MELT CONVEYING IN COUNTER-ROTATING TWIN-SCREW EXTRUDERS

by

LIN-TANG RICHARD ARTHUR LAI-FOOK, BSc(Eng.), MPHIL. (U.W.I.)

A THESIS SUBMITTED FOR THE DEGREE OF

DOCTOR OF PHILOSOPHY OF THE UNIVERSITY OF LONDON

AND FOR THE

DIPLOMA OF IMPERIAL COLLEGE

July 1984

Department of Mechanical Engineering,

Imperial College of Science and Technology,

Exhibition Road, London SW7 2BX.

ABSTRACT

Twin-screw extruders for polymer processing are still designed mainly by trial and error using expensive experimental methods. An attempt is made to establish a theoretical method of predicting melt flow behaviour in counter-rotating twin-screw extruders for the purpose of readily obtaining information relevant to extruder design and operation. The recent development of a part-empirical mathematical model for Newtonian flow in this type of extruder is used as the basis for further research towards the development of a similar model for predicting the non-Newtonian flow behaviour of polymer melts in intermeshing screws. In general, the greatest difficulty that arises in the analysis of the twin-screw extrusion process is the complicated geometry of the flow passages between the intermeshing screws. An analysis of the non-Newtonian melt flow in the screw channel and leakage clearances is carried out using a power law constitutive equation to characterise the non-Newtonian property of polymer melts. The deep-cut channels of a typical twin-screw extruder requires the use of a deep-channel flow analysis whilst in the leakage clearances one and two dimensional narrow channel flow analysis is employed. The theoretical equations are those derived by application of continuum mechanics and are solved on a digital computer using numerical methods, which include finite difference and finite element techniques. The geometric flexibility of the finite element method makes it suitable for use in the analysis of the intermeshing region, and a method of predicting the leakage flow which goes from one screw to the other through this region is developed. A mathematical model is developed for predicting a relationship between throughput rate and axial pressure drop for melt conveying in the twin-screw extruder. Experimental results are obtained from tests performed on a plasticating twin-screw

laboratory machine extruding polymer melts. Comparison of theoretical and experimental results shows that satisfactory agreement can be obtained for the extrusion of Newtonian fluids and for the highly non-Newtonian polymer melts extruded.

ACKNOWLEDGEMENTS

The author wishes to express his sincere thanks to his supervisor, Dr. D.P. Isherwood for helpful advice, encouragement and continued guidance throughout the investigation, and also to Dr. R.T. Fenner for many helpful discussions.

Grateful thanks is also due to BP Chemicals Limited for the use of facilities at their Research and Development Department at South Wales, and to members of the engineering and technical staff for their assistance, in particular, Dr. G.L. Pitman for organising the experimental work and for practical advice during the course of the work.

The author wishes to express his appreciation to the Science and Engineering Research Council for their financial support during this project.

CONTENTS

LIST OF FIGURES

LIST OF TABLES

LIST OF SYMBOLS

A	Aspect ratio
a_i, a_j, a_k	Triangular element dimensions for the x' direction in the finite element analysis
b_i, b_j, b_k	Triangular element dimensions for the y' direction in the finite element analysis
B	Axial width of the screw flight
b_o	Temperature coefficient
B_r	Brinkman Number
C	Centre-line distance of screws
C_p	Specific Heat at constant pressure
C_v	Specific Heat at constant volume
D	Diameter of screws
f_d, f_p	Shape factors for drag and pressure flows respectively
F_{pc}, F_{dc}	Correction factors for pressure and drag components of downchannel flow with curvature
h	depth
H	Channel depth
H_s	Side gap depth
H_c	Calender gap depth
I_1, I_2, I_3	Invariants of the rate of deformation tensor
k	Thermal conductivity
L	Distance between nodal points at the boundary in the finite element analysis
L_i	Length of the intermeshing or overlap region
m	Number of channels per turn of screw
n	Power law flow index
N	Screw rotational speed
p	pressure
P	Axial pressure

ΔP	Axial pressure drop between adjacent C-shaped chambers
P_e	Péclet Number
Q	Downchannel Flow Rate, and Net Throughput Rate of the twin-screw extruder
Q_{cd}	Rigid drag flow component or component of flow without shear for the calender leakage
Q_c	Calender gap leakage
Q_d	Rigid drag flow or flow without shear for the side leakage
Q_f	Flight gap leakage
Q_L	Sum of the leakages of the twin-screw extruder
Q_s	Side gap leakage
Q_t	Tetrahedron gap leakage
R	Radius of the screws
r_l, r_r	Radial coordinates for determining the clearance between flight flanks or tetrahedron clearance
s	Reciprocal of the power law index = 1/n (and the coordinate in the finite element analysis)
S	Screw pitch
t	Time
T	Temperature
T_o	Reference temperature
U	Internal Energy
v	Fluid velocity
v_x, v_y, v_z	Component velocities of cartesian coordinate system
v_r, v_θ, v_z	Component velocities of cylindrical polar coordinate system
V	wall velocity
V_a	Relative axial velocity between a chamber and the barrel wall
V_b	Barrel wall velocity
V_{bz}, V_{bx}	Components of barrel wall velocity resolved in the downchannel and transverse directions respectively
V_c	Relative wall velocity of the calender gap

V_d	Mean drag velocity of the side gap
V_{dp}	Mean velocity of combined drag and pressure flow in the side gap
V_m	Maximum mean wall velocity of the side gap
V_r	Screw root wall velocity
V_1	Flight wall velocity at a channel depth of $(H-\sigma)$
V_2	Flight tip velocity
V_θ	Angular wall velocity
Vol.	Volume of one C-shaped chamber
Vol_1	Volume of one barrel half over one pitch length
Vol_2	Volume of the screw core over one pitch
Vol_3	Volume of one screw flight with straight sides
w	width
W	Channel width
W_c	Calender gap width
W_s	Side gap width
x,y,z	Cartesian coordinates
r,θ,z	Cylindrical polar coordinates
α	Overlap angle
β	Helix angle
β_l, β_r	Angular coordinates for determining axial clearance between flight flanks or tetrahedron clearance
$\dot{\gamma}$	Shear rate
δ_f	Radial clearance between flight tip and barrel wall
ϵ	Total axial distance between flight flanks
ε	Side gap
η	Shear rate dependent viscosity
ϑ	Dimensionless velocity
μ	Apparent viscosity
μ_o	Reference viscosity at $\dot{\gamma}_o = 1\ s^{-1}$

ξ	Dimensionless coordinate, y/h
ξ^*	Dimensionless coordinate at zero shear stress or shear rate of a velocity profile
π_Q	Dimensionless channel flow rate
π_p	Dimensionless pressure gradient
ρ	Density
σ	Calender gap
τ	Shear stress
$\tau_{xx}, \tau_{yy}, \tau_{zz}$ $\tau_{xy}, \tau_{xz}, \tau_{zy}$	Components of shear stress in cartesian coordinates
$\tau_{rr}, \tau_{\theta\theta}, \tau_{zz}$ $\tau_{r\theta}, \tau_{rz}, \tau_{z\theta}$	Components of shear stress in cylindrical polar coordinates
ψ	Stream function
ω	Vorticity
ψ'	Flank angle

CHAPTER 1

INTRODUCTION

Extrusion is widely used in the plastics industry for the continuous processing of polymeric materials into useful products. Continuous shapes such as sheets, tubes and rods are made using screw extrusion. Although single-screw extrusion is the generally accepted method in common use, the practise of twin-screw processing is steadily increasing. Over the past decade, the introduction of more demanding processing operations has brought with it the need for more sophisticated and specialised machines. For many of these applications, a twin-screw extruder is often used as an alternative to, and offers decisive advantages over, a single-screw machine.

1.1.1 Screw extrusion of polymers.

In the screw extrusion of plastics, screw-barrel type of extruders are used to deliver a continuous supply of polymer melt usually to a die or mould to form a product of required shape. Because polymer melts can be very viscous, high pressures and consequently large amounts of power are required for plastic extrusion. Although melt extruders are quite common, the most widely used extrusion machine is the plasticating type of extruder.[1*] It efficiently and continuously converts solid polymer into melt and pumps the highly viscous melt through a die at high pressures. Solid polymer usually in the shape of pellets, chips, beads or powder is fed to the extruder hopper; the solid feed may consist of compounds of polymer blends or a compound with additives. The process consists of essentially three distinct operations, namely, solid conveying, melting and melt conveying (Figure 1.1.1). The condition

*Numbers refer to a list of references given on page 194

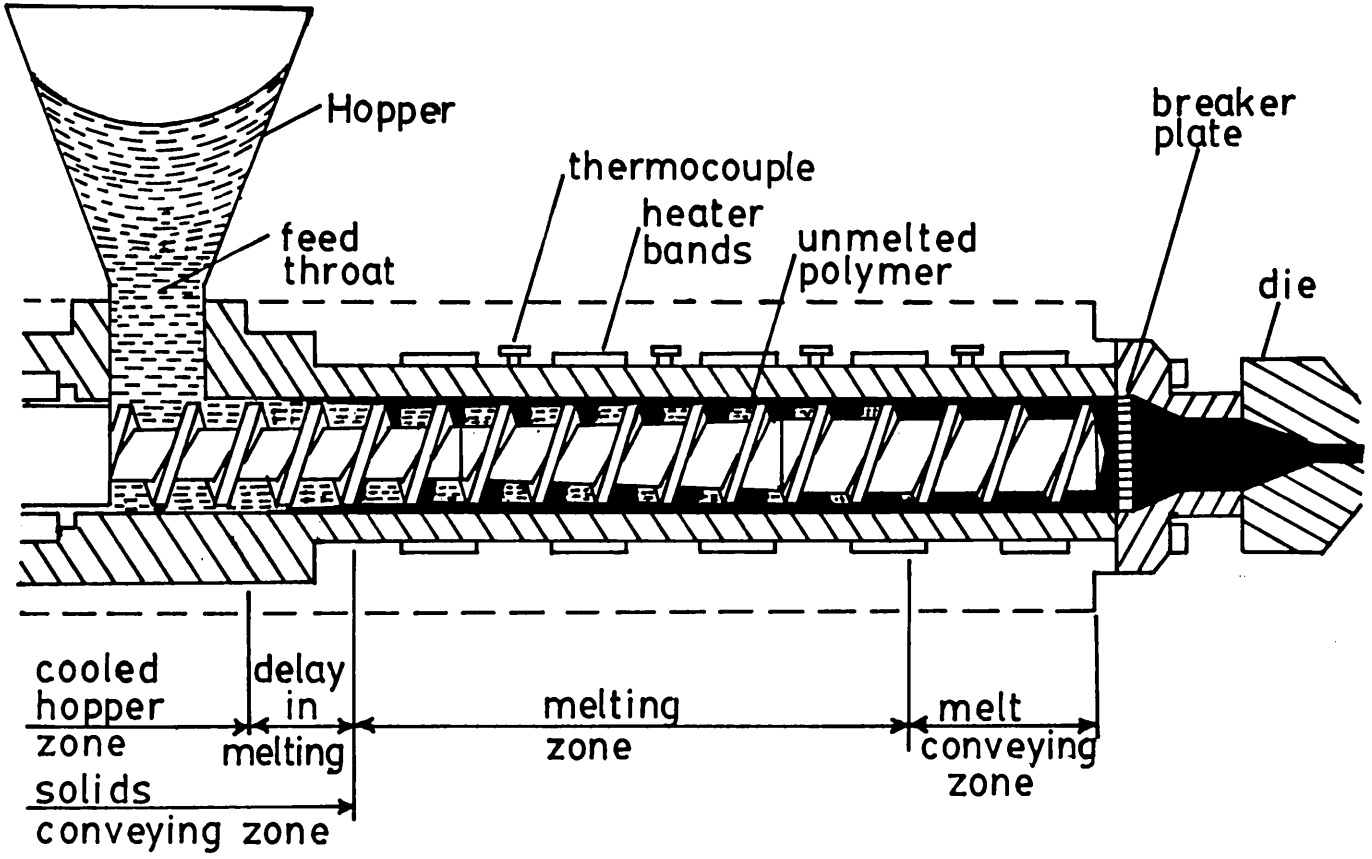

Figure 1.1.1 Cross-sectional view of a typical single screw plasticating extruder.

of the polymer in each functional zone depends a great deal on screw design and operating conditions. In addition to melting and conveying the polymer to the die, the screw extruder mixes and homogenizes the melt at high temperatures. The heat for melting is supplied by conduction from heaters in the barrel and can be generated in the material from the viscous dissipation of mechanical drive energy transformed into thermal energy. One measure of quality in the product is the temperature uniformity and homogeneity of the extrudate or melt leaving the extruder. Normally the plasticating extruder can accomplish all these tasks without the possibility of thermal degradation of the polymer. Barrel temperature setting is selected according to the polymer extruded and the temperature has to be high enough to melt the polymer without causing thermal degradation. The frequency of screw rotation at which the extruder will operate depends on the size of the extruder and production rate requirements, the limiting factor in a given size extruder being quality. Higher screw speeds will produce higher throughput but will normally result in deterioration of quality.

1.1.2 Single-screw extruders.

The most common type of screw extruder consists essentially of a single Archimedian screw rotating in a closely fitting cylindrical barrel. The principle of operation is like a screw pump in which the material is dragged along the screw channel by the relative motion of the screw and barrel.[1] The material is conveyed from the driven to the free end of the screw with generally increasing pressure. The pressure developed along the extruder depends largely on screw design but is normally quite high at the die because of the high viscosity of polymer melts. The condition of the polymer in each functional zone (Figure 1.1.1) depends a great deal on screw design and operating conditions. The principle

geometrical variable of the screw is the channel depth. A common type of screw is the 'metering screw' which has three geometrical sections, as illustrated also in Figure 1.1.1 , namely, a deep feed section, a tapered compression or transition section and a relatively shallow metering section. The relatively deep feed section enables the lower density feed solid to be conveyed at the same rate as the polymer in the other sections of the screw thus preventing starvation along the extruder. Conveying of melts in shallow channels also enables the polymer to undergo high shear levels which can raise the melt temperature from viscous heat dissipation but increases mixing and ensures homogenization of the melt before it reaches the die.

The mechanism of conveying the polymer depends largely on frictional forces between the polymer and barrel to push the material forward.[1,2] If the material filling the screw channels of a single screw extruder sticks to the screw and slips on the barrel it simply rotates with the screw without being pushed forward. To advance along a barrel material should slide as freely as possible on the screw and adhere as much as possible to the barrel; the forward motion of the leading edge of the screw flights producing the force necessary for the material to advance along the screw channel. Because of the finite clearance between the screw and barrel and the pressure gradient along the screw channel some polymer leaks across the screw flights. This reduces the effectiveness with which the screw can pump the material forward but can improve mixing in the extruder.

1.1.3 Twin-screw extruders.

In twin-screw extruders, the mechanism of conveying materials to the die can be quite different from that in single-screw machines. In principle the operating stages are the same in both extruders, these being solid conveying, melting and melt pumping but, in a typical twin-screw machine, the pumping action is positive if the screws intermesh.

A typical twin-screw machine consists essentially of two extruder screws rotating next to each other in a figure of eight section barrel.

Figure 1.1.3.1 illustrates arrangements of twin screws which can be either intermeshing or non-intermeshing. In non-intermeshing twin-screw extruders, screws are placed side by side with the distance between their centres equal to at least the diameter of one screw. Such extruders are still very dependent on frictional forces for conveying materials and their behaviour is not very different from a single-screw unit, although there is some interaction between the screws[3]. In intermeshing twin-screw extruders the flights of one screw penetrates the channel of the other forming C-shaped chambers which can positively convey the material from the hopper to the die when the screws rotate, thus behaving like a positive displacement pump[4,5]. Twin screw machines with intermeshing screws are those most commonly used for processing polymers.

Positive conveyance of the material in twin screw equipment is largely independent of the frictional relations that control conveying of the material in a single screw unit[2]. Thus, intermeshing twin screw extruders will convey, with comparable efficiency, materials of very high or very low viscosity and materials with very high or very low coefficients of friction against metal surfaces. It is possible and customary, also, to operate twin screw equipment with partially filled chambers only. A twin screw machine with intermeshing screws will convey a material with approximately the same efficiency whether the channels are completely

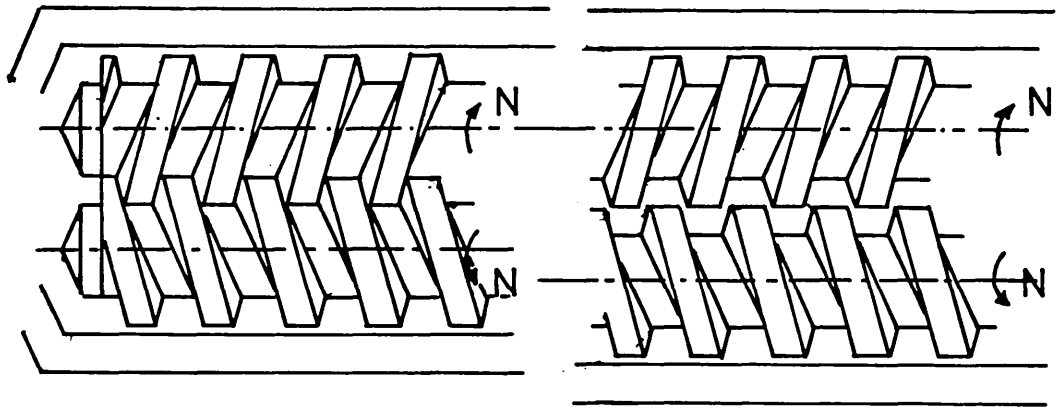

counter-rotating

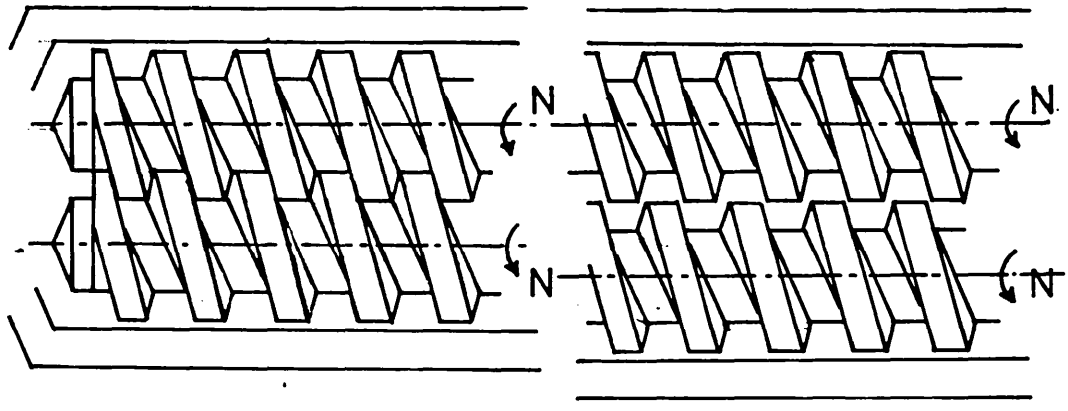

corotating

intermeshing non-intermeshing

Figure1.1.3.1 Arrangements of counter and co-rotating screws of twin-screw extruders.

filled with material or only partially filled.

Twin-screw extruders are often used, therefore, for materials which are inherently difficult to process with a single-screw extruder.[6,7,8,9,10,11] Such problems are, for instance, slip which can occur at the metal/polymer interface and can seriously reduce the transporting capability of the extruder, and/or too much viscous heat generation which can cause overheating of degradation sensitive materials, both conditions produced mainly by the high screw speeds(100-200rpm) necessary to obtain the required throughput rates in shallow channels of single-screw machines. These difficulties are largely overcome in twin-screw extruders by operating, with comparable output rates, at low speeds(10-60rpm) using screws with deep channels positively to convey the required quantity of material in chambers where, in any case, slip at the walls is irrelevant.[5,10]

Positive conveying behaviour in twin screw extruders is largely dependent, however, on how well the various screw channel sections are closed off when the screws are intermeshing.[2,5,12] In some screw geometries there can be very little sealing off of the C-shaped chambers formed even when the screws are fully intermeshing. The formation of partly-closed chambers creates the opportunity for material to leak back into upstream channel sections and adversely to affect the positive conveying behaviour of the extruder. Because of the need for mechanical clearances, the chambers tend not to be completely sealed, even for closely intermeshing screws.

Intermeshing screws of twin screw extruders can be designed to rotate either in the same direction(co-rotating screws) or in opposite directions (counter-rotating screws). In both types of extruders, a high degree of positive conveying can be achieved with the minimum clearances that the closely intermeshing screws would allow. Normally the highest degree of positive conveying can be achieved with the

counter-rotating extruder because it allows a screw geometry with a maximum sealing of the screw channel sections.[5] In general, twin screw extruders with small mechanical clearances, have to run at low speeds to avoid build up of high local pressures that could cause machine wear.[2] Co-rotating intermeshing twin screw extruders with only a small degree of positive conveying are those with self-wiping type screws.[13,14,15] Such screws can normally be designed with relatively small flight tips and consequently, with an almost fully-opened channel from one screw to the other. The mechanism of conveying in this type of machine is similar to that of a single-screw extruder and requires the machine to operate at high screw speeds (up to 500rpm).

It is generally accepted that twin screw extruders can be designed to provide far better mixing than basic single screw machines (i.e. without mixing devices).[2,11,12,16,17] Usually effective mixing can be accomplished in twin screw extruders by exchange of material between screws and the transfer of material from one screw channel to the other. In single screw extruders, there is no equivalent mechanism.

Leakage flow is limited by the small clearance between screw flights and barrel and usually, the local movement of melt in the shallow channels of rather long metering sections has to be relied upon for adequate mixing to occur.[1] By varying the clearance between the screws the degree of positive conveying can be controlled by varying the positive conveying of the screws which also affects the homogenization and residence time distribution.[5,12]

also be produced. To examine fully the performance of such machines, it is important to include the effects leakages have on melt conveying. Only when these flows are fully accounted for can their contribution towards power consumption and mixing be determined.[5,18,19] It is, however, the presence of leakages which makes the process more complex and difficult to analyse[5] and, for this reason, twin-screw machines for polymer processing are still designed largely by using practical trial and error methods.

1.1.4 Leakages in Twin screw extruders.

Some of the theoretical principles of the main types of multi-screw extruders were first introduced by Schenkel.[4] The theory for twin screw extruders with intermeshing screws considers the working material to be contained in a number of separate closed spaces. These include the three distinct working regions shown in Figure 1.1.4.1, that is: the C-shaped spaces(a) between the annular flanks of the two screw flights, the cylindrical surfaces of the screw roots and the barrel wall; the spaces(b) between the cylindrical surfaces of the root of one screw and the flight land of the other; and the wedge region(c) between the overlapping flanks of the two screw flights. The positive conveying capacity of the completely filled C-shaped volumes(which includes all working regions and which are assumed to be more or less hemetically sealed by the screw flights and barrel) of twin screws rotating at screw speed N is taken simply as the number of chambers becoming free at the die per unit time multiplied by the volume of one chamber. The ideal theoretical output of a twin screw extruder for screws with m starts(or channels per pitch) can be calculated from the equation,[4,5]

$$Q = 2mNVol. \qquad 1.1.4.1$$

where Vol. is the volume of each chamber for identical uniform intermeshing screws. Because the chamber volumes cannot be completely sealed, the actual output is always a little less due to leakage flow, Q_L, thus;

$$Q_a = Q - Q_L \qquad 1.1.4.2$$

For closely intermeshing screws of small radial clearance, Schenkel[4] states that the leakage flow is between 5 and 10 percent of the ideal pumping capacity, depending on the die pressure and the viscosity of the melt. For larger axial distance between the flanks of the flights and/or a larger radial distance between the cylindrical surfaces, pressure flow appears in opposition to the positive conveyance and back flow increases, just as in a single-screw extruder. Other workers determined the

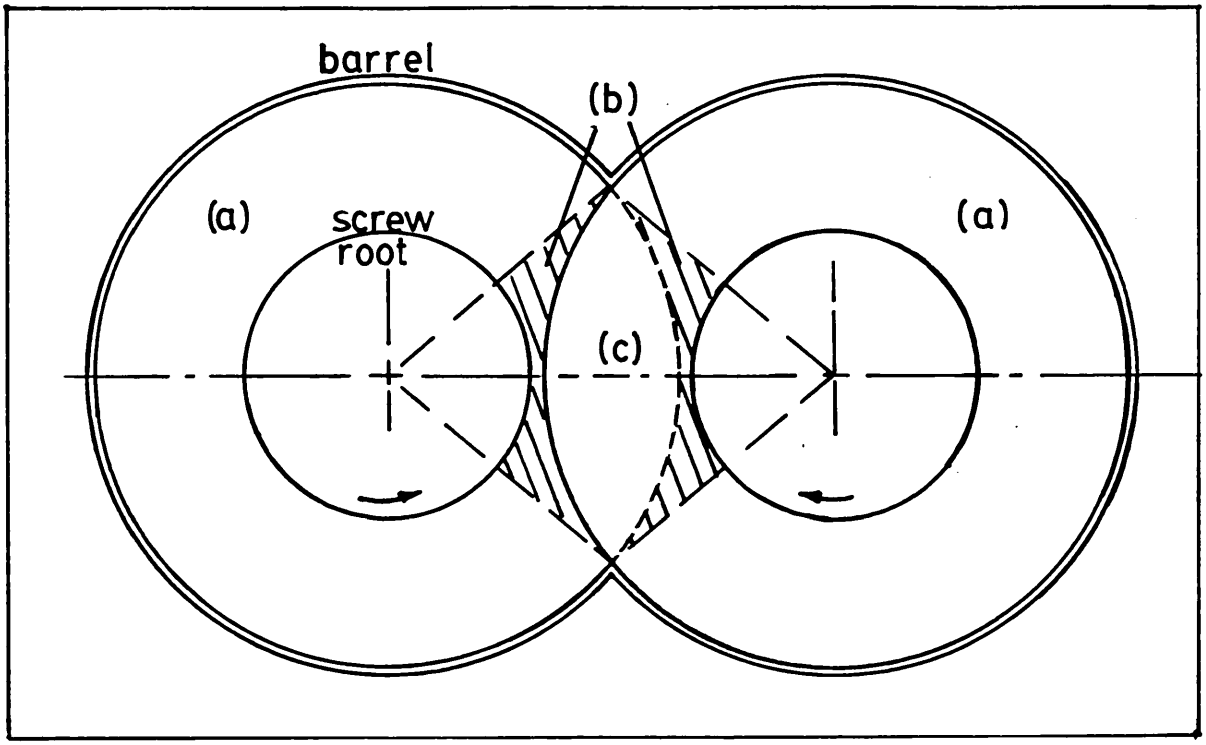

Figure1.1.4.1 Cross-sectional view showing working regions.

leakage flows of twin extruders by using a correction factor(less than one) with the ideal positive conveying capacity to calculate the actual output.[5] This correction factor was usually an undefined experimental constant not related directly to the mechanisms that occur in the twin screw extruders.

In recent years, attempts have been made to examine and understand the mechanism of flow in twin screw extruders. Most studies, however, completely neglected the leakage flows and concentrated only on the flow behaviour in sealed chambers of intermeshing screws with shallow channels.[20,21] One exception is the study made by Janssen[22] on the phenomena in counter-rotating twin screw extruders. He realised the importance of the leakages and their effects on the throughput and suggested suitable mathematical treatment for predicting leakage flow of isoviscous fluids. A Newtonian analysis, however is likely to be appropriate only for polymer melts which are mildly non-Newtonian.[23] Polymer melts are extremely non-Newtonian and studies on single-screw extrusion have shown that output rates can be seriously overestimated if these melts are treated as Newtonian fluids.[1] Nevertheless, from Janssen's work further research can be carried out towards the development of a similar mathematical model for predicting flow behaviours of actual melts in twin-screw extruders.

In the analysis, the ideal theoretical output of a twin screw extruder is given by equation 1.1.4.1 and it is reduced by the presence of leakages in the machine. Figure 1.1.4.2 shows the arrangement of counter rotating intermeshing screws with the leakages which have been described in detail by Janssen.[5] The four leakages shown are as follows:
(1) The flight leakage, Q_f, through the small clearances between the screw flights and barrel and is similar to that in a single screw extruder.
(2) The calender leakage, Q_c, through the clearance between the flight tip of one screw and the screw root of the other and goes from one C-shaped chamber to the other of the same screw.

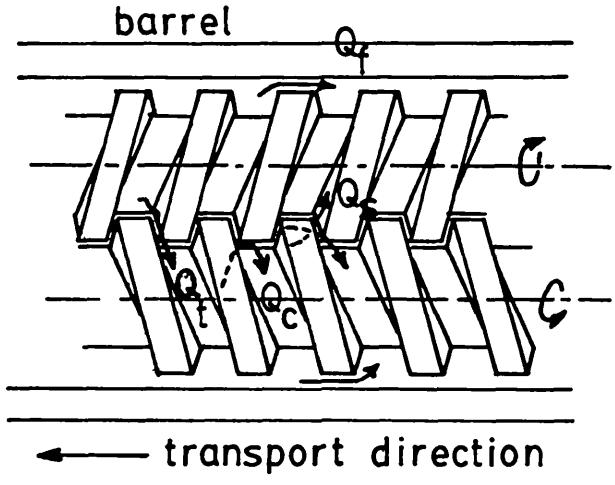

Figure1.1.4.2 Leakages in counter-rotating screws.

(3) The side leakage, Q_s, through the clearance between flanks of the screw flights and goes in a direction perpendicular to the plane through the screw axes.

(4) The tetrahedron leakage, Q_t, through the clearance that goes from one screw to the other between the flanks of the flights of the two screws.

The analytical mathematical model developed by Janssen for predicting the leakage flow rates was partly empirical. A formula developed from experiments performed on stationary models of the gap was used to predict the tetrahedron leakage.[5] It is mainly the complex shape of the intermeshing region that makes the flow difficult to analyse.

1.2 Objective and scope of the present work.

The object of this investigation is to attempt to establish a theoretical method for predicting polymer melt flow behaviour in counter-rotating twin-screw extruders. Such a theoretical procedure would be useful in solving the practical industrial problems of operation and design.

The study involves examining both theoretically and experimentally, melt flow in counter-rotating twin-screw equipment. Janssen's approach towards the development of the Newtonian flow model is extended to include non-Newtonian flow in the extruder. A flow analysis is carried out to attempt to find a general theoretical method which can be used to predict melt flow in the extruder. The treatment used is to be verified by comparison with experimental results obtained from the extrusion of polymer melts.

Chapter 2

Melt Conveying Zone

2.0 Introduction.

A review of literature relevant to the melt conveying process of a counter-rotating twin-screw extruder was carried out to determine the important aspects which are to be considered in the development of the mathematical flow model for the extruder. A satisfactory theoretical model for the melt conveying zone of the plasticating extruder should stipulate the equations for calculating the flow rate, pressure, temperature and velocity distributions in the various flow passages. These equations should include the pertinent physical properties, geometrical information about the intermeshing screws and barrel and operating condition and, finally, supply information relevant to extruder design and operation. For the understanding of plasticating counter-rotating twin-screw extruders, a good understanding of the melt conveying process is of paramount importance. In this chapter, therefore, an account is given of the working principles which include the mechanism of conveying and flow behaviour likely to occur in the channel and leakage gaps of the extruder. Mathematical flow models which have been developed for examining melt flow in channels of single-screw extruders and which may be relevant to flow behaviour in twin-screw extruders are discussed with the effects melt properties and operating conditions are likely to have on extruder throughput.

2.1 Conveying Mechanism.

A twin-screw extruder with intermeshing screws behaves like a positive displacement pump. The intermeshing screws form series of C-shaped chambers which convey the material from the hopper to the die by the displacement effect of the intermeshing screw threads produced by screw rotation. The mass of the material rotating in these chambers and becoming free at the die per unit time determines the throughput of the machine.[4,5] At the free end of the screws, a high pumping pressure is normally generated due to the restriction offered by the die to the positive conveying action of the extruder.

This positive pumping action can be reduced by leakage in the extruder. Because of the need for mechanical clearances the chambers are not completely sealed even for closely intermeshing screws, and material leaks back along the extruder from chamber to chamber. Consequently, the pumping capacity of the machine can be reduced by these leakages which allow the die pressure to be transmitted back through the chambers of the extruder. When this die pressure is transmitted as far back as the feed end of the machine, the twin screw extruder is operating with all the chambers completely filled with material and the feeding process and thus machine output can be influenced by the pressure developed at the die.[5] For instance, the higher die pressure which can be generated as a result of using a smaller die, would reduce extruder output by producing larger leakages from the steeper build up of pressure in the extruder.

In general, it is customary to operate twin-screw extruders with partly-filled chambers in the feed zone. Under this condition, back pressure due to the restriction at the die can only be generated when the chambers at the die end of the extruder become filled with material. Leakage flow from these chambers may in turn become full depending on the amount of back

pressure and the size of the clearances. In other words, this effect can be imagined also as a gradual falling or relieving of the pressure developed at the die when the material leaks or overflows from each chamber in turn. This type of behaviour can be found in plasticating twin-screw extruders (illustrated in Figure 2.1.1) in which the pressure builds up only as the die end is approached and the chambers become completely-filled with melt over this length of the machine[5]. Over the remaining part of the extruder, the chambers are only partly-filled with material i.e. from the hopper to the point where the die pressure falls to zero, and the conveying mechanism in these earlier regions can no longer be influenced by what happens at the die. The throughput of the machine is now governed mainly by the feeding process at the entrance region of the extruder and is independent of the die pressure[5]. It is obvious, therefore, that the amount of material entering the extruder from the hopper directly determines the output rate while the required leakage is the additional amount necessary to produce complete filling and to raise the pressure over each chamber at the die. Once the feed rate to the extruder is kept constant both output and leakages at a given screw speed would also be constant. For isothermal Newtonian flow, by generating a higher pressure at the die, for instance by pumping the same extruder output through a smaller die, the leakages and associated back-pressure drop remain unchanged and there must be an increase of the completely-filled length of the extruder. The number of completely-filled chambers in the extruder, therefore, is likely to increase with increasing die pressure as long as the back-pressure generated in the extruder is confined to the metering zone[5]. Only by increasing the rotational speed of the screws can there be both a pressure rise and a constant fully-filled length in the metering zone. Then the machine will deliver the same output as a result of the increased leakages generated from the larger back-pressure gradients and higher screw speed. Knowledge of the number of fully-filled chambers is necessary for determining screw performance and extrudate quality[5].

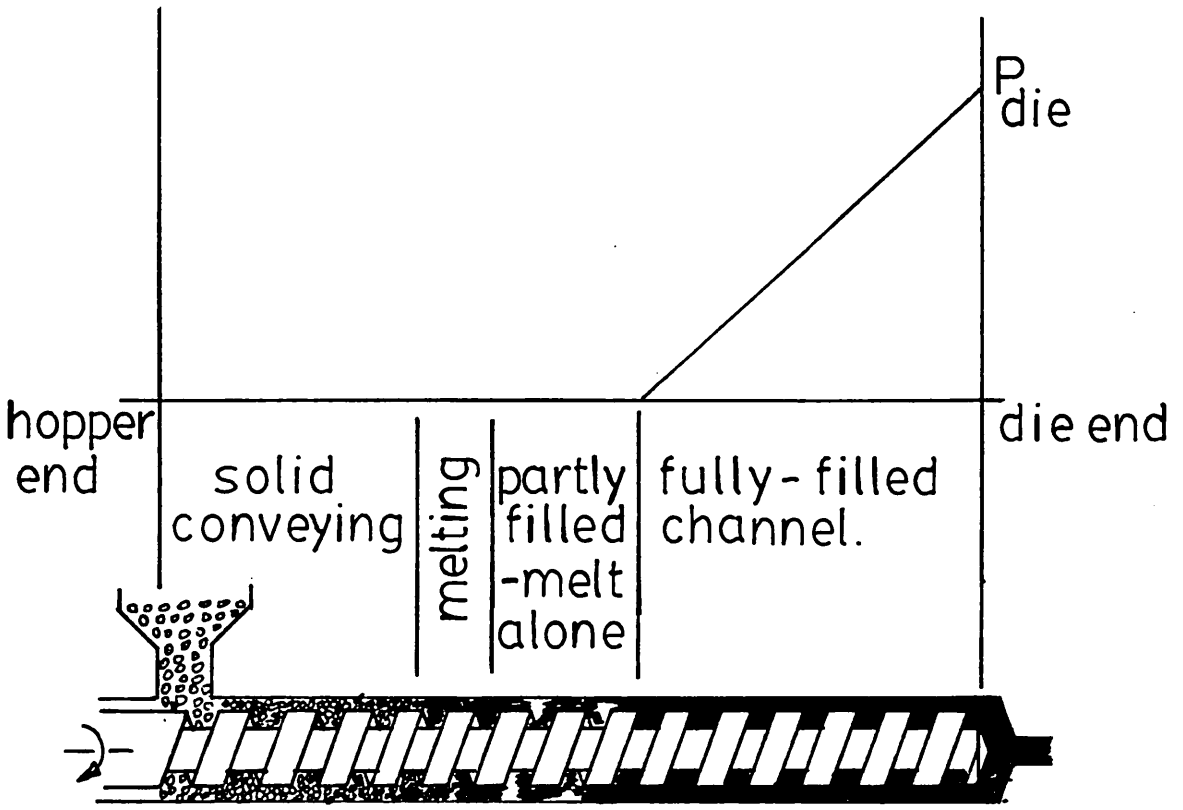

Plasticating twin-screw extrusion process.

Figure 2.1.1.

2.2 Flow behaviour in counter-rotating intermeshing screws.

The flow of melt in chambers of counter-rotating twin-screw extruders is produced by the drag effect of the rotating screws and the pressure forces developed in the extruder. The back-pressure generated along the screws due to die pressure is only partly responsible for the flow behaviour in the twin-screw extruder. Melt is also conveyed through the leakage clearances and within each chamber by drag flow due to the moving surfaces together with pressure flow produced by internal pressure generation as a result of the flow within each passage. The net effect of these flows is the result of the pressure difference between adjacent chambers in the extruder.[5] The working regions which can be examined separately, therefore, are the C-shaped spaces themselves and then the regions which join each of the chambers together i.e. the leak passages previously described and illustrated in section 1.1.4, Figure 1.1.4.1.

In each separate chamber, the material is exposed to the drag effect of the rotating surfaces and pressure gradients are developed resulting in complicated counter-currents in the screw channel. These are comparable, in principle, to the pressure flows which occur in the single-screw extruder, resulting in the material travelling in a helical path in the channel.[1] The material rotates with the screw channel but also sticks to the barrel where it can be dragged across the channel in the direction (of screw rotation) perpendicular to the screw axis, Figure 2.2.1. This motion can be resolved into two mutually perpendicular directions, one component acting in the direction along the channel and the other perpendicular to the flights, the angle of inclination of the flight being the helix angle. The net flow perpendicular to the flight is zero and counter-pressure flow produces recirculation. If the pressure flow generated along the channel is equal and opposite to the drag flow, there is no net downstream movement and recirculation occurs, with the material at the

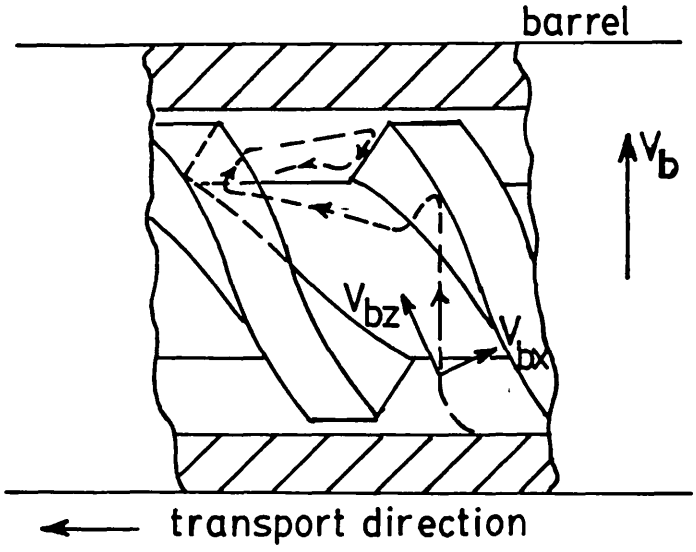

Figure 2·2·1 Channel flow due to relative motion, with stationary screw and rotating barrel.

flight moving towards the screw root and returning along the bottom of the channel in the direction of screw rotation. For a smaller back-pressure flow which would produce only a reduction in the drag flow, a net downstream flow would exist with material turning over at the flight wall but this time proceeding along the bottom of the channel in a helical path, the closer the net flow is to pure drag flow the more forwarding motion and the more open would the loops of the helix.

In counter-rotating extruders, however, the pressure flow along the channel is generated in the opposite direction to screw rotation. Where the screw surfaces converge in the intermeshing region, high pressure regions can be found on this side of opposed chambers of the extruder and low pressure regions at the opposite end when the surfaces diverge,[2,5,20] Figure 2.2.2. This would always produce a pressure flow in the downstream direction of each chamber with a flow larger than that due to drag and the production of a shorter helical path than that produced with pure drag flow. For chambers with very little pitch (helix angle almost zero), material would be conveyed directly from one end of the chamber to the other as illustrated in Figure 2.2.3, without travelling along the complicated helical path as in the case of screws with finite pitch.

Because the channels of twin-screw extruders tend to be almost closed at the intermeshing region, the enclosed volume of melt would be recirculated in each chamber. The closed nature of the chambers and this recirculatory flow would produce a complex flow field of a three-dimensional character. In the region far from the intermeshing zone, the influence of the rotating flight walls on the counter-pressure flow generated in the channel produces a flow profile with a zero velocity layer which is stationary with respect to the barrel or intermeshing zone.[5] For flow in this region, it has been found that velocity profiles are not influenced by screw rotation and a relative velocity can be used to define the flow.[5]

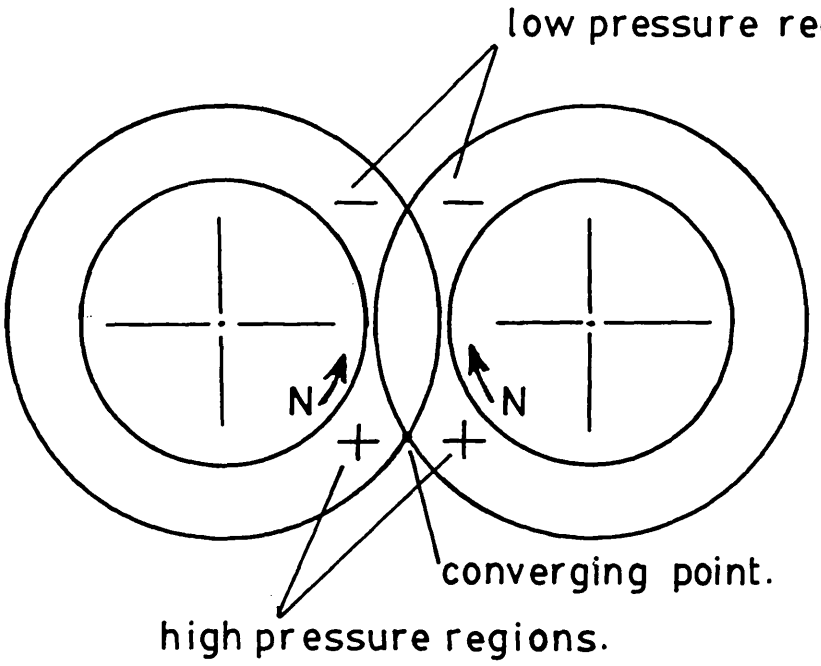

Figure 2-2-2 High and low pressure regions of opposed chambers.

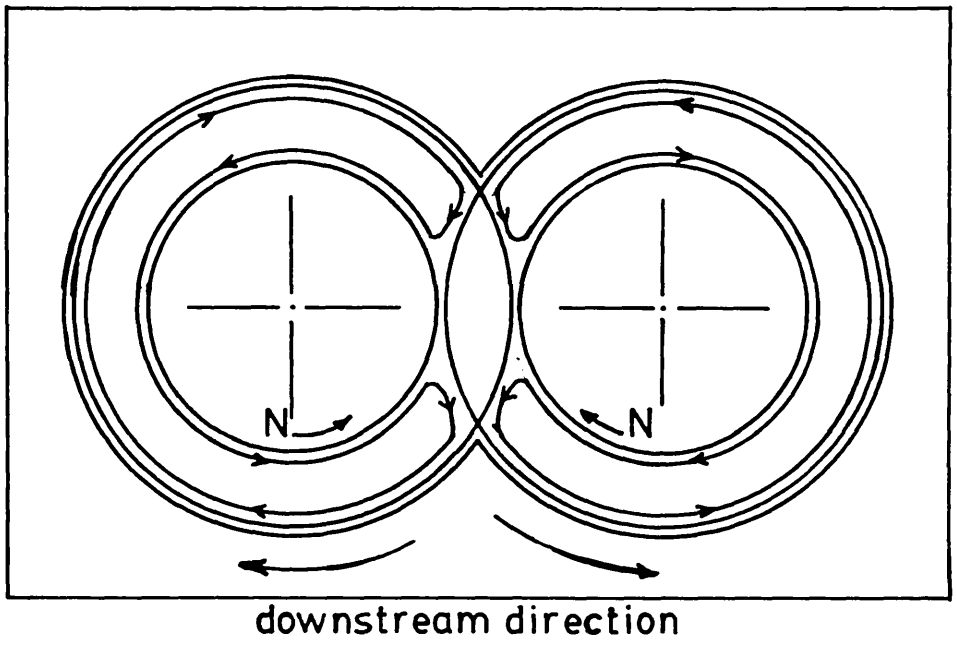

Figure 2-2-3 Recirculatory flow in opposed chambers.

This is similar to the case of slow flow of melts in channels of single-screw extruders for which the stationary screw and rotating barrel assumption used is found to be adequate enough for determining flow fields of this type in which inertia effects are not significant.[1] Velocity profiles in the chamber can be influenced by the leakage over the flight complicating the heat transfer and generation processes which affect flow fields in deep channels.[1,24]

Flow over the flights of intermeshing screws occurs in much the same way as that in single-screw equipment.[1] The melt rotates with the screw but sticks to the barrel surface where it is dragged across the channel and over the advancing flight into the adjacent chamber. The drag flow tends to build up pressure towards the flight wall and the pressure then drops across the flight associated with the flow through the flight gap, hence creating a pressure drop across the channel and flight. Figure 2.2.4 shows what form the axial pressure profiles are likely to take for two sets of clearances.[5]
Although there is a constant pressure drop over each channel and flight, the axial pressure in the channel can vary depending on the magnitude of the leakages over the flight and through the intermeshing region.[22]

Similar flow mechanisms occur in the calender and side gaps but considerable drag flow can be produced in these clearances because both surfaces rotate in the same direction and with almost equal speed, a relative velocity between the surfaces produced because of the linear variation of surface velocity over the flight depth. The drag flow for these leakages, therefore, consists of rigid material transport from motion of the surfaces with equal velocity plus, shear flow due to the relative surface velocity.

In the calender gap, drag flow can generate internal pressure flow, similar to the mechanism of squeezing melt through the convergent-

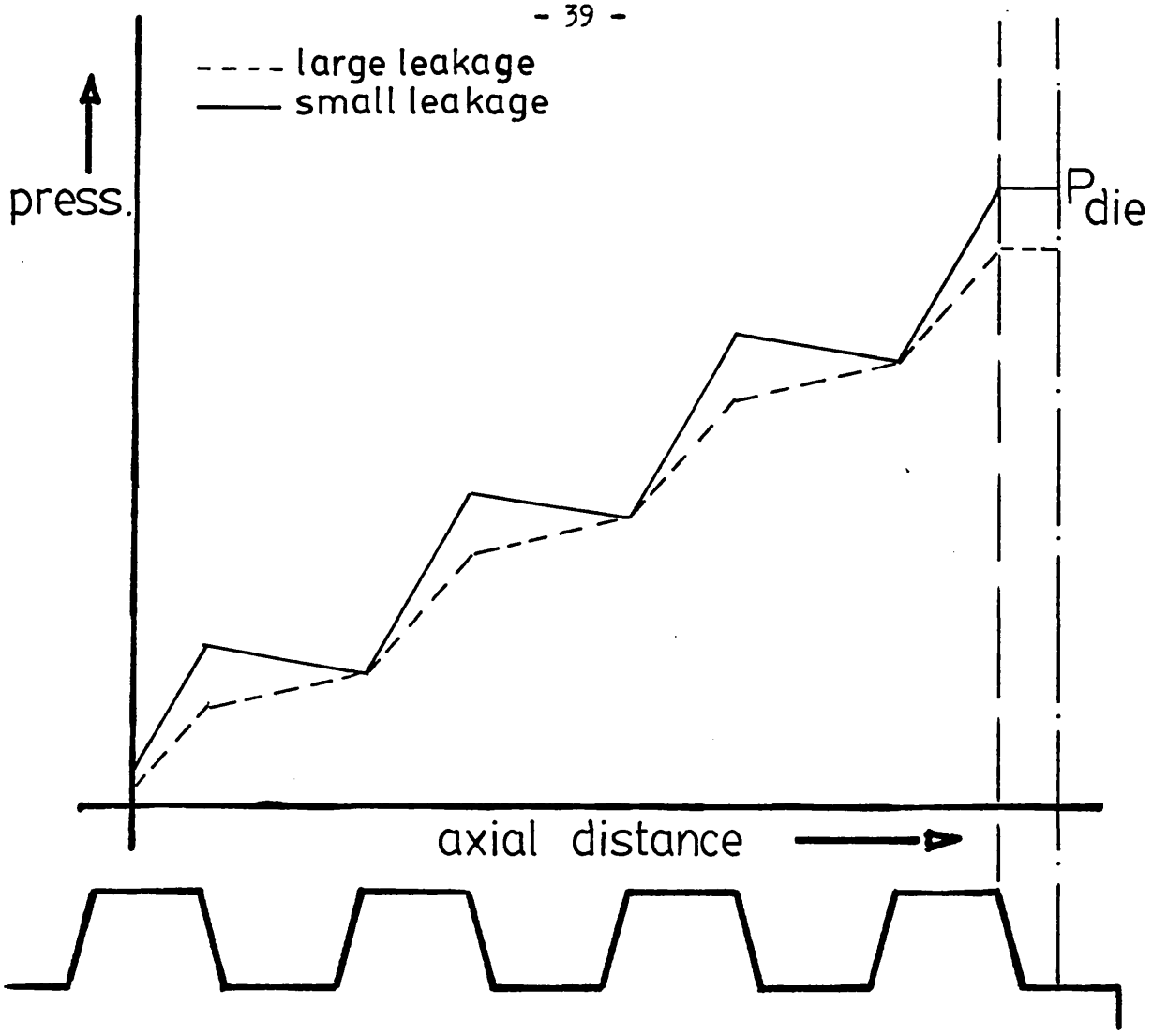

Figure 2·2·4 Axial Pressure Distribution with chamber pressure included.

divergent gap between rotating parallel rollers in a calendering process.[25] Hydrodynamic pressures can be developed with pressures rising to a maximum in the convergent section and falling to a minimum in the divergent section, similar to the pressures developed in a journal bearing.[27] The pressure in the extruder at inlet and outlet of the gap, however, must be high enough to prevent the pressures falling to a value below zero in the divergent section, since most fluids cannot sustain negative pressures.[27,28] This is only likely to occur when operating the extruder with very little or no pressure at the die but such an operating condition renders the extruder useless as a pump and is not likely to be important. With the addition of the influence of a high pressure drop due to die pressure across the chamber, there can be shear flow dominated by pressure flow in the calender clearance with the result that no maximum or minimum levels would be produced.

The flow through the overlapping area of the two screws flights is complex and consists of a combination of the leakages through the side and tetrahedron gaps. In the direction of screw rotation, material is carried along by the surfaces through the side gap, from the high pressure regions of the intermeshing channels (see Figure 2.2.2) to the low pressure regions of adjacent channel sections. Perpendicular to this direction, there is tranverse flow through the tetrahedron gap which allows material to be transferred from one screw to the other solely by the influence of the pressure drop due to die pressure existing between opposing chambers of the screws.[5] Although rotation produces drag flow through the side gap, there is no net drag flow through the tetrahedron gap according to experimental evidence.[5] It appears that the components of the drag velocities of the counter- rotating screws in the direction of the tetrahedron leakage are equal and opposite and tend to cancel. The flow through the side and calender gaps are directly influenced, therefore, by the flow in the channel produced by screw rotation whilst the tetrahedron leakage is influenced only by back-pressure in the extruder.[5]

Melt flow in twin screw extruders, unlike Newtonian flow, is affected by the amount of shear it experiences due to the drag effect of screw rotation. This shear thinning effect increases melt temperature and both reduce the viscosity.[1] This means also that all melt flows are inter-dependent and the local viscosity is influenced by the rate of deformation of the material resulting from flow in every direction. For isothermal conditions, flow characteristics of dimensionless flow rate versus pressure drop of a counter-rotating machine extruding Newtonian fluids show that the flow rate is dependent only on the geometry of the screws and independent of both viscosity and screw speed.[5] From the extrusion of highly non-Newtonian polymer solutions, flow curves show the strong dependence of viscosity on screw speed for a given geometry.[22]

Flow curves for the extrusion of polymer melts are dependent on temperature, although it is uncertain whether or not the variation of temperature and its effect is significant along a typical twin-screw extruder. Although there is little energy dissipation in deep channels of twin-screw extruders, this is not likely to be the case in the relatively small leakage gaps. It has been suggested that because of the continuous changing of the surfaces of the small gaps in the intermeshing region, the heat generated may be dissipated and distributed by conduction rapidly and evenly in twin-screw extruders.[5] Because of the recirculating flow that occurs in twin screw extruders from one end of a chamber to the other, the mixing and heat transfer is increased in a manner which is most likely to produce uniform melt temperature in each chamber.[5,26]

The temperature of the polymer, however, is not likely to be uniform throughout the extruder and measurements of temperatures of extruded polymer indicate a higher temperature at the die.[5] The pressure gradient will vary along the extruder and may be lowest at the die end. This is indicated also by the number of fully filled channels in the extruder which

increases less than proportionately with increasing die pressure. A uniform melt temperature is produced when the fully filled length is short, i.e. near the die, and also when it is very long.[5] From the experimental results it has been deduced that the temperature profile of the polymer in the extruder is hardly affected by changing die pressure.

2.3 Melt Properties of Polymers.

Viscosity under simple shear is an important material property of flowing liquids. Viscosity is defined as the ratio of the shear stress to the rate of shear (or rate of deformation) of the fluid. Most commonly used fluids exhibit Newtonian behaviour, that is, there is a linear rise in shear rate with increasing shear stress. For flow between parallel plates, Figure 2.3.1, the shear stress between layers of fluid in flow is given by the equation,

$$\tau_{xy} = \mu \frac{\partial v_x}{\partial y} = \mu \dot{\gamma} \qquad 2.3.1$$

where τ_{xy} is the shear stress, $\frac{\partial v_x}{\partial y}$ is the time derivative of shear strain and is termed the shear rate $\dot{\gamma}$. This relationship is plotted in Figure 2.3.2 in which the "flow curve" is a straight line of slope μ which is called the viscosity. It is not uncommon, therefore, to think in terms of only a single viscosity of the fluid.

Most polymer melts exhibit "pseudoplastic" behaviour i.e. there is a less than proportionate rise in shear stress with shear rate. In this case, the ratio of shear stress to shear rate which is termed the "apparent viscosity" falls progressively with increase of shear rate and the flow curve becomes linear at very high rates of shear (Figure 2.3.3). The physical interpretation of this phenomenon is probably that with increase in the rate of shear molecules progressively align until no further alignment is possible and the flow curve becomes linear.[29] The alignment of molecules normally takes place instantaneously (or too quickly to be measured in viscometers) as the rate of shear is increased and therefore polymer melts are often regarded as time-independent fluids. Other examples of time-independent fluids are dilatant and Bingham fluids which exhibit the non-Newtonian behaviour shown in Figure 2.3.3.

When the polymer melt flow curve is plotted on a logarithmic scale, the graph usually appears to be a straight line over one or two

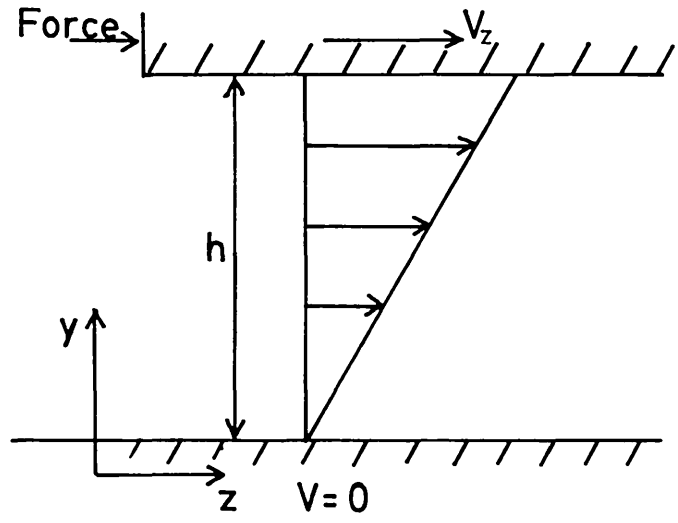

Figure 2·3·1 Laminar flow between parallel plates, top surface moving, bottom surface stationary.

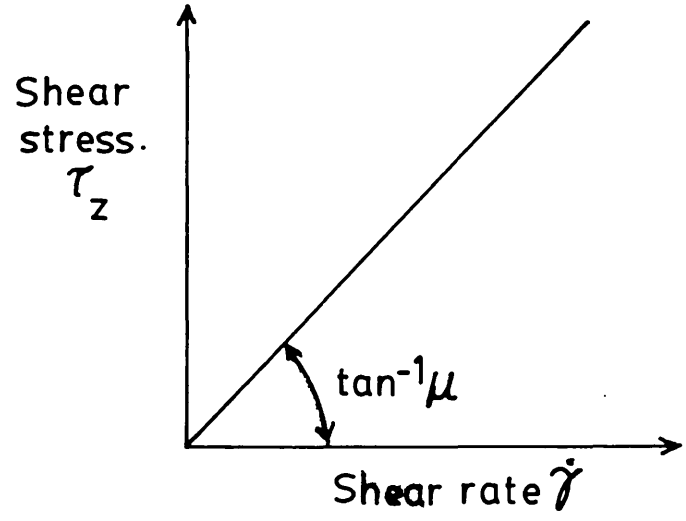

Figure 2·3·2 Flow curve of a Newtonian fluid.

decades of shear rate, Figure 2.3.4. At low shear rates of up to about 0.01 sec.$^{-1}$ the curve becomes a straight line with slope of unity, indicating Newtonian behaviour and again at very high shear rates Newtonian behaviour is observed. For most polymer melts, however, the relationship between shear stress and shear rate can be represented, over limited ranges of shear rates, by a power-law equation of the form,

$$\tau = k'\dot{\gamma}^n \qquad 2.3.2$$

which may be written in logarithmic terms as,

$$\log\tau = \log k' + n \log \dot{\gamma} \qquad 2.3.4$$

where k' and n are constants; k' is a consistency coefficient and n is a measure of the degree of non-Newtonian properties of the polymer. It is important to remember that n is a constant only over a limited range of shear rate, therefore, in engineering applications, all that is required is the rheological equation which describes the polymer over the particular problem.

Because negative values of shear rate are not allowed in the power law equation 2.3.2, an analytically useful form is,

$$\tau = \mu_o \dot{\gamma} \left| \frac{\dot{\gamma}}{\dot{\gamma}_o} \right|^{n-1} \qquad 2.3.5$$

where μ_o is the apparent viscosity at reference shear rate $\dot{\gamma}_o$ and n is the slope of the log shear stress/log shear rate curve. Alternatively, a plot of log $(\tau/\dot{\gamma})$ versus log $(\dot{\gamma}/\dot{\gamma}_o)$ would give a slope of n-1.

The flow curves of polymer melts are influenced by temperature and pressure. Viscosity of polymer melts, like that of most liquids, decrease with temperature. A temperature dependent term can be added to the power law equation to account for the shift of the flow curve in the vertical direction and the viscosity equation becomes,[1,30]

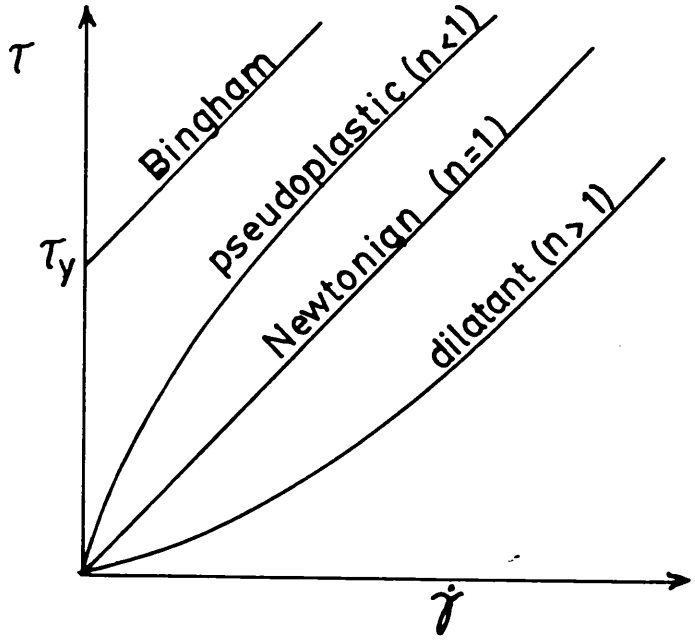

Figure 2.3.3 Flow curves of pseudoplastic, Newtonian, dilitant and Bingham fluids.

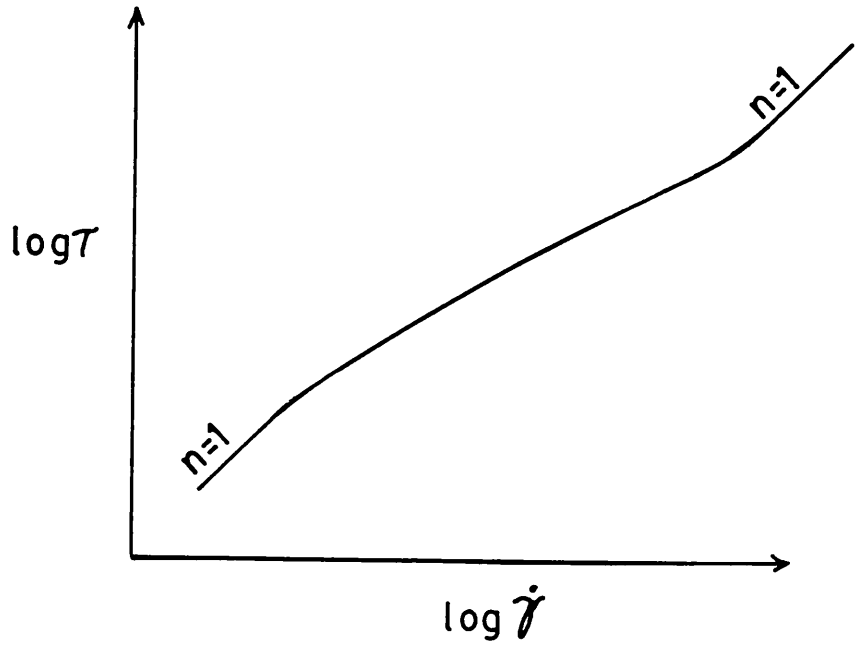

Figure 2.3.4 Logarithmic Flow curve for a polymer melt.

$$\tau = \mu_o \dot{\gamma} \left| \frac{\dot{\gamma}}{\dot{\gamma}_o} \right|^{n-1} \exp(-b_o(T-T_o)) \qquad 2.3.6$$

where b_o is a temperature coefficient determined from curves obtained over a range of temperature and T_o is the reference temperature of the apparent viscosity μ_o. This equation is usually limited in application to narrow range of shear rates. If temperature dependence over a wider range is needed to be incorporated more complex expressions with more terms are required. In addition high pressure can increase the viscosity of polymer melts. It appears that this effect in polymers may be reduced with increasing shear rate and temperature.[1]

To include the effects of temperature and pressure requires a more complicated analysis. In this case, additional coefficients have to be determined from "regression analysis" using a digital computer whereas the power law equation can be fitted to the polymer flow curves directly from graphical data. In addition, the use of the empirical models which overcome the difficulty of the power law model at the very low shear rates (Ellis model) or at the very low and high shear rate ranges (Reiner-Phillipoff and Powell-Eyring models) are more complicated to use than the power law model and usually do not offer any compensating advantages.[1]

Viscosity data for polymer melts under conditions relevant to extrusion processes is usually obtained using a capillary Rheometer.[31] Melt maintained at a uniform temperature is forced from a resevoir through a capillary tube by means of a piston,driven usually at constant speed. The volumetric flow rate and the resevoir pressure are measured and the shear rate and shear stress at the wall determined from the dimensions of the capillary die. To obtain reliable results, allowances must be made for variable resevoir pressure drop, capillary end effects (Bagley correction[32]) and Rabinowitsch shear rate correction.[33]

The density of polymer melts depends on temperature and pressure and variations can be determined with a capillary rheometer. Under extrusion conditions the variations are usually small and it is reasonable to assume the density is constant.[1,31] Thermal conductivity and specific heat are also functions of temperature and pressure but variation appears to be small under extrusion conditions and they are usually assumed to be constant.

2.4 Constitutive Equation for Polymer melts.

The general relationship between stress and deformation in fluid flow is the constitutive equation for the material. Constitutive equations relate the stress tensor to the rate of deformation tensor and also to the deformation tensor for elastic fluids. The stress tensor is a measure of forces that act between neighbouring elements in a fluid and has components of the form τ_{ij} where i and j can take values from 1 to 3 and define directions in a general coordinate system, i being the direction of the stress components and j the direction of the normal to the plane on which it acts. In cartesian coordinates the suffices become x, y and z and in cylindrical polar coordinates they become r, θ and z . The stress tensor is symmetrical i.e. $\tau_{ij} = \tau_{ji}$. The stress τ_{ii} act normal to the surfaces and are called the normal stresses and the stresses τ_{ij} $(i \neq j)$ are called shearing stresses. The linear relationship between shear stress and shear rate for an incompressible Newtonian fluid, equation 2.3.1, is a special case of the general constitutive equation and applies only to unidirectional shear. The six components of the general constitutive equation for a Newtonian fluid is given in Appendix IV, omitting the volume viscosity which is assumed to be negligible.[1]

For a non-Newtonian fluid, it has been shown that a general constitutive equation can be derived in which stress tensor is related to rate of deformation tensor by viscosity and cross viscosity which depends also on temperature and pressure.[30] The material properties η are, therefore, scalar quantities and are functions of the three principal invariants of the rate of deformation tensor (given in Appendix VII),

$$\eta = \eta(I_1, I_2, I_3, T, p) \qquad 2.4.1$$

Assuming polymer melt flow to be incompressible, $I_1 = 0$ and neglecting the dependence of pressure, the viscosities simplify to,

$$\eta = \eta(I_2, I_3, T) \qquad 2.4.2$$

To obtain a suitable empirical constitutive equation for polymer melts, the viscosities are correlated as far as possible with the viscosity data obtained from capillary rheometer measurements. In capillary flow, i.e. axial flow in a tube - Couette flow, $I_3=0$ but in many complex flow situations, as for example, axisymmetrical flow in a channel of varying diameter, I_3 varies and only because the dependence of η on I_3 cannot yet be determined experimentally, it is commonly assumed that,[1,41]

$$\eta = \eta(I_2,T) \qquad 2.4.3$$

In cylindrical polar coordinates,

$$I_2 = \frac{1}{2}\left[\left(\frac{\partial v_r}{\partial r}\right)^2 + \left(\frac{1}{r}\frac{\partial v_\theta}{\partial \theta} + \frac{v_r}{r}\right)^2 + \left(\frac{\partial v_z}{\partial z}\right)^2\right] + \frac{1}{4}\left[r\frac{\partial}{\partial r}\left(\frac{v_\theta}{r}\right) + \frac{1}{r}\frac{\partial v_r}{\partial \theta}\right]^2$$
$$+ \frac{1}{4}\left[\frac{1}{r}\frac{\partial v_z}{\partial \theta} + \frac{\partial v_\theta}{\partial z}\right]^2 + \frac{1}{4}\left[\frac{\partial v_r}{\partial z} + \frac{\partial v_z}{\partial r}\right]^2 \qquad 2.4.4$$

In capillary flow the simple one-dimensional shear rate measured at the wall reduces to $I_2 = \frac{1}{4}\left(\frac{\partial v_z}{\partial r}\right)^2 = \frac{1}{4}\dot{\gamma}^2$. The power law form of the constitutive equation for the material which is found to be applicable to many non-Newtonian fluids, particularly for many polymer melts is,[1,30]

$$\mu = \mu_0 \left|\frac{\sqrt{4I_2}}{\dot{\gamma}_0}\right|^{n-1} \exp\left(-b_0(T-T_0)\right) \qquad 2.4.5$$

2.5 Mathematical models for flow in channels.

Shear deformation of a fluid between infinitely parallel plates is the simplest channel flow that can be analysed. By assuming the fluid is Newtonian, flow rate and pressure expressions can normally be obtained for many flow situations. The momentum equation (or force balance of a fluid element) of one dimensional flow between infinitely wide parallel plate, Figure 2.3.1 reduces to,

$$\frac{dp}{dz} = \frac{\partial \tau_{zy}}{\partial y} \qquad 2.5.1$$

For a Newtonian, isothermal fluid this equation becomes,

$$\frac{dp}{dz} = \mu \frac{\partial^2 v_z}{\partial y^2} \qquad 2.5.2$$

This equation integrated and the constants of integration obtained for the boundary conditions given in Figure 2.3.1, of $v(0) = 0$ and $v(h) = V_z$, the velocity is,

$$v_z = V_z \frac{y}{h} + \frac{y^2 - hy}{2\mu} \frac{dp}{dz} \qquad 2.5.3$$

where μ is the Newtonian viscosity and $\frac{dp}{dz}$ is the pressure gradient.

The flow rate through the cross section becomes,

$$Q_z = V_z \frac{wh}{2} - \frac{wh^3}{12\mu} \frac{dp}{dz} \qquad 2.5.4$$

This equation is the simple addition of two terms, namely drag and pressure flows respectively (Figure 2.5.1). For two dimensional flow (or flow between parallel plates of finite width) the fluid is also sheared in the perpendicular direction because of the influence of the sides and

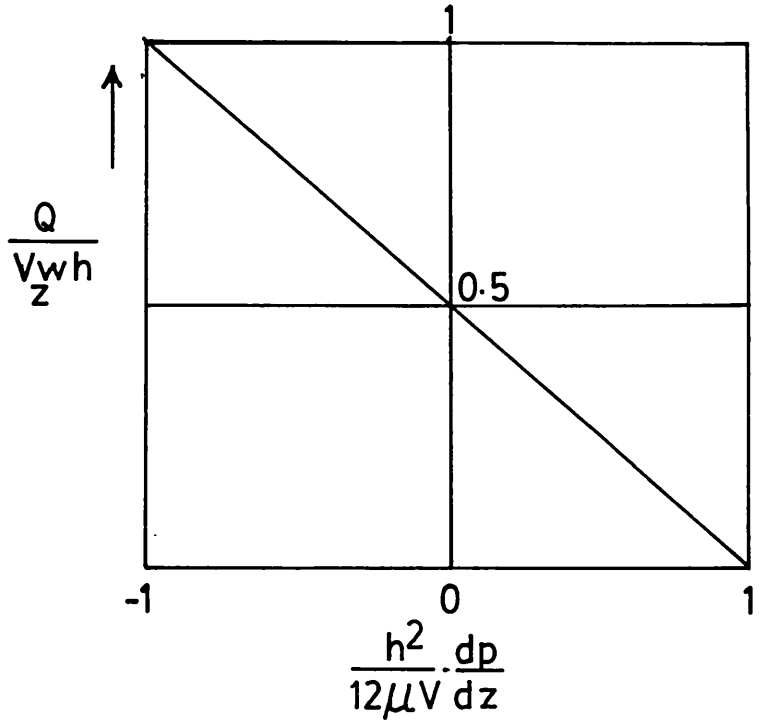

Figure 2·5·1 Dimensionless flow rate as a function of pressure gradient.

equation 2.5.2 is replaced by:

$$\frac{dp}{dz} = \mu\left(\frac{\partial^2 v_z}{\partial x^2} + \frac{\partial^2 v_z}{\partial y^2}\right) \qquad 2.5.5$$

This differential equation has been solved for a rectangular channel to give the flow rate equation,[45]

$$Q_z = \frac{V_z w h}{2} f_d - \frac{w h^3}{12\mu} \frac{dp}{dz} f_p \qquad 2.5.6$$

where f_d and f_p are 'shape factors' for the drag and pressure flow respectively. These factors are functions of the depth to width ratio (h/w) of the rectangular passage between the plates and are smaller than unity for flows other than between infinitely wide plates. For a h/w ratio which is very small f_d and f_p are approximately equal to unity; this is normally the case for the relatively shallow and wide channels in the metering section of single screw extruders and the equation becomes identical to equation 2.5.4.

Equation 2.5.4 can be written in terms of dimensionless flow($Q/V_z wh$) and pressure gradient $\frac{h^2}{12\mu V_z} \cdot \frac{dp}{dz}$ as follows,

$$\frac{Q}{V_z wh} = \frac{1}{2} - \frac{h^2}{12\mu V_z} \frac{dp}{dz} \qquad 2.5.7$$

The graphical representation of this equation is shown in Figure 2.5.1. It is seen that the flow rate and consequently the velocity profile are dependent on the magnitude of $\frac{dp}{dz}$. The different forms of velocity profiles are given in Figure 2.5.2.

For a pressure gradient of zero, the dimensionless flow rate is equal to 0.5, which is identical to the case of pure drag flow given in Figure 2.3.1. For a positive pressure gradient, two extreme cases can exist (a) predominantly drag flow and (b) predominantly pressure flow with dimensionless flow rate less than 0.5. For a negative pressure gradient two cases

of predominantly drag (c) and predominantly pressure(d) flow exist, with the dimensionless flow rate limited to the range $0.5 \leq \frac{Q}{V_z wh} < 1$. It is important to note, also, that the dimensionless flow rate per unit width is equivalent to the total area under the V_z versus h curve.

Both pressure and drag flow can exist if there is a restriction of the flow between the surfaces. In this case, a pressure is built up in the direction of motion and a positive pressure gradient is produced by, for instance, a gradual decreasing clearance depth between the surfaces, a steady state condition is normally reached in which case the flow remains constant along the tapered clearance (of infinite width). In other words the area enclosed by each velocity profile along the clearance should be the same. To satisfy this condition in a channel with gradually decreasing depth, different velocity profiles must exist. This situation is shown in Figure 2.5.3 in which a positive pressure gradient exists at the larger clearances due to the kind of velocity profile satisfying the flow condition in this region, until the pressure gradient becomes zero where pure drag flow exists. This is the net flow of the clearance and is equal to $Q = V_z wh/2$ or dimensionless flow rate $Q/V_z wh = 0.5$. From then on, the pressure gradient is negative and the dimensionless flow rate becomes greater than 0.5 because of the further decrease of clearance depth. Therefore, for any tapered clearance in which hydrodynamic pressures are developed, there will be a pure drag (or net) flow at a particular clearance depth which is dependent on the geometry of the clearance. Furthermore, the flow equation for a Newtonian fluid, equation 2.5.4, completely describes the flow rate existing anywhere along the clearance and therefore, the actual velocity profiles produced are unimportant because they do not affect viscosities.

In practice, isothermal conditions rarely exist in Newtonian fluid flow especially for cases of very high shearing of the fluid and viscosity decreases with increase in temperature. This can complicate

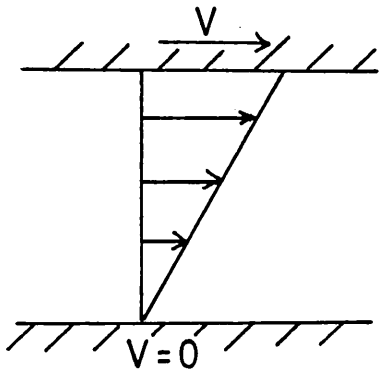

(i) Drag flow.

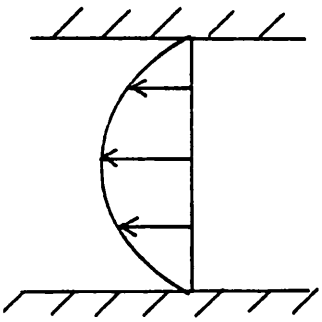

(ii) Pressure flow.

Positive Pressure Gradient.

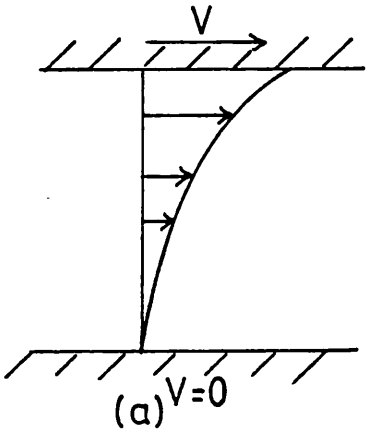

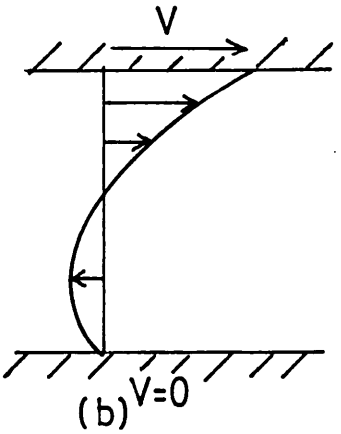

Negative pressure gradient.

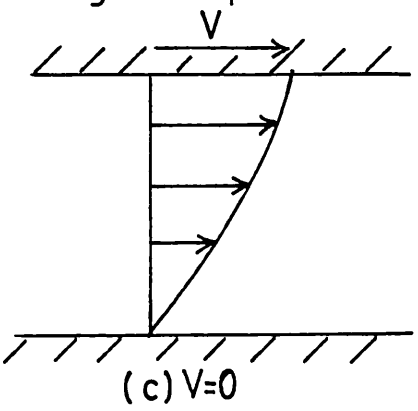

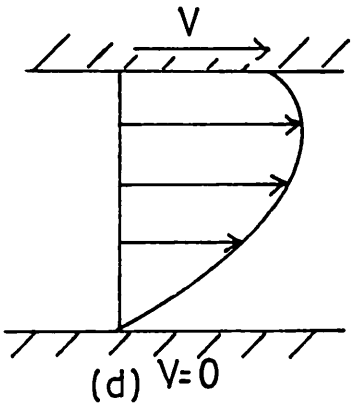

Predominantly Drag Flow. Predominantly Pressure Flow.

(iii) Pressure and Drag flows combined.

Figure 2.5.2. Velocity Profiles for different flow conditions.

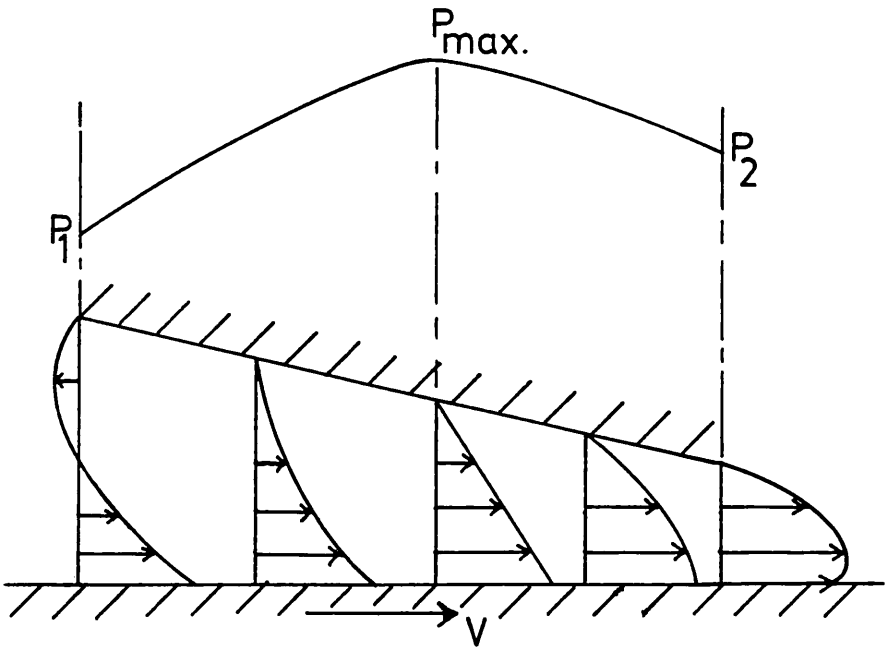

Figure 2.5.3. Typical Velocity Profiles in a tapered clearance.

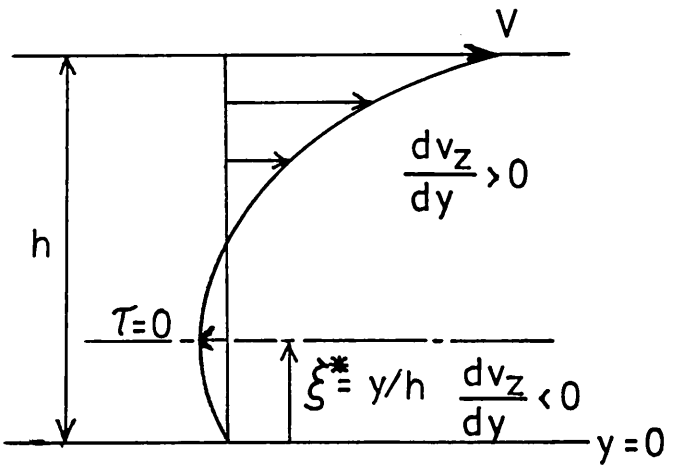

Figure 2.5.4. Coordinate system for predominantly pressure flow by Krosser & Middleman(37).

the analysis of Newtonian flow but this problem is sometimes tackled by assuming an effective viscosity determined at the mean temperature of the flow passage. Various approximate methods have been used from which a mean viscosity can be determined.[28]

Newtonian fluid analysis can be used for flow of slightly non-Newtonian melts in which the shear stress dependence on shear rate is small. Mc Kelvey[23] used the simple theory to predict flow of polymer melts in a screw channel. He concluded that the theory can accurately predict extruder behaviour for isothermal flow of mildly non-Newtonian fluids. However, the correct viscosity has to be calculated using flow rates from actual extrusion experiments. It has been found that an apparent viscosity at the volume average shear rate or at the drag flow shear rate (V/h) will give reasonable results.[1]

Weeks and Allen[34] developed a better method for determining apparent viscosities based on the simple and power law fluid theory. They used the theories to determine an equivalent Non-Newtonian melt viscosity which when used with the Newtonian flow equations would produce the pressure gradients of the melt flow for a given flow rate. They predicted results within 25% of measured flow rates for a single screw extruder using this method for highly non-Newtonian melts.

Large errors can be obtained if the Newtonian equation is used to predict flow of pseudoplastic fluids as shown in Figure 2.5.5. Jacobi[35] assumed the error would not be significant using the super-position principle, for a modified pressure flow based on the power law model added to the drag flow. Glyde and Holmes-Walker[36] and later Krosser and Middleman[37] showed that the error is significant and for the case of a positive pressure gradient, showed that the flow can be considerably overestimated using this method. For the case of a negative pressure gradient, which can also be generated in a single screw extruder, the flow calculated by super-position can be underestimated. The reason is that the velocity profile obtained

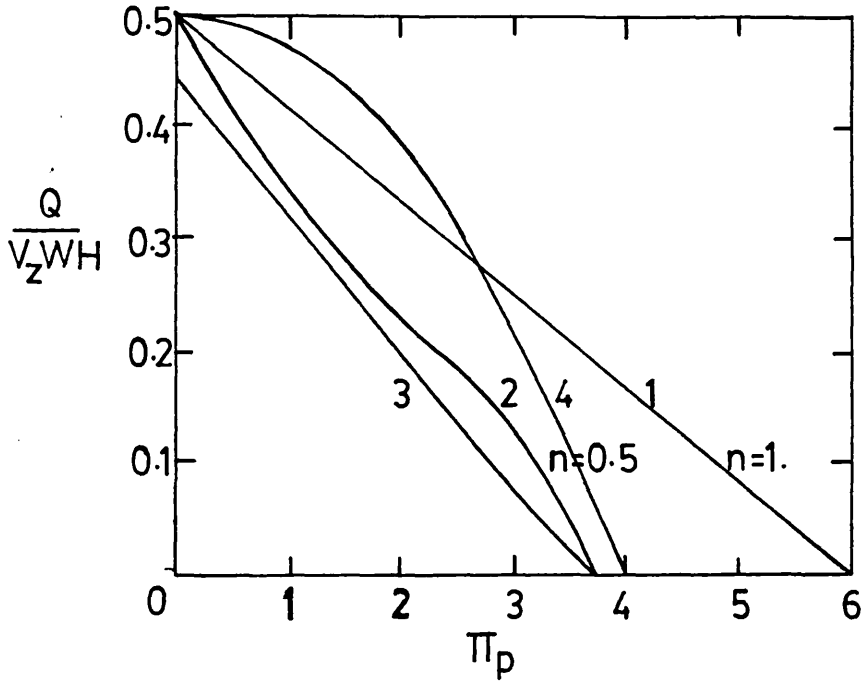

Figure 2.5.5. Reduced Flow Rate as a function of Dimensionless Pressure Gradient: Newtonian case
(1) Superposition of pressure and drag flow.
(2) Combined pressure and drag flow. ref(37).
(3) Combined flow with a cross-channel velocity. ref (39).
(4) Superposition of drag flow and pressure flow of a power law fluid. (ref.35).

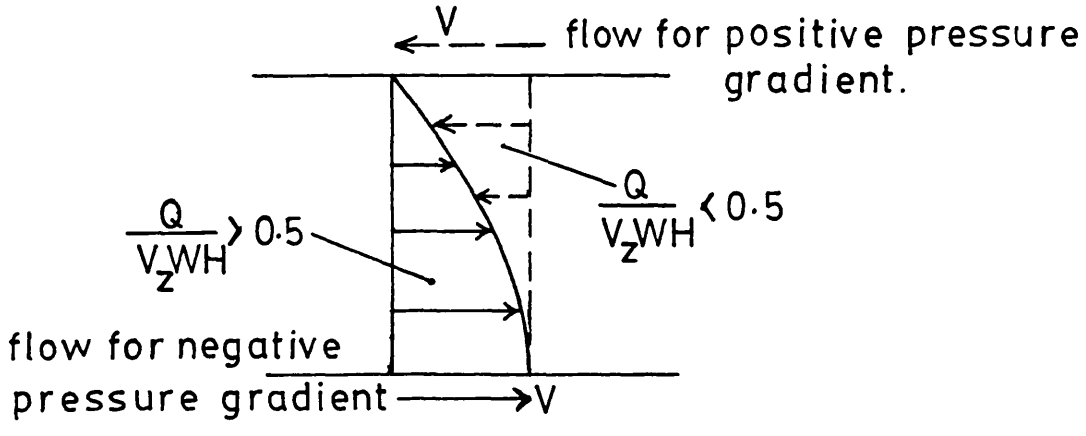

Figure 2.5.6. Method of determining the flow rate for a Negative pressure gradient.

with superimposing the shear rate profile of a drag and pressure flow is different from the shear rate profile of a "combined" pressure and drag flow because of the shear rate dependence of viscosity.

The analysis with a non-Newtonian fluid is done in a similar manner to that with a Newtonian fluid except that the rheological equation is different. In this case, the momentum equation for one-dimensional isothermal flow between infinitely parallel plates becomes,

$$\frac{dp}{dz} = \mu_o \, d\left|\frac{dv_z}{dy}\right|^n = \mu_o \frac{d}{dy}\left|\dot{\gamma}\right|^n \qquad 2.5.8$$

in which the shear rate can be either positive or negative. It is possible therefore to obtain only individual solutions for positive and negative shear rates and there is no single equation which describes pseudoplastic fluid flow for all flow conditions in a tapered clearance.

For predominantly pressure flow in which separate regions of positive-negative shear rates exist, solutions have been obtained using various coordinate systems to define this type of velocity profile.[36,38] The simplest and least complicated to use was given by Krosser and Middleman.[37] They used a dimensionless coordinate ξ which defined the position of zero shear stress/shear rate from the stationary surface, Figure 2.5.4. This point of zero shear stress also divides the shear rate profile into two regions of positive and negative values. The flow rate equation was obtained by summing the individual solutions determined for each region. The one-dimensional flow equations are given in Appendix V. Their solutions predicted a reduction in the flow rate with increase in pressure gradient for values of flow index $n < 1$, as compared with Newtonian results. This is illustrated in Figure 2.5.5 for $n = 0.5$. Griffith[39] showed that a further reduction of the flow can occur with a zero net transverse flow (or circula-

tory flow in a screw channel). He used a lengthy trial and error method on a digital computer to solve the simultaneous differential equations obtained for flow in each direction and confirmed his results by experiments on a screw extruder with actual polymer melts. The effect of the transverse flow on viscosity is to reduce the down channel flow rate even at pure drag flow conditions.

Using the coordinate system by Krosser and Middleman[37], it appears that a flow rate expression cannot be obtained for a negative pressure gradient because of the negative sign of the pressure gradient. However, Weeks and Allen[34] obtained a flow rate equation for a negative pressure gradient using a different coordinate system. On examining their equations, it was found that the dimensionless flow rate for a negative pressure gradient is equal to one minus the dimensionless flow rate for a positive pressure gradient. It appears that the dependence of viscosity on shear rate (for isothermal flow conditions) is no different for a flow either with a positive or a negative pressure gradient. All these power law flow equations were found to converge to the Newtonian solutions for a flow under n = 1.

In the polymer processing field, the power law constitutive equation is used to describe flow of polymer melts. The complex flow in screw extruders has been satisfactorily predicted using this fluid model.[1,30,40] Logarithm
Flow curves of polymer melts are known to be quite linear over the range of shear rates normally encountered in polymer processing i.e. in the range from about 6 $sec.^{-1}$ up to 200 $sec.^{-1}$ There is a danger of underestimating flow rates, however, if the melt is described over the very low range of shear rates by the power law equation. This error resides in the difference between the predicted and the true velocity profiles. A velocity profile contains a wide range of shear rates with a proportion of very low shear rates i.e. Newtonian behaviour can exist. This is particularly significant in the case of "pressure flow" between two parallel plates,

Figure 2.5.7. The power law equation can describe the fluid only over a limited range of shear rates. The magnitude of the error introduced by comparing the power law fluid and the measured flow can be less than 5% if the proportion affected by the Newtonian behaviour is 50% of the total area of flow.[1,41] If the affected area is large, the error can be as high as 50 - 100%. This may be the case also for regions of very high shear rates and therefore, the position of the flow curve in the high range of shear rates will become more important. This kind of effect would be important when considering pressure flow of melts in narrow channels, as in dies.[42,43,44]

There are rheological factors which may affect the flow rate and pressures developed in leakage clearances. Polymer melts are elastic as well as viscous and thus, have the ability to store and recover shear energy. The visco-elastic properties of polymer melts are less important in single-screw extruders because the fluid flow is contained in a closed channel bounded by the flights, screw root and barrel wall,[1] and therefore, the elastic effects are not likely to affect the flow. In twin-screw extruders, in which there are likely to be sudden changes of shear rates from the chamber through the leakage gaps into the other chamber, visco-elastic effects are likely to be significant and therefore the flow resistance of gaps will increase. On the other hand, increase of shear rates in small gaps is likely to reduce the viscosity and the resistance to flow, and it has been suggested[5] that the shear dependency and visco-elasticity in twin-screw extruders act in opposite directions and the net effect may be small.

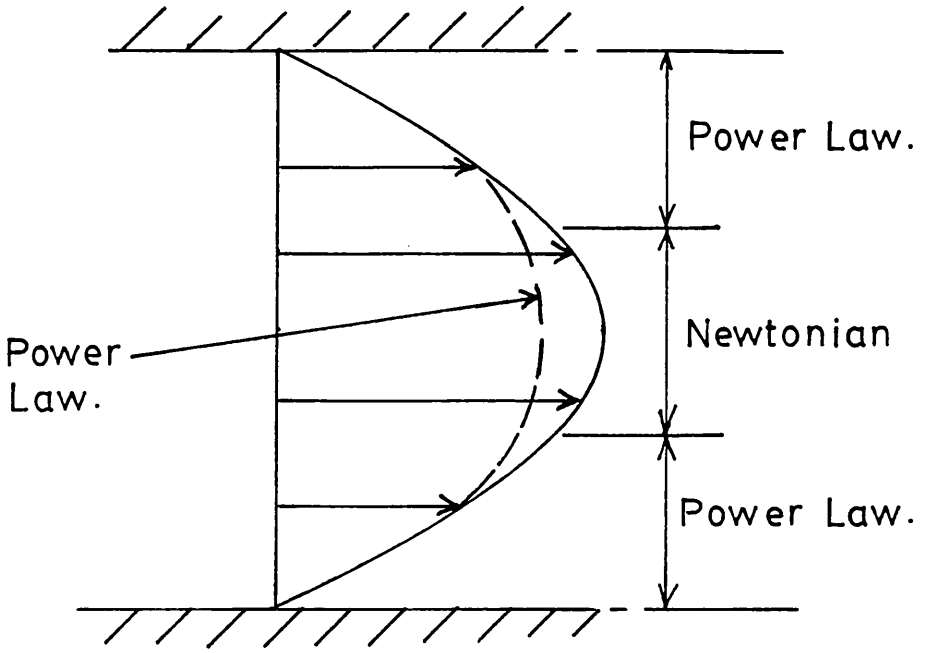

Figure 2.5.7. Error introduced by using the Power Law Model for pressure flow between parallel plates.

2.6 Flow in Deep Channels.

The flow in an extruder may be considered to occur in a straight rectangular channel if the channel is shallow[+]. The metering zone of a typical single-screw extruder usually satisfies this requirement without introducing significant error[1]. The channels in the metering zone of typical twin-screw extruders are never shallow[5] and significant errors can, therefore, be introduced by simply neglecting the effect of curvature.

The effect of curvature may be visualised by comparing the velocity profile of fluids between two infinite parallel plates (plain rectangular flow) with that between two infinite concentric cylinders (cylindrical flow), with the outer cylinder rotating at the same speed as in the rectangular flow situation and the inner cylinder stationary. The velocity profile is now nonlinear and leads to an increase of flow rate for Newtonian flow of 8% and of 20% for a non-Newtonian power law fluid with n = 0.5 for a ratio of outer to inner radius of 2[1].

An analysis of isothermal Newtonian fluids in deep curved channels was carried out by Booy[45] in which the effects of helix angle and its variation with radius was also included. The barrel was assumed to rotate about a stationary screw with helical flights and cylinder polar coordinates were used. From the flow model, correction factors for pressure, F_{pc}, and drag, F_{dc}, components of flow were obtained as functions of curvature (or relative channel depth, H/D) and helix angle β; the channel width and helical length at the barrel surface are used for comparison i.e. conditions used to determine flow in the parallel plate model. For example, the results show that there is an increase of the correction factors from unity (parallel plate flow) with increasing relative channel depth and decreasing helix angle for $\beta \leqslant 20^{\circ}$. The net effect due to the presence of the typical square-pitch helix angle is to reduce the parallel plate flow of drag and back pressure, with a further reduction produced for smaller helix angles. However the parallel

[+]means a channel width to depth ratio of at least 10.

plate flow at unity does not account for the changed flow due to curvature which occurs between concentric cylindrical surfaces. This was taken into account by McKelvey[23] for pure drag flow of a power law model using a curvature correction factor based on the ratio of flow rate between infinitely long concentric and parallel plates. This special case represents the tangential flow in a channel with zero helix angle and infinite aspect ratio and was solved for isothermal non-Newtonian drag and pressure flow by Tadmor.[41] The analysis produced correction factors for the error introduced by superimposing drag and pressure flows for non-Newtonian fluids and a curvature correction factor for pressure flow.

Besides curvature, the effect due to the flights in deep channels is also likely to be significant (i.e. when H/W is significantly greater than zero). The problem of isothermal downstream plain flow in a deep channel (i.e. neglecting transverse flow) has been solved for Newtonian[23] and power law fluids,[30,46,47] and in general the flight wall is seen to have the effect of reducing the drag flow rate as H/W increases. There have been attempts, however, to solve the complete problem of fully developed non-isothermal non-Newtonian flow in deep channels. Dyer[48] assumed axially symmetric geometry (zero helix angle) and used cylindrical polar coordinates to account for curvature due to channel depth. Martin[24] used cartesian rectangular coordinates and produced solutions for plain flow in deep channels. There appears to be a significant net effect on the downstream flow rate in relatively deep channels when the transverse flow, curvature and temperature variations are all included. The problem of isothermal non-Newtonian flow in deep channels including also curvature effects due to helix angle has been solved using a helical coordinate geometry.[49,50] The effects of curvature for this case shows a smaller reduction of the throughput than is predicted using Booy[45] correction method.

The validity of the assumption that the flow is isothermal depends on operating conditions and screw geometry. Non-isothermal effects may be introduced if excessive heat is generated by viscous dissipation or by simple heat transfer through the channel boundaries. In general at low screw speed and not very shallow channels, the heat generation will not be significant, and normally heat transfer through the barrel will not introduce significant non-isothermal effects, if the melt conveying zone is long enough and the barrel temperature is kept at a constant level.[1] The factors relevant to heat generation and heat transfer in polymer melt flow processes have been discussed by many workers[24,51,52,53] and attention is drawn to the physical and operating approximations that arises in a mathematical formulation of flow problems. The equations which govern problems are the conservation equations plus the appropiate rheological equation of state for the melt and the relevant boundary conditions. In order to make the solution obtained to have a wider applicability it is usual therefore to make the equations dimensionless.[24,53] To obtain simple solutions it is usually common to treat properties of density, thermal conductivity and specific heat as constant. There are many dimensionless ratios which become important. For example, the Péclet number which represents the ratio between convective heat transfer and conductive heat transfer is usually very large ($P_e \gg 1$) due to the extremely small thermal conductivity of polymers, i.e. $Pe = \rho c V h^2/k$, where ρ is the density, c is the specific heat, V is the velocity, k is the thermal conductivity, h is usually a small dimension measured perpendicular to the flow lines.

In general, temperature distributions are strongly dependent on the aspect ratio of the channel, and the value of such a dimensionless quantity indicates how important convective and conductive heat transfer is on the flow field in the channel.[24]

Therefore, by combining the physical variables to form dimensionless parameters, dimensional analysis can be used to generalise solutions to the energy equation and behaviour is then characterised in terms of the parameters.

The energy conservation equation for the flow can be generalised in terms of dimensionless variables[24,31,53] and the dimensionless parameters, besides Péclet number (which has been already defined above), the Nahme/ Griffith number, G and the Graetz number, G_z for the flow are,

$$G = \frac{b_o \bar{\tau} \bar{\dot{\gamma}} h^2}{k} \qquad 2.6.1$$

$$G_z = \frac{\rho c V h^2}{k l} \qquad 2.6.2$$

where b_o is the temperature coefficient of viscosity introduced in equation 2.3.6, $\bar{\tau}$ and $\bar{\dot{\gamma}}$ are mean shear stress and shear rate respectively and l is a length measured along flow lines. In the dimensionless energy equation, the thermal convection and viscous dissipation terms include the parameters P_e or G_z and G respectively, while the thermal conduction term remains unscaled. Hence, P_e and G_z are measures of thermal convection, and G is a measure of heat generation, all relative in importance to thermal conduction. An additional thermal parameter, Brinkman number, B_r enters the temperature analysis via the boundary conditions and determines the relative importance of viscous dissipation and imposed differences in boundary temperature in bring about temperature changes in the flow,

$$B_r = \frac{\bar{\tau} \bar{\dot{\gamma}} h^2}{k(T_b - T_o)} \qquad 2.6.3$$

where T_b is the set operating temperature boundary condition and T_o is an inlet or reference temperature of the fluid. It should be noted that Martin[24] and Pearson[67] defined a Brinkman number similar in form to what is now commonly called the Griffith number, equation 2.6.1, and only where reference is made to their work (in subsequent chapters), would the number

be referred to as the Brinkman number.

Péclet number in melt flows is usually very large, typically of the order of 10^3 - 10^5, implying that thermal convection is an important mode of heat transfer. The Graetz number is a measure of the importance of thermal convection in the direction of flow relative to conduction normal to the flow and, although is often large in some melt flows, it may be of order of unity or less. Hence, G_z can vary from 10^{-1} to 10^4. The Griffith number, besides quantifying the ratio between heat generation and thermal conduction, also determines whether heat generation will lead to temperature differences within the melt sufficient to affect the velocity distribution locally. G varies in practice from 0 to 200. For G=0, there is no coupling between energy and equilibrum equations and the flow is isothermal.

For the purpose of analysis, these heat transfer parameters can be used to distinguish between different flow situations.[31,53] For example, if both G and $G/B_r < 1$, then the temperature variations due to heat generation and boundary conditions respectively do not greatly affect velocity profiles and the flow may be treated as isothermal.

If $G_z < 1$ (irrespective of the value of G), then heat transfer is dominated by thermal conduction to and from the boundaries i.e. the flow is thermally fully developed and the temperature profile does not change in the direction of flow.

If $G_z \approx 1$, then both thermal convection and conduction are important and temperature profiles should be treated as developing (and so should the velocity profiles if $G>1$).

If $G_z \gg 1$, then thermal convection is dominant but conduction must still take place. Temperature profiles develop very slowly in the direction of flow. This causes slight changes in the velocity profiles but it is reasonable to assume locally fully developed velocities.

It is evident that when analysing the effects temperature has on

flow both the Griffith and the Graetz numbers must be examined. It is important to note also, that in single-screw extruder channels, the convective effects caused by the overturning of the flow at the flight walls would strongly influence temperature distribution in the downchannel direction.[53] From theoretical results of fully developed two-dimensional channel flow analysis of a single-screw extruder, it has been concluded that when both heat generation and convection are included, the flow rate was found to be closer to the isothermal case than when convection is ignored.[24] It was suggested that this behaviour may be attributed to the effect that convection has towards keeping the screw temperature down, thus preventing hot-low viscosity layer of melt forming on the surface.

Chapter 3

Theoretical Analysis

3.0 Introduction.

The purpose of a theoretical model for melt conveying in a plasticating counter-rotating twin-screw extruder is the prediction of flow rate, pressure, temperature and velocity distributions and the dependence of these parameters on the nature of the polymer, the geometry of the screws and the operating conditions. From these predictions additional information relevant to extruder design and operation can be supplied, for instance, the number of completely-filled chambers in the metering zone[5], the power input required for this zone, and the shear rate history and the residence time distribution of the polymer melt leaving the extruder, which may have a decisive influence on product quality.[1]

In any theoretical flow analysis, the choice of mathematical model is determined by the geometry of the channel and the boundary conditions. Usually, the complexity of the solution depends on the coordinate system used and the differential equations to be solved. Making appropriate assumptions can simplify the equations and reduce the effort involved in obtaining solutions without losing sight of the actual problem. Very often, complex problems can only be approximately solved by adopting simplifying assumptions. Trying to solve such a problem, can sometimes result in the loss of the benefit that is to be gained from the use of a theoretical approach. Although the analysis must be as realistic as possible, it must not be allowed to develop into a theoretical procedure which is as expensive or even more uneconomical to use than the practical methods it replaces. The approach used here,

therefore, is to find simple and efficient methods of simulating the flow processes, while still retaining as much as possible aspects of behaviour which are most likely to be significant.

For polymer processing problems, the main considerations appear to be the effects due to the non-Newtonian nature of the melt and geometric aspects, like curvature etc., which for twin-screw extruders cannot be neglected. The effect of pseudoplastic behaviour appears to indicate that, in order to obtain proper simulation of the conveying process, all flows should be coupled, especially the leakages in the intermeshing region between the screws where the gaps are interrelated. However, because of the complex flow behaviour in the intermeshing region plus the simple lack of or limitations of the theoretical methods available for solving such a problem, a simple approach is adopted. This is essentially to analyse each channel or gap separately and then to connect the flows by matching the variables accordingly to predict the overall performance. The theoretical treatment of the melt conveying process described in this chapter can be used to obtain solutions, with a reasonable amount of effort, only by using a high speed digital computer.

3.1 Screw geometry.

The twin screw extruder consists essentially of two intermeshing screws rotating next to each other in a figure-of-eight section barrel. In a counter-rotating extruder, rotation of screws is such that the surfaces converge below and diverge above the intermeshing region. Figure 3.1.1a and 3.1.1b show the typical arrangement of counter-rotating intermeshing screws. Viewing the extruder from the direction of the hopper to the die, Figure 3.1.1a, the screw on the right has a left hand thread and rotates clockwise while the screw on left has a right hand thread and an anticlockwise rotation. This choice of rotation allows a high degree of filling of each chamber to occur from a hopper feed.

Figure 3.1.1b gives a top-sectional view of intermeshing screws defining the geometry. R is the outer radius of each screw (D is the diameter) ; H is the channel depth, the distance between the root of the screw and the tip of the flight; δ_f is the radial clearance between the barrel and flight tip; S is the flight pitch, the axial distance of one full turn; β is the helix angle of the flight and is related to the pitch and diameter by $\tan^{-1}(S/\pi d)$; B is the width of the flight tip measured axially. The number of channels in one full turn (or number of starts) of each screw is m (a double start screw, m= 2, is shown in Figure 3.1.1b). The rotational speed of each screw is N revolutions per unit time and the direction of rotation produces a foward motion of the flights and consequently the chambers , from right to left.

Figure 3.1.2 shows an axial cross- section of the middle of the intermeshing region taken perpendicular to the plane through the axis of the screws. The axial cross-section of the screw channel is of trapezoidal form, that is, a screw with constant depth across the channel and with uniformily inclined flight walls with flank angle, ψ'. The calender gap is σ, the minimum distance between the screw root of one screw and

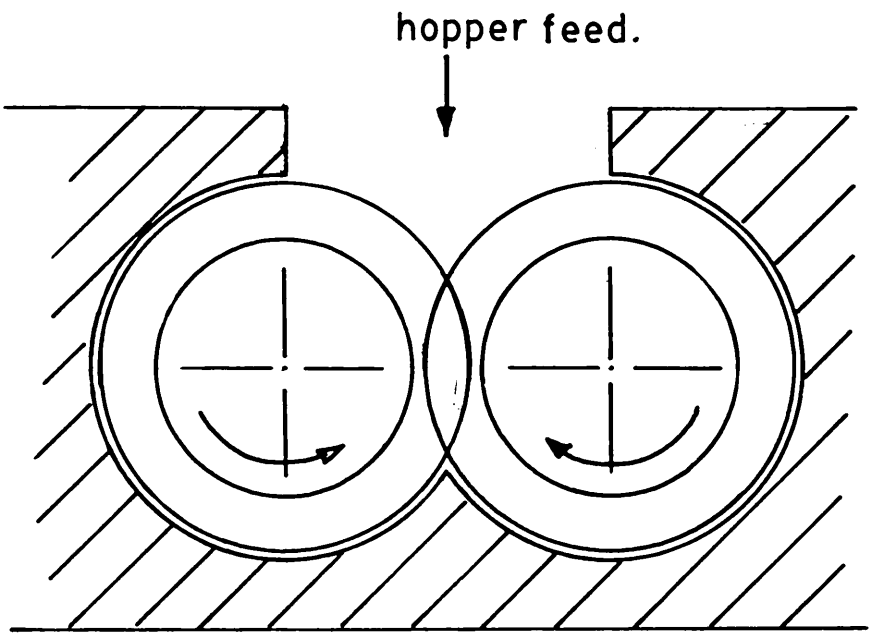

(a)

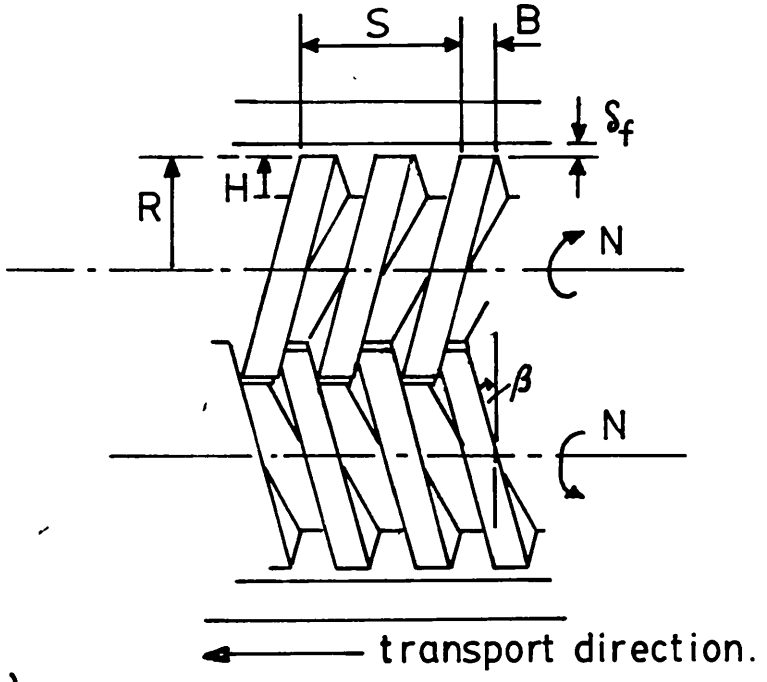

(b)

Figure 3.1.1 Geometry.

the flight tip of the other; ε is the side gap, the minimum axial distance between the flanks of adjacent flights and is given by,

$$\varepsilon = \frac{S}{2m} - B - H \tan\psi' \qquad 3.1.1$$

The total minimum axial distance between adajacent flanks of the flights is influenced by the side gap and the calender gap and is;

$$\epsilon = \varepsilon + \sigma \tan\psi' \qquad 3.1.2$$

C is the distance between barrel centres and for centrally positioned screws, the minimum calender gap is calculated from,

$$\sigma = C - (2R - H) \qquad 3.1.3$$

The depth of the calender passage measured perpendicular to the root of one screw can be calculated from the general expression, (see Figure 3.6.1)

$$H_c = ((\sigma + 2R - H - \sqrt{R^2 - x^2})^2 + x^2)^{1/2} - R + H \qquad 3.1.4$$

where x is a coordinate distance measured from the line joining screw centres along the middle of the intermeshing zone. The maximum length of the intermeshing zone can be found from, (see Figure 3.5.1a)

$$L_i = 2 R \sin\alpha/2 \qquad 3.1.5$$

where α is the overlap angle. When there is no calender gap,

$$\alpha = 2 \tan^{-1}\left(\frac{\sqrt{RH - H^2/4}}{R - H/2} \right) \qquad 3.1.6$$

and with a calender gap, σ, the overlap angle is calculated by reducing the channel depth H to $H-\sigma$ in equation 3.1.6.

The axial distance between the flight flanks of any point in the intermeshing region can be determined from the formula derived by Janssen[5] from the summation of the distances due to: screw pitch, inclination of

the flight walls,and the clearance ϵ given by equation 3.1.2 . Using coordinates shown in Figure 3.1.3 the expression reduces to;

$$E = \frac{S}{2\pi}(\beta_l - \beta_r) + (r_r + r_l - 2R + H)\tan\psi' + \epsilon + \sigma\tan\psi' \qquad 3.1.7$$

where β_l, β_r refer to the angular coordinates and r_l, r_r refer to the radial coordinates of left and right screws respectively.

The volume of one C-shaped chamber formed by closely intermeshing screws can be found by elementary calculations[5] as,

$$\text{Vol.} = \frac{\text{Vol}_1 - \text{Vol}_2 - \text{Vol}_3}{m} \qquad 3.1.8$$

where; the volume of one barrel half over one pitch length is,

$$\text{Vol}_1 = S\left((\pi - \alpha/2)R^2 + (R - H/2)\sqrt{(R-H-H^2/4)}\right) \qquad 3.1.9$$

The volume of the core of the screw over one pitch length is,

$$\text{Vol}_2 = \pi S(R - H)^2 \qquad 3.1.10$$

and the volume of one screw flight with straight sides of width in the axial direction defined by, $b(r) = B + 2(R-r)\tan\psi'$ is,

$$\text{Vol}_3 = 2\pi\left((RH - H^2/2)B + (RH^2 - 2/3\,H^3)\tan\psi'\right) \qquad 3.1.11$$

where B is the width of the flight tip in the axial direction. By defining the flight width in the axial direction the effect of the pitch on the chamber volume is small and the error introduced was found to be in general less than one per cent of the chamber volume.[5] The effect of the presence of the calender gap on chamber volume is to increase the volume of one barrel half by a small amount. This can be accounted for in the expression Vol_1, equation 3.1.9, by substituting $H - \sigma$ for H and using the overlap angle α calculated with a calender gap (equation 3.1.6) .

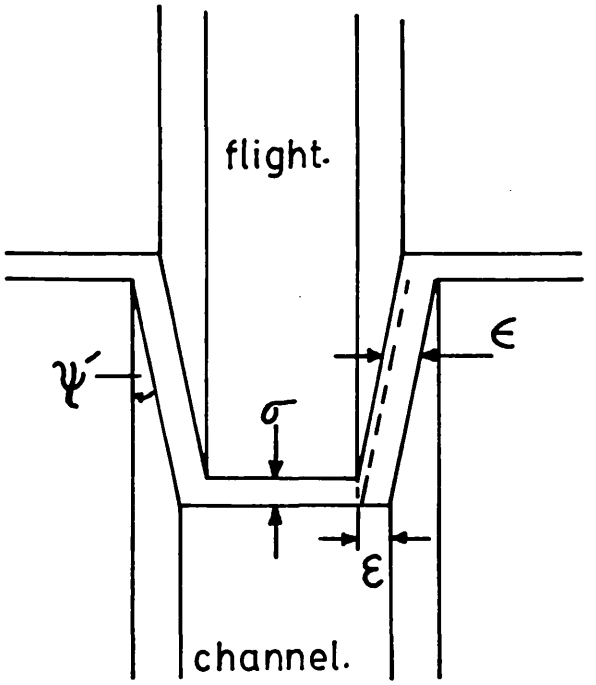

Figure 3.1.2 Geometry of gaps in the intermeshing region.

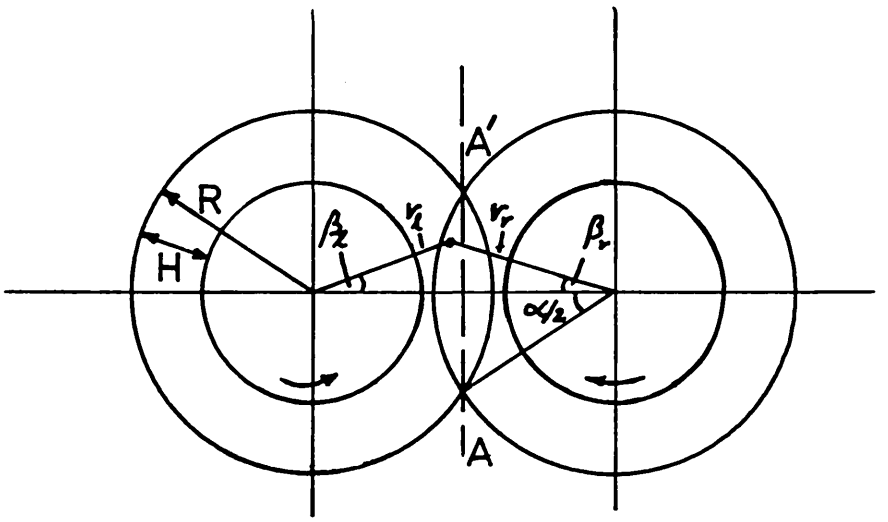

Figure 3.1.3 Geometry for determing the clearance between screw flanks.

3.2 The Governing differential equations of flow.

The differential equations governing flow of fluids are those of conservation of mass, momentum and energy, and they express fundamental laws of nature which are obeyed by all continuous materials. The equations are given in Appendices I,II and III and are expressed in both cartesian and cylindrical polar coordinates.[1] The choice of the particular coordinate system depends on the problem to be solved but generally the complexity of the solution depends on the system selected. Usually the choice of the coordinate system is dictated by the boundary conditions.

The conservation of mass principle states that, in a steady flow process, the net rate of flow of mass into any control volume is zero. For polymer flow, the melt is assumed to be incompressible and thus, for a constant density, the equation of continuity, equation A, Appendix I, in cartesian coordinates reduces to,

$$\frac{\partial v_x}{\partial x} + \frac{\partial v_y}{\partial y} + \frac{\partial v_z}{\partial z} = 0 \qquad 3.2.1$$

where v_x, v_y, and v_z are the velocities in the respective component directions x, y and z.

For conservation of momentum in a differential element of constant mass in a fluid, pressure, viscous and gravitional, inertia forces acting on the fluid element are balanced to give the differential equations of motion (or force balance) of the fluid element, equations A, B and C, Appendix II . It is further assumed that; the flow is steady, that is, independent of time; the flow is sufficiently slow (and laminar) so that centrifugal inertia forces (i.e. Reynold's number for the flow is small); and body forces due to gravity are likewise negligible compared with the other forces, then the equations of motion in Cartesian coordinates and in terms of the viscous shear stress components and local pressure

gradients reduce to ;

$$-\frac{\partial p}{\partial z} = \frac{\partial \tau_{xz}}{\partial x} + \frac{\partial \tau_{yz}}{\partial y} + \frac{\partial \tau_{zz}}{\partial z} \qquad 3.2.2$$

$$-\frac{\partial p}{\partial x} = \frac{\partial \tau_{xx}}{\partial x} + \frac{\partial \tau_{yx}}{\partial y} + \frac{\partial \tau_{zx}}{\partial z} \qquad 3.2.3$$

$$-\frac{\partial p}{\partial y} = \frac{\partial \tau_{xy}}{\partial x} + \frac{\partial \tau_{yy}}{\partial y} + \frac{\partial \tau_{zy}}{\partial z} \qquad 3.2.4$$

Now, conservation of energy yields in Cartesian coordinates the following scalar equation with only one component, T , simplified from equation A, Appendix III, to ;

$$\rho C_p \left(\frac{\partial T}{\partial t} + v_x \frac{\partial T}{\partial x} + v_y \frac{\partial T}{\partial y} + v_z \frac{\partial T}{\partial z} \right) = k\left(\frac{\partial^2 T}{\partial x^2} + \frac{\partial^2 T}{\partial y^2} + \frac{\partial^2 T}{\partial z^2} \right)$$

$$- \left(\tau_{xx} \frac{\partial v_x}{\partial x} + \tau_{yy} \frac{\partial v_y}{\partial y} + \tau_{zz} \frac{\partial v_z}{\partial z} \right)$$

$$- \left(\tau_{xy}\left(\frac{\partial v_x}{\partial y} + \frac{\partial v_y}{\partial x} \right) + \tau_{xz}\left(\frac{\partial v_x}{\partial z} + \frac{\partial v_z}{\partial x} \right) + \tau_{yz}\left(\frac{\partial v_y}{\partial z} + \frac{\partial v_z}{\partial y} \right) \right)$$

3.2.5

where C_p is the specific heat of the fluid at constant pressure (for an incompressible fluid, $C_p = C_v$, the specific heat at constant volume) and k is the thermal conductivity of the fluid; both are assumed to be constant. In order to solve these conservation differential equations, the constitutive equation relating the stress tensor to the rate of deformation tensor, equation 2.4.5, supplies the information on the flow properties of a particular melt.

3.3 The Lubrication Approximation.

A useful simplification introduced to extrusion theory is the Lubrication approximation.[1,30,54] This is basically the replacement of the flow in a tapered - small gap by uniform flow between plane parallel surfaces. This approach has been discussed in detail by Pearson,[54] in reference to the analysis of flow problems in polymer processing, who showed that the resulting uniform flow is a valid first approximation to the flow of an elastic non-Newtonian fluid in a narrow channel (i.e. one which is relatively shallow in comparison with its width and length). For isothermal Newtonian fluids, it has been shown (in the previous chapter) that the velocity profile is a function of the clearance depth $h(x,z)$. The pressure profile is also a function of the coordinate x and z only i.e. the local pressure gradients are $\frac{dp}{dx}$, $\frac{dp}{dz}$ and the flow and pressure normal to the surfaces (y direction) is neglected. Therefore, the pressure or velocity profile can be evaluated at any point (x,z) as if the flow would occur between two infinite plates at a distance $h(x,z)$ from each other. This is the only way to treat non-Newtonian flow in a tapered section which can be described as a series of parallel sections.[1] It has been found by Benis[55] that the lubrication approximation applied to isothermal flows in channels is valid for most non-Newtonian fluids if the local angle between the surfaces is less than 10^{o} .

The application of the lubrication approximation to channel flow assumes that the velocity and temperature profiles are fully developed. Therefore, considering the downchannel flow in the z direction to be fully developed, assumes that there are no differentials of shear stress and velocity with respect to z and the equations of motion 3.2.2 , 3.2.3 and

3.2.4 reduce to ;

$$-\frac{\partial p}{\partial z} = \frac{\partial \tau_{xz}}{\partial x} + \frac{\partial \tau_{yz}}{\partial y} \qquad 3.3.1$$

$$-\frac{\partial p}{\partial x} = \frac{\partial \tau_{xx}}{\partial x} + \frac{\partial \tau_{yx}}{\partial y} \qquad 3.3.2$$

$$-\frac{\partial p}{\partial y} = \frac{\partial \tau_{xy}}{\partial x} + \frac{\partial \tau_{yy}}{\partial y} \qquad 3.3.3$$

It can be seen that the pressure $\frac{\partial p}{\partial z}$ is a constant and independent of x and y since the pressure gradients in these directions are also independent of z.

Similarly the energy equation 3.2.5 reduces to ,

$$\rho C_p\left(v_x \frac{\partial T}{\partial x} + v_y \frac{\partial T}{\partial y} \right) = k \left(\frac{\partial^2 T}{\partial x^2} + \frac{\partial^2 T}{\partial y^2}\right) - \left(\tau_{xx} \frac{\partial v_x}{\partial x} + \tau_{yy} \frac{\partial v_y}{\partial y} \right)$$

$$- \left(\tau_{xy} \left(\frac{\partial v_x}{\partial y} + \frac{\partial v_y}{\partial x} \right) + \tau_{xz} \frac{\partial v_z}{\partial x} + \tau_{yz} \frac{\partial v_z}{\partial y} \right) \qquad 3.3.4$$

If the flow is assumed to be fully developed also in the cross-channel x direction, the differentials with respect to x become insignificant and the momentum and energy equations are further reduced to,

$$-\frac{\partial p}{\partial z} = \frac{\partial \tau_{yz}}{\partial y} \qquad 3.3.5$$

$$-\frac{\partial p}{\partial x} = \frac{\partial \tau_{xy}}{\partial y} \qquad 3.3.6$$

$$-\frac{\partial p}{\partial y} = \frac{\partial \tau_{yy}}{\partial y} \qquad 3.3.7$$

and $$k \frac{\partial^2 T}{\partial y^2} = - \tau_{xy} \frac{\partial v_y}{\partial y} - \tau_{yz} \frac{\partial v_z}{\partial y} \qquad 3.3.8$$

These are the equations for simplified two-dimensional flow in which the

two independent velocity components are dependent only on the channel depth coordinate y . From equation 3.3.7 can be determined the pressure distribution in the y direction and neglecting normal stresses in comparison with the local pressure, it is assumed that the pressure is constant throughout the channel depth. The two independent shear stress components which are obtained from equations D and E, Appendix IV, reduces to ,

$$\tau_{yz} = \eta \frac{1}{2} \frac{\partial v_z}{\partial y} \qquad 3.3.9$$

$$\tau_{xy} = \eta \frac{1}{2} \frac{\partial v_x}{\partial y} \qquad 3.3.10$$

and hence, the viscosity can be determined from equation 2.4.5 where the second invariant of the rate of deformation tensor in cartesian coordinates is,

$$I_2 = \frac{1}{2} \left(\left(\frac{\partial v_x}{\partial x}\right)^2 + \left(\frac{\partial v_y}{\partial y}\right)^2 + \left(\frac{\partial v_z}{\partial z}\right)^2 \right)$$

$$+ \frac{1}{4} \left(\frac{\partial v_y}{\partial x} + \frac{\partial v_x}{\partial y}\right)^2 + \frac{1}{4} \left(\frac{\partial v_z}{\partial y} + \frac{\partial v_y}{\partial z}\right)^2 + \frac{1}{4} \left(\frac{\partial v_x}{\partial z} + \frac{\partial v_z}{\partial x}\right)^2 \qquad 3.3.11$$

and is reduced for the simplified two-dimensional flow to,

$$I_2 = \frac{1}{4} \left(\left(\frac{\partial v_z}{\partial y}\right)^2 + \left(\frac{\partial v_x}{\partial y}\right)^2 \right) \qquad 3.3.12$$

For one-dimensional flow, a further simplification can be made to the above equations by neglecting the cross-channel flow components of shear and velocity and consequently, its effect on viscosity and the required momentum and shear stress equations are 3.3.5 and 3.3.9 respectively and the energy equation reduces to,

$$k \frac{\partial^2 T}{\partial y^2} = - \tau_{yz} \frac{\partial v_z}{\partial y} \qquad 3.3.13$$

and

$$I_2 = \frac{1}{4} \left(\frac{\partial v_z}{\partial y}\right)^2 \qquad 3.3.14$$

To all the above cases the 'isothermal' condition can be applied by neglecting the energy equation and assuming that velocity profiles are independent of the temperature profiles and therefore, any temperature variations do not significantly affect the viscosity of the fluid.

3.4 The flight leakage.

In Figure 3.4.1 is given the axial cross-sectional view of the flight gap showing the geometry and coordinate system used. The flow in the gap is analysed for leakage occurring in the axial direction since this is influenced by the axial pressure drop in the extruder.

The screws are assumed to rotate concentrically in the barrel sections so that the flight gap δ_f is constant and equal to the radial clearance between the screw and barrel. A coordinate system fixed relative to the screw is used and the barrel is treated as if rotating about a stationary screw. Because of the positive conveyance of the C- shaped chambers of material, there is an axial relative velocity component between the material in the screw channels and the barrel wall of,

$$V_a = NS \qquad 3.4.1$$

The flight gap is normally relatively shallow i.e.,

$$\delta_f \ll D \qquad 3.4.2$$

so that curvature effects are negligible and the gap can be unrolled and Cartesian coordinates x, y used. The depth of the flight gap is also relatively small compared with its width and length i.e.,(Figure 3.4.1),

$$\delta_f \ll W_f, \delta_f \ll B \qquad 3.4.3$$

so that end effects can be ignored and the gap can be treated as infinite parallel plates. The leakage is treated, therefore, as isothermal one-dimensional flow and the equations to be solved are 3.3.6 , 3.3.10 , 3.3.14 and 2.4.5. The boundary conditions are,

$$v_x = 0 \text{ at } y = 0 \text{ and } 0 \leqslant x \leqslant B$$

$$v_x = V_a \text{ at } y = \delta_f \text{ and } 0 \leqslant x \leqslant B \qquad 3.4.4$$

Analytical solutions have been obtained[1,37] for this isothermal one-dimensional combined drag and pressure flow of a power law fluid between parallel plates and the equations relating dimensionless flow rate and pressure gradient terms for the various flow conditions are given in Appendix V. The power law parameters are taken at a characteristic shear rate, V_a/δ_f

3.5 The side leakage.

When analysing the leakage through the side gap, flow from one end of the intermeshing zone to the other is to be examined. The material is conveyed through a passage which is narrow and deep at the inlet and outlet, and wide and shallow at the middle, and the transverse flow is the tetrahedron leakage. (Figure 3.5.1a) Because of its narrowiness at the inlet, the tapered form of the depth over the gap length (due to the flank angle) is not likely to build up pressures but to encourage the material to leak from the sides of the gap and relieve the pressure. The side gap leakage is treated, therefore, as flow through a rectangular channel with constant dimensions over the length of the intermeshing region (Figure 3.5.1a), and was the approach adopted by Janssen[5] for this gap. The dimensions of the side gap passage is taken as,

$$\text{depth, } H_s = \frac{\epsilon}{\cos\psi'} \quad ; \text{ width, } W_s = \frac{H}{\cos\psi'}$$

and $$\text{length, } L_i = 2R \sin \alpha/2 \qquad 3.5.1$$

The leakage consists of rigid drag flow and combined drag and pressure flows. There is a linear variation of surface velocity across the gap resulting in both top and bottom surfaces rotating with the same minimum velocity, Figure 3.5.1b,

$$V_1 = 2\pi N \left(R - (H - \sigma) \right) \qquad 3.5.2$$

and up to a maximum mean velocity of,

$$V_m = 2\pi N \left(R - \left(\frac{H-\sigma}{2}\right) \right) \qquad 3.5.3$$

The mean velocity responsible for rigid drag flow through the gap is taken as,

$$V_d = \frac{V_1 + V_m}{2} \qquad 3.5.4$$

and this flow is,

$$Q_d = V_d W_s H_s \qquad 3.5.5$$

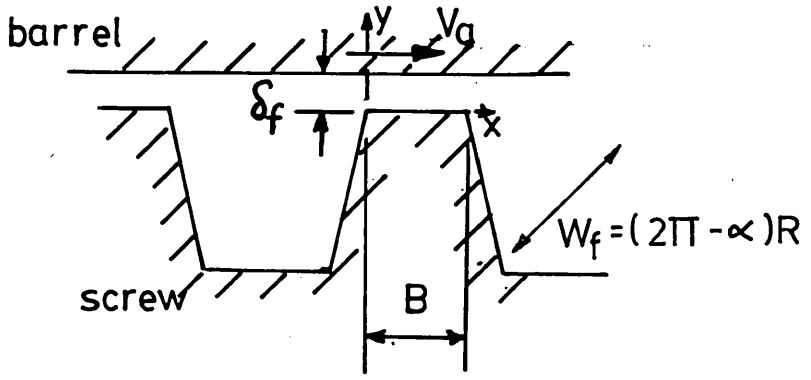

Figure 3.4.1 Flight gap

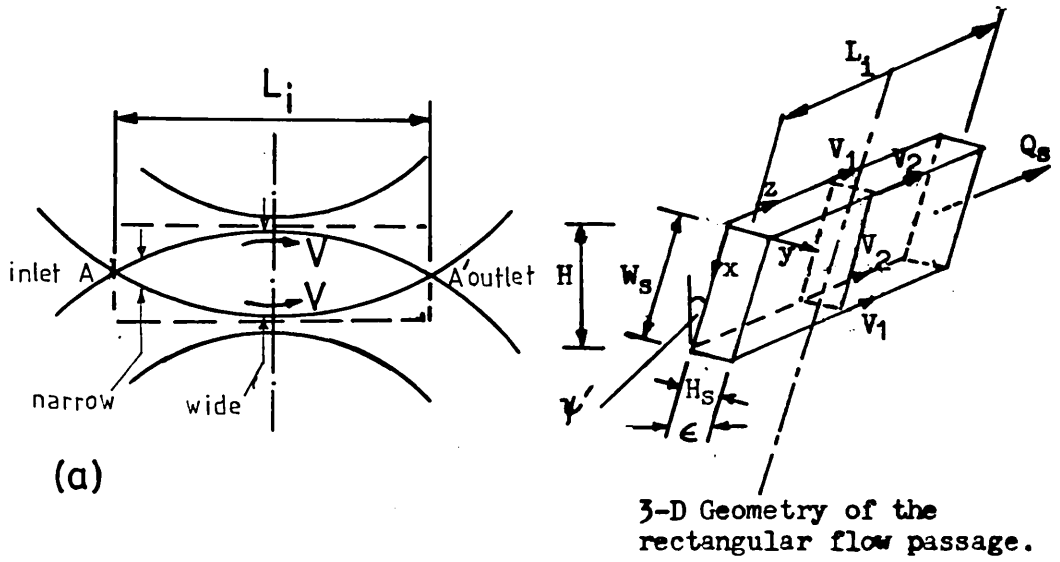

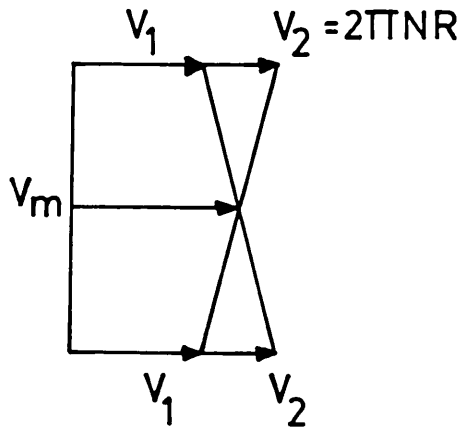

(b) Velocity of the surfaces.

Figure 3.5.1 Side gap.

For the combined drag and pressure flows through the full width of the gap, a mean relative drag velocity is used,

$$V_{dp} = \frac{V_2 - V_1}{2} \qquad 3.5.6$$

and the viscosity is taken at the mean maximum shear rate, $(V_2 - V_1)/H_s$.

The shear flow is treated as being isothermal and fully developed, and occuring in the direction of screw rotation (downchannel z direction). The coordinate system is taken relative to either flight flank surface, since the geometry is symmetrical. Because the side gap canbe large, i.e. H_s/W_s can be as large as 0.45 for metering screw sections, deep channel flow is appropiate. The equations to be solved are 3.3.1, 3.3.9, 3.3.10, 3.3.12 and 2.4.5 . The boundary conditions are,

$$v_z = 0 \text{ at } y = 0 \text{ and } 0 \leq x \leq W_s$$

$$v_z = 0 \text{ at } x = 0 \text{ , } x = W_s \text{ and } 0 \leq y \leq H_s$$

$$v_z = V_{dp} \text{ at } y = H_s \text{ and } 0 \leq x \leq W_s \qquad 3.5.7$$

Solutions have been obtained for non-Newtonian plain downstream flow in deep channels[30,59] and dimensionless flow characteristics for a range of H/W values are given by Fenner.[30] Deep channel combined downstream and transverse flow analysis is considered later in section 3.9 and this can also be used to obtain solutions for this case.

When the flow is to be treated as one-dimensional, equations for combined drag and pressure flow of a power law fluid between infinite parallel plates (Appendix V) are used to obtain solutions. The boundary conditions for this case are,

$$v_z = 0 \text{ at } y = 0 \text{ and } 0 \leq z \leq L_i$$

$$v_z = V_{dp} \text{ at } y = H_s \text{ and } 0 \leq z \leq L_i \qquad 3.5.8$$

3.6 The calender leakage.

The leakage flow through the calender gap consists of drag and pressure flows. There is rigid material transport or drag flow with no shear due to all surfaces rotating in the same direction with component of velocity equal to the screw root velocity (Figure 3.6.1), 3.6.1b),

$$V_r = 2\pi N (R - H) \qquad 3.6.1$$

and drag and pressure flows taken stationary with respect to the screw root and generated by the relative velocity of the flight tip of one screw and the root of the other,

$$V_c = 2\pi N H \qquad 3.6.2$$

Since the root and flight walls of the same screw are responsible for most of the drag flow through the passage, the coordinate system is fixed relative to the screw channel and the radial clearance of the calender passage can be taken as H_c given by equation 3.1.4. The width of gap is taken as the axial width of the flight tip,

$$W_c = B \qquad 3.6.3$$

The flow through the gap is assumed to be isothermal and fully developed, with rigid drag flow component at any depth in the passage of,

$$Q_{cd} = V_r H_c W_c \qquad 3.6.4$$

The calender passage is rather deep at the inlet and outlet, becoming shallower at the minimum calender gap. There is no drag velocity across the passage but there is likely to exist a transverse pressure flow which is assumed to be small compared with the downstream calender flow and is therefore neglected. Deep channel flow analysis is appropriate for this case and cylindrical polar coordinates are used to account for curvature of the deep channel. The simplified equations to be solved are for cylindrical coordinates and are similar to those used for plain flow in the previous section 3.5 . Using the general conservation equations

given in Appendices I to IV, together with the assumptions given in section 3.3, equations for axisymmetric flow can be simplified in a similar manner to those for plain flow. The simplified version of the second invariant of the rate of deformation tensor I_2 can be obtained from equation 2.4.4 . The boundary conditions are,

$$v_\theta = 0 \text{ at } r = R - H \text{ and } 0 \leqslant z \leqslant W_c$$
$$v_\theta = 0 \text{ at } z = 0 \text{ , } z = W_c \text{ and } R-H \leqslant r \leqslant R$$
$$v_\theta = V_c \text{ at } r = R \text{ and } 0 \leqslant z \leqslant W_c \qquad 3.6.5$$

Axi-symmetric flow in deep channel is analysed in section 3.9 and the method is used to obtain solutions for this case. The non-Newtonian viscosity used is determined for the range of mean shear rates, V_c/H_c, generated in the calender passage.

When the flow is to be treated as one-dimensional, occurring as if in a shallow channel, the equations for combined drag and pressure flow of a power law fluid between infinite parallel plates (Appendix V) are used to obtain solutions for this gap. The boundary conditions are for this case,

$$v_x = 0 \text{ at } y = 0 \text{ and } -\frac{L_i}{2} \leqslant x \leqslant \frac{L_i}{2}$$
$$v_x = V_c \text{ at } y = H_c \text{ and } -\frac{L_i}{2} \leqslant x \leqslant \frac{L_i}{2} \qquad 3.6.6$$

The non-Newtonian viscosity is obtained for each position along the calender passage at the mean shear rate, $\overset{drag}{\Delta}$, V_c/H_c.

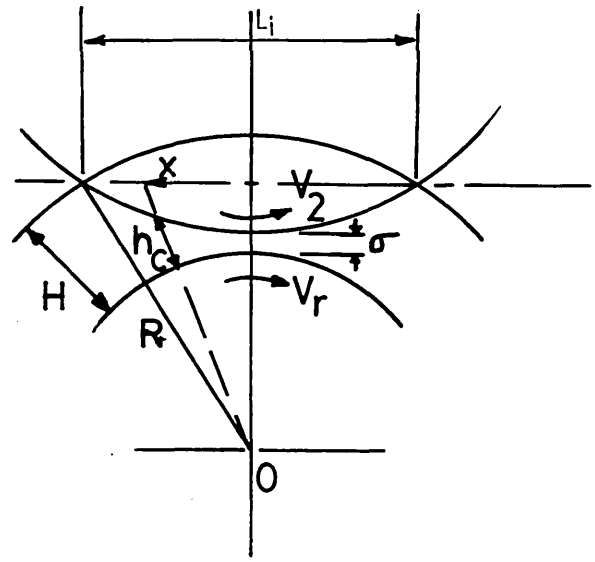

Figure 3.6.1 Calender gap.

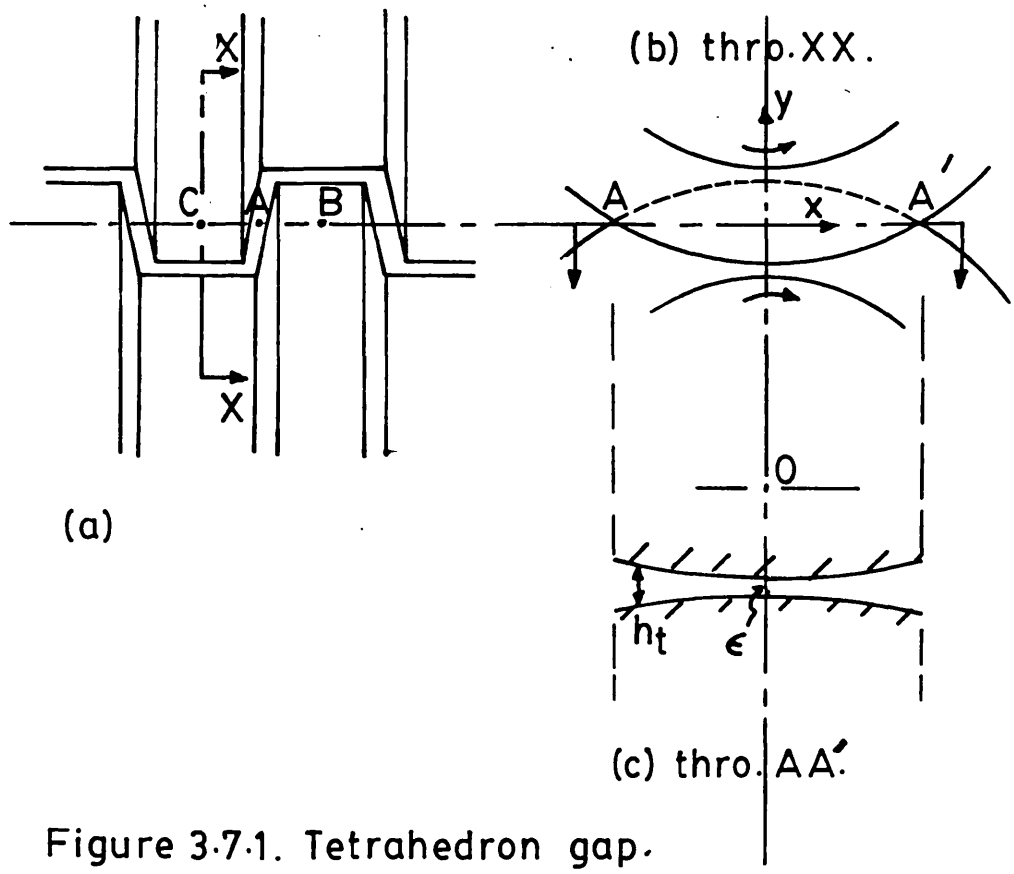

Figure 3.7.1. Tetrahedron gap.

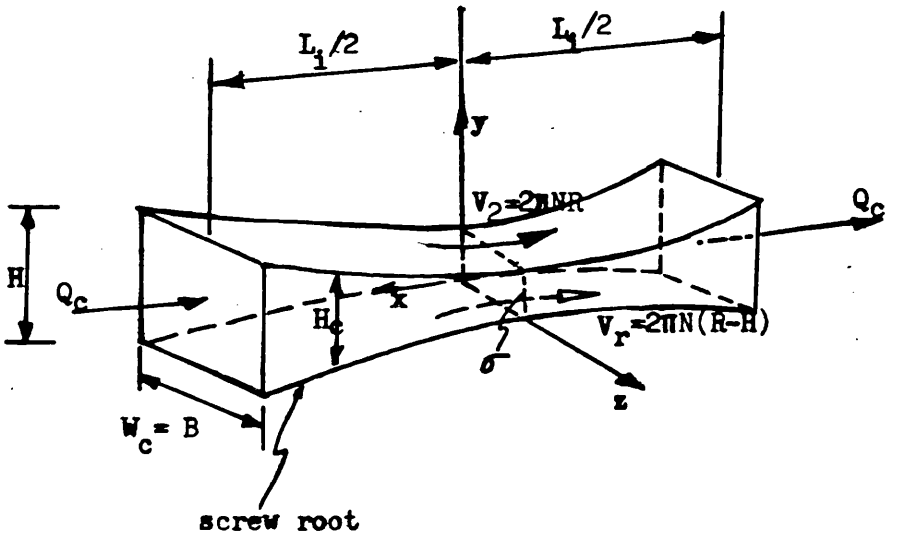

Figure 3.6.1b Three dimensional geometry of the calender gap. H_c used is the depth measured perpendicular to a screw root so that when $x=\pm L_1/2$, $H_c=H$ and when $x=0$, $H_c=\sigma$ (see equation 3.1.4).

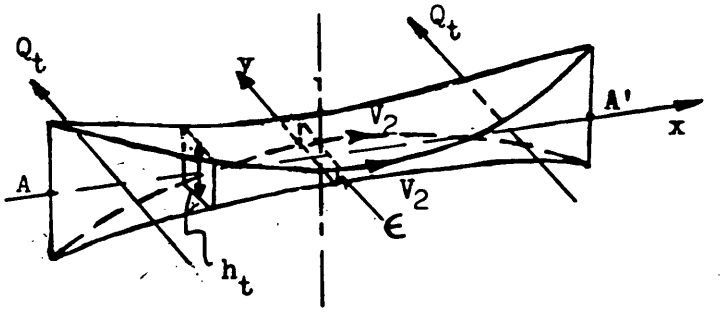

Figure 3.7.1d Three dimensional geometry of the tetrahedron gap.

3.7 The tetrahedron leakage.

The geometry of the tetrahedron gap is approximated by the gap between intermeshing flights without any pitch (or between intermeshing discs), Figure 3.7.1a. The effect of the screw pitch on gap depth (in equation 3.1.7) is assumed to be negligible. Over the length of the gap (y direction), the depth is constant and is equal to that determined at the middle of the intermeshing region, AA' (which is like taking a mean depth of the clearance), Figure 3.7.1b and 3.7.1d.

The effect of drag velocity on melt flow through this gap is likely to be small. Figure 3.7.2a illustrates the surface velocity distribution in the gap. Because of the symmetrical shape of the intermeshing region, the velocity components resolved in the x direction gives the distribution shown i.e. zero along the middle line AA' increasing to a maximum relative value at the outer boundaries of $V_2 - V_1$. This velocity component is small and is equal to the difference between the velocities of the surfaces with radius R and $R - (H - \sigma)$, or $2\pi N(H - \sigma)$, and is confined to the region near the outer boundaries. The component of velocity resolved in the y direction, is shown as, zero at the centre and increases to a maximum at A or A'. Figure 3.7.2b shows this drag velocity of top and bottom surfaces in the y direction direction. The addition of these velocities i.e. the velocity taken relative to either surface is the same but the net drag effect is zero. The maximum drag occurs near the edge of the intermeshing region A and A' and B and B'. The flow is likely to be largest due to pressure flow through the region near A and A', where the gap tends to be shortest and widest. It may be significant, therefore, that the shear due to drag is likely to be relevant only near this region where, also, the leakage is generated by a predominantly pressure flow with high shear.

Because there is no net drag flow through the tetrahedron gap,

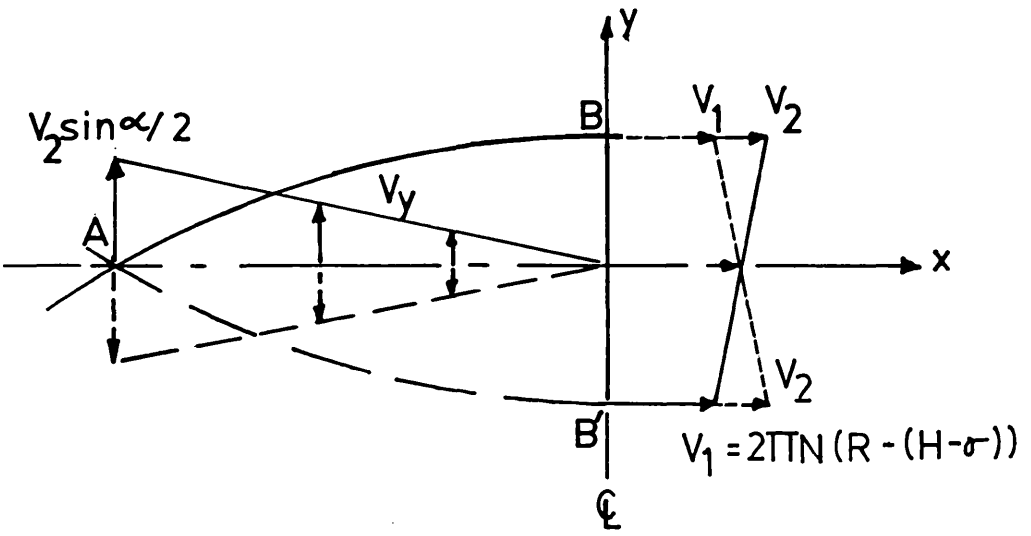

(a) velocity distribution of surfaces.

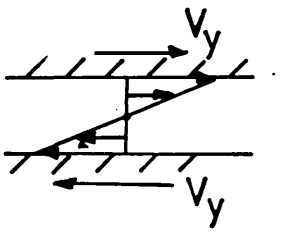

(b) y - component of drag velocity.

Figure 3.7.2. Tetrahedron gap wall velocities.

the leakage is generated only by the pressure drop between opposed chambers in the extruder. It is assumed that this pressure drop is generated at the edge of the intermeshing zone , Figure 3.7.1a , from B in the middle of one chamber, through A to C in the middle of the other chamber. Along BAC and in the intermeshing region, the flow is not influenced by the drag effect of the axial relative motion of the barrel and screw and only pressure flow is likely to exist. Now, in the intermeshing region, the pressure drop and associated leakage flow would vary across the tetrahedron gap because of its irregular shape, i.e., length and depth of the clearance varying with gap width. and the unknown pressure distribution at the boundaries of the gap would be dependent also on the transverse flow that passes through the calender passage since this flow would be also influenced by the same pressure drop over BC.

Figure 3.7.3 shows a simplified model of the intermeshing region. The three leakage gaps of the overlapping region are placed in a single plane by wrapping a calender passage around the inlet and outlet of the tetrahedron gap. BB' and CC' are the centre lines of each calender flow passage. The pressures at points B and C (and also B' and C') remote from the tetrahedron gap are assumed to be the pressures in the opposed chambers of the extruder and thus, ΔP is the pressure drop between these points. Across the calender gap the pressure drop is equal to that generated between adjacent chambers in the same screw i.e. $2\Delta P$, or for screws with m channels per pitch, $2m\Delta P$.

These pressure boundary conditions can only account for the pressure flow through the intermeshing region produced by the pressure drop due to die pressure in the extruder. This pressure drop is assumed to be mainly responsible for producing leakage flow through the tetrahedron gap.

Although this was found from experiment to be the case for both Newtonian and non-Newtonian flows in the tetrahedron gap[5], melt flow would be influenced, to some extent, also by the drag flow generated by the

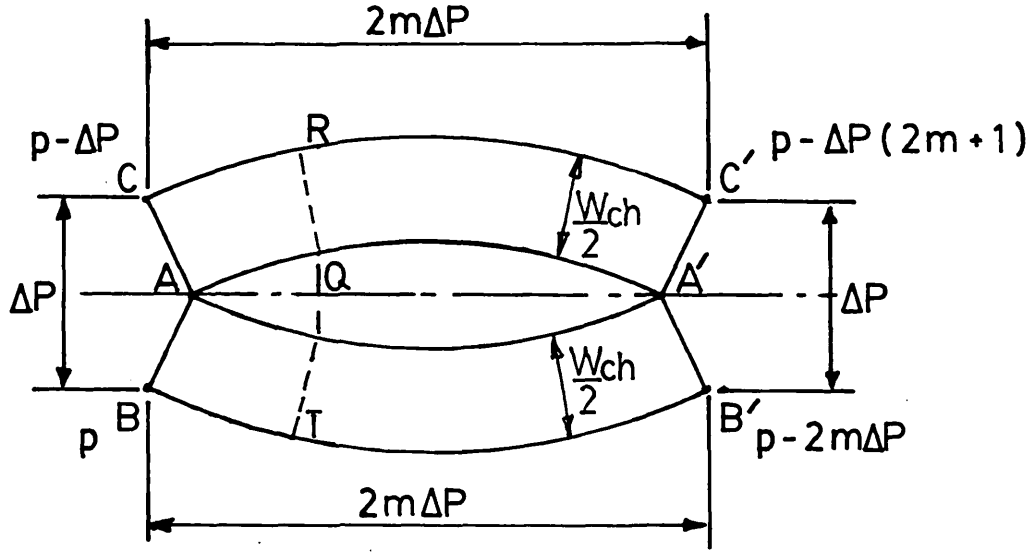

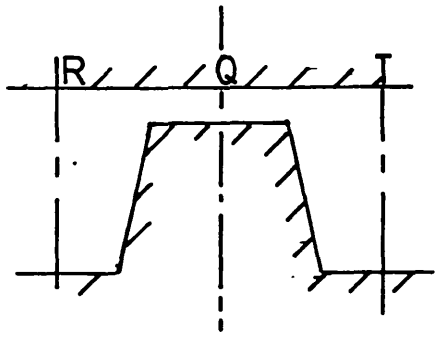

section thro. RQT.

Figure 3.7.3 A model of the intermeshing region

rotating surfaces of the gap. To include drag flow, requires an analysis which would be three-dimensional in the sense that, even if the full lubrication approximation is used for flow in the two component (x,z) directions alone, the local viscosity and thus the velocity profiles would be dependent on an additional variable, namely, the coordinate of the stress neutral surface of each profile which would itself be influenced by the combined shear rates varying in the third component (y) direction. The analysis would be similar to that described by Griffith[39] for combined downstream and zero net transverse flow in single-screw extruder channel, but in the general case, the transverse flow would be required to take any value with no special condition prescribed. It would be required then to use such a solution of the analysis at every point in the flow region. Considering the effort which is usually involved in obtaining each solution numerically on a digital computer, this method would be uneconomical to use, although such an analysis would be useful for solving the problems of flow,not only through the tetrahedron gap, but also through the entire intermeshing region i.e. including the combined drag and pressure flows through the side and calender passages.

Since there is, however, no net drag flow through the tetrahedron gap, what is really required is only the effect that drag shear rates would have on the local viscosity in the region of the gap where the greatest amount of melt flows. It was previously shown that most of the leakage flow is likely to go through the shortest part of the gap where, also, the surfaces rotate with the largest relative velocity and thus generate large drag shear rates which would probably become more significant as the screw speed is increased. In order to simplify the analysis, it is proposed to include the effect of drag flow on viscosity by using the combined drag and pressure flow shear rates at the screw wall to define the viscosity to be used. The method used is given as an extension of the pressure flow analysis of narrow clearances described in the next section.

3.8 Finite Element Analysis of the tetrahedron leakage.

In the previous section is described a simplified arrangement of the leak passages of the intermeshing region which makes the flow amenable to mathematical treatment (Figure 3.7.3). A non-Newtonian pressure flow analysis of narrow channels (as in dies) which was first introduced by Pearson[42] is used for the flow over the entire region. Such an analysis has been described by Fenner and Nadiri[44] for application to pressure flow in cable-coating dies and the differential equation solved using the finite element method.[56] The finite element method allows a mesh of small triangular elements to be constructed on the intermeshing region so as to follow as closely as possible the form of the boundaries. In Figure 3.8.1 is shown the finite element mesh used for the flow region plotted on the x, y plane.

If Q_x , Q_y represent the volumetric flow rates per unit length in the x and y directions respectively in the two-dimensional flow, then in terms of a stream function $\psi(x,y)$,

$$Q_x = \frac{\partial \psi}{\partial y} \quad , \quad Q_y = -\frac{\partial \psi}{\partial x} \qquad 3.8.1$$

This stream function automatically satisfies the equation of conservation of mass in incompressible steady flow (equation 3.2.1),

$$\frac{\partial}{\partial x}(Q_x) + \frac{\partial}{\partial y}(Q_y) = 0 \qquad 3.8.2$$

Applying the lubrication approximation to flow in each direction separately, the equation of motion 3.2.3 and 3.2.4 together with their shear stress component equations 3.2.7 and 3.2.8 respectively can be solved for a power law fluid, equation 2.4.5 with the no-slip boundary conditions, $v_x = v_z = 0$, at $y = h$ to give the pressure gradients,[23,31]

$$\frac{\partial p}{\partial x} = -\, Q_x \frac{\bar{\mu}}{\lambda h^3} = -\frac{\partial \psi}{\partial y}\frac{\bar{\mu}}{\lambda h^3} \qquad 3.8.3$$

and

$$\frac{\partial p}{\partial y} = -\, Q_y \frac{\bar{\mu}}{\lambda h^3} = -\frac{\partial \psi}{\partial y}\frac{\bar{\mu}}{\lambda h^3} \qquad 3.8.4$$

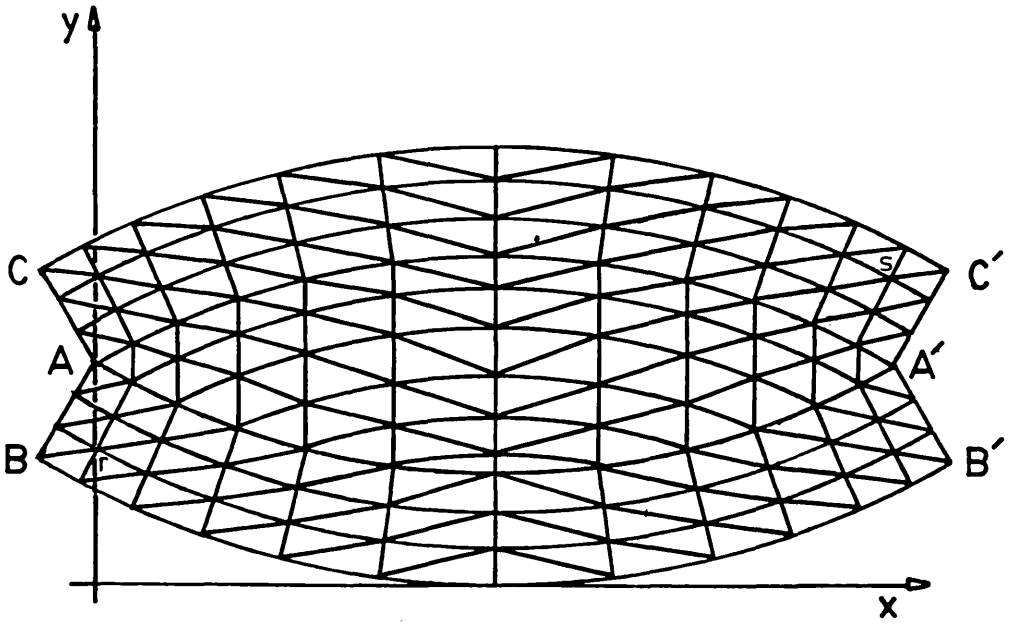

Figure 3.8.1. Finite element mesh.

Number of nodal points = 127.
Number of elements = 216.
Number of boundary points = 36.

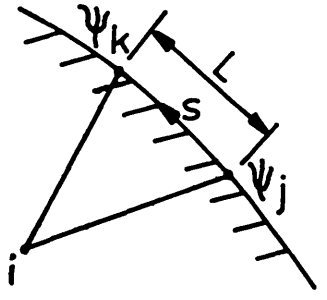

Figure 3.8.2 Typical boundary showing the direction of positive stream function and pressure variation.

where for pressure flow of a non-Newtonian fluid,

$$\lambda = \frac{1}{2^{2n+1}}\left(\frac{2n}{2n+1}\right)^n \qquad 3.8.5$$

$$\bar{\mu} = \mu_o \left(\frac{Q_s}{h^2}\right)^{n-1} \qquad 3.8.6$$

* being the viscosity evaluated at the resultant flow rate,

$$Q_s^2 = Q_x^2 + Q_y^2 \qquad 3.8.7$$

In order to eliminate the pressure gradients, equations 3.8.3 and 3.8.4 must satisfy the following,

$$\frac{\partial}{\partial x}\left(\frac{\partial p}{\partial y}\right) - \frac{\partial}{\partial y}\left(\frac{\partial p}{\partial x}\right) = 0 \qquad 3.8.8$$

and therefore, the final governing differential equation is,[44]

$$\frac{\partial}{\partial y}\left(\frac{\bar{\mu}}{\lambda h^3}\frac{\partial \psi}{\partial y}\right) + \frac{\partial}{\partial x}\left(\frac{\bar{\mu}}{\lambda h^3}\frac{\partial \psi}{\partial x}\right) = 0 \qquad 3.8.9$$

In the finite element method, a varational principle equivalent to the equilibrum condition expressed by equation 3.8.9 is used to formulate the problem. The condition to be satisfied by the nodal point variables is that the total viscous dissipation over the flow region should be a minimum.[57,60] The variational approach used to solve the partial differential equation, is to seek a stationary value for a functional χ which is defined by an appropiate integration of the unknowns over the solution domain.[56] It has been shown that the required stationary condition is obtained when,

$$\frac{\partial \chi}{\partial \eta} = \iint \left(\frac{1}{2}\frac{\bar{\mu}}{\lambda h^3}\frac{\partial}{\partial \eta}\left(\frac{\partial \psi}{\partial x}\right)^2 + \frac{1}{2}\frac{\bar{\mu}}{\lambda h^3}\frac{\partial}{\partial \eta}\left(\frac{\partial \psi}{\partial y}\right)^2\right) dx\, dy - I = 0 \qquad 3.8.10$$

holds for all of the unknowns, η where,

$$I = \iint \left(\frac{\partial}{\partial x}\left(\frac{\bar{\mu}}{\lambda h^3}\frac{\partial \psi}{\partial \eta}\frac{\partial \psi}{\partial x}\right) + \frac{\partial}{\partial y}\left(\frac{\bar{\mu}}{\lambda h^3}\frac{\partial \psi}{\partial \eta}\frac{\partial \psi}{\partial y}\right)\right) dx\, dy \qquad 3.8.11$$

and in terms of the first derivative of ψ normal to the boundary,

$$I = \oint \frac{\partial \psi}{\partial \eta}\frac{\bar{\mu}}{\lambda h^3}\frac{\partial \psi}{\partial n}\, ds \qquad 3.8.12$$

* h for a triangular element taken as a mean depth $h = 1/3(h_i + h_j + h_k)$.

where the line integral is performed in the anticlockwise direction around the boundaries. Integral I = 0, if on the boundaries either the value of ψ is prescribed (independent of the unknown ψ) or its first derivative $\frac{\partial \psi}{\partial n}$, with respect to the distance normal to the boundary (boundary of equal pressure) , is zero. In the present problem, the integral I (equation 3.8.12) is probably not equal to zero (see previous section) since not all of the above conditions can be prescribed at the boundaries. However, it can be seen that I is related to the flow along the boundary and therefore, it is possible to prescribe pressure gradients, since the equation can be modified to,

$$I = \oint \frac{\partial \psi}{\partial \eta} \frac{\partial p}{\partial s} \, ds \qquad 3.8.13$$

where $\frac{\partial p}{\partial s}$ is the pressure gradient at the boundary. Considering stream function values ψ_j and ψ_k at any two nodal points on the boundary, distance L apart, Figure 3.8.2 , and assuming a linear distribution of both ψ and pressure between the nodal points, then,

$$I = \frac{\partial}{\partial \eta} \int_0^L \left(\psi_j + \frac{s}{L} (\psi_k - \psi_j) \right) \frac{\overline{dp}}{L} \, ds \qquad 3.8.14$$

where $\overline{dp}$ is the pressure drop between the points. Integrating produces,

$$I = \frac{\partial}{\partial \eta} (\psi_k + \psi_j) \frac{\overline{dp}}{2} \qquad 3.8.15$$

Now, for a solution domain divided into small triangular elements of geometry shown in Figure 3.8.3 a linear distribution of stream function over each element is given by the shape function,

$$\psi (x',y') = C + C_2 x' + C_3 y' \qquad 3.8.16$$

The three parameters of the shape function C_1, C_2, C_3 can be obtained in terms of the three nodal point velocities ψ_i, ψ_j, and ψ_k as,

$$C_1 = \psi_i \quad , \quad \begin{bmatrix} C_2 \\ C_3 \end{bmatrix} = \frac{1}{2 \Delta m'} B \begin{bmatrix} \psi_i \\ \psi_j \\ \psi_k \end{bmatrix} \qquad 3.8.17$$

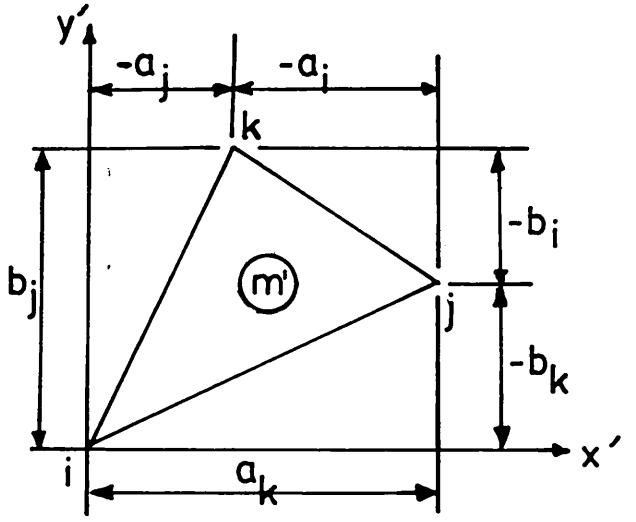

Figure 3.8.3 Triangular element dimensions.

where B is a dimension matrix,

$$B = \begin{bmatrix} b_i & b_j & b_k \\ a_i & a_j & a_k \end{bmatrix}$$

and the area of the element $\Delta m' = \frac{1}{2} (a_k b_j - a_j b_k)$

The form of the functional used is,

$$\chi = \iint (\frac{1}{2} \frac{\bar{\mu}}{\lambda h^3} (\frac{\partial \psi}{\partial x})^2 + \frac{1}{2} \frac{\bar{\mu}}{\lambda h^3} (\frac{\partial \psi}{\partial y})^2) \, dx \, dy - (\psi_k + \psi_j) \frac{\overline{dp}}{2} \qquad 3.8.18$$

where ψ_k, ψ_j are points only at the boundaries.

For integration $\chi^{m'}$ performed over the area of each element, numbered m', the required solution is obtained when the value of χ is stationary with respect to the nodal point stream function values i.e. when,

$$\frac{\partial \psi}{\partial \psi_i} = \sum \frac{\partial \chi}{\partial \psi_i}^{m'} = 0 \qquad 3.8.19$$

The derivative of ψ^m with respect to the three nodal stream function values of m' is obtained and for all elements in the solution domain the summation gives,[56]

$$[K] [\delta] - [p'] = 0 \qquad 3.8.20$$

where $[\delta]$ is a vector containing the stream function values for all the nodal points in the mesh, $[K]$ a square matrix is often referred to as the overall stiffness matrix contains coefficients assembled from the properties and dimensions of the individual elements and $[p']$ a matrix contains pressure drops which would be non-zero only at the boundary nodal points.

Equation 3.8.20 is solved for the unknown values of ψ using the Gauss-Seidel back-substitution iterative method with overrelaxation, where the overrelaxation factor f is in the range $1 < f < 2$. The convergence criterion used for the variable is that the sum of the relative errors should be less than 10^{-5}

Prescribing pressure drops on the boundaries in this type of finite element formulation is equivalent to prescribing on the boundary derivatives of ψ alone without specifying any values of ψ. Attempts to solve such a problem will result in failure of the Gauss-Seidel method to converge[44] and to prevent this occurring, at least one value of ψ must be specified.[61] For the present problem, it was found convenient to specify $\psi = 0$ at two selected nodes in the mesh i.e. near the two extreme corners as shown in Figure 3.8.1, nodes marked r and s. It has been recommended,[44,47] also, that elements should be acute or right-angled and as equilateral as possible otherwise the rate of convergence would be reduced.

For non-Newtonian flow in each element, the mean viscosity is determined from the resultant flow or local gradients of stream function, using equations 3.8.6 and 3.8.17 and a mean depth over the element. For this reason, the equations become non-linear and are solved by initially, assuming a constant value of $\bar{\mu}$ for the element viscosities and then using the new values of stream function,obtained after a few iterations, to update the viscosities, repeating the process until satisfactory convergence is achieved.

The flow rate of melt passing the inlet or outlet boundary between adjacent pair of nodal points is equal to the difference between the stream function values of these points, $\Delta\psi$. The leakage flow rate through the tetrahedron gap is determined from the difference in the values of the stream function between points A and A', $\psi_{A'} - \psi_A$ (Figure 3.7.1).

For polymer melts, if the leakage is produced by a pressure flow which is large compared with the drag component of flow, the analysis described above is likely to give a good estimate of the leakage flow rate. Because of the high viscosity of melts, the pressure gradients are most likely to be relatively large in order to generate significant leakages

and therefore, the analysis could be valid for the low screw speeds normally encountered in this type of extruder. In addition, the tetrahedron leakage is not considered to be important over the range of small pressure gradients, near pure drag flow conditions, where the simple addition of a drag flow and a relatively small pressure flow of a non-Newtonian fluid tends to be most seriously in error[35] (Figure 2.5.5). For large pressure gradients, the net flow is most likely to be influenced mainly by the shear rates due to the pressure flow than that due to a drag flow which is relatively small compared with the pressure flow, and using a combined flow which is strongly dependent on a mean drag shear rate is likely to produce significant errors.

It is important to know, however, the significance of the effect that drag shear rates could have on the net flow rate through large tetrahedron gaps. Because the transverse flow was shown to have but only a small effect towards decreasing the downsteam flow,[1,39,30] the combined flows for this problem are assumed to have a negliglble effect on flow rates in any direction and the influence of drag on the pressure flow is considered to be more significant. In this case, therefore, the combined flow in the two component directions is treated as one-dimensional but the common viscosity is determined from an overall shear rate at the wall.

The main assumptions made, therefore, are that,

(a) the effect of drag shear rates in one component direction on the flow in the other direction is small and can be neglected.

(b) the two-dimensional non-Newtonian leakage can be treated as pressure flow alone, because the flow rate is generated mainly by a pressure flow and there is also no net drag flow through the gap.

However, the effect of the drag shear rates on pressure flow is included by using the shear rate at the wall of the combined drag and pressure flow to determine the non-Newtonian viscosity.

(c) the gap is narrow and therefore velocity profiles are influenced mainly by the shear stress at the wall, so that the two components of flow can be coupled by a common viscosity determined from an overall shear rate which is defined by the resultant shear stress at the wall,

$$\tau_R^2 = \tau_x^2 + \tau_y^2 = \mu^2(\dot{\gamma}_x^2 + \dot{\gamma}_y^2) \qquad 3.8.21$$

where $\dot{\gamma}_x, \dot{\gamma}_y$ are the shear rates at the wall of the combined drag and pressure flow in the x and y directions respectively.

The additional procedure which is to be used with the finite element analysis previously described, is to determine the local viscosity (at each nodal point) which must be used with the Newtonian form of the flow equations to obtain the non-Newtonian solutions. The equivalent viscosity method has been used in a finite element type formulation to solve non-Newtonian pressure flow problems[65,66] but, in this case, the method for determining the equivalent viscosity described by Weeks and Allen[34] was found to be suitable and is employed directly in the present FE formulation of the problem. An account of this method has been described by Tadmor and Klein[1] (Appendix VI) and is consistent with the dimensionless coordinate system employed by Krosser and Middleman[37] for one-dimensional non-Newtonian flow (Appendix V).

The procedure used in updating the equivalent viscosity was to determine , firstly, the combined net flow rates in the two component directions from the algaebraic sum of the ideal drag flow rate and the pressure flow rates computed with the previous value of viscosity, and to use these to determine, the velocity profiles for a power law fluid, their individual shear rates at the wall, and the overall shear rate which is

then used to compute the viscosity from the constitutive equation for the melt and thus the equivalent viscosity to be used in the FE formulation to solve the equation once again for the flow rate. In order to include the changing equivalent viscosity in both directions, the additional term, $C_R = k_R(1+K_1)^{s-1}$ is inserted in the transpose of determinant of the dimensions matrix which becomes,

$$B^T = \begin{vmatrix} C_{Rx}b_i & C_{Ry}a_i \\ C_{Rx}b_j & C_{Ry}aj \\ C_{Rx}b_k & C_{Ry}a_k \end{vmatrix} \qquad 3.8.22$$

For zero drag flow, the analysis converges to the pressure flow solutions. For the relevant range of pressure drop used in determining the non-Newtonian solutions, the overrelaxation factor varied from about 1.6 for the lowest value, to 1.8 for the higher values of pressure drop. For the Newtonian solutions, the optimum factor was found to be about 1.5.

3.9 Screw channel flow.

The screws of counter-rotating extruders are usually designed with relatively deep channels and small helix angles in the metering zone. The width to depth ratio, A (aspect ratio) of typical screw channels can vary from 10 to as low as one (square channel) and normally with a pitch to diameter ratio of less than the square-pitch value of one (which is equivalent to a helix angle of about 17.65 degrees). The variation of the helix angle and consequently, also the variation of the width of the channel from top to the bottom of the screw channel is dependent on the depth of the channel, or depth to diameter ratio, H/D. For example, a square-pitched screw with a typical value of H/D = 0.14, the helix angle at the screw root is increased to about 23 degrees and the width decreased by about 5 percent.[1,45] For screws with smaller helix angles, therefore, the variation in dimensions due to the screw pitch is further reduced and is not likely to be significant. In addition, however, the channels of counter-rotating screws are normally trapozoidal-shaped with inclined flight walls. The influence of the flight wall angle on the calculated flow rate along the channel has been found in general to be small for flank angles $\psi' < 12$ degrees and can be neglected.[5] The channel can be treated, therefore, as approximately rectangular-shaped with straight sides.

The helical flow generated in screw channels of extruders consists of a downchannel flow and a cross-channel two-dimensional recirculatory flow with leakages over the flights. In deep channels of twin-screw extruders the downstream flow is likely to be influenced by (a) the flight walls (b) curvature (c) the transverse flow on which the effective viscosity of the melt is dependent (and which includes the turning over of the melt at the flight walls with flow occurring also across the depth of the channel) (d) changes in melt viscosity with increases in temperature produced by the shearing of the non-Newtonian melt and (e) leakages.

The effect of curvature in this problem is likely to be due mainly to the linear variation of velocity from top to bottom of the channel and become significantly larger the deeper the channel. In comparison with the flow in deep channels, the flight leakage is small and therefore, its influence on the channel flow is assumed to be small enough to be neglected.

In order to calculate a downchannel flow rate influenced by the above factors all the governing equations (Appendices I-IV) derived and simplified for two-dimensional flow must be solved simultaneously. This problem of isothermal and non-isothermal non-Newtonian flow in deep rectangular channels have been solved by Dyer[48] using axisymmetrical geometry which approximately accounts for curvature effects. The differential flow equations (together with a suitable constitutive equation for the material and the relevant boundary conditions) were solved using a finite difference method developed by Gosman et al[58] for formulating recirculating flow problems. This method was found by Fenner[30] to produce correct solutions for isothermal Newtonian and non-Newtonian flow in deep channels. It is this FD method of analysis which is used to obtain solutions of flow rate for the deep channels of twin-screw extruders.

For the axi-symmetrical geometry assumed (i.e. with zero helix angle) cylindrical polar coordinates are employed, Figure 3.9.1. The coordinates are taken with reference to the screw and thus, the barrel is treated as rotating about a stationary acrew which is a valid procedure for slow viscous flows. However, the correct barrel velocity components relative to the channel are used in the downchannel and transverse directions respectively,

$$V_{b\theta} = V_b \cos\beta \qquad 3.9.1$$

$$V_{bz} = V_b \sin\beta \qquad 3.9.2$$

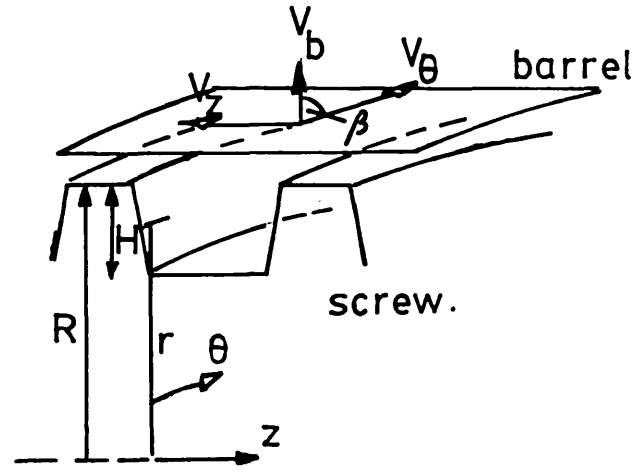

Figure 3.9.1 Channel geometry -axisymmetric, cylindrical polar coordinates.

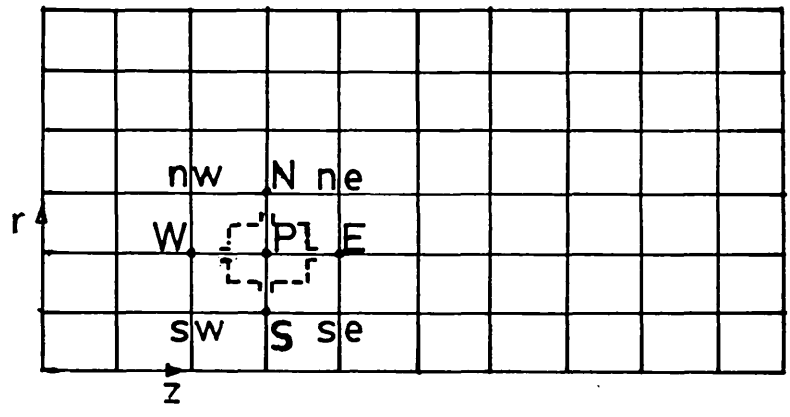

Figure3.9.2 FD grid of rectangular channel.

The flow is assumed to be steady (time - independent), laminar (Reynold's number for the flow is small) and incompressible (constant density). The governing differential equations (of conservation of mass, momentum and energy) can be written to fit a standard form.[58] The momentum equations for the directions r and z are reduced to a single equation by eliminating the pressure gradients $\frac{\partial p}{\partial r}$, $\frac{\partial p}{\partial z}$, from differentiation and subtraction (see equation 3.8.8) and the velocity components v_r and v_z are replaced by the dependent variables, stream function ψ and vorticity ω , defined as,

$$\omega = \frac{1}{r}\left(\frac{\partial v_r}{\partial z} - \frac{\partial v_z}{\partial r}\right) \qquad 3.9.4$$

$$r\rho v_z = \frac{\partial \psi}{\partial r} \quad , \quad r\rho v_r = -\frac{\partial \psi}{\partial z} \qquad 3.9.5$$

the latter, automatically satisfying the continuity equation for conservation of mass (equation B, Appendix I), in two-dimensional flow,

$$\frac{\partial}{\partial z}\left(\frac{\partial \psi}{\partial r}\right) - \frac{\partial}{\partial r}\left(\frac{\partial \psi}{\partial z}\right) = 0 \qquad 3.9.6$$

For the remaining momentum and energy equations, the dependant variables are velocity v_θ , and internal energy U, respectively and are defined as,

$$v_\theta = r\, V_\theta \qquad 3.9.7$$

$$U = C\, T \qquad 3.9.8$$

where C is the specific heat and is taken as a constant, and V_θ is the angular speed in radians.

The boundary conditions for each of the four dependent variables are specified on all four channel walls. The vorticity condition is not usually known and therefore is not specified directly at any of the walls but is obtained from the values of velocity and stream function at and near the wall. A general equation for the vorticity condition on each of the horizontal and vertical walls have been obtained for this problem from a one-dimensional analysis of flow near the wall.[48] There is no net flow

through any of the walls, thus, the stream function must have the same value at all the walls which for convenience is taken as zero, $\Psi = 0$. The angular velocity of the barrel at the top wall is prescribed as the downchannel velocity component, equation 3.9.2, and on the stationary screw surfaces, $v_\theta = 0$. There are various temperature conditions which can be specified at the boundaries. For adiabatic operations, where no heat is gained or lost through the screw surfaces, the temperature gradient $\frac{\partial U}{\partial n} = 0$ can be prescribed, where n is the direction normal to the surface of interest. Also, the temperature of the barrel is known and the condition, $U = C\ T_o$ can be prescribed at the top wall, where T_o is a referance temperature which, for this problem, is taken as the barrel temperature.

The information on the properties of the polymer melt is supplied by the power law form of the constitutive equation given by equation 2.4.5. The viscosity is related to I_2, the second invariant of the rate of deformation tensor which in equation 2.4.4 is the form used in cylindrical coordinates.

The differential equations are transformed into finite difference equations derived for a grid, shown in Figure 3.9.2, covering the flow area using the 'tank and tube' finite difference analogue of the equation suggested,[58] in which integration is performed over the finite areas around a typical node P. Each FD equation is expressed in terms of the value of the variables of the surrounding nodes and the integration of the differential equation is performed over the area shown by the broken lines which enclose the nodal point P. The set of algebraic equations derived from the differential equations and the boundary conditions connect the values of the dependent variables at the grid nodes with each other. The algebraic equations for all the grid nodes are solved using the Gauss-Seidal iterative successive substitution method. The successive-substitution technique is used to update the values of the variables at each node after each cycle of

iteration. When the equations are numerous and are made non-linear (as in this case, by the non-Newtonian nature of the flow), this technique must be employed. For non-Newtonian flow, the viscosity is computed from the power law constitutive equation and also updated after each cycle of iteration. The criterion for convergence employed is when the relative error is less than a small tolerance, 10^{-5}. Although overrelaxation to improve convergence can be used, it can sometimes cause divergence of vorticity[58] and for this problem, this was found to be the case. The grid size used was 15 rows by 21 columns and the digital computer employed for solving the equations was a CDC 7600.

The flow characteristic is plotted for each screw channel geometry using dimensionless flow rate and pressure gradient terms,

$$\text{flow rate, } \pi_Q = \frac{Q}{V_{b\theta} WH} \qquad 3.9.9$$

$$\text{pressure gradient, } \pi_p = \frac{H}{\bar{\tau}} \frac{\partial p}{\partial \theta} = \left(\frac{H}{V_{b\theta}}\right)^n \frac{H}{k'} \frac{\partial p}{\partial \theta} \qquad 3.9.10$$

where $\bar{\tau}$ is the average shear stress, $\frac{\partial p}{\partial \theta}$ is the pressure gradient, and Q is the upchannel flow rate (taken relative to the intermeshing region) since this is the channel flow which influences the leakages through the intermeshing region, and this flow is normalized with the maximum plain downstream flow rate, $V_{b\theta}WH$, which is convenient to use because the FD flow rate solutions can be compared directly with the parallel plate solutions for plain flow and, also is the form employed in the numerical procedure, described in the next section, for matching the channel and leakage flows.

The dimensionless numbers, the Péclet number which represents the ratio between convective heat transfer and conductive heat transfer, and the Brinkman number which determines whether imposed barrel temperatures or heat generation are dominant in effective temperature changes in the melt, are used in the form,[24,53]

$$Pe = \frac{\rho c_p H V_{b\theta}}{k} \quad , \quad Br = \frac{b_o \mu_o V_{b\theta}^{n+1} H^{1-n}}{k} \qquad 3.9.11$$

This Brinkman number is in a similar form to what was defined by Martin[24] and is now referred to as the Griffith number (see section 2.6).

3.10 Numerical Procedure for matching channel and leakage flows.

In the previous sections, the analysis of the individual flow in each gap and chamber resulted in the solution of flow equations which can now be used to simulate the performance of the machine. For each chamber and associated leakage gaps, the flow rates are inter-dependent because of the flows generated internally in the passages due to drag and pressure and also because of the axial back-pressure drop over each chamber. It is assumed that the drag and pressure flow component in the direction along the channel influences the leakages through the calender and side gaps, whilst the component in the axial direction influences the leakages over the flight and through the tetrahedron gap. Because the net flow through the calender gap, side gap and channel are all dependent on the net axial pressure drop over each chamber, the leakages must be balanced simultaneously against the channel flow, Figure 3.10.1a. This is not the case, however, for the flight and tetrahedron leakages because the latter has already been determined at the net axial pressure drop and only the flight leakage has to be coupled to the net flow rate resulting from the difference between the axial channel component of flow and the tetrahedron leakage, Figure 3.10.1b.

To obtain the required leakages for a given pressure drop and net flow rate through the channel and gaps, a numerical procedure was employed on a digital computer. A trial-and-error iterative procedure[62] which was developed for one-dimensional lubricating melt flow in a tapered clearance is adopted. In the procedure, the pure drag flow, VHW/2 (which is the one-dimensional net flow rate for a tapered clearance; section 2.5) is used to compute pressure gradients for flow through small elements of the clearances and the pressure summed over the clearances and compared with the prescribed value at the boundaries. The procedure is repeated each time for a new position of drag flow rate, until the correct net flow rate and pressure drop is obtained for the clearances.

The pure drag flow condition can be found by trial-and-error since it is related to the final pressure computed at the boundary.

The application of the method to the matching of the channel and leakage flows involves obtaining, first of all, the pressure drop over each flow passage for a selected drag flow rate and then comparing the net pressure drop obtained with the prescribed value over a chamber. For the tapered calender gap, the net drag flow is situated somewhere along its length between the maximum channel depth and the minimum calender depth. However, if the flow generated locally in the calender gap is overshadowed by the effects of back-pressure flow, the iterative procedure will converge to pure drag flow in the channel, a condition which is unlikely to exist in the extruder because a high pressure is always developed where the rotating screw surfaces converge.[2,5] Now, when considering the balanced flow through the side gap (which has a constant clearance depth) and the channel, the net pure drag flow rate can be cho sen, using the iterative procedure, from a linear tapered passage with a maximum depth equal to that of the screw channel at one end, and a minimum depth equal to that of the gap at the other end. For flow in the axial direction, however, the net flow rate can be larger than the pure drag flow in the channel if there exists a large flight and tetrahedron leakage (see Figure 2.2.4) and for this case, the pure drag flow rate is chosen from a tapered passage with a maximum depth equal to twice that of the screw channel.

When there is only one leakage flow to be matched to the channel flow, the iterative procedure is no longer required when the flow is Newtonian because there would then be a linear relationship between the net pressure drop and flow rate and the leakage can be determined exactly by linear interpolation from two computed solutions. For two leakages to be balanced simultaneously against the channel flow, the iterative

procedure is carried out, firstly, for each leakage gap separately and, because both leakages must decrease when coupled under the same pressure conditions at the boundaries, the estimates obtained can be used as upper limits in the same procedure but this time using the combined leakages as the net flow rate required for computing the pressure gradient in the channel.

To determine the pressure gradient for a given flow rate the relationships obtained from the analyses given in the previous sections are used. To obtain a one-dimensional solution from the non-Newtonian flow equations (given in Appendix V), the dimensionless coordinate, ξ, for each type of flow is computed as a root of the equation using Newtonian's approximate method when the equation is expressed as a function equal to zero.[63] For each dimensionless flow rate assumed, the dimensionless coordinate obtained is used to determine the dimensionless pressure gradient term and consequently, the constant pressure drop for flow through either, the uniform gap, or small elemental sections of the tapered calender gap. For deep channel flow, the required solution is obtained by linear interpolation between chosen points on the flow characteristic. For this purpose, the characteristic is defined by ten or more points which are conveniently choosen so that each short section of curve is represented as accurately as possible by a straight line.

Non- Newtonian viscosity of the melt at the operating temperature and for a limited shear rate range can be used for determining solutions. To obtain solutions at individual screw speeds and to cover a wider range of shear rates at each speed, the melt viscosity at the mean shear rate V/H for each flow passage is obtained from the viscosity flow curve (see Figure 2.3.5) by using linear interpolation - similar to the procedure already described above for obtaining deep channel solutions.

Finally all the leakage flow rates computed for the twin-screw extruder are summed using the equation,

$$Q_l = 2Q_f + Q_t + 2m\,(\,Q_c + Q_s\,) \qquad 3.10.1$$

and these leakages are subtracted from the theoretical output to give the actual output rate,

$$Q = 2mNVol. - Q_l \qquad 3.10.2$$

The throughput rate versus pressure drop characteristic for each screw geometry is plotted using dimensionless terms,

$$\frac{Q}{2mNVol.} \quad ; \quad \frac{\Delta P}{k' N^n} \quad \text{or} \quad \left(\frac{\Delta P}{k'}\right)^{1/n_1} \frac{1}{N}$$

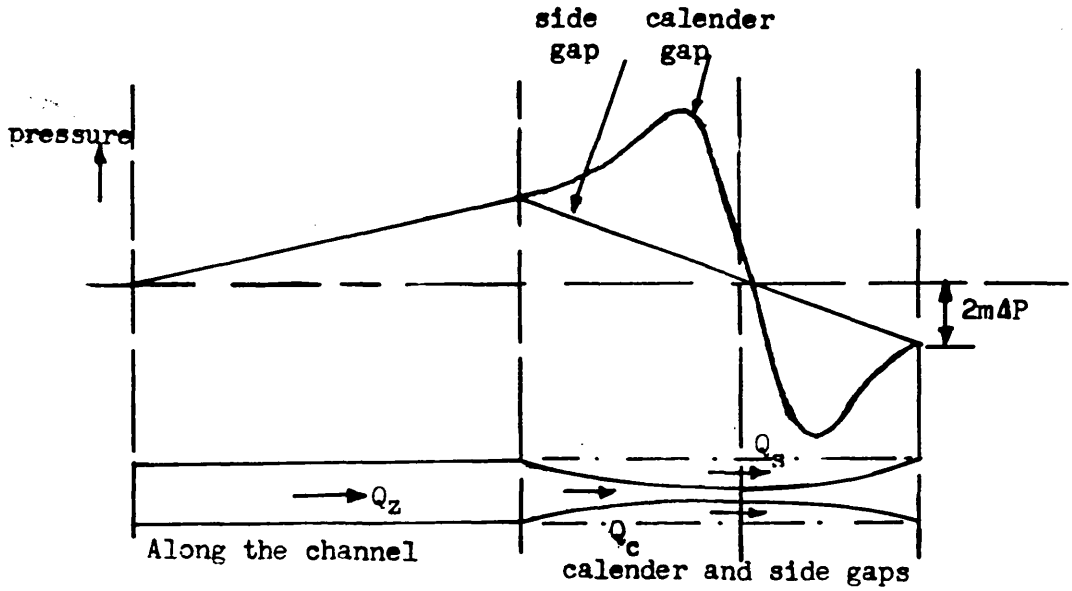

(a)

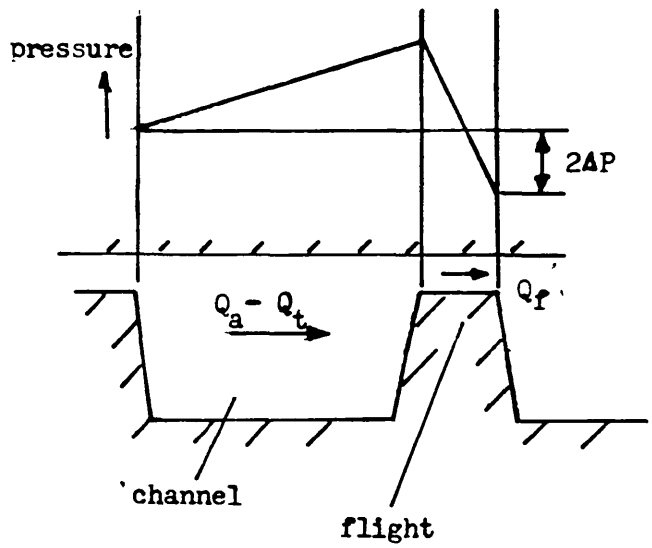

(b)

Figure 3.10.1 Pressure distributions to be computed in the channel and, (a) calender and side gaps, (b) flight gap.

3.11 Theoretical solutions.

In this section, typical solutions obtained from the various flow analyses are presented and comparisons made, where possible, with published solutions. For deep channel flow with curvature, Fenner[30] found errors in Dyer's computer program and therefore, no satisfactory comparisons could be made with published solutions.[48] However, since the only other isothermal and non-isothermal solutions for flow in very deep channels available, were those published by Martin[24] for plain flow in rectangular channels, the solutions of the finite difference analysis used were checked against Martin's results. The plain flow solutions in deep channels were obtained using cartesian coordinates which was included in the general coordinate system used in the FD analysis.[58] In Table 3.11.1 are given a few comparisons of theoretical solutions for isothermal and non-isothermal flow. In general, the agreement was found to be within 5% which was considered to be good.

In Figure 3.11.1 is plotted the deep channel and one dimensional solutions for Newtonian flow in a screw channel using dimensionless flow rate and pressure gradient terms. These solutions were obtained for the dimensions of the extruder screws used by Janssen[5] and are given for flow in the up-channel direction taken relative to the intermeshing region (since this is the channel flow which influences the leakages: see Section 2.2). In comparison with the one-dimensional solutions, higher channel flow rates and consequently, higher leakage flow rates can be expected when using these deep channel solutions for the same pressure gradients. Therefore, for Newtonian flow in twin-screw extruders with relatively deep screw channels, there is a strong case for using deep channel solutions to determine leakage flow rates. There is a significant difference, however, between the deep channel solutions with and without the effects of curvature included, as expected, with a lowering

Table 3.11.1 Comparison of Two-dimensional Deep channel solutions.

Cartesian coordinates: Aspect Ratio, A = W/H = 1.0

Helix angle, $\beta = 20^{\circ}$

Newtonian: n=1.0

	Martin (ref.24)	finite difference method used.
π_p	π_Q	π_Q
0	0.250	0.2505
4	0.115	0.117

Isothermal non-Newtonian: n=0.6

	Martin (ref.24)	FD method used.
π_p	π_Q	π_Q
0	0.2064	0.2124
3	0.110	0.1085

Non-isothermal non-Newtonian: n=0.6, A = 5.0, $\beta = 17.7^{\circ}$, $B_r = 4$, $P_e = 3500$, $T_b = 150^{\circ}C$.

	Martin (ref.24)	FD method used.
π_p	π_Q	π_Q
0	0.409	0.420
2	0.085	0.081

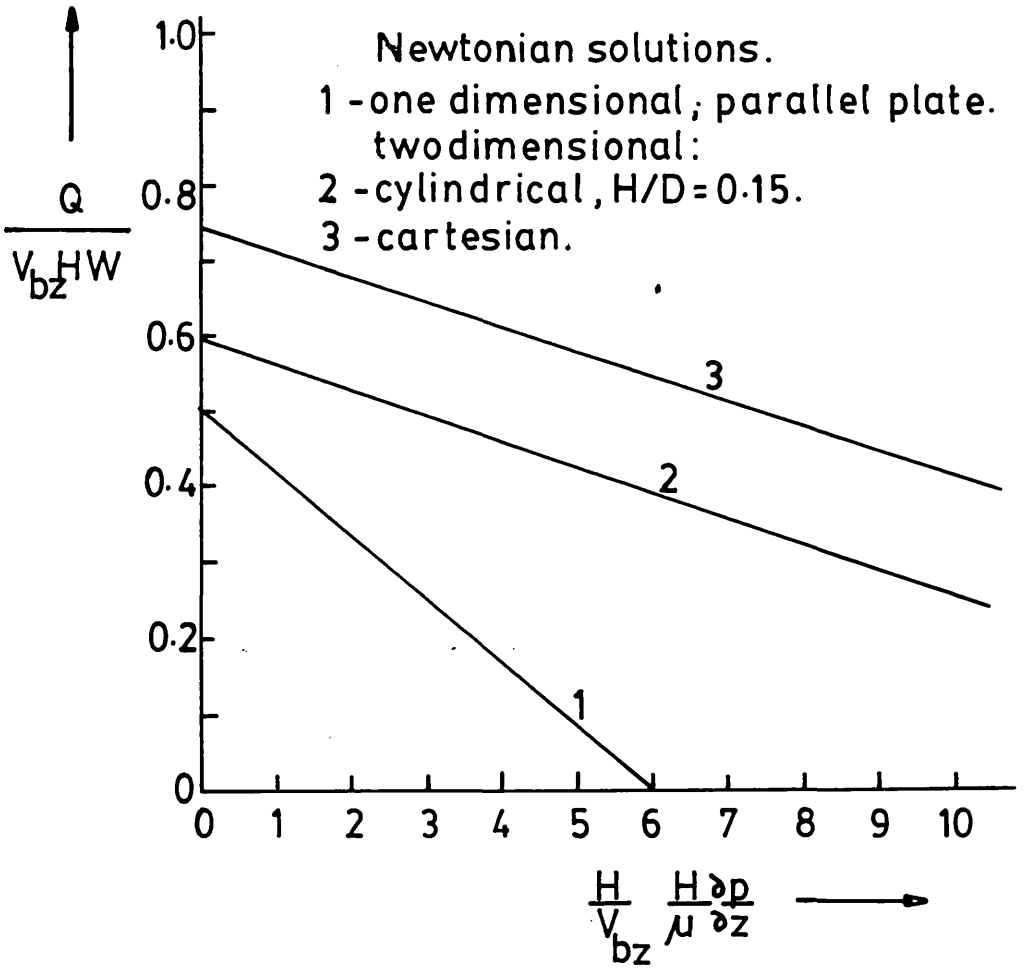

Figure 3.11.1 Dimensionless flow rate against pressure gradient, A = 1.

of the flow rate due to curvature because of the linear reduction of the surface velocity from top to bottom of the screw channel. There is likely to be, therefore, gross overestimation of flow rates if plain deep channel solutions are used to determine leakages.

Figure 3.11.2 gives typical solutions for isothermal and non-isothermal non-Newtonian flow in deep channels together with the isothermal one-dimensional solutions. For isothermal non-Newtonian flow in curved deep channels, the flow rate is increased compared with one-dimensional flow but is significantly reduced compared with plain flow in deep channels. When temperature effects are included, however, the non-Newtonian flow with curvature is further reduced and the solutions become closer to those of isothermal one-dimensional flow. These temperature effects are accounted for by using the boundary conditions for an insulated screw and isothermal barrel which are considered to be appropiate for melt flow in deep channels.[24,48] If these are valid operating conditions in twin-screw extruders, then the results indicate that, with melt flow, using the isothermal deep channel solutions with curvature is likely to produce an overestimation of the throughput rate in the channel and consequently an overestimation of the leakage flow rates.

Considering Newtonian flow through the tetrahedron gap, an empirical formula for the flow rate was obtained by Janssen[5] from tests performed with stationary models of the gap. Solutions of this formula shows that the relationship between leakage flow rate through the tetrahedron gap, Q_t, and the axial pressure drop is linear and goes through the origin. Table 3.11.2 gives the solutions obtained from the empirical formula and from the FE two-dimensional flow analysis used. The results given are equal to $Q_t \mu / \Delta P$ and are for dimensions taken from the two different pairs of screws tested by Janssen. The two-dimensional solutions given are for constant pressure gradients prescribed at the

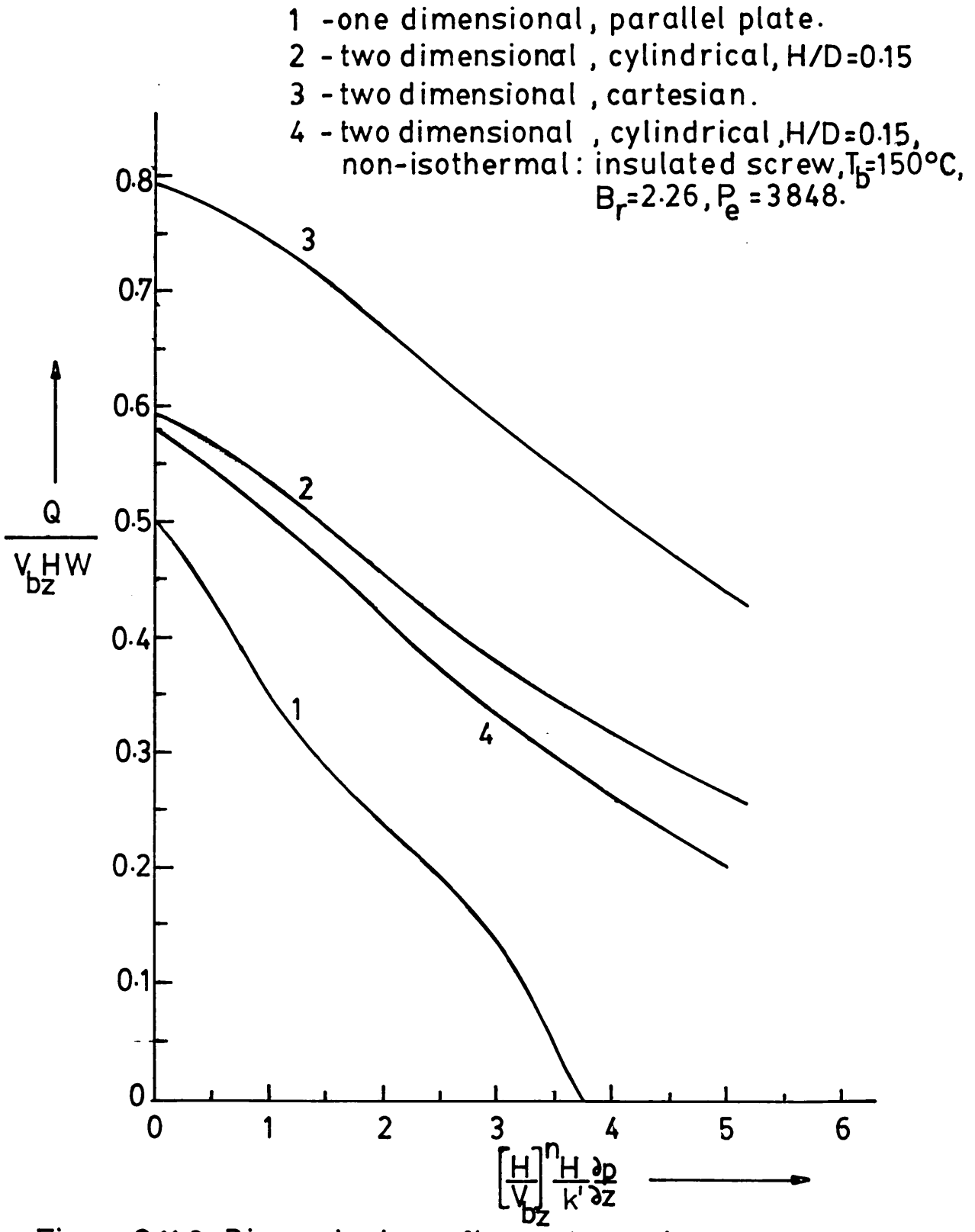

Figure 3.11.2 Dimensionless flow rate against pressure gradient. n = 0.466, T_o = 150°C, β = 5.19°, A = 1.

Table 3.12.2 Comparison of Tetrahedron leakages - Newtonian Solutions.

	Newtonian solutions: $\frac{Q_t \mu}{\Delta P}$ (x 10^{-8}), $\mu = 1.0$			
calender gap, σ mm.	1.25	0.76	0.34	0.2
(ε = 0.05mm., ref.5)				
Formula (ref.5) given below.*(1)	0.243	0.207	0.179	0.170
2D- Finite element method.*(2)	0.224	0.207	0.186	0.181
2D- FE method.*(3)	0.207	0.193	0.183	0.170
calender gap, σ mm.	1.5	0.2		
(ε = 4.0mm, ref.5)				
Formula (ref.5).*(1)	2.036	1.934		
2D- FE method.*(2)	1.810	1.741		
2D- FE method.*(3)	2.003	1.991		

*(1) Janssen's formula (ref.5) for the tetrahedron gap:

$$Q_t = 0.0054 \frac{\Delta p}{\mu} R^3 \left(\frac{H}{R}\right)^{1.8} \left(\psi' + 2 \left(\frac{\varepsilon + \sigma \tan \psi'}{H}\right)\right)^2$$

*(2) full pressure boundary condition prescribed.

*(3) zero pressure drop prescribed along the calender passage.

boundaries and in comparison with the experimental results, are the correct order of magnitude and there is satisfactory agreement. Comparison of solutions obtained with a constant pressure gradient and a zero pressure gradient at the boundary along the calender passage showed a reduction for small but an increase for large side gaps. High pressure boundary conditions of this type are likely to have a significant effect on shear flow of non-Newtonian melts and is considered to be important and must be included. Flow rates were also obtained with stream function type boundary conditions by assuming no flow to occur through parts of the boundary where constant values are prescribed. Specifying flow only through the boundaries along the calender duct, i.e. in through BB' and out through CC' and assuming no pressure gradient along these boundaries, Figure 3.7.1, produced a leakage flow rate (corresponding to a pressure drop of ΔP) which was approximately twice the empirical value and which was about equal to that obtained from a one-dimensional analytical solution for pressure flow, equation 3.8.4, integrated and summed numerically over the whole flow region. In order accurately to predict leakage flow rates, therefore, it appears that flow through parts of the boundary cannot be neglected. In general, the results show that most of the leakage flow is concentrated near the edge of the intermeshing region at A and A', Figure 3.7.1, where the gap tends to be shortest and deepest with only a small proportion distributed over the relatively large and shallower area at the middle. The leakage flow rate of the tetrahedron gap is influenced, therefore, mainly by the flow behaviour in the region near the sides of the gap.

Figure 3.11.4a gives the dimensionless throughput rate plotted against pressure gradient for Newtonian flow in a completely filled counter-rotating twin-screw extruder. The experimental and theoretical results from Janssen's work are given and compared with predictions obtained for a power law index of n=1 from the non-Newtonian flow model

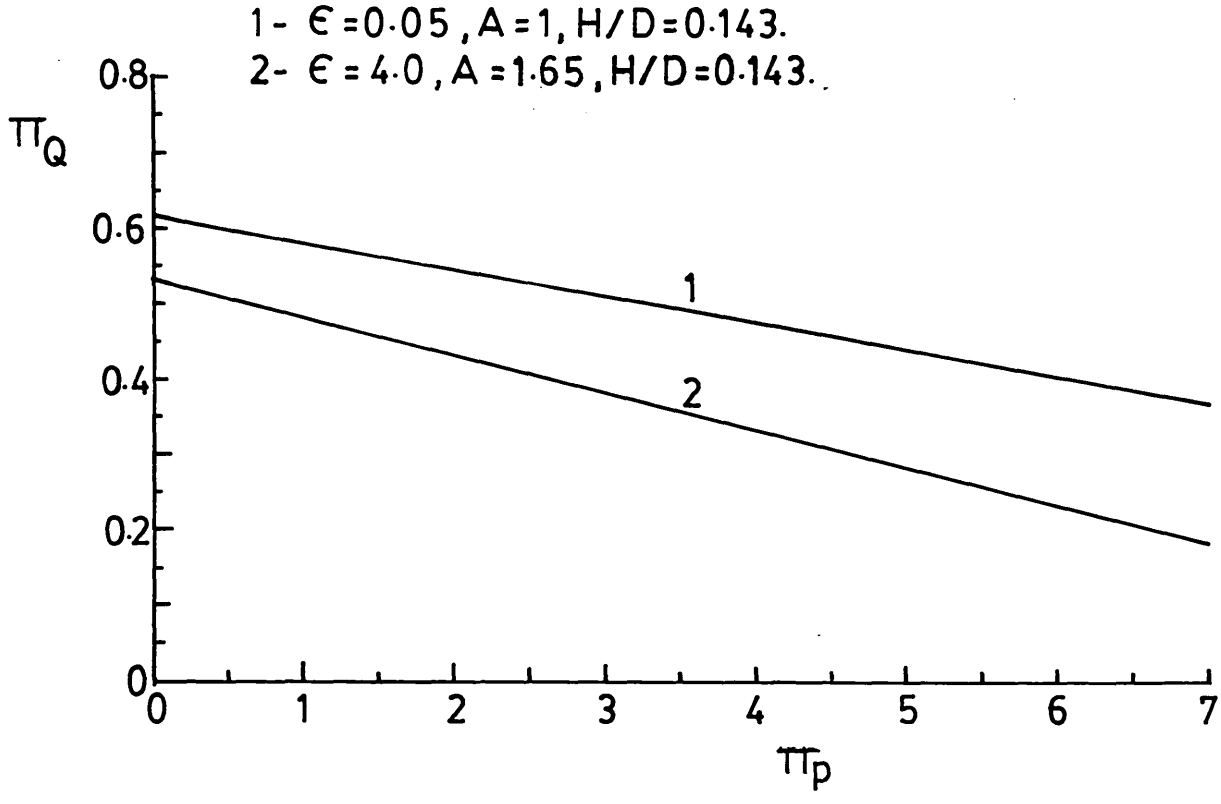

Figure 3·11·3 Dimensionless flow rate versus pressure gradient. Newtonian flow in channel of screws used in ref (5).

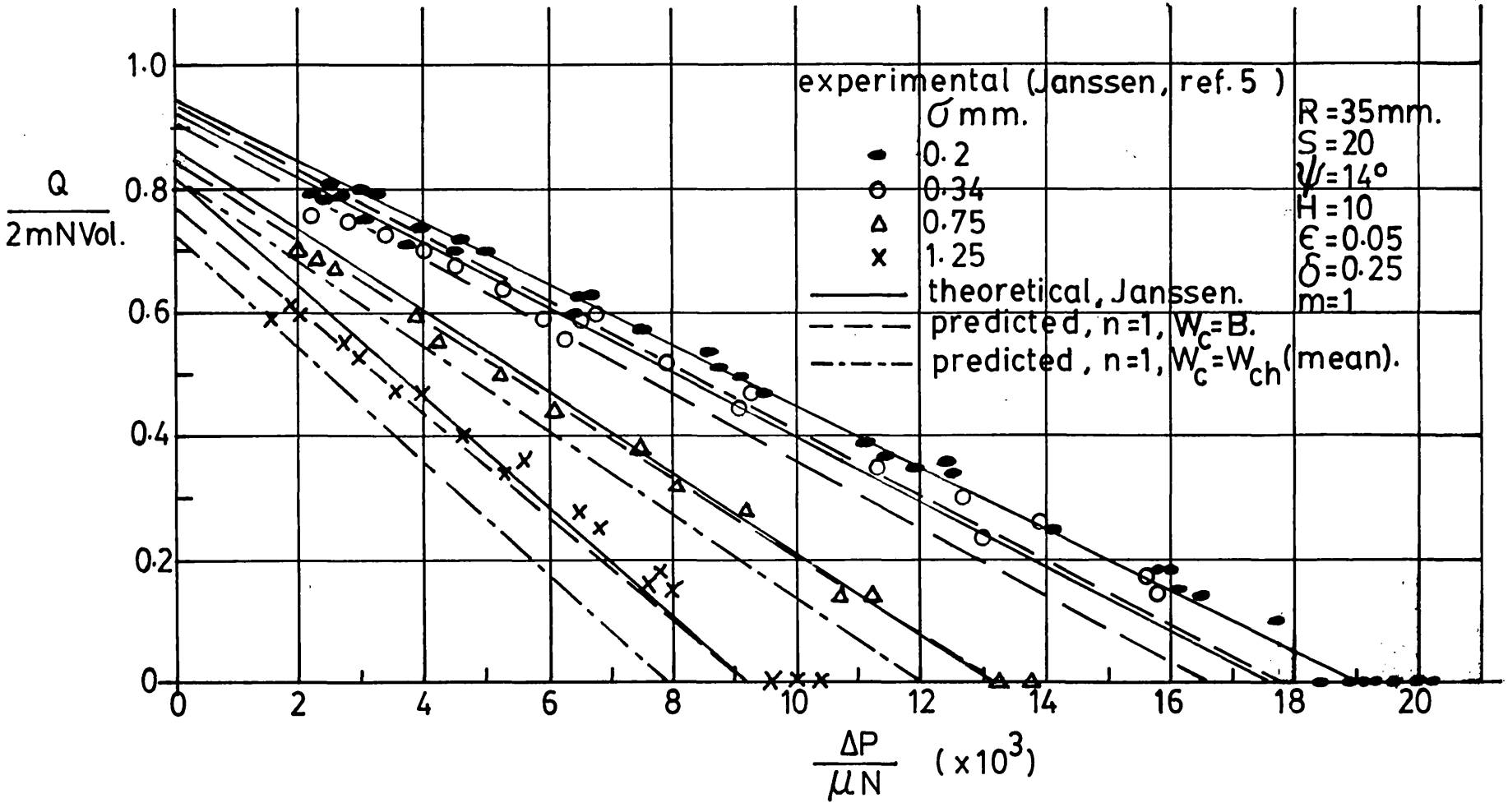

Figure 3.11.4a. Dimensionless throughput rate versus pressure drop, Newtonian flow.

Figure 3.11.3 gives the deep channel flow solutions used for the predictions. developed. The experimental results were obtained from tests performed on a twin-screw extruder with a split barrel arrangement in which the depth of the calender gap was varied by altering the centre-line distance of the two screws (and the degree of intermeshing) with shims packed between barrel halves, and as a result the tetrahedron and side gap dimensions were also varied. For each calender gap examined, the plot of dimensionless terms produced a characteristic which was linear and independent of both the screw rotational speed and the fluid viscosity. With the extruder opened at the die, the back pressure drop is zero and the machine produces the largest throughput rate possible for each geometry, limited by the leakages which can be produced only by the drag and pressure flows generated internally in each chamber and associated leakage gaps. When there is a build up of back pressure along the extruder, however, as a result of the flow restriction at the die, leakages are increased in order to reduce the output rate, thus balancing the net throughput rates of the machine and die, the limiting value of pressure gradient and leakages for zero output determined by the size of the gaps.

For the set of screws examined, the side and flight gaps were small so the significant leakages passed mainly through the tetrahedron gap, and through the calender gap when its depth was significantly increased. When flow was treated as one-dimensional in the side and calender clearances, an overestimation of the total leakage flow rate was obtained, as illustrated, but in general, the error produced in predicting throughput rates was not very large. For instance, the error in the flow rate obtained when comparing the predictions for very small calender gaps with Janssen's theoretical curve was less than 5% of the ideal theoretical throughput, but was a large proportion of the actual net throughput rate at large pressure drops. The calender and side gaps were so small that their contribution to the overall error was negligible. The largest leakages generated with these small calender gaps,

therefore, are those due to flow through the flight and tetrahedron gaps and only a small overestimation of the leakage through the latter was sufficient to magnify the error considerably, especially with large pressure drops.

When deep-channel downstream solutions were used for these gaps, the improvement was small without producing much of an increase in the throughput rate of the machine. This was because deep-channel solutions had more influence on the flow through the deepest end of the calender passage near the inlet where the pressure gradients and thus pressure build up tended to be small compared with those for the much shallower clearances, and therefore the effect on the overall pressure drop was small.

For large calender gaps, however, a comparison of Janssen's predicted and experimental results show that the predicted throughput rate at zero pressure drop is overestimated and the estimated curves should not have been so steep. There was a small improvement in the throughput rates at $\Delta P = 0$ compared with Janssen's predictions using the one-dimensional flow in the calender passage and a calender width equal to the axial width of the flight, i.e. with $W_c = B$. However, when the calender gap width was put equal to the mean width of the channel (as did Janssen[5] who used instead the width of the top of the channel) the throughput rate at $\Delta P=0$ became comparable to the value which the experimental measurements appear to converge to but the curves remain approximately parallel to the origional predicted curves. This effect was negligible with the low values of calender gap which suggests that overestimation of the leakage flow rate could have been due to an error in predicting the tetrahedron leakage. It was found also that the analytical equation for one-dimensional flow through the calender gap derived by Janssen[5] produced a larger leakage for a given pressure drop than the present numerical method used here. Although the flow through the calender passage was found to be sensitive to the dimensions near the minimum gap, large variations of

depth dimensions at the deeper end can be tolerated without producing significant variations in the leakage flow rate. This was because the pressure gradients in the deeper end tended to be relatively small compared with those at the much shallower region in the middle and the overall pressure drop was influenced mainly by the larger pressure gradients in the latter region. When comparing theory with experiment, therefore, it is important to have an accurate measurement of the calender gap.

Figure 3.11.4b gives similar results for the other set of screws which contained a much larger side gap than the first tested by Janssen.[5] For this set of screws which contained very large side gaps, there was an underestimation of the leakage flow rate which in general was not very large, but the slope of the predicted curves showed a behaviour which was similar to the experimental measurements. Again, the use of the width of the channel for the calender gap width instead of W_c=B, produced a better correlation of throughputs at ΔP=0 but gross overestimation of the leakages was obtained with the large calender gap and very little with the smaller gap. In this case, therefore, there is instead an underestimation of the leakage flow rate, probably due to the effect of the increased side gap. Using one-dimensional solutions for flow in the screw channel would further reduce the leakages and therefore make the predictions worse. The predictions obtained from the non-Newtonian flow model for n=1 are considered to be in good agreement with the experimental results over the range of geometries examined and it appears that one-dimensional solutions are adequate for simulating leakage flow behaviour in the flight, calender and side gaps whilst deep channel solutions must be used for the screw channel flow.

Figure 3.11.5 gives the throughput rate versus pressure drop relationship for non-Newtonian flow in the tetrahedron gap. The dimensions are for the twin-screw extruder used in the melt conveying experiments (Chapter 4). The solutions given are for pressure flow and a constant pressure gradient prescribed along all boundaries. There is, initially, a less than proportionate rise in leakage flow rate with

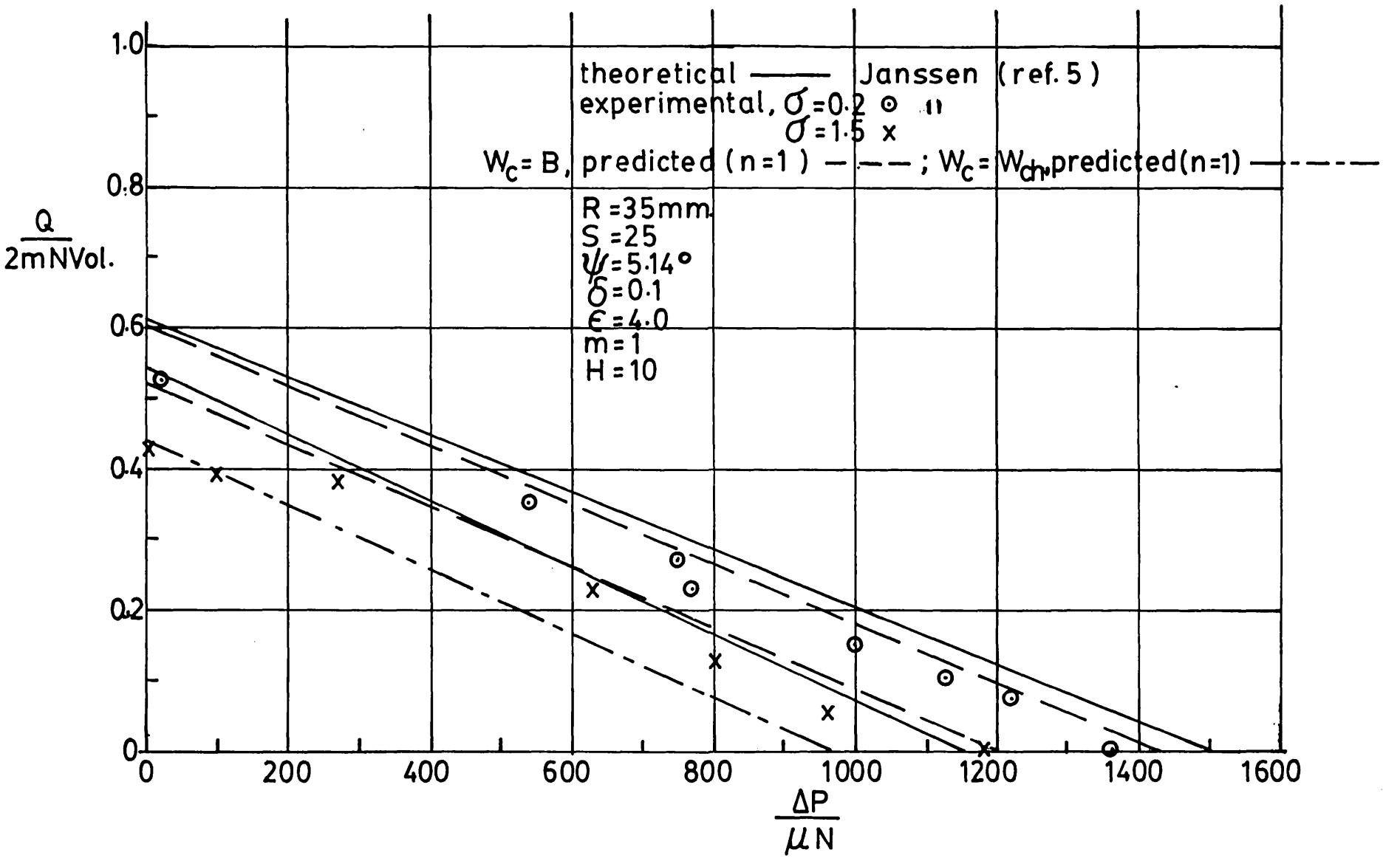

Figure 3.11.4b. Dimensionless throughput rate versus pressure drop, Newtonian flow.

increasing pressure drop but finally a rapid increase occurring at higher pressure drops. In the region of very low pressure drop, the pressure flow is most likely to be influenced by shear rate due to pure drag flow and the viscosity will be constant in each small element of flow, dependent only on the local drag shear rate. The flow behaviour, in this case, is given by the linear characteristic which was obtained for a rotational speed of the screws of 30rpm. For higher speeds, similar characteristics can be drawn which would be situated not very far above the linear characteristic given. Similar flow behaviour has been found in the tetrahedron gap by Janssen[64] from tests performed on rotating screws extruding a polymer solution. The fluid was highly non-Newtonian and a screw speed of up to 60 rpm. and a pressure drop of up to 3.2 kN/m^2 were used. The relationship between tetrahedron leakage and pressure drop with screw rotation was found to be linear over the range of pressure drop used, even at very low screw speeds, and as would be expected, the flow rates and thus the gradients of each characteristic increased with speed. The flow curve for no rotation was of a similar shape to that given in Figure 3.11.5. The linear form of the characteristics indicates that fluid viscosity is dependent mainly on screw speed at low pressure drops. In other words, the velocity profile generated at each point in the flow is dependent on a viscosity which is kept constant as a result of the shear rate produced only by the resultant drag of the surfaces rotating at a constant relative speed. This flow is likely to become non-linear only when a large proportion of it is generated by die pressure. Figure 3.11.6 shows the throughput rate versus pressure drop characteristic for a tetrahedron gap with a relatively small clearance depth. The large drag shear rate developed over the speed range in this case, has a significant effect on leakages even at very large pressure drops but the flow rates are much smaller because of the reduced gap size. The effect of

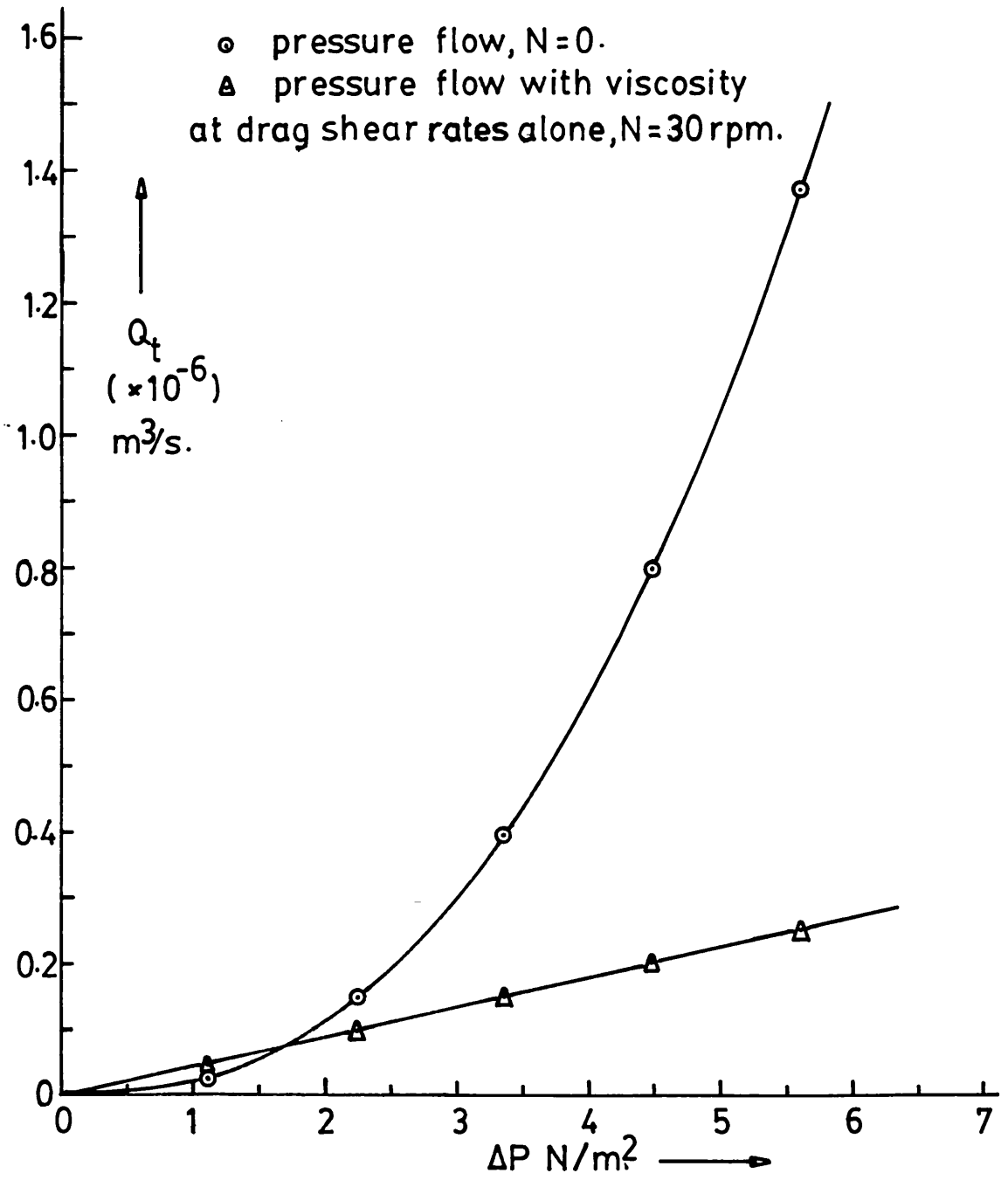

Figure 3.11.5 Tetrahedron leakage flow rate against pressure drop, $n = 0.41$, $\mu_o = 18.5\ kNs/m^2$, - large gap. (screws A, Chapter 4)

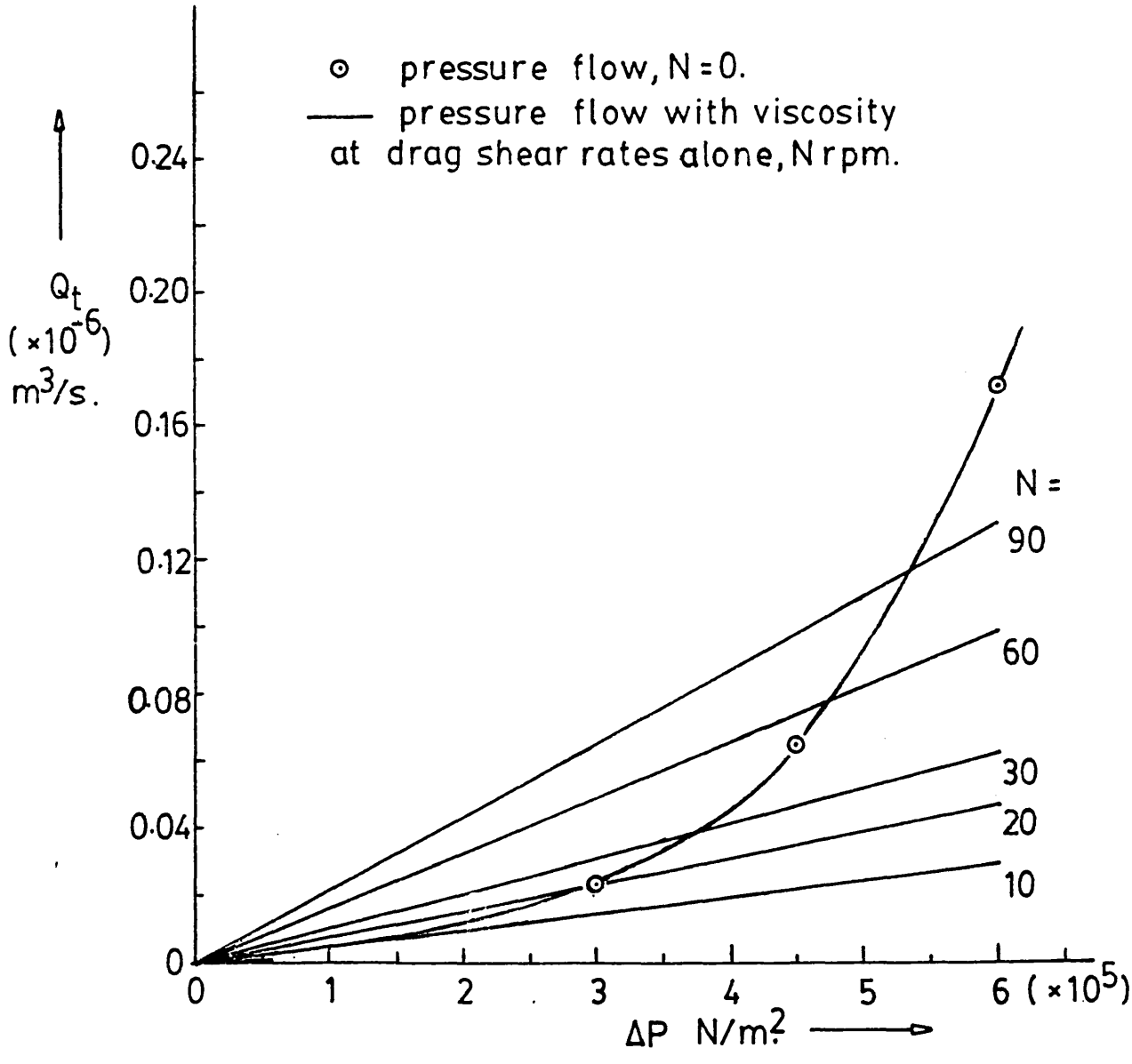

Figure 3.11.6 Tetrahedron leakage flow rate against pressure drop, $n = 0.326$, $\mu_o = 17.5 kNs/m^2$, - small gap. (screws B, Chapter 4)

screw speed on leakages is much less significant (as shown in Figure 3.11.5) when tetrahedron gaps and thus leakage flow rates are larger. Low-pressure flow through large tetrahedron gaps, however, is not likely to exist during normal operations since the extrusion of high viscosity melts usually require large pumping pressures at the die, resulting in the development of large pressure gradients along the melt conveying zone. The limitation on the range of pressure gradients that was obtained from extrusion tests conducted with screws containing large tetrahedron gaps tends to suggest that this is the case (see Chapter 4). An examination of the theoretical results obtained using typical back-pressure gradients reveals that most of the leakage flow passes through the shortest part of the tetrahedron gap.

Figures 3.11.7 to 3.11.9 give the relationships for non-Newtonian leakage flow rate against pressure drop for the tetrahedron gap of screws used in the experiments described in Chapter 4. These solutions were obtained from the approximate method described (in section 3.8) for including the effects of a combined drag flow with the pressure flow. In Figure 3.11.8, the solutions are given for a large tetrahedron gap, a speed range of 0-50rpm, and for the range of pressure drops measured in typical experiments. The largest computed solution of about $1.36 \times 10^{-6} m^3/s$ for pressure flow (N=0), corresponds to a leakage of about 4.6 kg/hr. which is a significant proportion of the ideal throughput rates for this screw at the speeds 30 and 50rpm (see section 4.7), but the effect of screw speed is only to increase the leakage by a small amount. It can also be seen that curves for rotational speed show almost a linear behaviour at the very low pressure drops, similar to that shown by experiment.[64] In Figure 3.11.8, solutions are given for the same screws but using parameters of a power law fluid which corresponds to a higher temperature and thus a lower viscosity. In this case there is a steeper rise of leakage flow rate

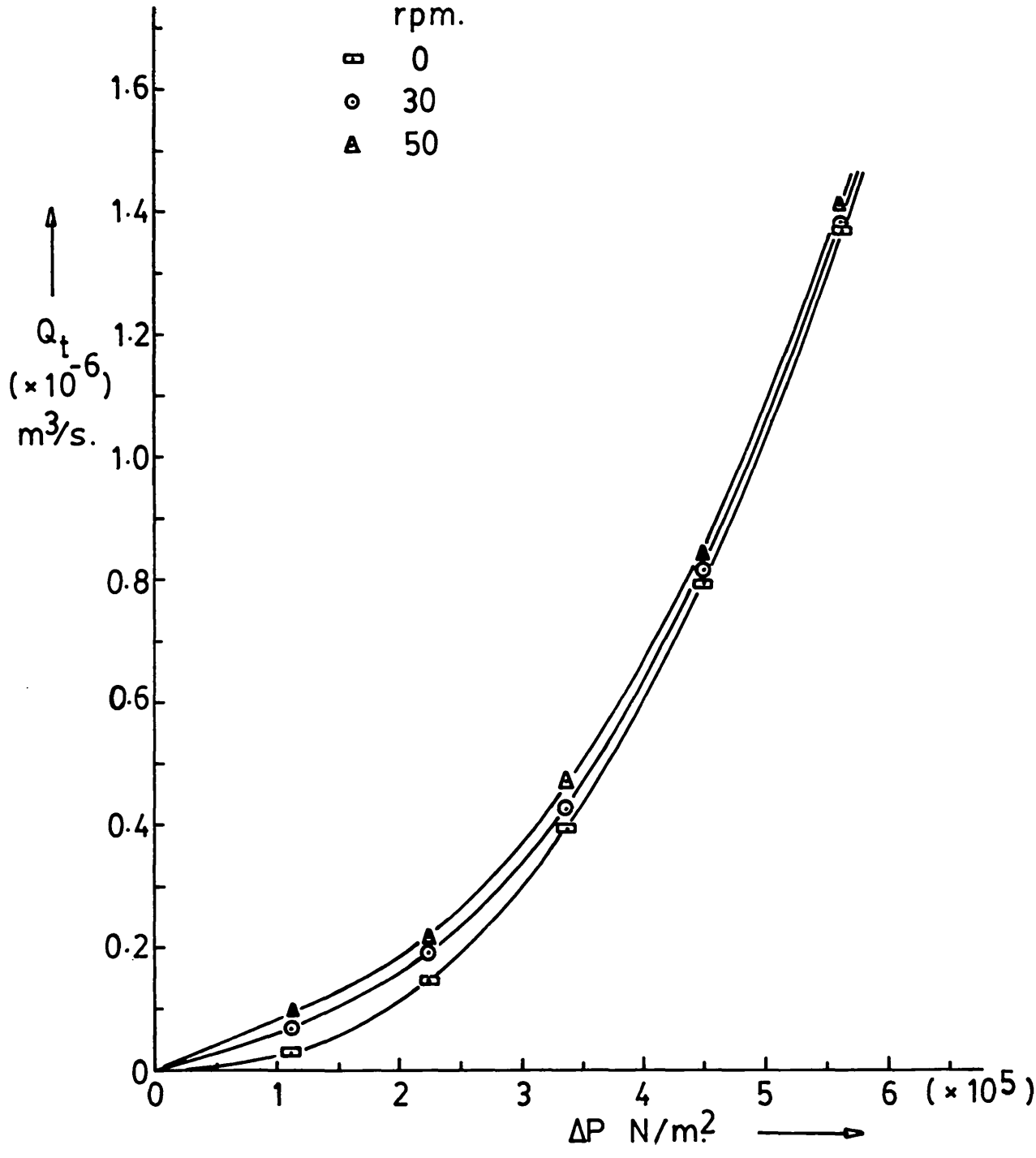

Figure 3.11.7 Leakage flowrate against pressure drop for the tetrahedron gap, $n = 0.41$, $\mu_o = 18.5\ kNs/m^2$, screws A.

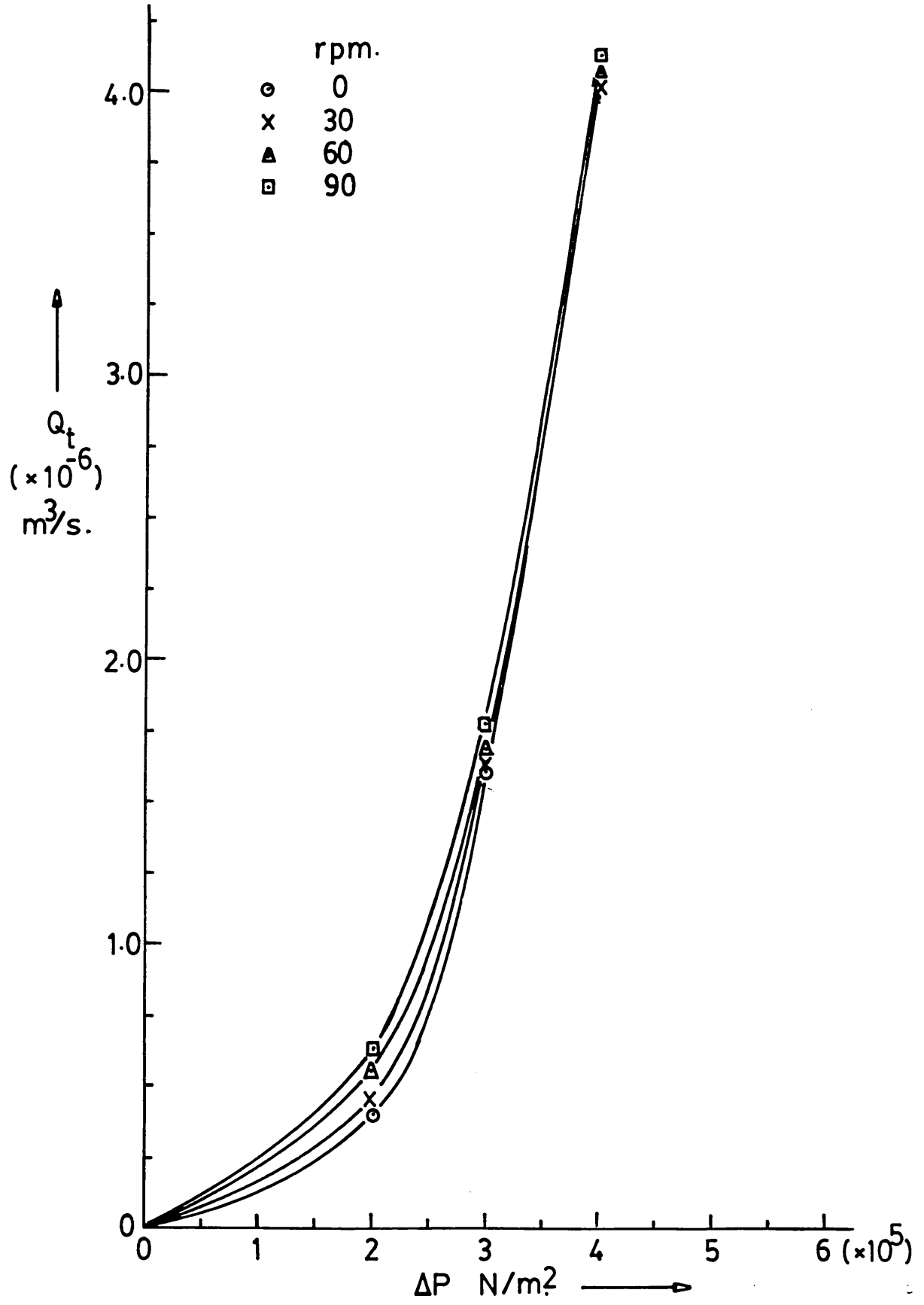

Figure 3.11.8 Leakage flow rate against pressure drop for the tetrahedron gap, $n = 0.356$, $\mu_o = 11.5\ kNs/m^2$, screws A.

with increasing pressure drop as would be expected with a lower viscosity. The maximum pressure drop measured by experiment with this viscosity would not be as high as in the previous case since small pressure gradients would be required to generate the same leakages through the gap. In Figure 3.11.9 are given the flow curves for a relatively small tetrahedron gap. The leakage flow rate for pressure flow alone is very small and although the effect of rotational speed inthis case is much more significant, the largest solution computed at 90rpm of about $0.55 \times 10^{-6} m^3/s$ (or 1.92kg/hr.) is still quite small and only likely to be significant at the very low screw speeds.

Figures 3.11.10 and 3.11.11 give some deep channel solutions computed for the geometry of screws used in extrusion experiments given later in Chapter 4. The dimensionless flow rate given is for the flow conveyed with the screw in the upchannel direction (and not in the direction of barrel rotation). There appears to be very little influence of the power law index on down-channel flow rates probably because the channels are very deep. The effect of increasing the aspect ratio of the channel is to reduce the downchannel flow rate and thus the upchannel value is increased.

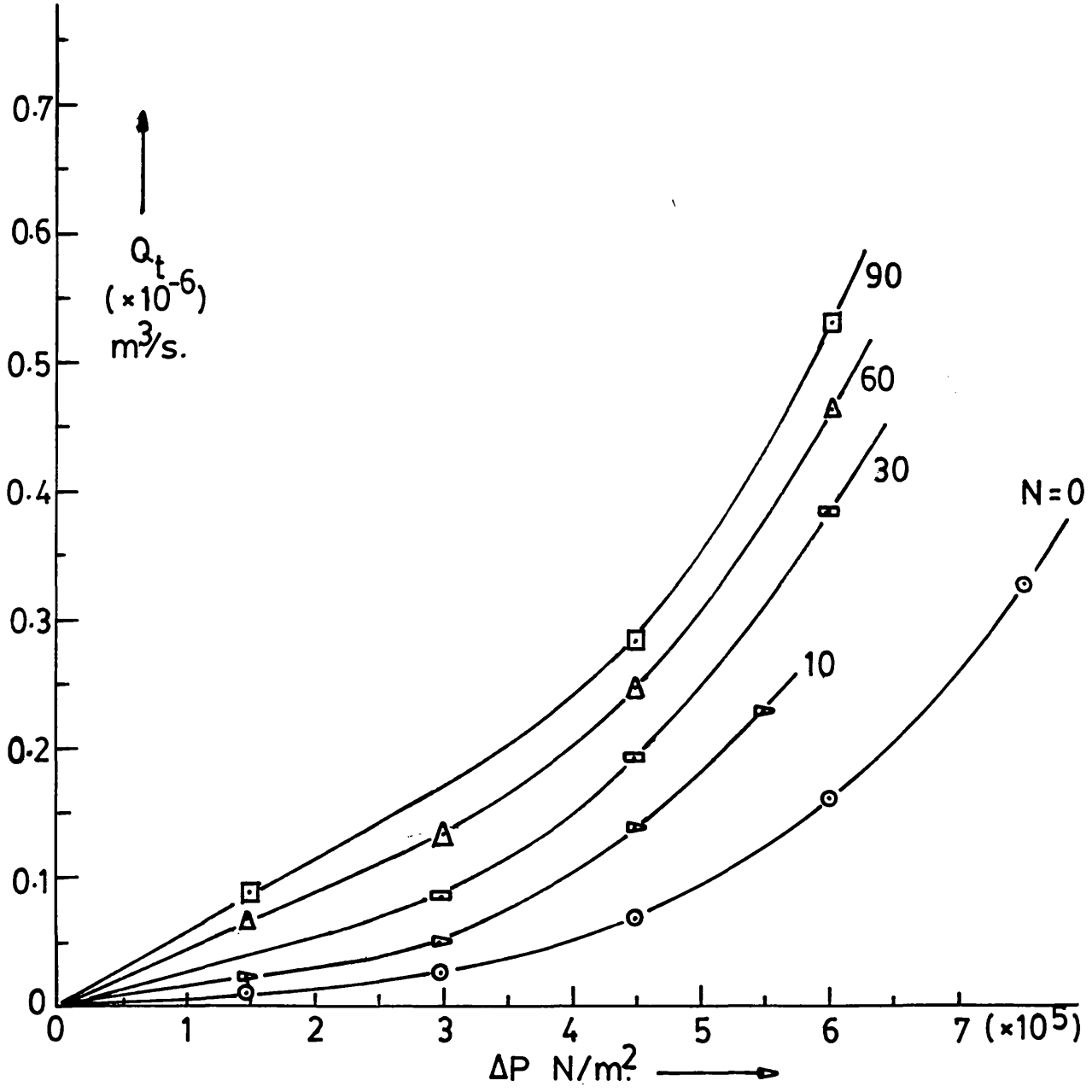

Figure 3.11.9 Leakage flow rate against pressure drop for the tetrahedron gap, $n = 0.326$, $\mu_o = 17.5 kNs/m^2$; screws B.

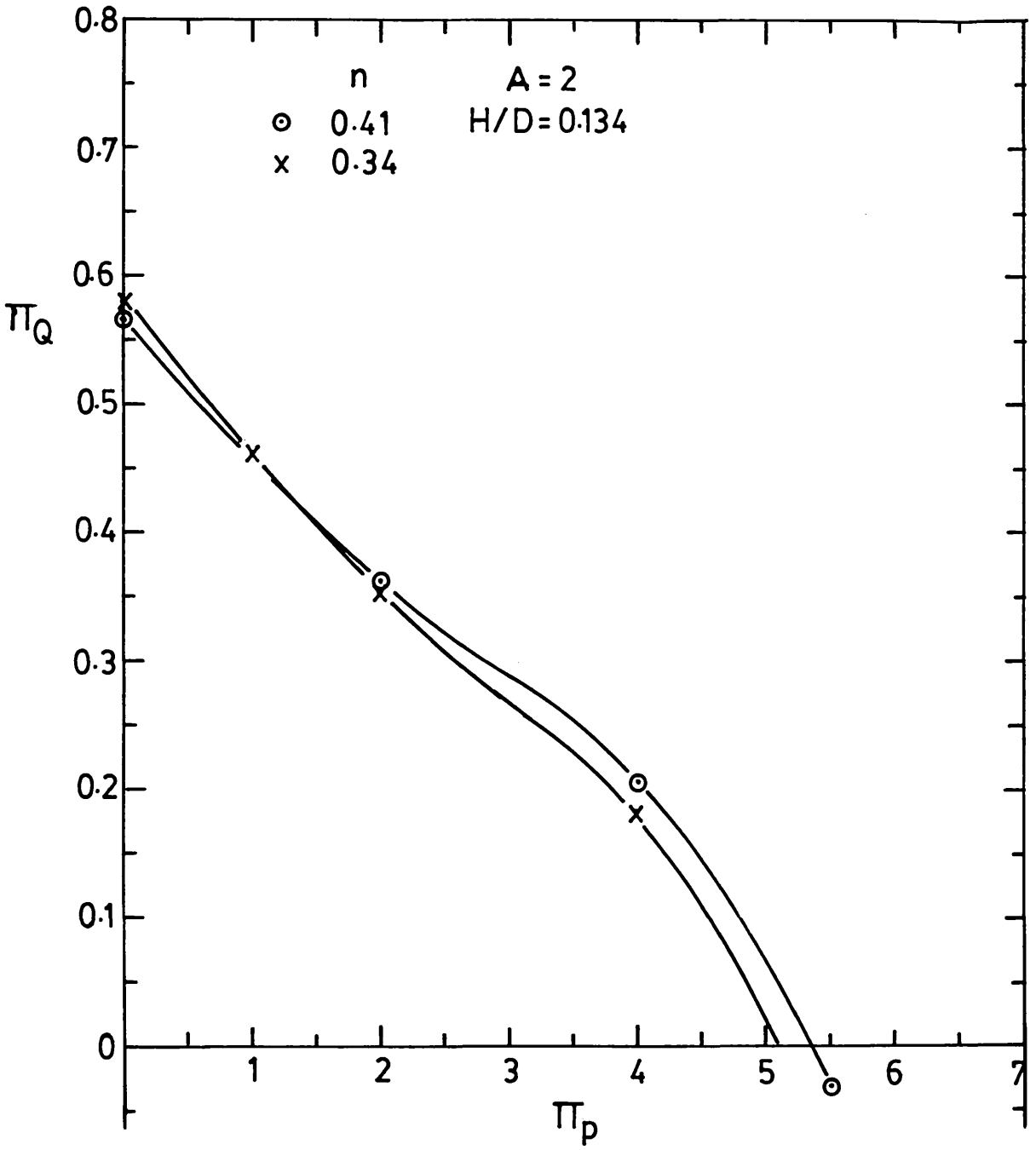

Figure 3.11.10 Dimensionless flow rate versus pressure gradient. for non-Newtonian deep channel flow.

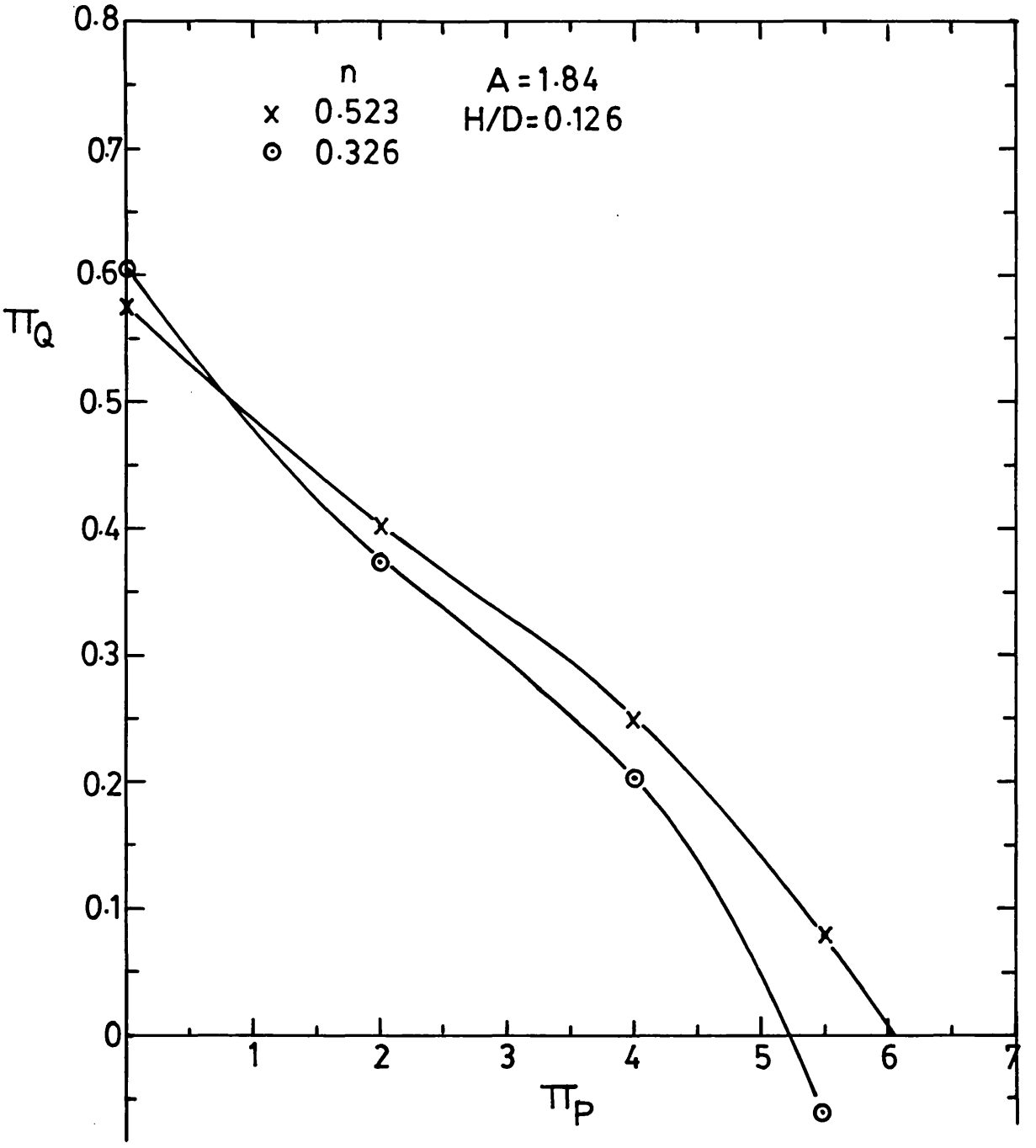

Figure3.11.11 Dimensionless flow rate versus pressure gradient. for non-Newtonian deep channel flow.

CHAPTER 4

MELT CONVEYING EXPERIMENTS AND COMPARISON WITH PREDICTIONS.

In the previous chapter, theoretical solutions of the flow equations for the channel and leakage gaps were obtained using a number of simplifying assumptions. The validity of these assumptions and thus the accuracy of the theoretical treatment described in simulating melt conveying is to be determined by comparison with measurements obtained from tests performed on a typical plasticating counter-rotating twin-screw machine extruding polymer melts. From such experiments, a comparison can be made only with the total amount of leakage or simply the net throughput extruded. This chapter describes experiments which provide information about the relationships between flow rates, pressures, and temperatures for the melt conveying process.

4.1 Experimental Twin-screw Extruder.

The counter-rotating twin-screw extruder used to carry out the experimental work was a fully instrumented Leistritz laboratory machine* with intermeshing screws. The screws were uniform and identical, and the barrel bores were a nominal 34 mm. with a centre distance of 30 mm. A general view of the extruder is shown in the photograph given in Figure 4.1.1. A photograph of the intermeshing screws is given in Figure 4.1.2.

The machine was a plasticating type extruder which consisted essentially of; a long heated barrel, screws with four different geometrical sections, hopper with feeder, heated die, infinitely variable speed mechanical drive and various measuring devices connected to instruments used for controlling, recording and monitoring the operating conditions of the extrusion process.

Figure 4.1.3 gives a cross-sectional view of the extruder. Both the barrel and screws were constructed of short separate sections connected together in series. Each barrel block was equipped with means of heating, cooling and controlling the temperature of the barrel. Pressures were measured directly from the barrel, at four points along the length of the metering region of the extruder using Dynisco pressure transducers situated 60 mm. apart. Before each experiment, the recording instrument connected to each transducer was zeroed and then adjusted to record pressures over a full-scale range of 0 - 27.6 MN/m^2. Thermocouples were used in place of the pressure transducers for measuring melt temperatures. Pressure and melt temperature were also measured at the output end of the extruder. Each screw was made up of standard elements of different screw geometries fixed together on a single shaft. By simply changing screw elements of the metering section it was possible to test different screw geometries. Screws were withdrawn via the die end of the extruder using a mechanical pulling device. The metering

*Extruder was located at BP Chemicals Ltd., Barry.

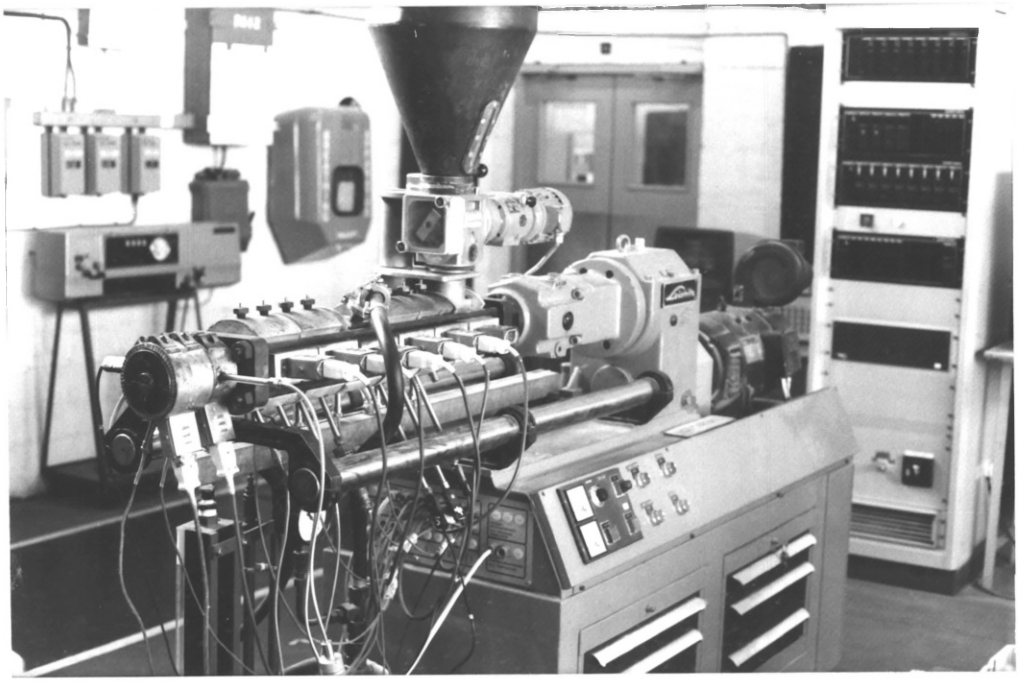

Figure 4.1.1 General view of the Leistritz laboratory Extruder.

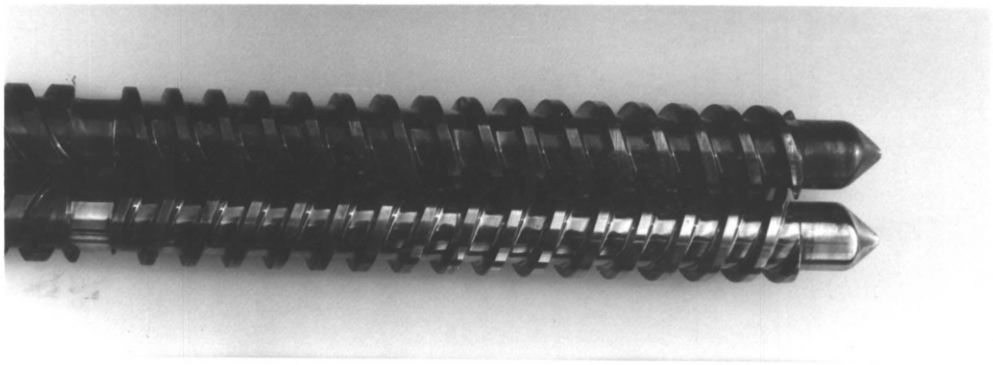

metering section.

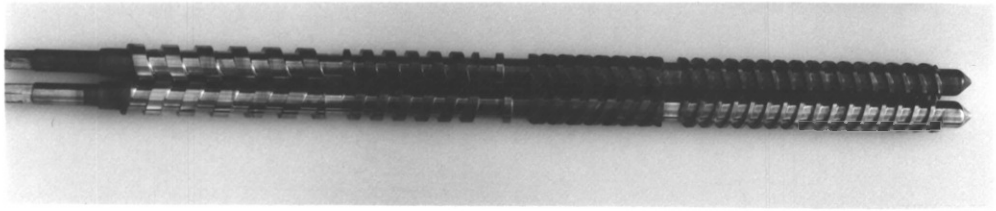

Figure 4.1.2 The Intermeshing Screws.

section of the screw was 180 mm. long. The screws were driven by a 5.5 kW electric motor through a gear box with a speed range capability of 7 - 233 rpm..

A rotary type feeder was used at the hopper to regulate extruder output which emerged from a heated 2 mm. by 20 mm. slit die. The feeding rate was varied by increasing or reducing the speed of the rotor using a graduated dial. The output rate of the machine was measured using a stop watch to time the mass of melt extruded over a convenient period.

Data logging equipment together with a digital computer was used to record a 100 scans of the changing pressures and temperatures and to compute and print out the minimum, maximum and mean values when required. All operating conditions were recorded after short time intervals and monitored continuously on a visual display unit (VDU), initially to ensure that all equipment was working correctly and then, to determine when conditions became steady. Figure 4.1.4 gives a photograph of the data logging equipment and the visual display unit used.

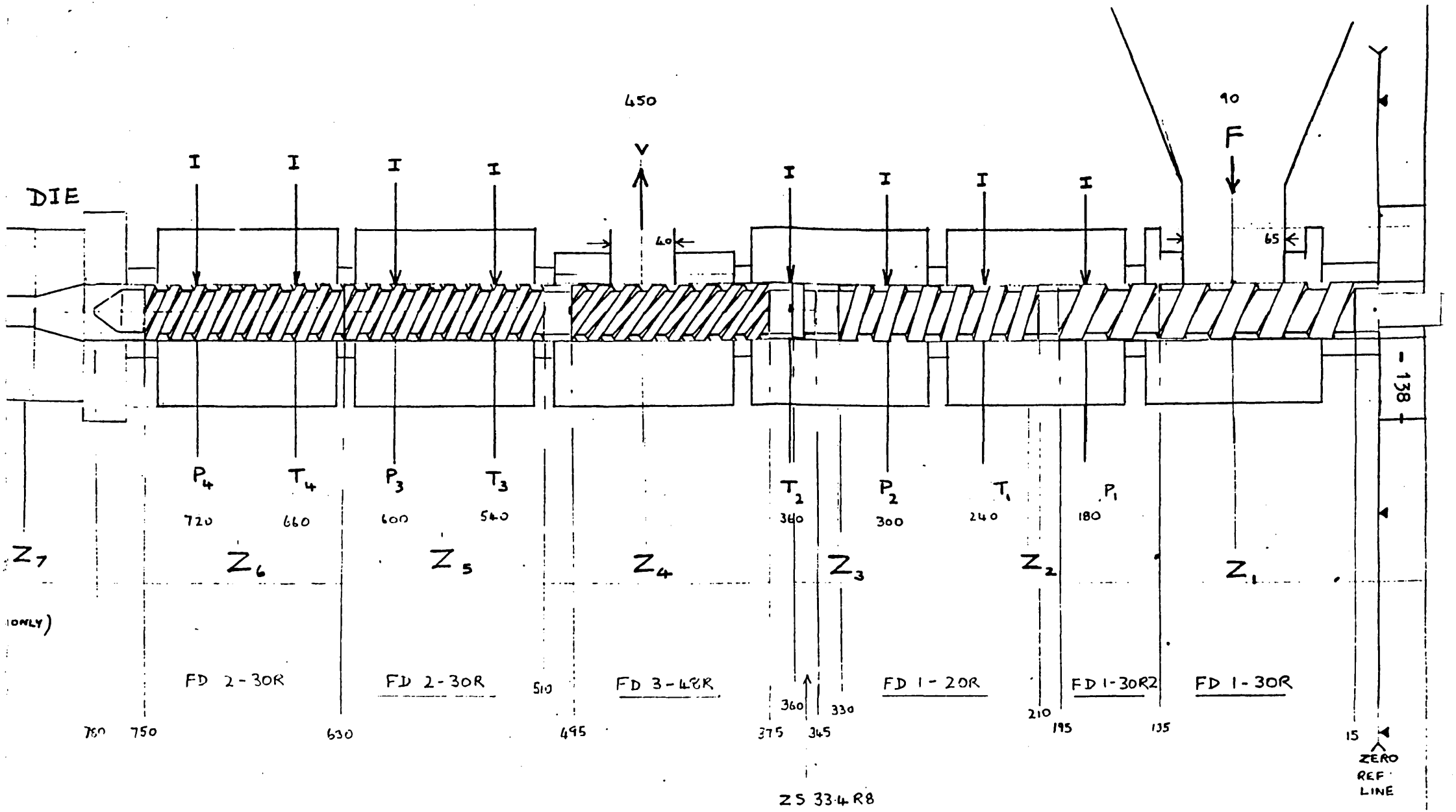

Figure 4.1.3 Cross-sectional view of the Counter-rotating Twin-screw Extruder - LEISTRITZ LS30.34

Figure 4.1.4 Data logging equipment and Visual Display Unit.

4.2 Screw dimensions.

Figure 4.1.2 gives a photograph of the intermeshing screws used in the experiments and Table 4.2 gives the dimensions of the screw elements of the metering section. All dimensions were measured to a tolerance of $\pm$ 0.02 mm. and were averaged over the length of both screws. Two different sets of screw elements with the same pitch of 30 mm. were tested, and these are called screws A and screws B. Screws A had a much larger clearance between the screw flanks in the intermeshing region than screws B and thus, the tetrahedron and side gaps were larger.

4.3 Polymeric material extruded.

The polymers used in the experiments were two grades of polystyrene, HS and CC37 beads, both manufactured by British Petroleum Chemicals Limited, South Wales, England. Polystyrene was chosen because it melts at a relatively low temperature, does not burn or degrade easily at relatively high temperatures and therefore can be extruded without problems over a large range of temperatures. Its flow behaviour was typical of most polymers used in extrusion processes, i.e. it was elastic, highly non-Newtonian (with a low flow index of the order of 0.3 - 0.4 over a normal operating range of average shear rate) and does not slip at relatively high shear rates. The significance of the additional effect of slip on melt flow could be determined from further work by using the material PVC which tends to have a very narrow temperature operating range and degrades easily if conditions are not properly controlled.

Table 4.2 Dimensions of the extruder screws.

All dimensions in mm.

Diameter of the barrel bores = 34.0 mm.

Screws	A	B
Diameter, D	33.70	33.76
Centre distance, C	30.0	30.0
Channel depth, H	4.53	4.27
Axial flight width, B	4.36	6.65
Pitch, S	30.0	30.0
Screw starts, m	2	2
Radial clearance, δ_f	0.15	0.12
Flank angle, ψ	15.42°	2.36°
Calender gap, σ	0.83	0.51
Side gap, ε	1.75	0.675
Helix angle, β	15.78°	15.78°

4.4 Experimental procedure.

The various measuring devices and instruments were connected to the experimental extruder (Figure 4.1.1) and the control, visual display unit and data logging equipment switched on. The data logging equipment was set to record every 20 seconds and to display the operating conditions on the VDU. The cooling water supplied to the barrel was turned on and the operating temperatures of the barrel and die were set. For all experiments a common temperature was maintained from hopper to die. Once this temperature was reached the pressure recording instruments were zeroed and calibrated for the required pressure range.

The polymer was extruded over a range of screw speeds commencing with the lowest speed. The extruder motor was started and screw rotation was slowly increased to the first operating speed. The feed rate was then increased slowly, in steps, until pressure was built up at the end of the screw and melt was seen to emerge from the die. Feeding rate was further increased until extruder inlet was just flooded with polymer - this produced the maximum output capability of the machine for that screw speed and was used as the first feeding rate. Operating conditions were now monitored for about 10-15 minutes or until approximately constant and recorded, with the final results stored in the computer and printed out when required. By weighing the amount of melt extruded over a two minute period, the throughput of the extruder was obtained. For smaller feeding rates, care was taken to ensure that the lowest level of starve feeding used was enough to build up sufficient back-pressure at the die, to be measured by the two transducers located nearest the screw end. This made it possible for a pressure drop to be determined for the melt flow between the two pressure measuring points. Before changing to the next screw speed, the feeding rate was increased once more to the flood-feed setting to prevent large fluctations in pressure which could be caused by overstarving when screw

speed is increased with a relatively low feeding rate. This tended to reduce the operating time required for the process to return to a steady state once again. The above procedure was repeated for each screw speed used.

4.5. Polymer Melt Properties.

The viscosity data were obtained from capillary rheometer measurements using an Instron Capillary Rheometer.* Two capillaries were used, nominally of length 25 and 50 mm. and 1.27 mm. diameter. Measurements were made at two temperatures, 180 and 200°C and over a wide shear rate range of 3.1 - 3073 $sec.^{-1}$ Allowances were made for resevoir pressure drop, (Bagley) capillary end corrections and Rabinowitsch shear rate correction. The accuracy of the measurements were not better than by about ±5%. Density was measured at each temperature by extruding the polymer melt through the 25mm capillary for one minute and an average taken over the range of temperatures used. The thermal conductivities and specific heats of both polymers were obtained from the manufacturers. Figures 4.5.1 and 4.5.2 give the log shear stress versus shear rate curves, with corrections, for the polymer melts extruded. Table 4.5 gives the values of the polymer properties used. The viscosity parameters given are for curve fitting of the empirical power law over the relevant shear rate range.(in brackets).

* This work was carried out at Mechanical Engineering Dept., Imperial College.

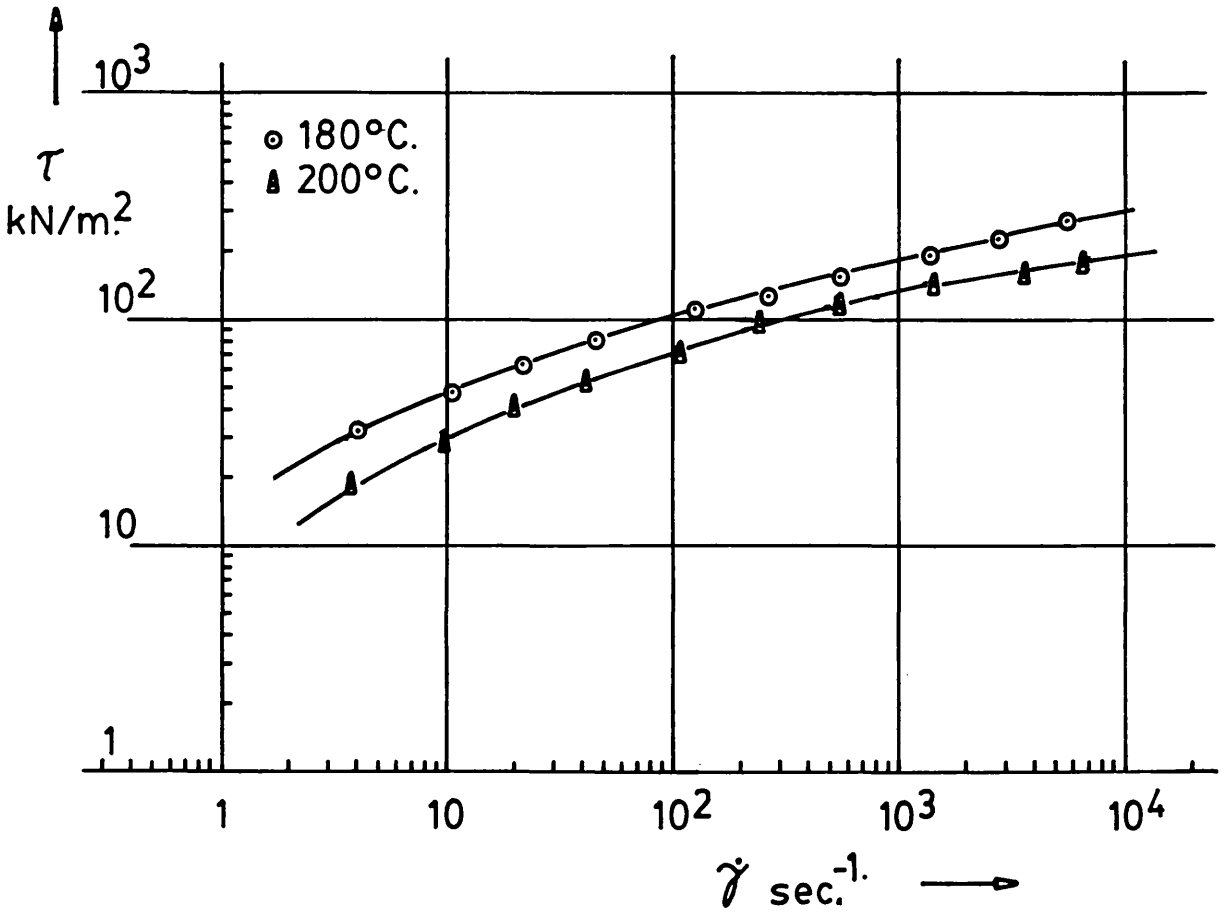

Figure 4.5.1 Flow curves for Polystyrene HS grade.

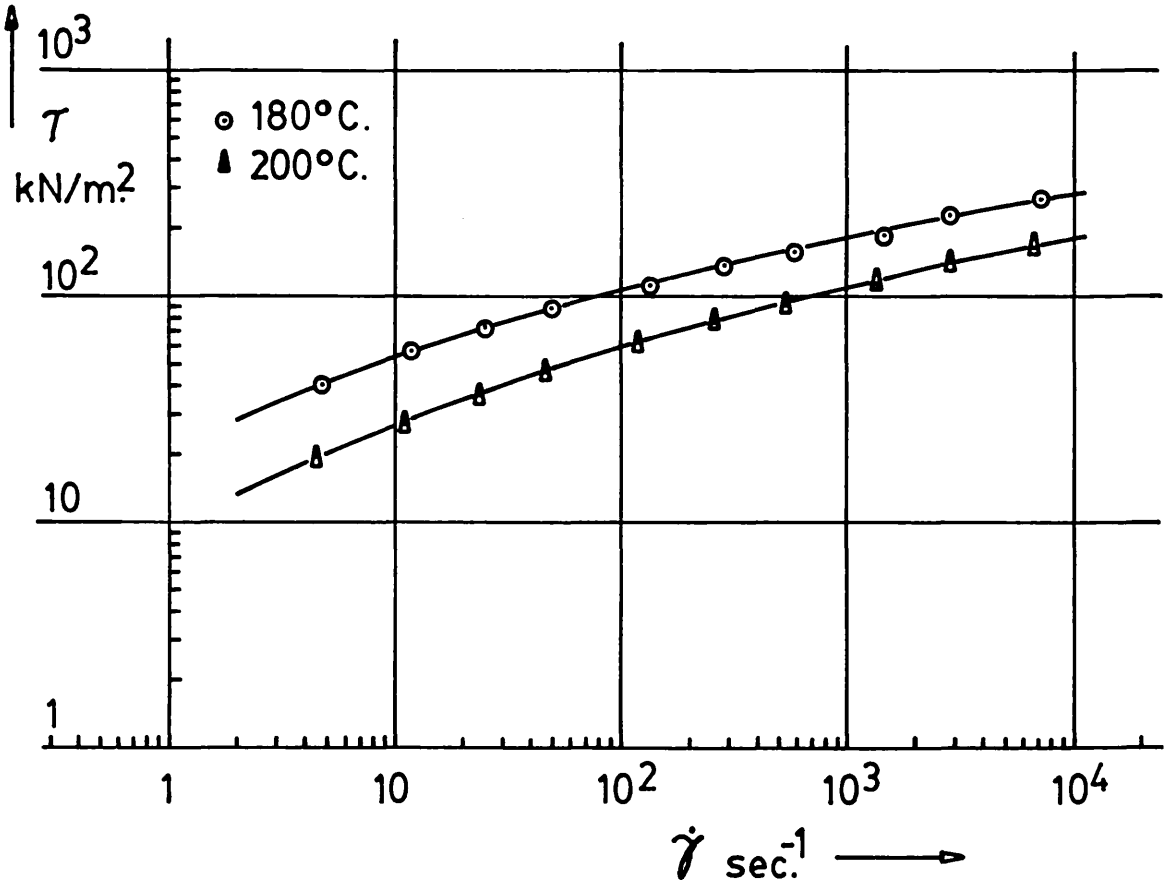

Figure 4.5.2 Flow curves for Polystyrene CC37 grade.

Table 4.5 Polymer melt Properties.

Polymer.	B.P. Polystyrene.	
Grade.	HS. beads.	CC37 beads.
n	0.41 ($3-40s^{-1}$)	0.356 ($3-60s^{-1}$)
μ_o kNs/m^2	18.5 ($\dot{\gamma}_o=1s^{-1}$, 180°C)	11.5 ($\dot{\gamma}_o=1s^{-1}$, 200°C)
n	0.27 ($40-700s^{-1}$)	0.28 ($40-700s^{-1}$)
μ_o kNs/m^2	29.0 ($\dot{\gamma}_o=1s^{-1}$, 180°C)	17.0 ($\dot{\gamma}_o=1s^{-1}$, 200°C)
b_o / °C	0.023 ($3-40s^{-1}$)	0.034 ($3-60s^{-1}$)
ρ kg/m^3	940	973
k W/m/ °C	0.125	0.125
C_p kJ/kg/ °C	1720	1740

4.6 Experimental Results.

Plasticating extrusion experiments were performed with the twin-screw extruder to measure operating conditions of flow in the melt conveying part of the process for comparison with the predicted solutions. The various twin-screw sets A, B (section 4.2) were tested over a range of screw speeds and the results of melt pressures and temperatures are given for various extruder output rates in Figures 4.6.1 to 4.6.12. The readings were recorded, simultaneously, from similar points in the chambers along the screw and therefore, the difference between the measurements represents a change of operating condition over an exact number of chambers in that length of extruder. For this case, the pressures were measured axially from points situated 60 mm. apart; therefore, a pressure drop can be determined for four consecutive chambers of the 30 mm. pitch intermeshing double-start screws (or for six chambers of 20 mm. pitch double-start screws).

Figures 4.6.1 to 4.6.3 give the distributions of mean values of pressure and temperature for the extrusion of polystyrene-HS beads using screws A at speeds 30,40 and 50 rpm.. For the operating temperature of 180°C, the maximum output rates (and consequently the smallest pressure gradients) given for the screws were obtained using flood-feeding at the extruder inlet. Melt temperatures were obtained at approximately the same extrusion rate as in the tests when pressures were measured instead of temperatures at the same points in the barrel. Although these may not be true melt temperatures because of the strong influence the heated barrel may have on the thermocouples flush-mounted in its wall[1], the trends produced are useful for indicating flow behaviour. Temperature profiles are almost independent of screw speed and feed rate, the maximum variation being about 3°C.

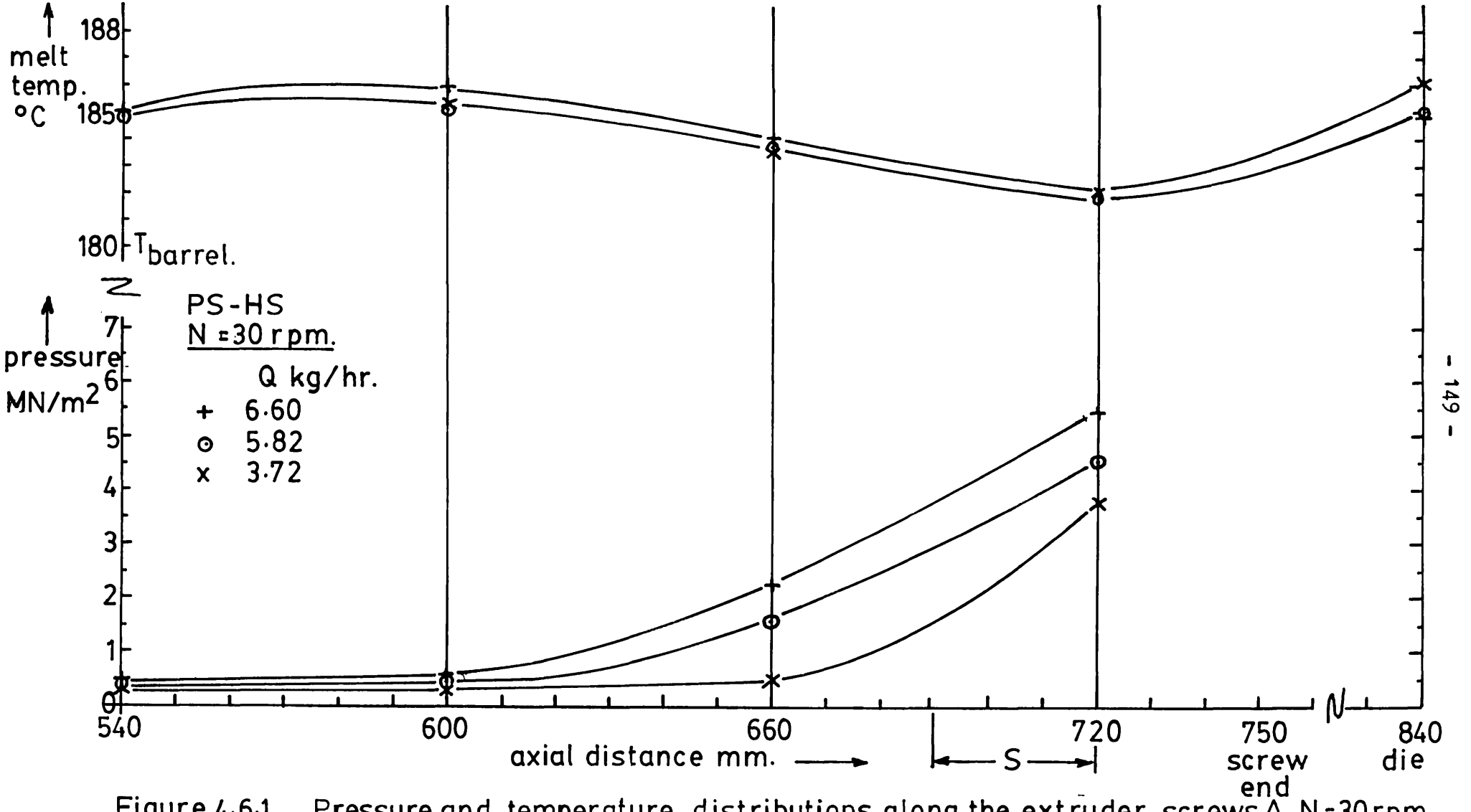

Figure 4.6.1 Pressure and temperature distributions along the extruder, screws A, N = 30 rpm.

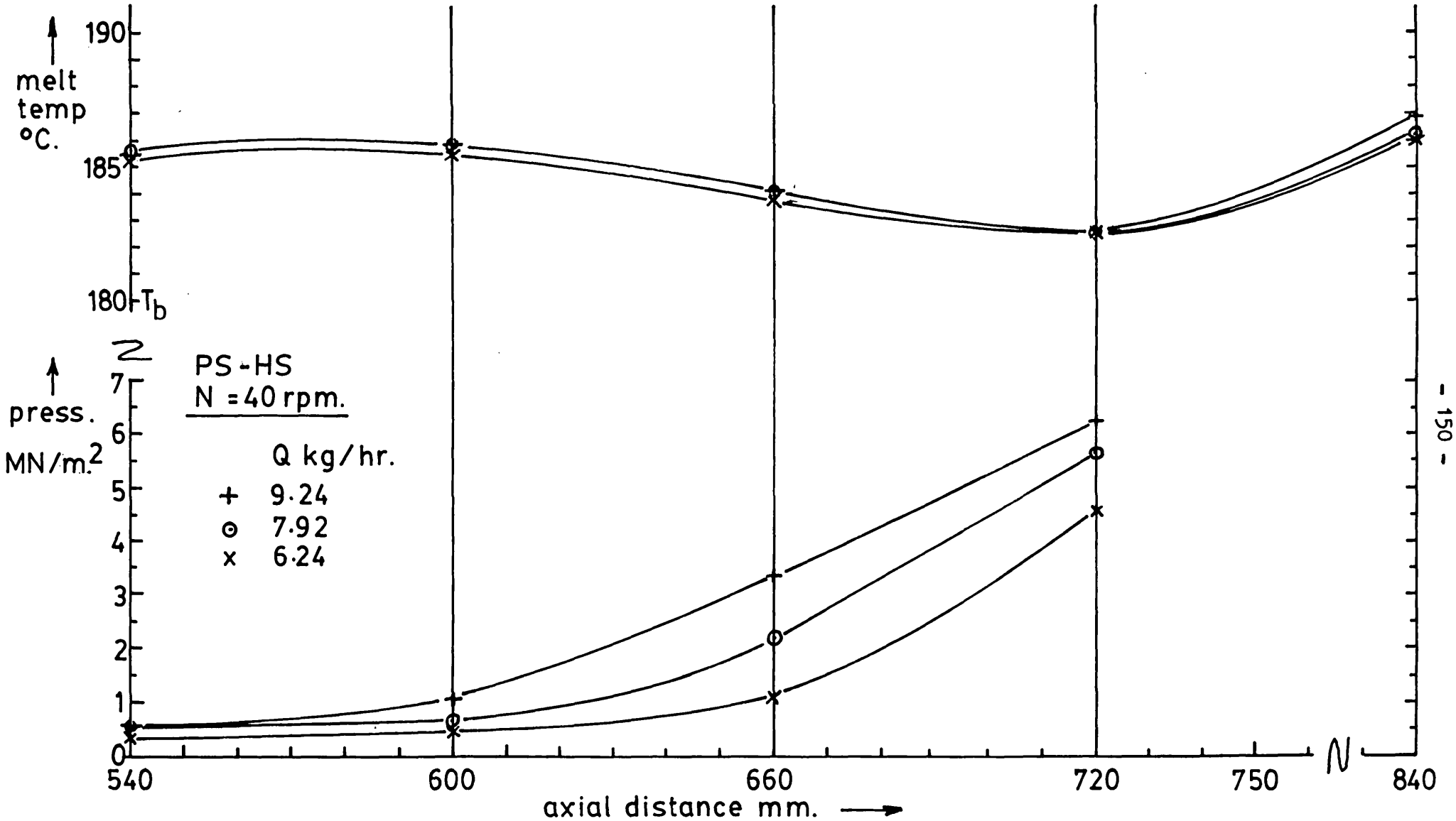

Figure. 4.6.2 Pressure and temperature distributions along the extruder, screws A, N = 40 rpm.

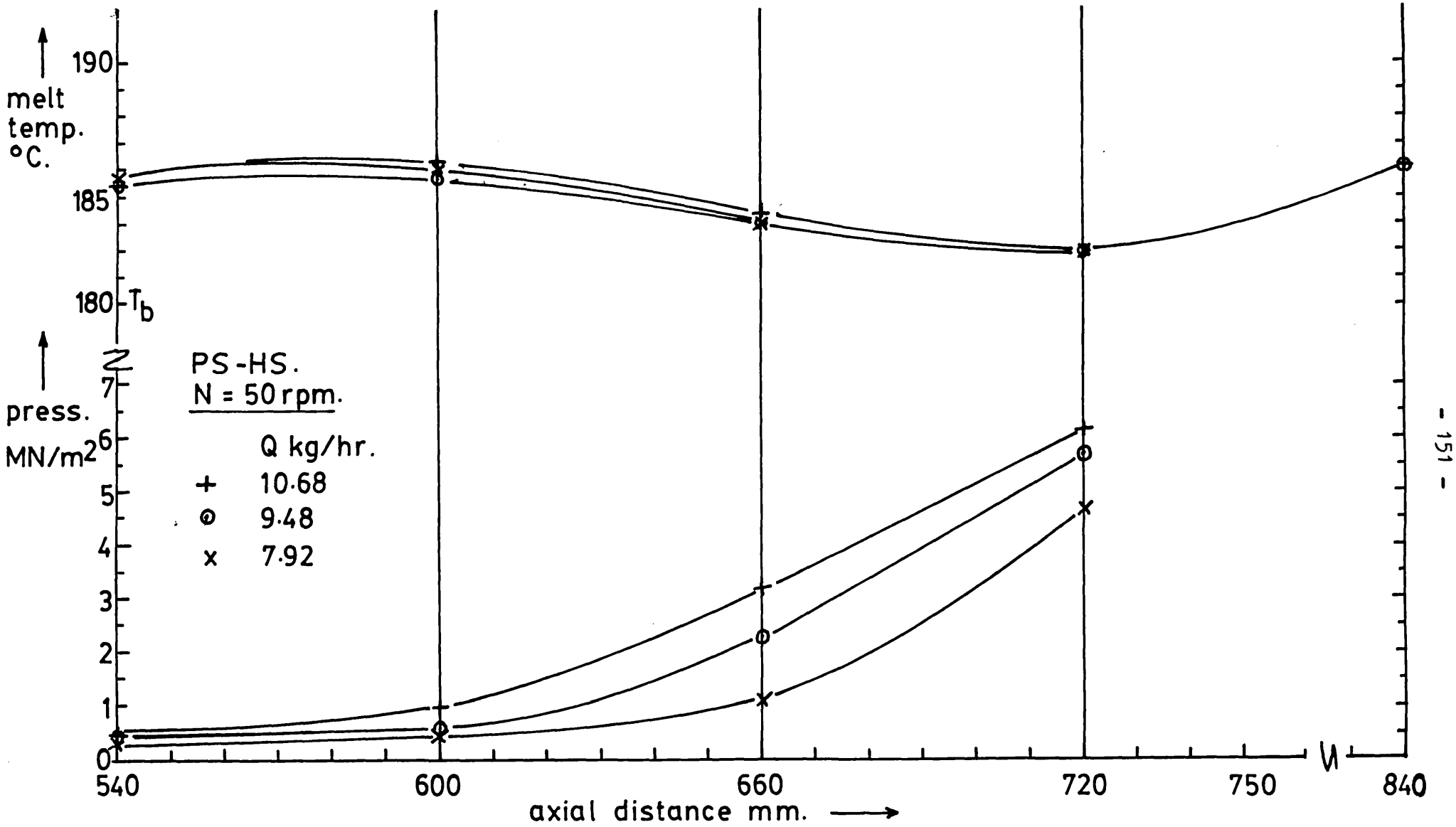

Figure 4·6·3 Pressure and temperature distributions along the extruder, screws A, N = 50 rpm.

The melt temperature over 8 chambers of the extruder remains almost constant, a condition which is also shown by the almost equal value of pressure drops generated (for the largest flow rate given) between the two equal lengths of the metering zone. It can be seen, also, that there is always a finite pressure generated where the chambers are supposed to be only partly filled with melt. This is because pressures were measured near to where the rotating screw surfaces converge and pile up material at the entrance to the intermeshing region, and where there would still be a tendency for the melt to build up pressure in the partly filled chambers. It has been confirmed, from examination of hot screws, that the chambers were only partly filled with melt over the region where the minimum value of pressure was recorded. A photograph of extracted screws filled with melt is shown in Figure 4.6.13 in which can be clearly seen the completely filled and partly filled chambers.

Similar results were obtained for screws A with polystyrene CC37 grade extruded at a temperature of 200°C and these are given in Figures 4.6.4 to 4.6.8. Because of the reduced viscosity due to the higher temperature, smaller pressure gradients were obtained with pressure distributions extending over a larger portion of the metering zone. At the lower screw speeds, the melt temperature profiles were similar to those previously shown for 180°C, but at 60 rpm and above the melt temperature increased instead of decreased, probably due to significant shear heating at these speeds. The operating results for screws B extruding polystyrene CC37 at 200°C are given in Figs 4.6.9 to 4.6.12. The maximum output rate obtained at each screw speed was limited also for these screws by flood feeding at the extruder inlet. In comparison with screws A, the smaller leakage gaps of screws B means larger pressure gradients to generate through the same die opening roughly the same leakage flow rate. In general, the pressure profiles obtained for the extrusion of

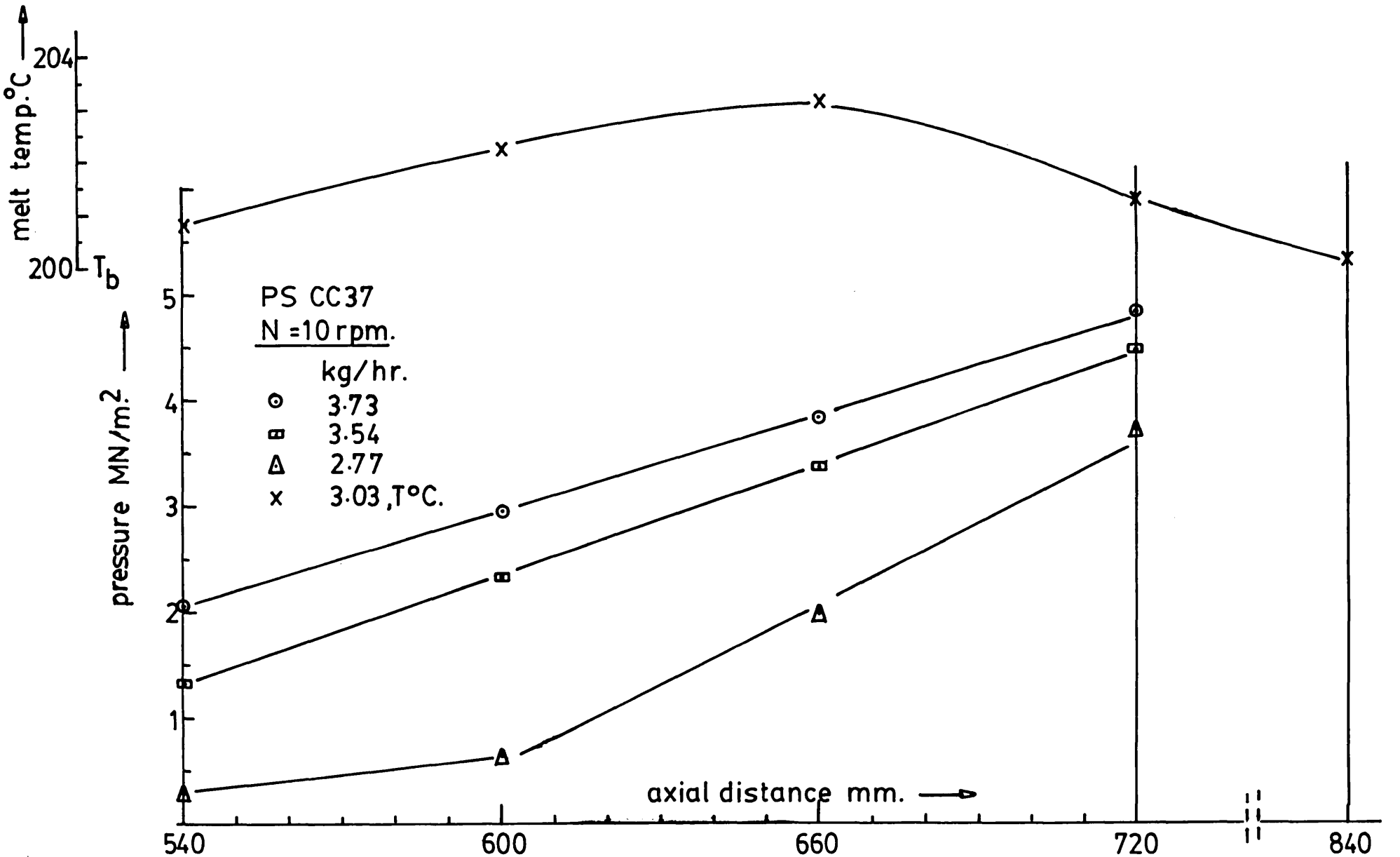

Figure 4.6.4. Pressure and temperature distributions, screws A, N=10 rpm.

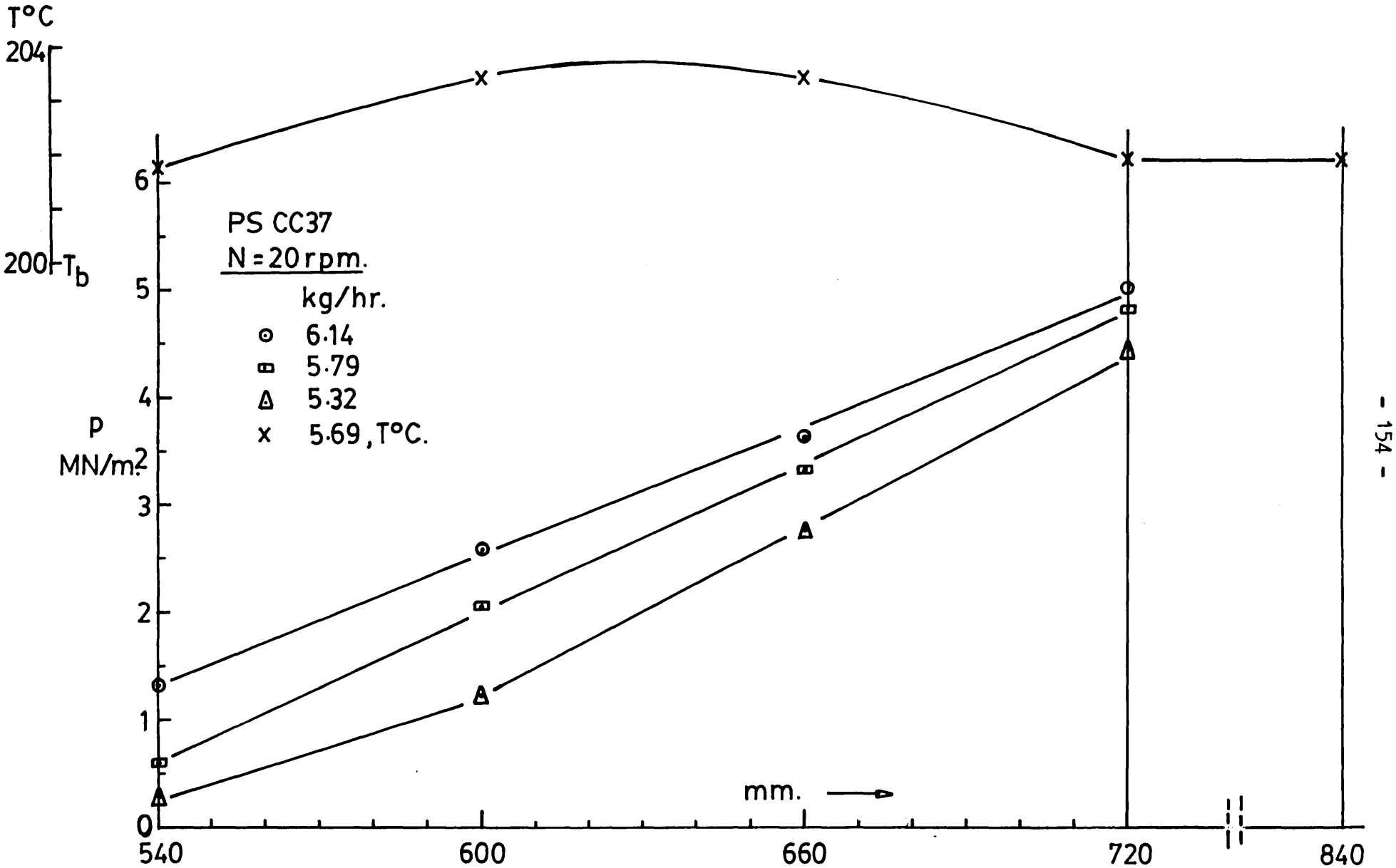

Figure 4·6·5. Pressure and temperature distribution, screws A, N = 20 rpm.

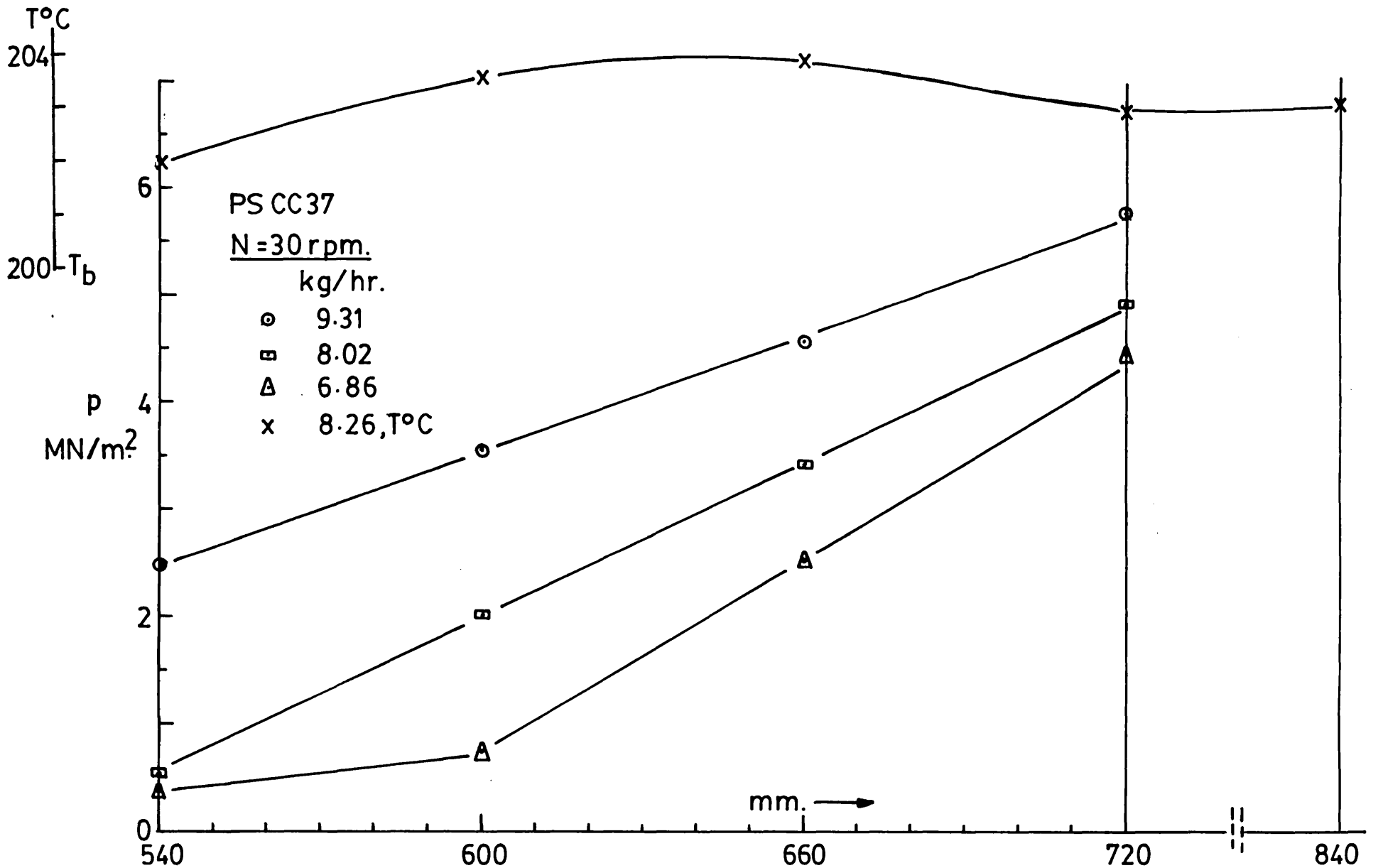

Figure 4.6.6. Pressure and temperature distributions, screws A, N = 30 rpm.

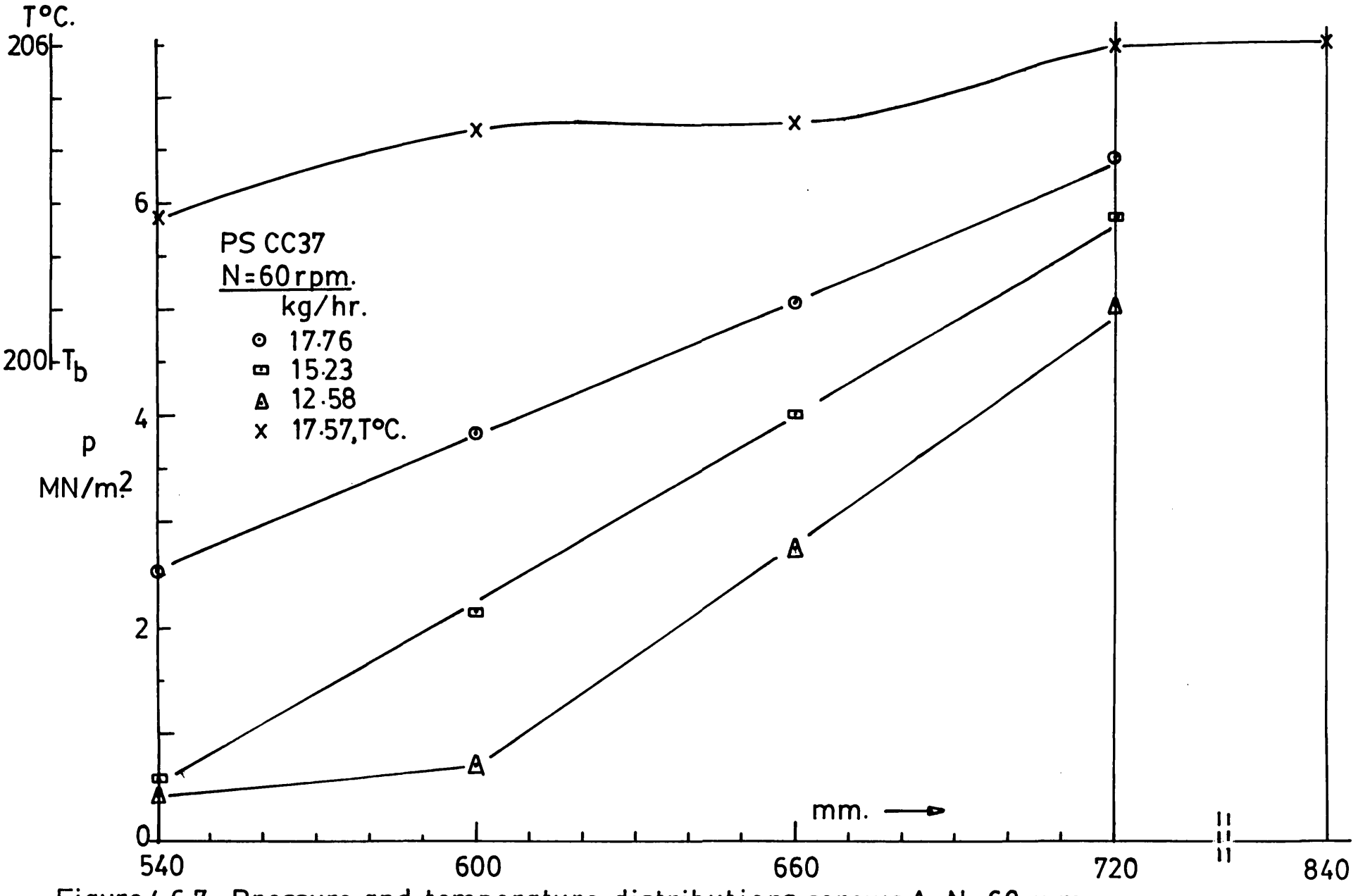

Figure 4.6.7. Pressure and temperature distributions, screws A, N = 60 rpm.

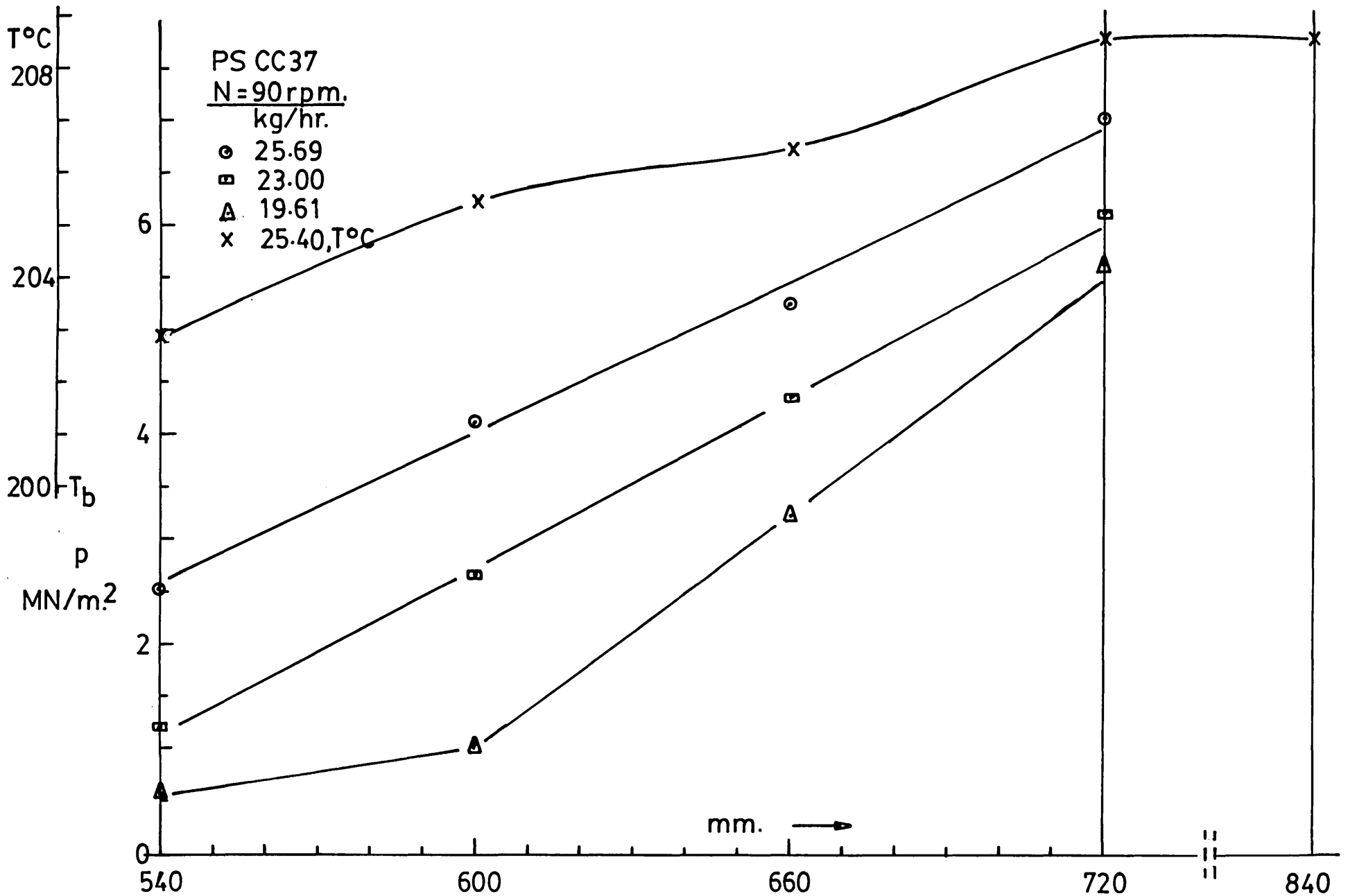

Figure 4.6.8. Pressure and temperature distributions, screws A, N = 90 rpm.

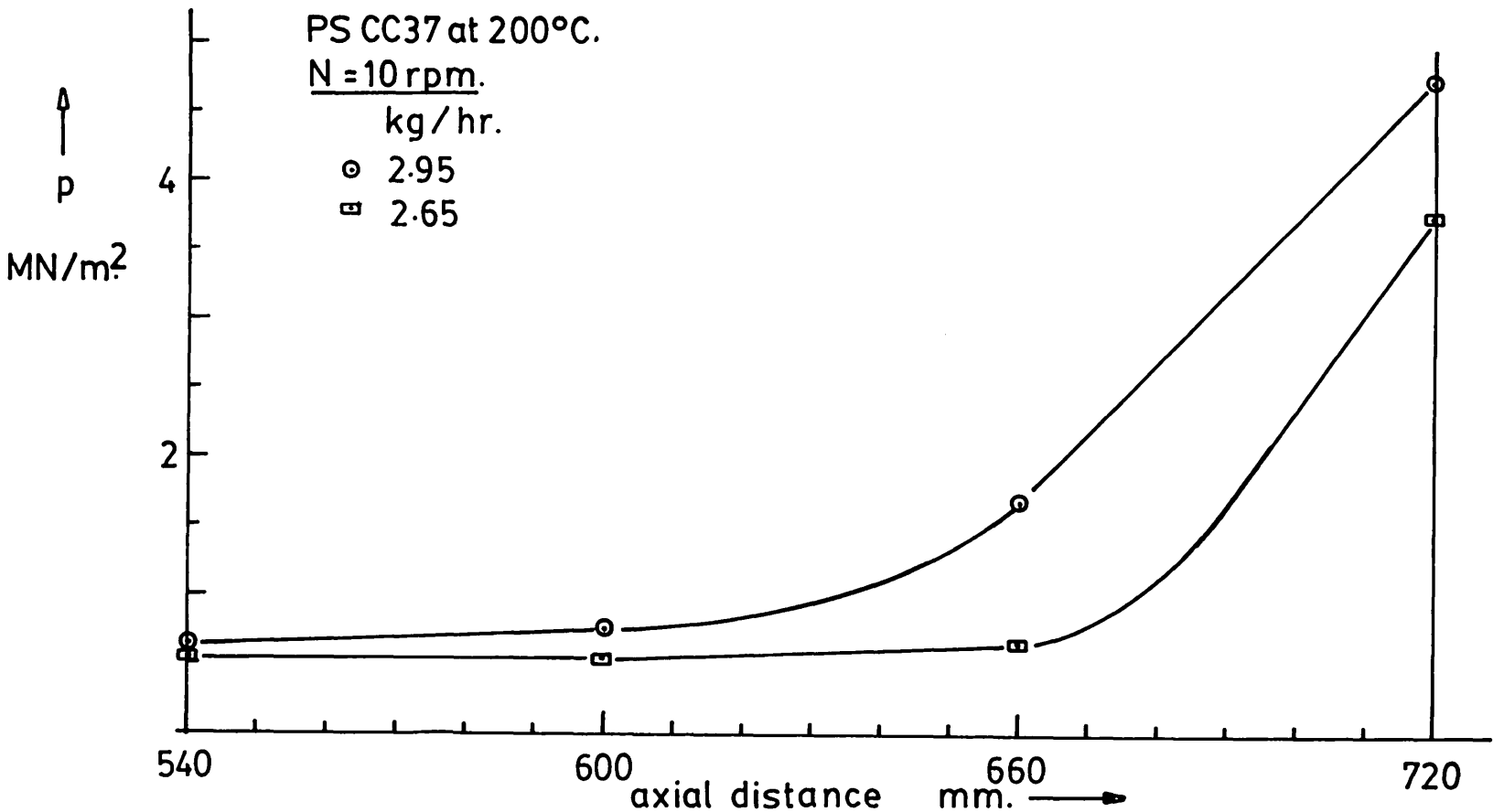

Figure 4.6.9. Pressure distributions, screws B, N = 10 rpm.

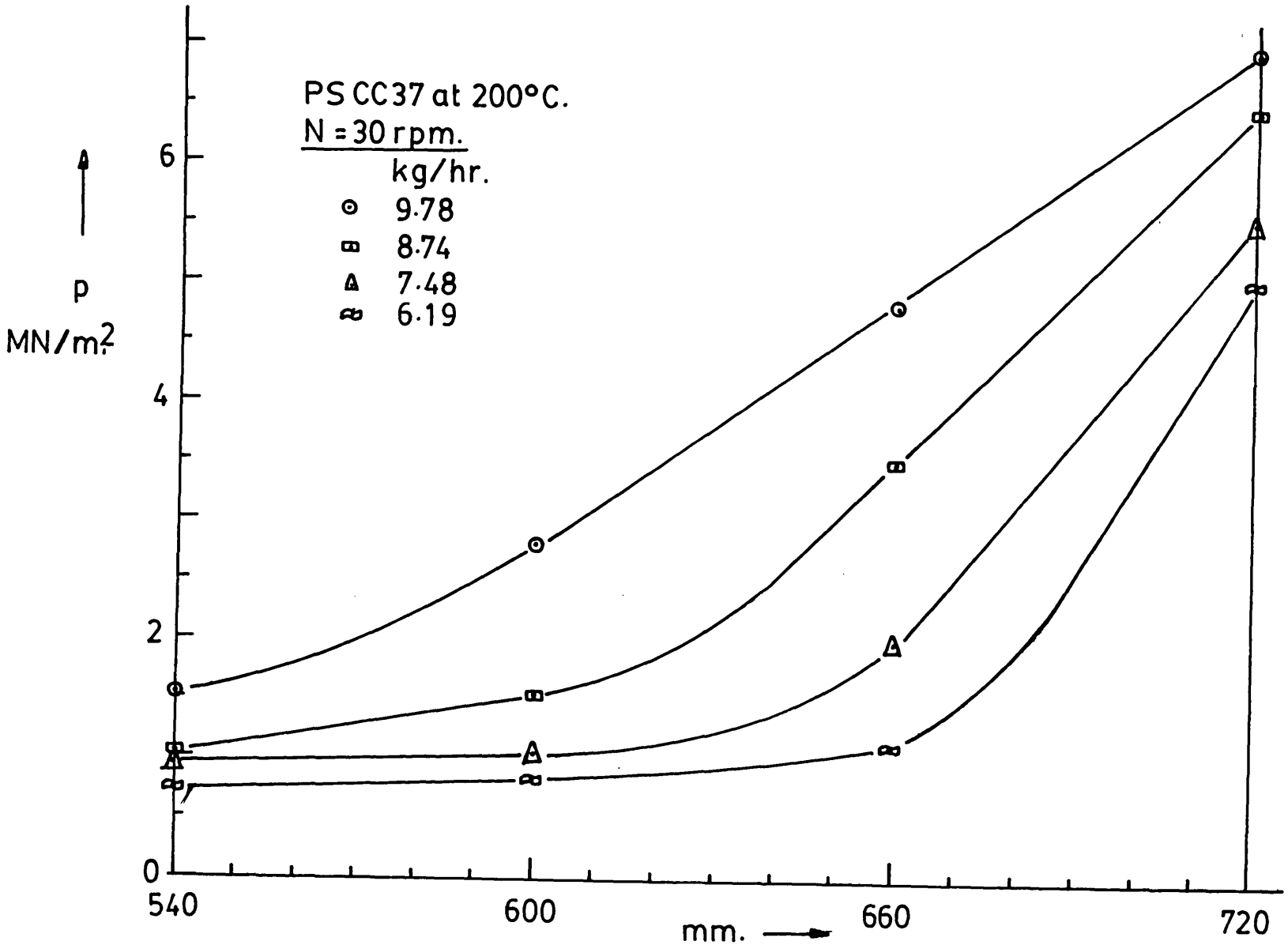

Figure 4.6.10. Pressure distributions, screws B, N = 30 rpm.

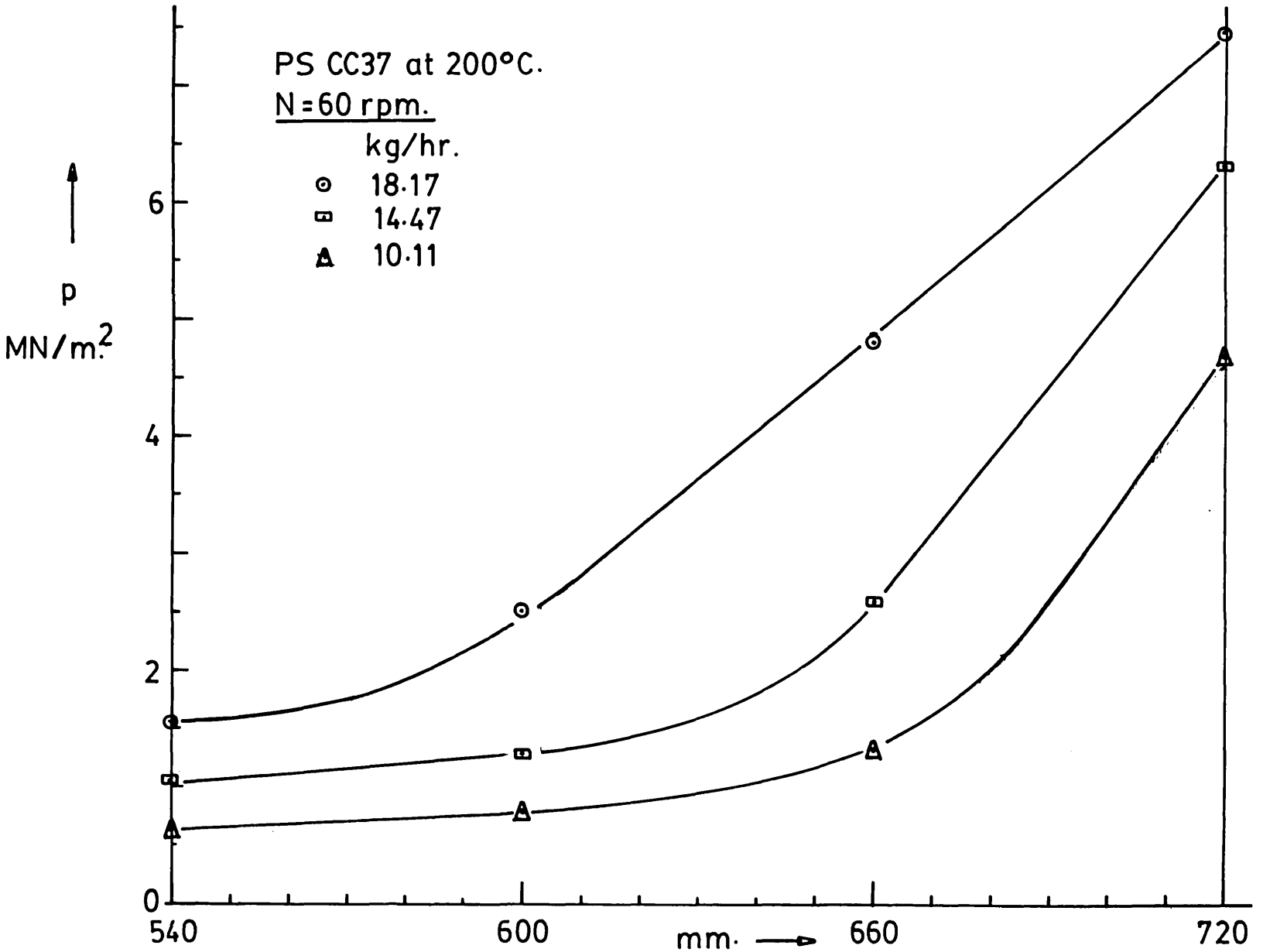

Figure 4.6.11. Pressure distributions; screws B, N=60 rpm.

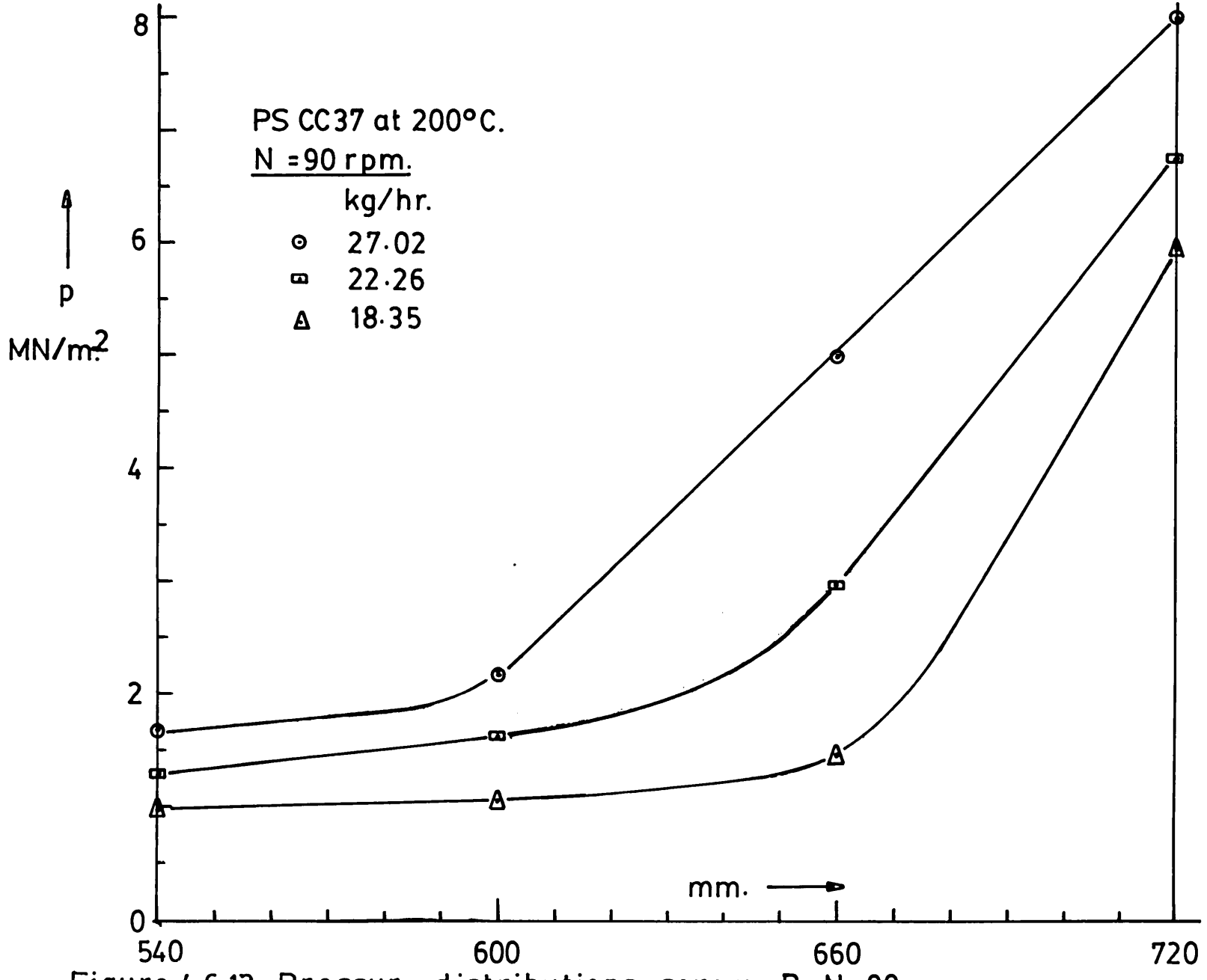

Figure 4.6.12. Pressure distributions, screws B, N =90 rpm.

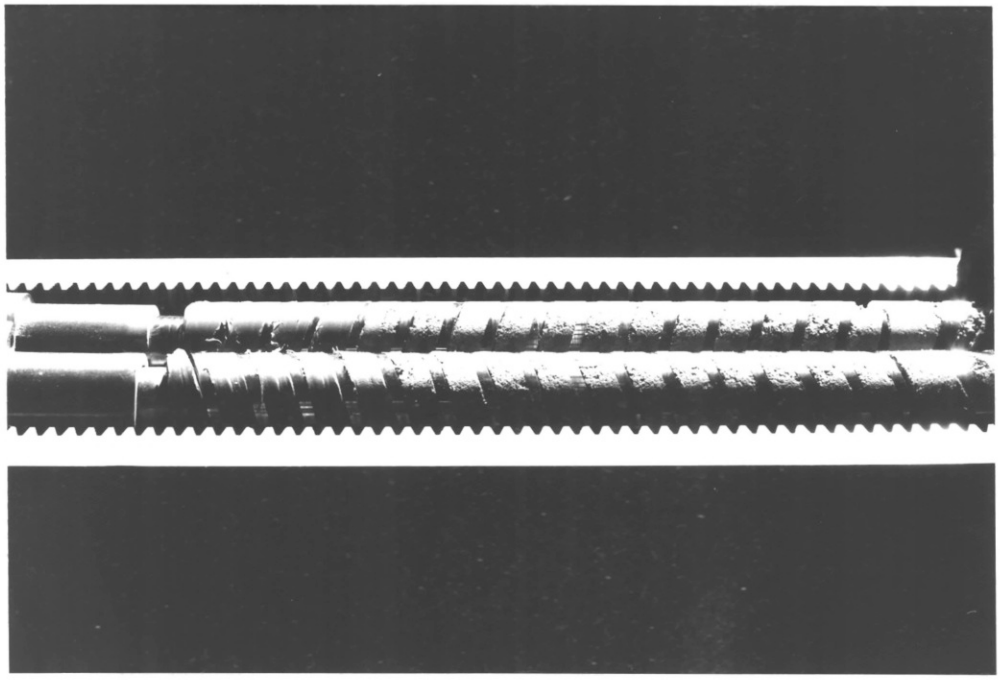

Figure 4.6.13 Extracted screws filled with a polymer melt - completely-filled chambers can be seen on the left, at the end of the screws.

melt in this machine using screws with varying degrees of positive conveying, was found to be approximately straight over the length of the metering zone examined indicating that the temperature variation is not significant. The trends shown by the melt temperature measurements indicate that there is significant shear heating in the extruder at screw speeds above 60 rpm. which is likely to raise the bulk mean temperature of the melt in each chamber but still maintain an almost constant temperature of the melt conveyed along the metering zone.

Figure 4.6.14 gives dimensionless throughput rate plotted against dimensionless pressure drop for screws A extruding polystyrene HS beads at 180°C and speeds of 30,40 and 50 rpm.. The viscosity, power law parameters, at the average shear rate in the screw channel is used to determine the pressure drop term. Because of the small range of screw speeds (and shear rates) used, the results are situated close together but it can be seen that a separate relationship for each screw speed exists for each set of points. For a given screw geometry and axial pressure gradient, therefore, the throughput of the extruder is reduced with increased speed. If the flow rates are plotted, instead, against the pressure drop term, $(\Delta P/\mu_o)^{1/n}N$, the characteristic becomes linear[5] as illustrated in Figure 4.6.15. The throughput rate of the extruder over the lower range of pressure drop can now be obtained and is seen to be very small. In general, this was found to be the case in all the extrusion tests performed, and the maximum possible throughput rate obtained was about equal to that for the machine, and for the cases shown in Figure 4.6.15, these values correspond to an axial pressure drop of about $\Delta P = 0.39\ MN/m^2$. The results for screws A extruding polystyrene CC37 at 200°C are given in Figures 4.6.16 and 4.6.17 plotted using the different pressure drop terms. The maximum possible throughput rates at this higher temperature corresponds to an axial pressure drop of about

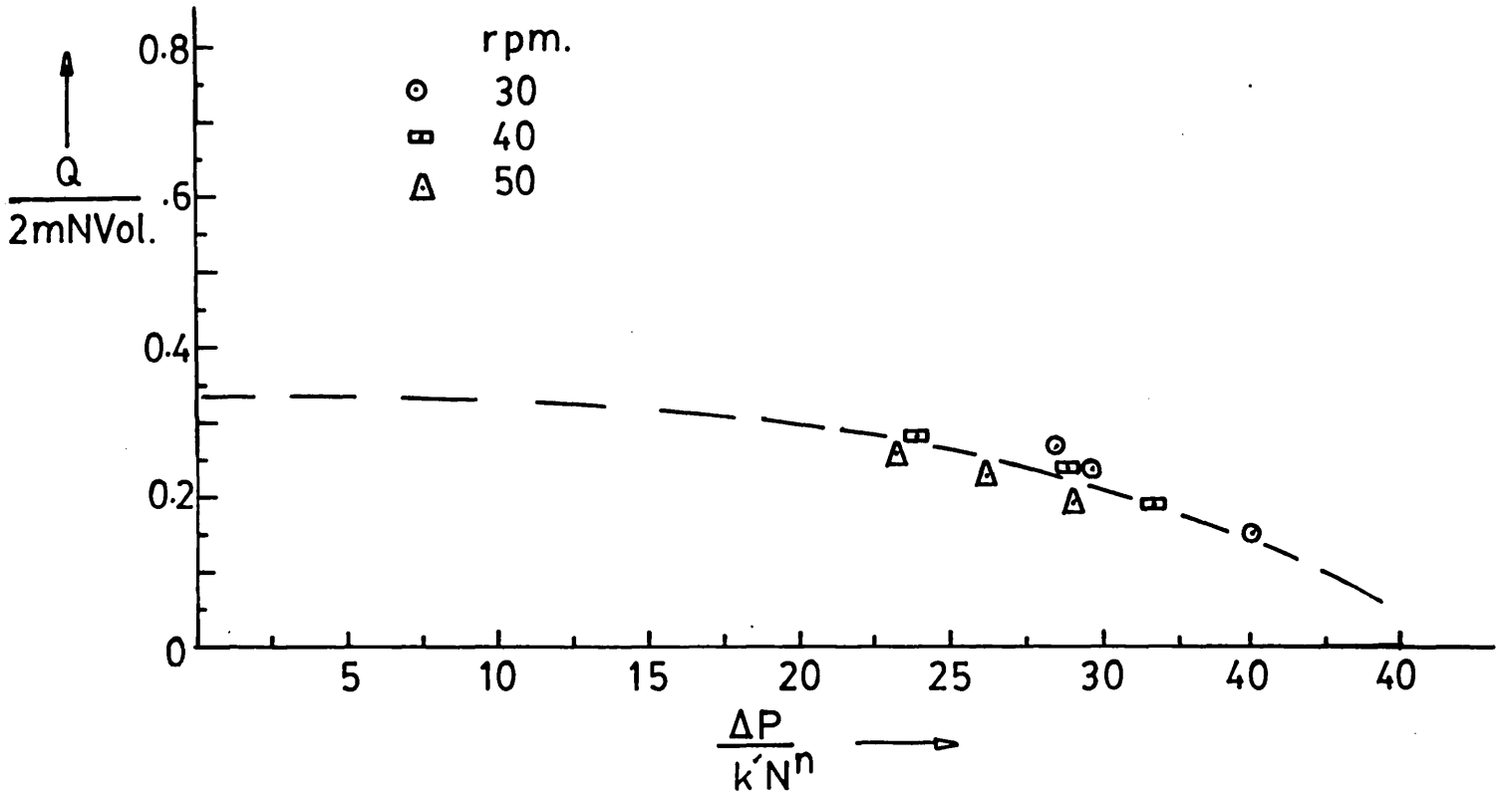

Figure 4·6·14. Dimensionless throughput rate versus pressure drop for Screws A, extruding Polystyrene-HS at 180°C, n = 0·41, μ_o = 18·5 kNs/m^2,
– – – approx. curve based on linear plotting of results, Figure 4·6·15 overleaf.

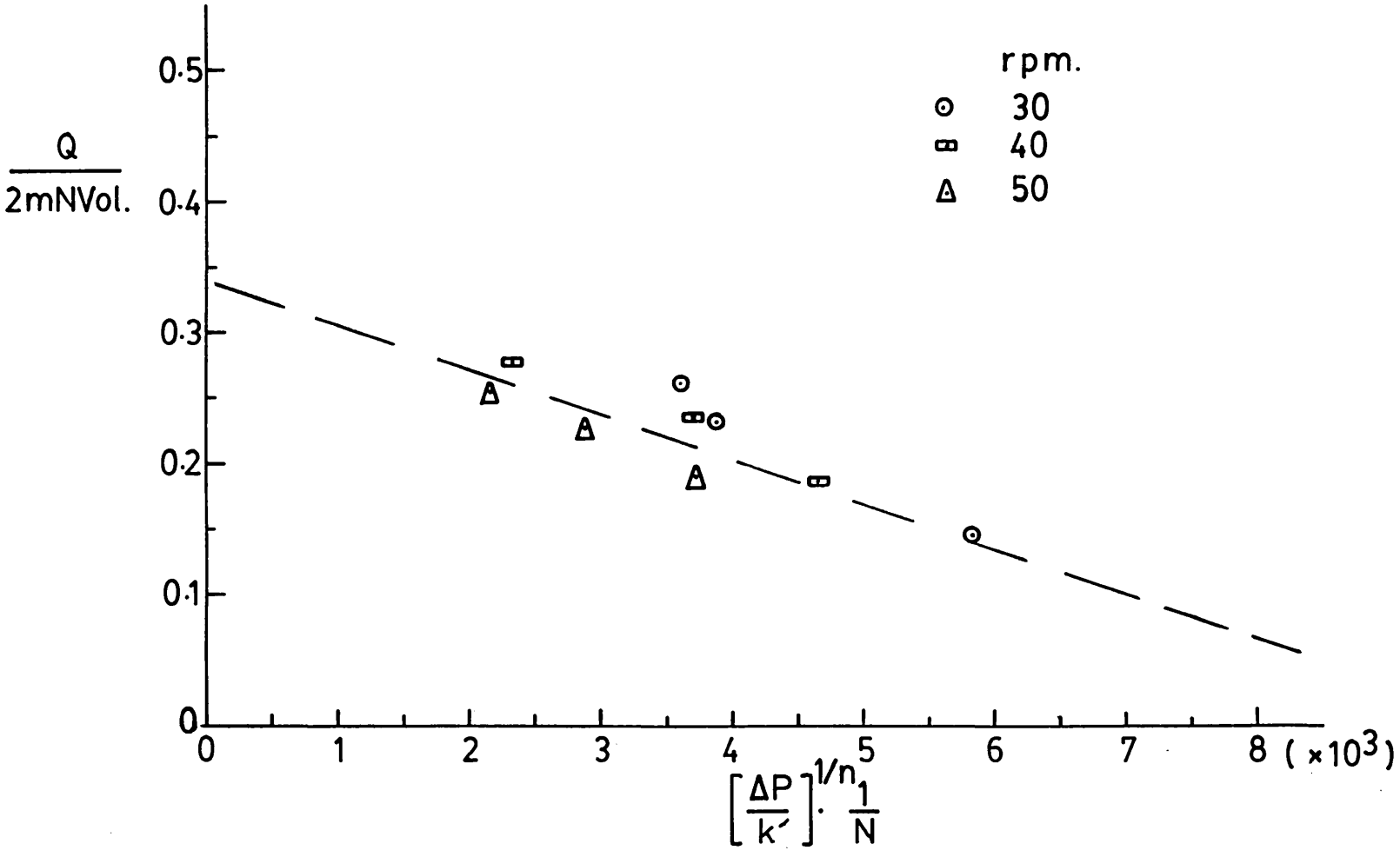

Figure 4·6·15. Dimensionless throughput rate versus pressure drop for screws A, extruding polystyrene-HS at 180°C, $n = 0{\cdot}41$, $\mu_o = 18{\cdot}5$ kNs/m., - linear characteristic.

$\Delta P = 0.15 MN/m^2$ which is still relatively high. Therefore, in order to generate significant leakages from the die pressure, a relatively high pressure drop must be developed.

Figure 4.6.17 gives approximate linear characteristics, drawn as broken lines, for the experimental results. At zero pressure drop (i.e. for an open-ended extruder), the throughput rate for each speed is seen to vary for the given screw geometry. The throughput rate at zero die pressure drop, Δ, is still dependent on the internal drag and pressure flow generated in each chamber and associated gaps, and it would become smaller as the melt viscosity is reduced with increased speed of the screws. Over this wide range of screw speeds, a strong dependence of the throughput on speed can be seen, especially at the lower end of the range from 0 to 60 rpm., but above this, the influence is reduced and the results for the higher speeds are situated very close together indicating a behaviour which is almost independent of screw speed and melt viscosity. This is probably due to fact that, at the higher shear rate range, most of the viscosity flow curve for the melt (Figure 4.5.2) is approximately straight and can be described by a single flow index and thus, for a given geometry, the dimensionless characteristics produced would still be independent of both screw speed and melt viscosity. It is at the lower shear rates where the power law behaviour of the melt flow is valid only over a limited range, that the flow characteristics are influenced by speed and viscosity because of the varying non-Newtonian flow index; this was found to be the case for the theoretical treatment used to simulate the melt conveying process.

Figure 4.6.18 gives the dimensionless relationship between throughput rate and pressure drop for screws A extruding the same polymer at two different temperatures. Each relationship for a given screw speed is seen to be independent of operating temperature which confirms the

result previously obtained when the experimental measurements for only one operating temperature were plotted i.e. that each flow curve was indeed independent of the viscosity of the melt in the channel.

In Figure 4.6.19 the dimensionless throughput rates are plotted against the axial pressure drops alone, and the relationship can be represented by a single curve which appears to be approximately linear over most of the range of pressure drops measured probably becoming non-linear at the very low and very high values. Although the relationship excludes the influence of the melt viscosity, it is useful in determining certain aspects of flow behaviour. For example, it is possible to generate the same pressure drop with a constant dimensionless throughput rate by increasing the screw speed, which means that for a given die size, the die pressure would increase as the flow rate is increased. Since the dimensionless output rate (or specific output rate) for this type of twin-screw extruder was found to be independent of the die pressure,[5] the pressure drop would also be constant and therefore the die pressure would be linearly related to the completely filled length of the metering zone. This is contrary to what has been found by Janssen[5] for he has shown that this was the case only when the number of fully-filled chambers were small or large and the relationship showed a proportionally smaller increase with increasing die pressure. Such a linear relationship, however, is what is expected when a uniform temperature is generated along the melt conveying zone, and this was found to be the case, as shown earlier, for the machine examined.

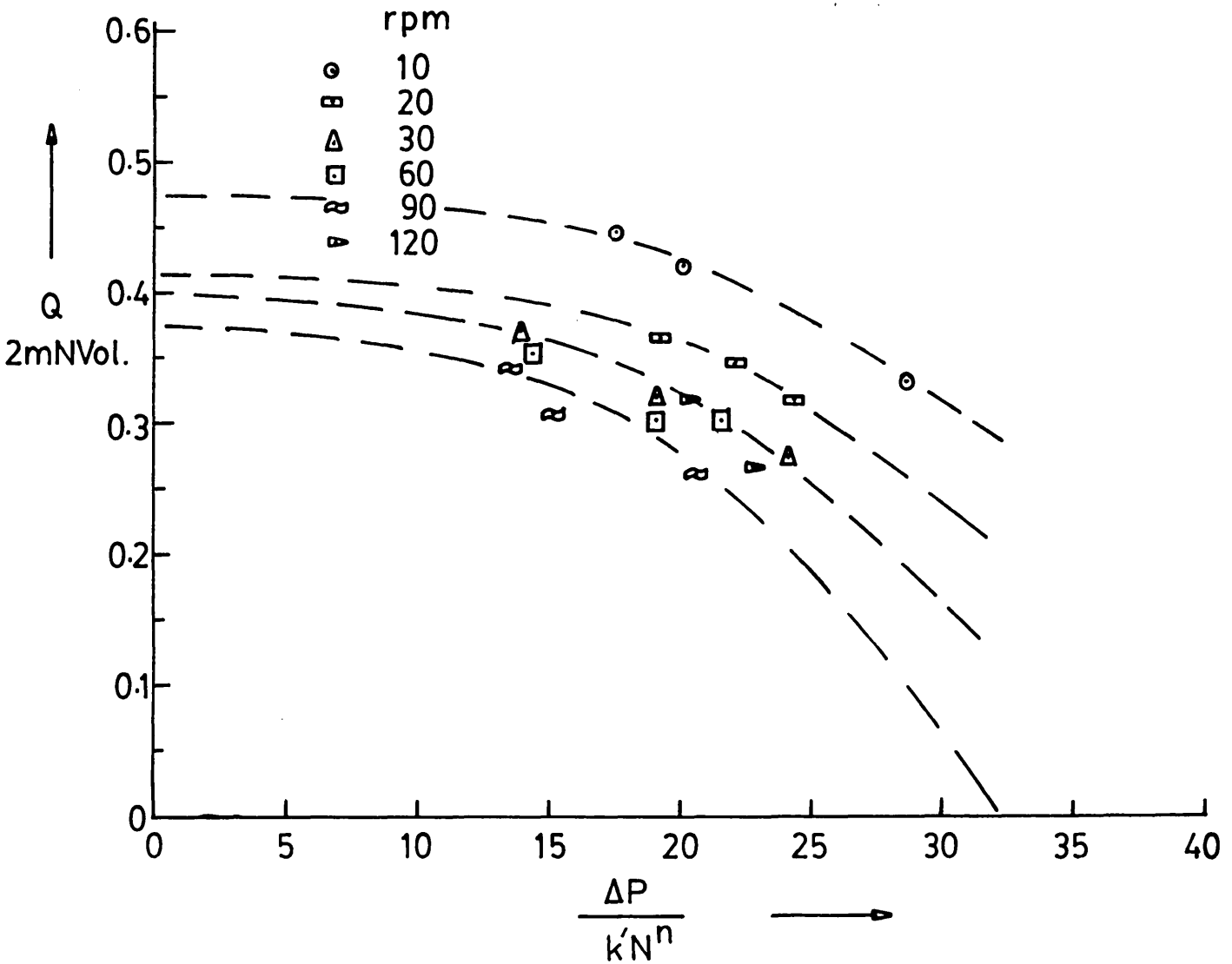

Figure 4·6·16. Dimensionless throughput rate versus pressure drop for Screws A, extruding polystyrene - CC37 at 200°C, n = 0·356, μ_o = 11·5 kNs/m^2, – – – approx. curve based on linear plotting of results, Figure 4·6·17 overleaf.

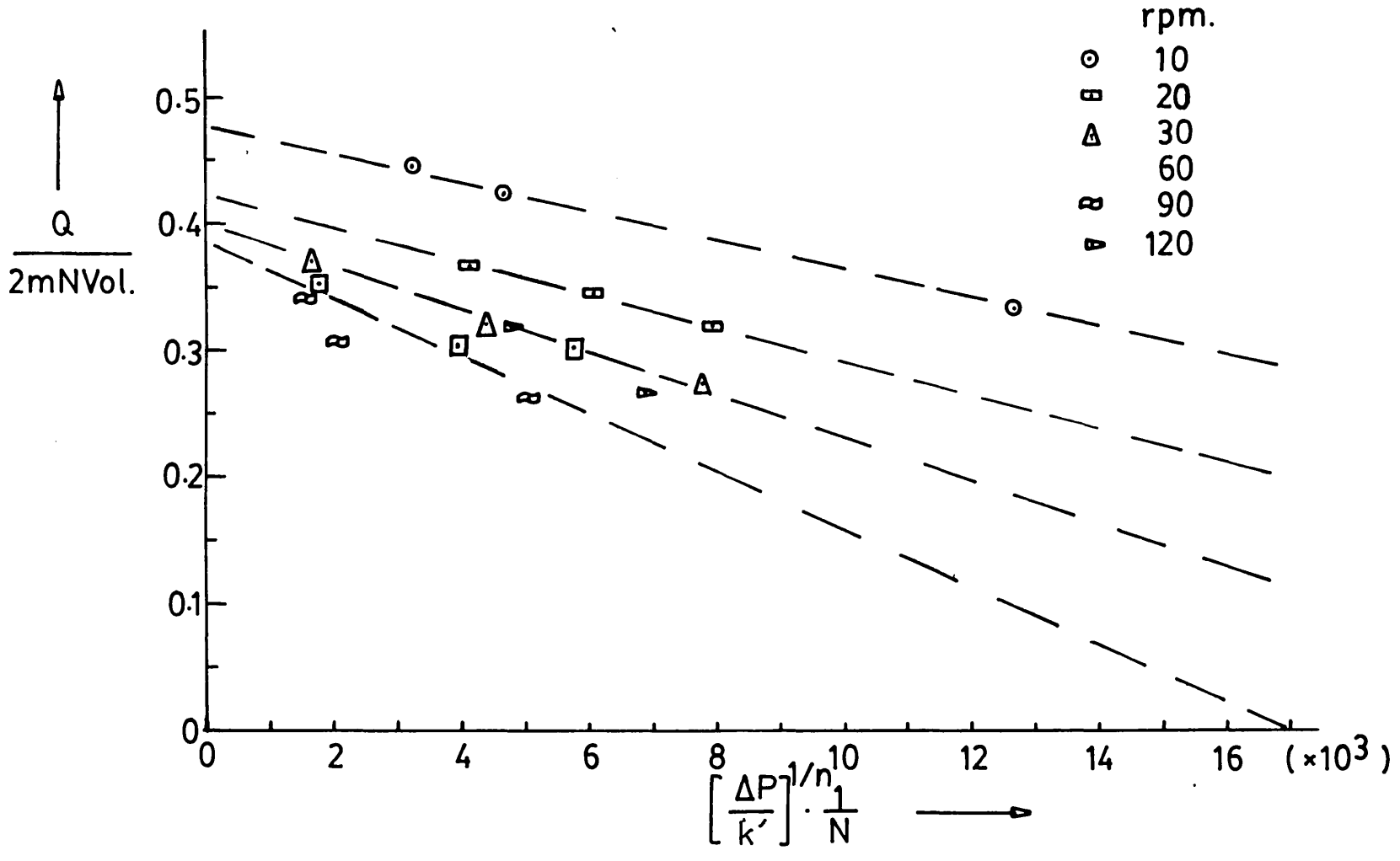

Figure 4·6·17. Dimensionless throughput rate versus pressure drop for screws A, extruding polystyrene - CC37 at 200°C, n = 0·356, μ_o = 11·5 kNs/m^2, --- approx. linear characteristic.

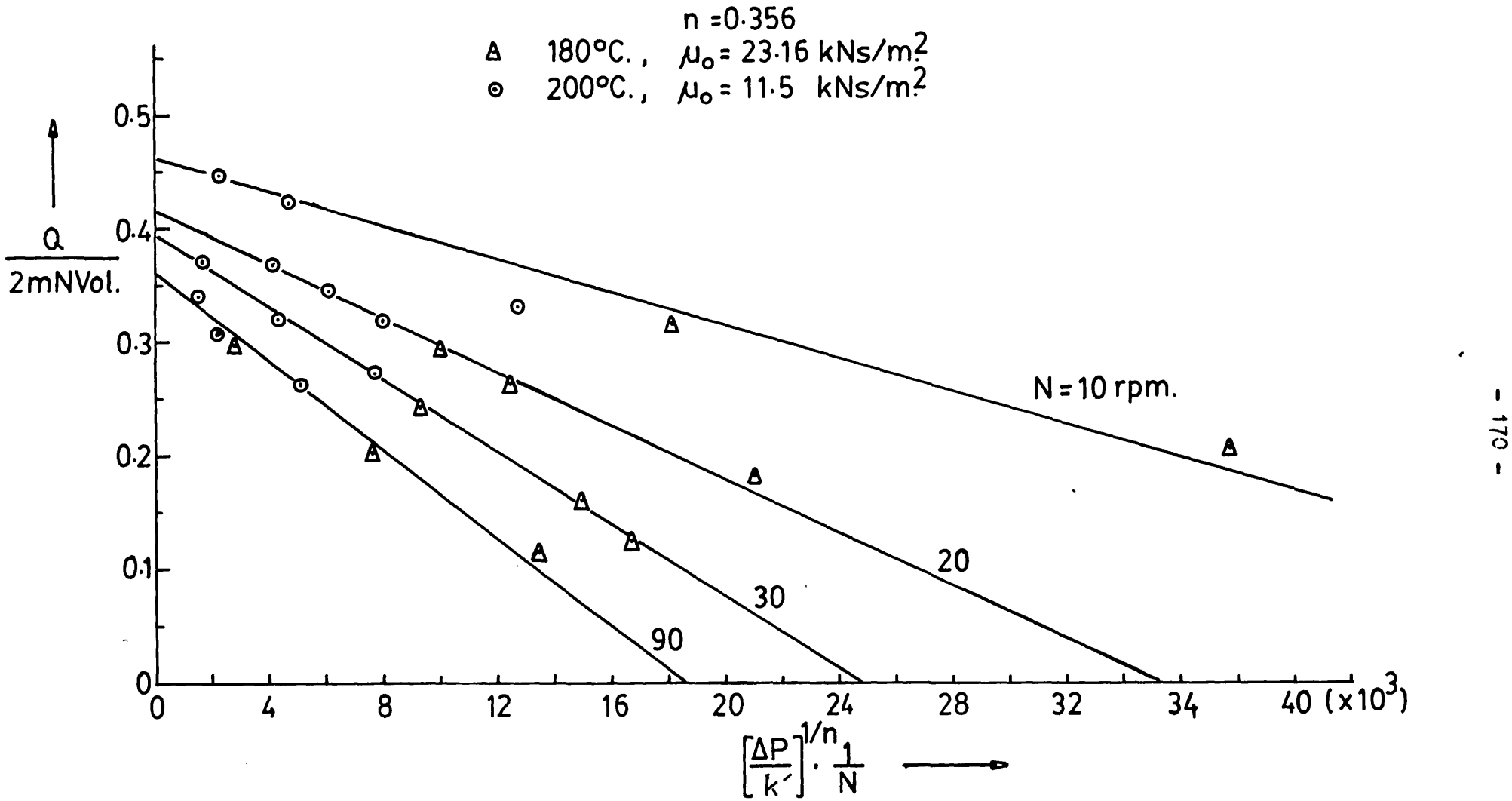

Figure 4·6·18. Dimensionless throughput rate against pressure drop for screws A extruding polystyrene CC37 at 180°C and 200°C. —— approximate relationship.

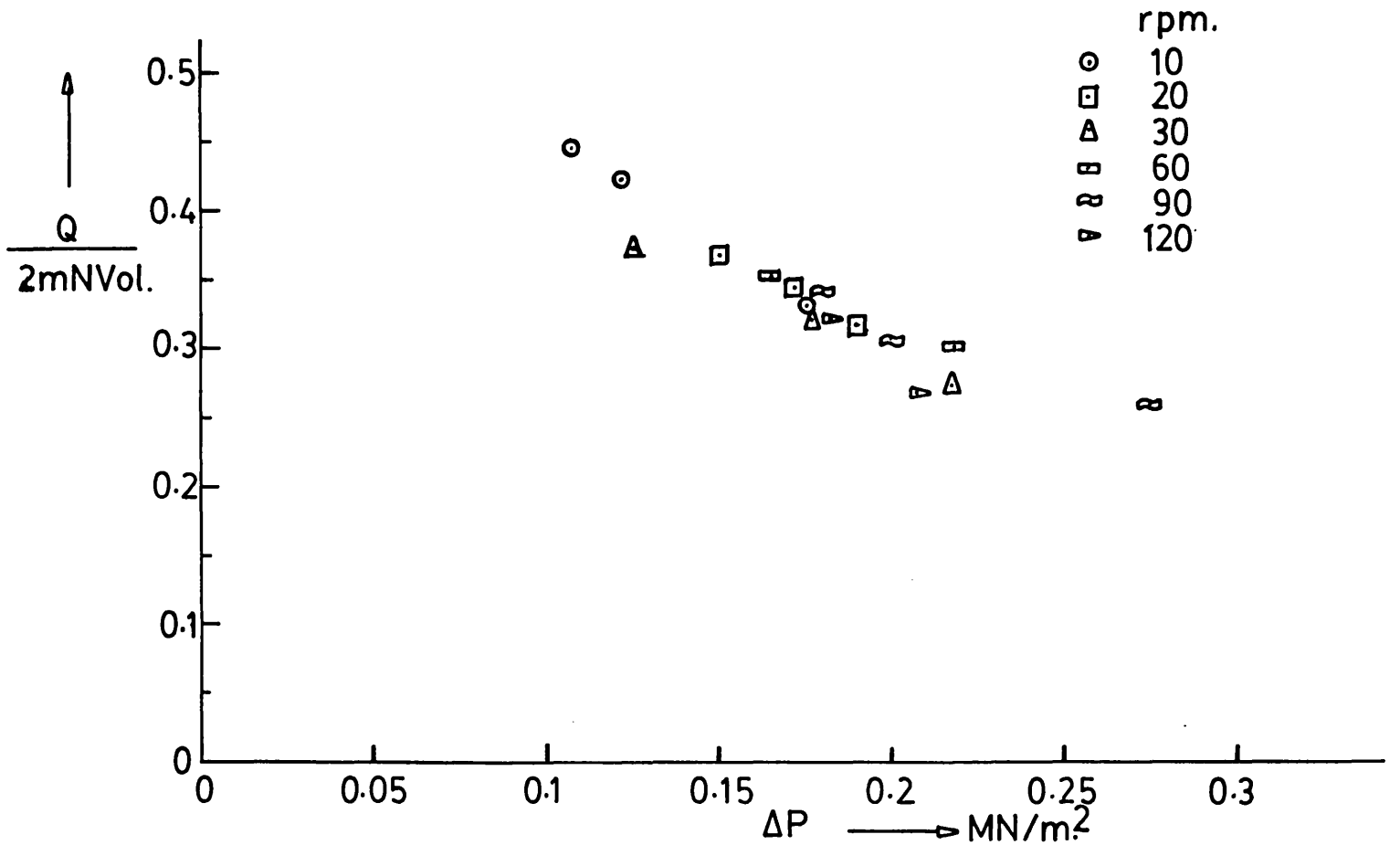

Figure 4.6.19. Dimensionless throughput rate against axial pressure drop, screws A extruding polystyrene-CC37 at 200°C. The relationship can be represented by a single characteristic.

4.7 Comparison of Experimental and Theoretical Results

In section 3.11, a comparison of experimental and theoretical results was presented for Newtonian flow. The predictions obtained from the non-Newtonian model developed were compared with experimental and predicted results of Janssen.[5] The agreement between experiment and theory was good and the theoretical results were comparable to Janssen's predictions except for overestimation of the leakage flow when both the side and calender gaps were relatively small compared with the tetrahedron gap. The main difference between the numerical flow model developed and Janssen's flow model is the method used for predicting the tetrahedron leakage flow rate. A theoretical method is used in the numerical model whilst an empirical flow equation is used in Janssen's model to predict the tetrahedron leakage. It is not surprising therefore, that Janssen obtained very good predictions when both the side and calender gaps were small because then, the leakage flow would be predominantly tetrahedron leakage flow which for this case would be an empirical flow rate and should be comparable with the experimental results. However, the discrepancy obtained amounted to less than about 10% reduction in the melt conveying throughput rate at zero die pressure which is an acceptable error considering the approximations used in modelling the flow in the intermeshing region. The non-Newtonian model developed therefore satisfactorily predicts the throughput rates for the twin-screw extruder and it can now be tested for melt flow. In general, comparison of the experimental and theoretical results for the screw arrangements tested indicated that leakage flow can be adequately represented by treating the flow in the calender, side and flight gaps as one-dimensional but a deep channel flow analysis must be used for the chamber in order to obtain the best prediction of leakage flow behaviour. A two-dimensional narrow channel analysis of the tetrahedron flow is found to give good predictions of flow rates.

Tables 4.7.1 to 4.7.3 give the experimental and predicted output rates for the screw arrangements tested and these results are also given in Figures 4.7.1 to 4.7.4. The experimental results are given also in Figures 4.7.1a and 4.7.1b. The flow-pressure characteristics used for determining the deep channel flow rates for the screws were given in Figures 3.11.10 and 3.11.11 and those for the tetrahedron leakage were given in Figures 3.11.7 to 3.11.9. For the other leakage flows and also for the channel flow, melt viscosity was determined at the mean drag shear rate (defined for each gap and the channel in chapter 3, based on the relative drag velocity of the walls) using linear interpolation of the viscosity logarithm flow curves (Figures 4.5.1 and 4.5.2) over small ranges of shear rate.

Before discussing the comparison of the theoretical results using the complete model developed, it is worth considering whether more simple analyses would give reasonable predictions of output rate, therefore, a Newtonian analysis, modified Newtonian analysis using viscosities based on local mean drag shear rates and a non-Newtonian analysis using a power law fluid of constant power law index were carried out. Figure 4.7.1a gives the experimental and some theoretical results for the extrusion of polystyrene CC37 at 200^{o}C using screws A. The results are plotted using dimensionless throughput rate and pressure drop terms. The viscosity of the melt in the channel was used to compute the dimensionless pressure drop term (because, it is the channel flow which determines the magnitude of the leakages and hence the throughput rate of the extruder). Curve 1 shows the behaviour predicted for all screw speeds with a constant melt viscosity i.e. Newtonian flow. These predictions were obtained using the non-Newtonian flow model developed but with a power law index n=1 and a melt viscosity determined for the channel is used throughout to give Newtonian representation. The solutions given above curve 1 (curve 2) show the flow behaviour when melt viscosities are determined at the relevant 'mean drag shear rate' for each

flow passage and n=1, thus representing Newtonian flow in each passage with a local viscosity based on local drag shear rates. For the tapered calender passage, the maximum drag shear rate computed at the minimum clearance σ was used to determine the viscosity. The solutions show a small dependence on speed but this is too small to be represented accurately by separate curves and therefore, the behaviour is illustrated as a single curve, curve 2. In comparison with the experimental results it can clearly be seen that Newtonian predictions greatly underestimates the leakage flow rates. This appears to be due to the fact that there is significant difference between the dimensionless flow rate - pressure gradient characteristics of Newtonian and non-Newtonian fluids giving large errors when the fluid is highly non-Newtonian (which in this case it is) and when pressure gradients are large (see Figure 2.5.5). This can be seen also as the inability of the Newtonian analysis to describe the non-Newtonian flow adequately with melt viscosities based only on the mean drag shear rates, especially, in this case, because the drag shear tends to be low for most flows in the twin-screw extruder.

Referring to the throughput rates of curve 1, Figure 4.7.1a, one would expect smaller throughputs (or larger leakage flow) when melt viscosities based on local drag conditions are used for the gaps, because of the lowering of the shear rate - dependent viscosities. In relation to curve 1, however, curve 2 shows the opposite behaviour i.e. less leakage flow. A reduction in the side gap leakage was found to be responsible for this behaviour because of a higher melt viscosity in the gap than in the channel due to a lower mean shear rate in the gap. Although the other leakage flows were increased because of the lower melt viscosities, the reduction due to the side gap was more significant and this flow rate (which was about 28% of the total leakage) was the dominant leakage. It should be noted also that, in comparison with screws B, the side gap is larger in these screws and such a predicted behaviour is not expected with screws B; this is shown to be the case later.

Curve 3 shows the theoretical behaviour when all flows were predicted using the parameters of n=0.356 and μ_o= 11.5 kNs/m^2 to determine viscosities for all the passages. This viscosity data was obtained from a power law fit of the logarithm flow curve using the mean drag shear rates in the channel of about 4 to 35sec^{-1} over the speed range of 10 -90rpm. The model predicts a single curve relationship for all speeds indicating that the melt conveying behaviour of the twin-screw extruder cannot, therefore, be adequately predicted using a single set of power law paramaters n and μ_o over the whole range of shear rates. The results displayed in Figure 4.7.1a clearly demonstrates that Newtonian analyses are completely inadequate in describing the extruder behaviour as they seriously overestimate the output rates. The attempts to improve on the Newtonian analysis using the same viscosity in all passages has failed for this geometry and a single power law index model for the fluid does not encompass the observed variations due to screw speeds.

Figure 4.7.1b gives similar experimental and theoretical results for the extrusion of polystyrene CC37 at 200^{o}C using screws B. Curve 1 shows the Newtonian behaviour (constant viscosity) and curve 2 shows the melt flow behaviour predicted from the non-Newtonian analysis with n=1 using melt viscosities obtained from local drag shear rates. The results represented by curve 2 also show a very small dependence on speed, similar to the behaviour with screws A, but in this case leakages are increased (or throughput rates are reduced). This is because the side and tetrahedron gaps are relatively small compared with the calender gap and the calender leakage being the dominant leakage flow rate reduces because viscosity tends to be lower in this gap than in the channel for these screws. The Newtonian melt-flow predictions, therefore, grosslyunderestimate leakage flows also for this screw geometry. Curve 3 is the predicted behaviour for viscosity data of n = 0.356 and μ_o = 11.5kNs/m^2. These were the same viscosity parameters determined for the channel mean drag shear rates of screws A and

is appropiate also for screws B because it channel is only slightly shallower giving similar mean shear rates at the speed range used. The curve was in agreement with experimental results at about 30rpm indicating that the range of shear rates is appropriate for melt flows generate but only at this speed.

Returning to the comparisons between experiment and theory using the full computer model, Figure 4.7.1 gives comparison of experimental and theoretical results for the speeds of 30 and 50rpm, for screws A extruding polystyrene HS at 180°C. The dimensionless pressure drop term used for comparing non-Newtonian results includes the power law viscosity parameters n and k' determined for the channel based on mean drag shear rates over the relevant speed range. There is good agreement between the results at 50rpm but an overprediction of leakages occurs at the lower speed. In fact, all predictions appear to lie approximately on a single straight characteristic. It is believed that this low speed underprediction of throughput may be due to the use of the power law curve obtained at relatively high shear rates to describe low shear rate behaviour. It is well known that this leads to an over estimate of viscosity at low shear rates since in the limit as shear rate tends to zero, viscosity predicted by a power law relationship tends to infinity. There a reduced viscosity of $\mu_o = 12.5 kNs/m^2$ with index, n=0.58 was used for lower shear rates to test this effect. The resulting prediction is curve(a) in Figure 4.7.1 and it can be seen that there is, indeed, an improvement in the accuracy which appears to be a little suprising since the effect of using lower viscosities at low shear rate is to reduce leakages. It is argued that the reason for this is that the effect of a reduction of viscosity is more significant in the chamber than in the leakage gap. In the chamber, pressure is built up as the flow approaches the intermeshing zone. After leaking through to the adjacent chamber it is also built up as it leaves the intermeshing zone. If chamber viscosity is reduced, then the pressure

build up is also reduced and for a given pressure drop ($2\Delta P$) between adjacent chambers it follows that the pressure drop across the leakage passage is reduced thus reducing leakage flow rate despite viscosity reduction in some of the gaps (see Figure 4.7.1c).

Figure 4.7.2 gives the results for the extrusion of polystyrene CC37 at 200°C and speed range of 10 - 90rpm for the same screws. In general, there is an overestimation of leakages (or underestimation of throughput rates) with the worse results at the lowest speed of 10rpm. The viscosity data used over the low shear rate range of 1 to $4s^{-1}$ was n = 0.44, μ_o= 10.0 kNs/m^2. If another estimate of the viscosity at the lower shear rates is used of n=0.49, μ_o= 8.5 kNs/m^2 over the shear rate range of 1 to $4s^{-1}$, the improvement shown by curve (b) is obtained. The same explaination advanced for polystyrene HS for the underestimate of leakages is believed to be appropriate here also. There is, however, an under prediction of leakages at 30rpm which appears to indicate that there may be additional effects influencing flow behaviour.

Figure 4.7.3 gives the results for the extrusion of polysryrene CC37 at 200°C using screws B. The viscosity data appears to be more appropriate for these screws at the lowest speed, as shown by the good agreement with the experimental results at 10rpm. This is probably because the melt flows through smaller gaps and shallower channels compared with screws A and the shear rates would be higher and be within the range used in determining the viscosity data. There is also good agreement between the experimental and predicted results at the high speeds of 60 and 90rpm (although some overprediction of leakages can be seen at very low pressure drops) but there is underestimation of leakages at 30rpm. The improved predictions with these screws at high speeds compared with results for screws A indicate that the effects which produce overprediction may be more significant in the side and tetrahedron gaps because these gaps are smaller in screws B.

Comparison of results appear to indicate also that this effect is reduced to zero somewhere within the moderate speed range 40 - 60rpm, as illustrated earlier by the very accurate predictions obtained at 50rpm for polystyrene HS, Figure 4.7.1. It is important to note, also, that it would usually be extruder operations at moderate instead of lower or very high speeds which would be of more interest, for it is very often the practice to extrude at the fairly high output rates which would still keep the viscous heat generation to a tolerable level. In general, the agreement between the experimental and theoretical results are within about 18% which is considered to be satisfactory.

Figure 4.7.4 gives the comparison of experimental and theoretical results for dimensionless throughput rate plotted against axial pressure drop alone. The distribution of the experimental results appears to indicate that there is a single-curve relationship when the effects of screw speed and melt viscosity are excluded. The majority of predicted solutions given (except two at 30rpm) are situated almost on the approximate theoretical curve shown, indicating a similar behaviour. Although theory underestimates the throughput rate, the form of the theoretical curve in relation to the experimental results illustrates that the model adequately simulates extruder flow behaviour over the range of screw speeds used.

An attempt was also made to verify the theory for the extrusion of a typical PVC formulation (manufactured by BP Chemicals Ltd.). From preliminary tests performed with screws A extruding the PVC material at the recommended maximum operating temperature of 180°C, it was found that the largest output rate or the longest pressure profile that could be obtained, was limited by the maximum allowable power consumption of the machine and, consequently, only one pressure drop could just be obtained for any speed used. In addition, there were difficulties in obtaining a satisfactory viscosity flow curve for the very viscous PVC melt at 180°C due to the inconsistency

Table 4.7.1 Comparison of experimental and theoretical results: screws A, extruding polystyrene-HS grade at 180°C.

N	Q_{th}	ΔP	Q kg/hr.	
rpm.	kg/hr.	MN/m^2	Exptl.	Theoretical.
30	24.22	0.49	3.72	3.03
		0.41	5.82	4.91
		0.40	6.60	4.66
50	40.37	0.50	7.92	7.53
		0.45	9.48	9.79
		0.40	10.68	10.76

Table 4.7.2 Comparison of experimental and theoretical results: screws A, extruding polystyrene-CC37 grade at 200°C.

N	Q_{th}	$4\Delta P$	Q kg/hr.	
rpm.	kg/hr.	MN/m^2	Exptl.	Theoretical.
10	8.35	0.70	2.77	2.35
		0.49	3.54	2.96
		0.43	3.73	3.22
30	25.05	0.87	6.86	7.29
		0.71	8.02	8.35
		0.50	9.31	9.32
60	50.10	1.00	15.23	12.97
		0.66	17.76	16.39
90	75.15	1.10	19.61	16.69
		0.80	23.00	21.05
		0.72	25.69	21.80

Table 4.7.3 Comparison of experimental and theoretical results: screws B, extruding polystyrene-CC37 at 200°C.

N	Q_{th}	ΔP	Q kg/hr.	
rpm.	kg/hr.	MN/m^2	Exptl.	Theoretical.
10	6.86	0.51	2.65	2.64
		0.38	2.95	3.26
30	20.59	0.65	6.19	6.56
		0.46	7.48	8.49
		0.37	8.74	9.21
		0.27	9.78	9.87
60	41.19	0.59	10.11	11.53
		0.47	14.47	14.27
		0.33	18.17	16.00
90	61.78	0.69	18.35	16.87
		0.47	22.26	21.31
		0.36	27.02	23.07

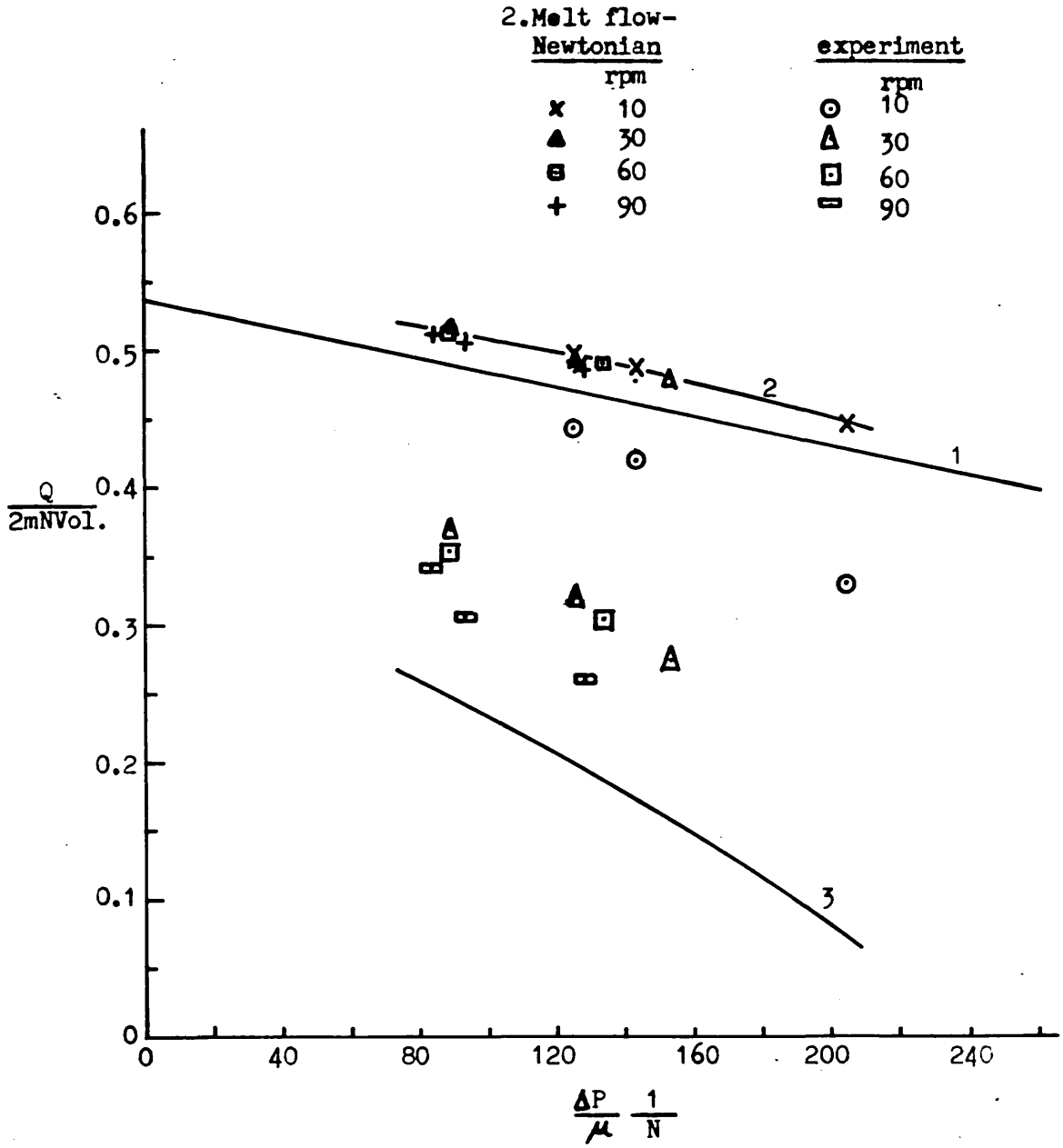

Figure 4.7.1a Dimensionless throughput rate against pressure drop for screws A extruding polystyrene CC37 at 200°C. Comparison of experimental results with, 1. Newtonian, 2. Newtonian with melt viscosities, 3. Non-Newtonian power law.

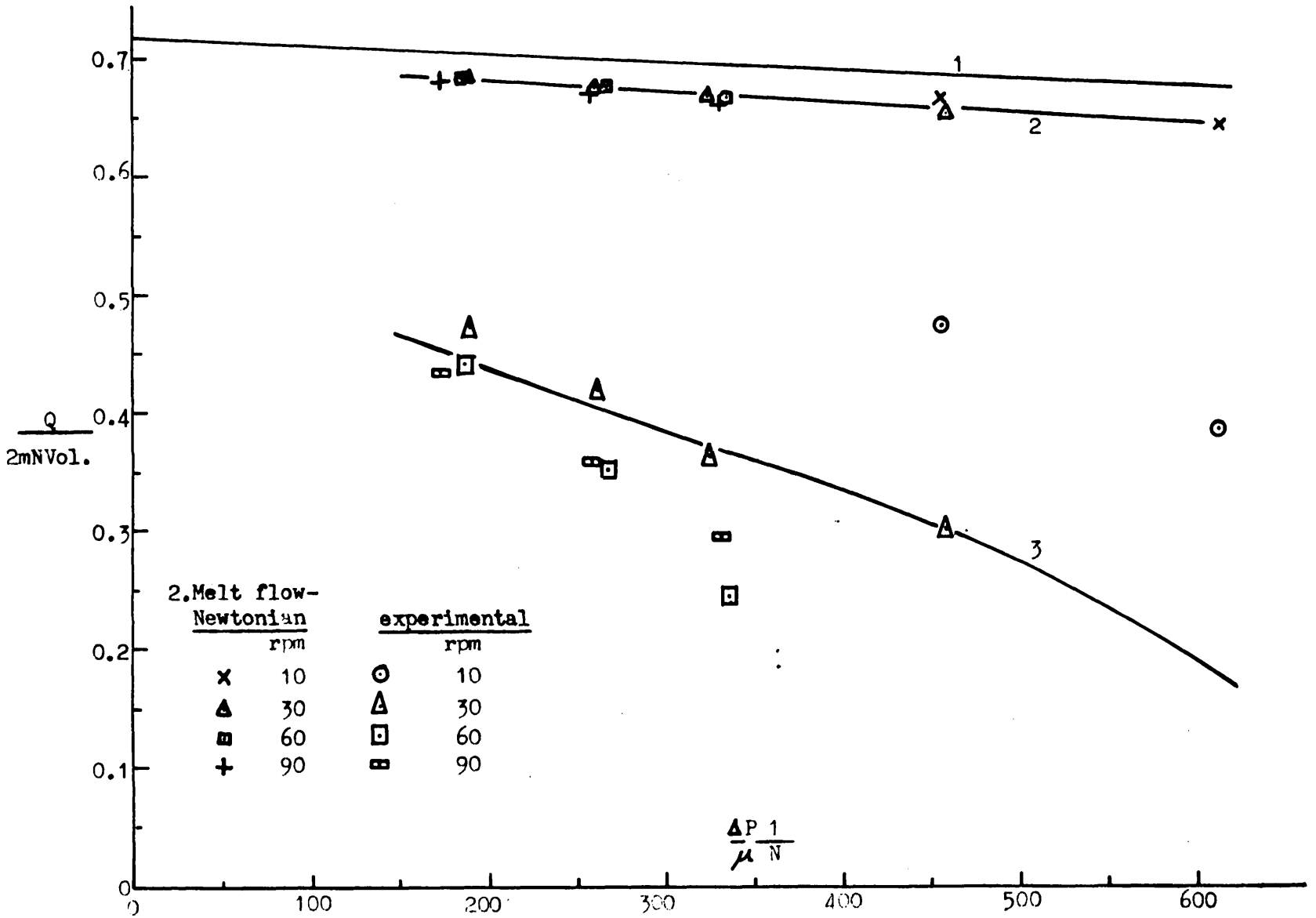

Figure 4.7.1b Dimensionless throughput rate against pressure drop for screws A extruding polystyrene CC37 at 200°C. Comparison of experimental results with, 1. Newtonian, 2. Newtonian with melt viscosities, 3. Non-Newtonian power law.

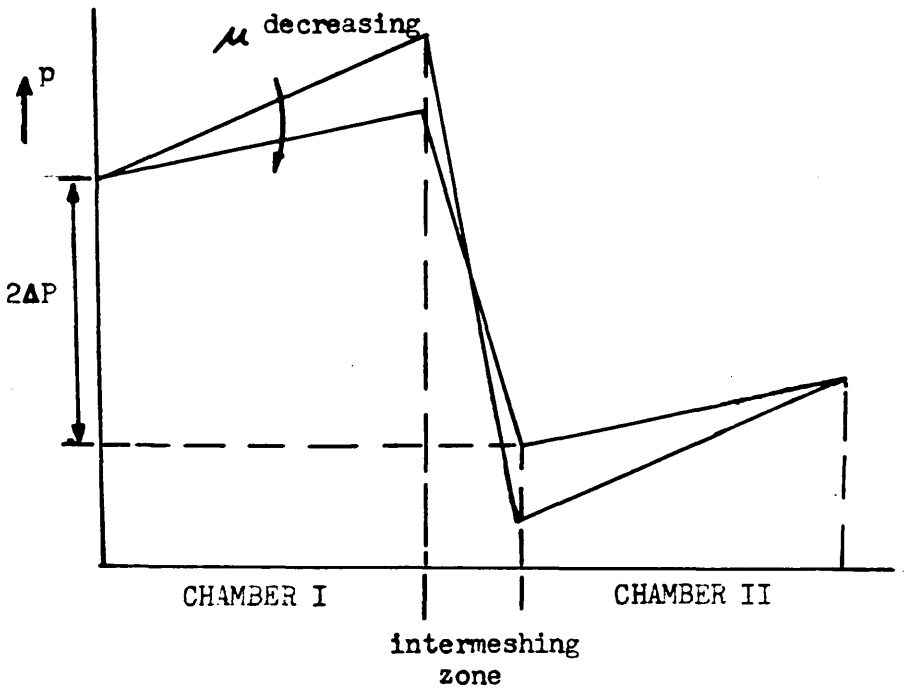

Figure 4.7.1c Pressure profiles for flow into and out of adjacent chambers through the intermeshing zone illustrating decreasing pressure gradient and leakage flow rate with reducing viscosity μ in the chambers.

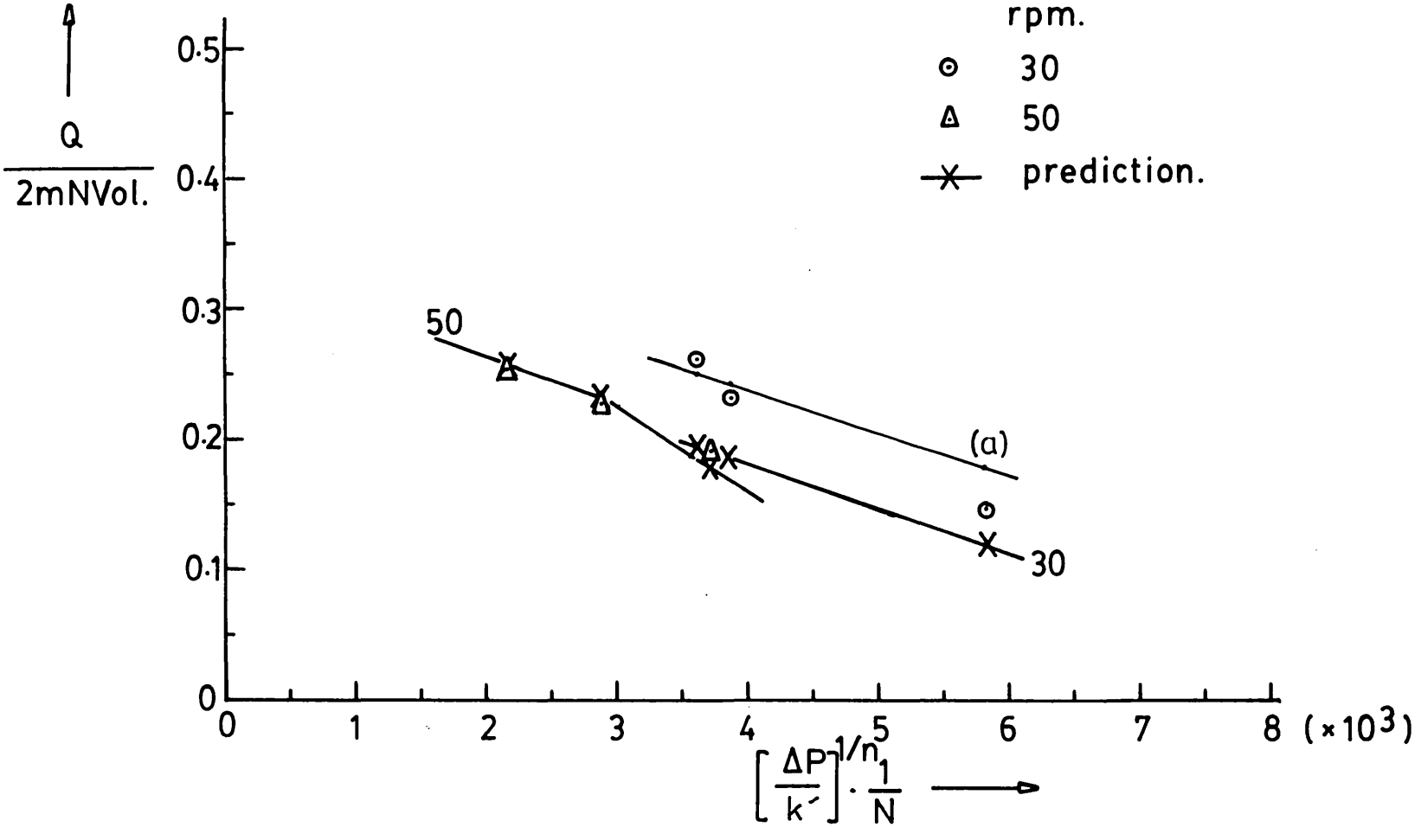

Figure 4·7·1 Dimensionless throughput rate versus pressure drop for screws A, extruding polystyrene-HS at 180°C, n = 0·41, μ_o = 18·5 kNs/m^2, -comparison with theory.

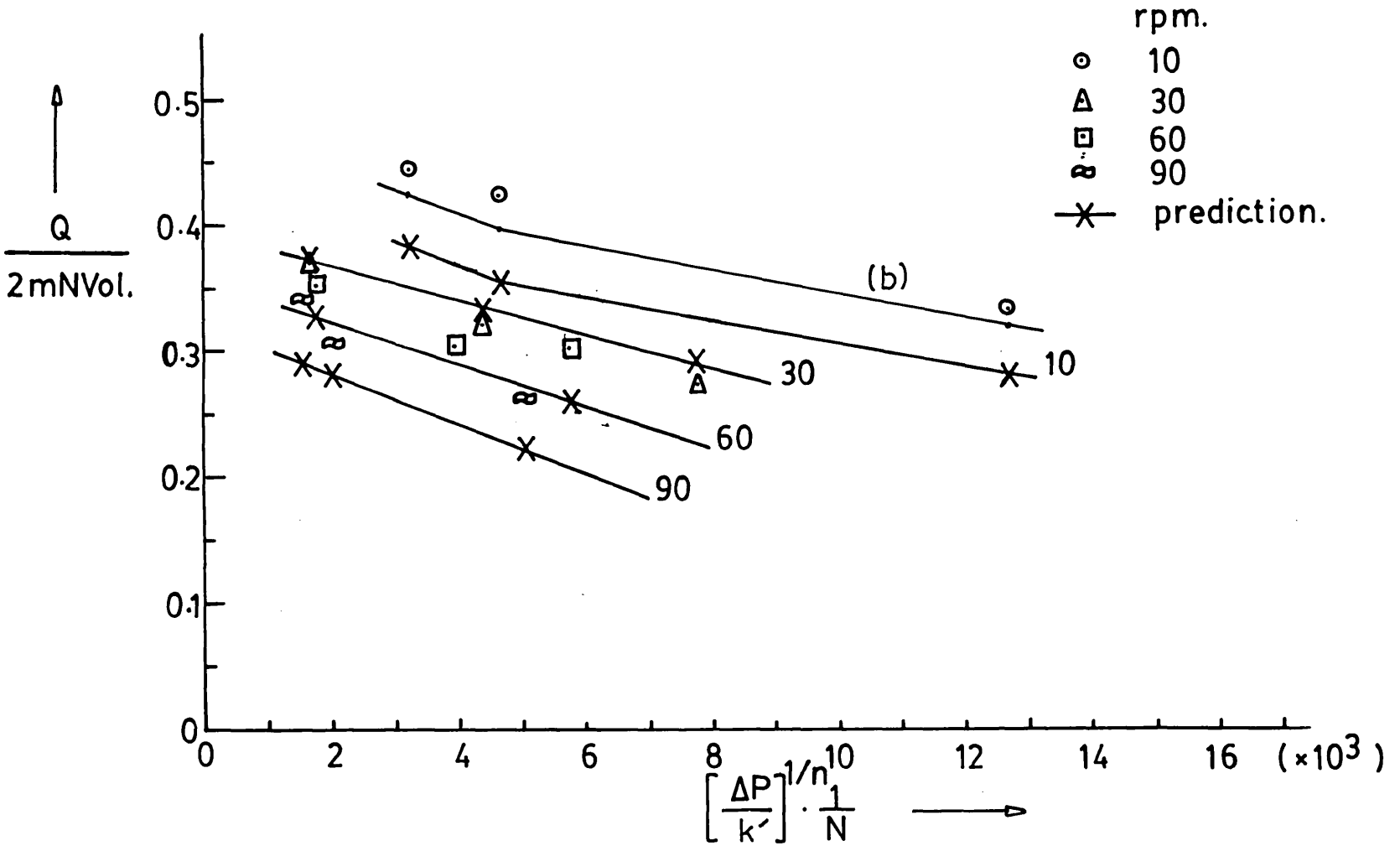

Figure 4.7.2 Dimensionless throughput rate versus pressure drop for screws A, extruding polystyrene - CC37 at 200°C, n = 0.356, μ_o = 11·5kNs/m^2, — comparison with theory.

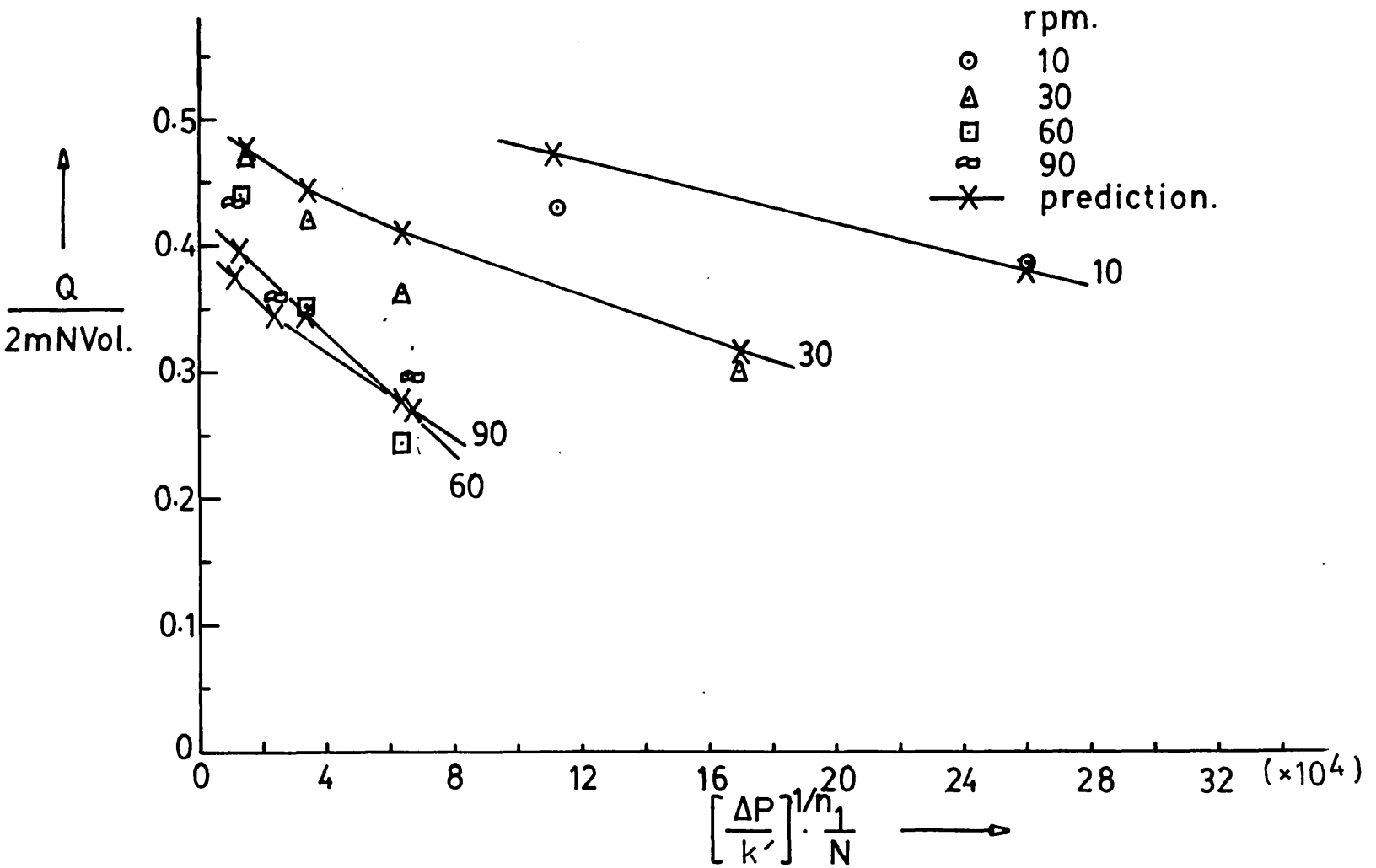

Figure 4.7.3 Dimensionless throughput rate versus pressure drop for screws B, extruding polystyrene - CC37 at 200°C, n = 0.356, μ_o = 11.5 kNs/m^2, – comparison with theory.

of the measurements produced by the combination of high elasticity and the large power required to extrude the melt through the small die, resulting in unsteady measurements even after long extrusion times. However, with the use of rough estimates of both pressure drop and viscosity for predicting the leakages, the agreement between the experimental and theoretical results was within 36% for a screw speed of 10rpm and 18% over the range of 30 - 60 rpm. The same behaviour as for polystyrene melt flow was observed i.e. an underestimation of leakage flow at 30rpm but overestimation at 10, 60 and 90rpm. In view of the inaccuracy of the data used, the larger discrepancy in the results obtained with this material can be considered acceptable, and it appears, therefore, that the theory is likely to be appropriate also for predicting PVC melt conveying in counter-rotating twin-screw extruders.

In general, the model predictions were consistent in behaviour for the two screw geometries tested, but the disagreement with experimental results were found to be different at low and high speeds. Major errors in the predictions are most likely to be due to inaccurate viscosities ($\pm$ 5%) due to unsteady temperature conditions during measurement but this should have the effect of either, over or under estimating throughput rates and showing consistent behaviour with increasing screw speed. Comparison of results shows that this was not the case over the speed range used and that other factors might be influencing the flow behaviour. The results show that these effects are not large enough to produce unacceptable errors but significant enough to warrent further examination. One such influencing factor could be the thermal effect. Although experimental measurement of channel flow conditions (given in section 4.6) indicate that heat generation did not have much effect on net pressure drops and hence channel melt viscosity, it may be possible that flows in the gaps are affected.

To obtain an insight of the likely effects of temperature in each flow passage, the dimensionless Griffith number, G and Graetz number, G_z for each

flow were examined. The Griffith number quantifies the ratio between heat generation and thermal conduction and it determines whether heat generation will lead to temperature differences within the melt sufficient to affect the velocity distribution locally. The Graetz number is a measure of the importance of thermal convection in the direction of flow relative to conduction normal to the flow. These numbers were defined in section 2.6. When G was determined for the tapered calender passage, a shear rate computed for a mean clearance depth was used. For the tetrahedron gap, the maximum mean shear rate at the largest clearance depth was used since this value gave a conservative estimate of G. For determining G_z, an average clearance depth was used for the whole length of the calender gap and a mean length and depth was used for the tetrahedron gap. The Griffith and Graetz numbers were estimated as follows:

Flow passage	Channel		Tetrahedron		Calender		Side		Flight	
rpm	10	90	10	90	10	90	10	90	10	90
Screws A										
G =	.4	3.6	.2	1.8	.026	.24	.012	.108	.057	.513
G_z =	55	495	453	4077	13	117	30	270	.34	3.1
Screws B										
G =	.41	3.69	.15	1.35	.018	.162	.008	.072	.045	.405
G_z =	49	441	118	1062	10	90	15	135	.146	1.31

For the calender, side and flight gaps, $G < 1$ over the speed range of 10 - 90rpm, indicating that temperature variations due to heat generation would not significantly affect the velocity profiles and the flow may be treated as isothermal for these gaps. This condition would also be valid for the tetrahedron leakage flow at the very low speeds and would probably be justified also at the moderate speeds since the G values given represent the worse cases. Assuming that $G \lesssim 1$ are acceptable limits producing only

small errors,[24] this condition for the channel flow occur at only the very low speeds and for about $N \geq 30$rpm, $G > 1$, which indicates that temperature effects would be significant in the deep channels. The Graetz values for all the flow passages, with the exception of the flight gap were large enough (i.e. $G \gg 1$) to indicate that thermal convection would be dominant in the direction of flow. Therefore, temperature profiles would develop very slowly in the direction of flow, with very little temperature development occurring from inlet to outlet due to the short length of the flow passages. For the flight gap, $G_z < 1$, indicating that heat transfer would be dominated by thermal conduction to and from the boundaries i.e. the flow would be thermallyfully developed and temperature profile would not change in the direction of flow. The results appear to suggest, so far, that the isothermal assumption would probably be justified for all flows at low speeds $N < 30$rpm and because of little development of temperature profiles in most passages, the assumption could be also valid for the whole speed range used.

In order to determine the extent of the heat generated in each chamber, the temperature rise was estimated by assuming adiabatic flow conditions in the extruder (i.e. no loss or gain of heat from the system). The Newtonian analysis introduced by McKelvey[23] for adiabatic extrusion was employed. The variation of viscosity as a function of the downchannel distance was obtained by performing an energy balance for both downchannel and cross-channel flows and also flow in the flight gap. It was assumed that all mechanical energy dissipated by the screw in a down channel increment equals the thermal and pressure energy gained by the melt in that increment. The temperature dependence of the viscosity given in equation 2.3.6 was used and temperature integrated over the length of the channel and flight gap. Using typical melt viscosities, the net bulk temperature rise for drag flow through two adjacent C-shaped chambers (m=2 for the screws) of screws A

was estimated to be about 12°C at 10rpm and 26°C at 90rpm. When the flow in the flight gap was neglected, the temperature rise was negligible (< 1°C) at 10rpm and less than 3°C at 90rpm. Higher or lower temperature changes would be expected when there is an additional superimposed pressure flow with gradient of either positive or negative values respectively. A positive pressure gradient would increase the shear rates at the barrel wall and hence increase the power due to shear in the channel whilst a negative pressure gradient would have the opposite effect i.e. reduce the power. It appears that melt temperature in the chamber is likely to rise significantly only as a result of the heat generated in the flight gap. This was shown earlier to be the case by a $G_z < 1$ for the flight gap indicating a fully developed temperature profile for the flow.

A bulk temperature rise of 12°C would produce a reduction of the melt viscosity of about 25% which is a significant change. For the channel flow alone, however, the heat generation appears to be negligible, although in the earlier analysis $G > 1$ at $N \geqslant 30$rpm indicating that significant thermal effects would be present for the higher speeds. This is probably due to the short length of the C-shaped chamber over which very little temperature development takes place.

The same analysis was used for one-dimensional flow through the remaining gaps to estimate temperature rises. For the calender passage , the depth equal to the smallest clearance was assumed to be constant over its length, and mean values of both depth and length were used for the tetrahedron clearance. Negligible temperature increases (< 1°C) were obtained for the calender and side gaps which was due to the presence of the low values of mean shear rates, even at 90rpm, whilst the same result was obtained for the tetrahedron leakage flow but in this case, was due mainly to its relatively short length. For screws B, a slightly larger temperature rise was obtained at each speed for channel and flight gap flows because of

the smaller depth of the flow passages. Although gap size was generally smaller in screws B compared with screws A, they were not small enough to produce a significant increase of shear rate and of temperature rise in the leakage flows.

From the analysis , therefore, it can be concluded that heat generation is not likely to significantly affect velocity profiles in all flow passages over the speed range used and it appears that the isothermal assumption used for all the flows is justified. There will be in each chamber, however, a temperature rise above extruder operating temperature mainly due to heat from the flight leakage flow. Some of this heat will be lost by convection through the barrel wall and the rest transferred to the channel by convection with the leakage flow and by conduction through the screw walls. Experimental evidence suggests that this may be the case, since melt temperature rise in the heated die was not greater than about $9^{o}C$ at 90rpm (see Figure 4.6.8). In screw channels of extruders, heat transfer would be improved by thermal convection produced by the recirculatory flow in the channel. Thermal convection produced by transverse flow would have the effect of cooling the screw by transferring the heat generated to the top of the channel where it could be lost more readily by conduction through the barrel wall. A theoretical study by Martin[24] of fully developed non-isothermal two-dimensional flow in screw channels has shown that this is the case when cross-channel thermal convection is included. He found that the down channel flow rate computed with transverse thermal convection was nearer to the isothermal case than when only heat conduction was considered. The additional effects of recirculation in the downchannel direction in each chamber would improve heat transfer and mixing and help in maintaining a uniform temperature.[5]

Now considering only flow in the flight clearance, a high temperature associated with the fully developed temperature profile would reduce viscosity.

In this case, leakage flow should be higher than when the viscosity at the barrel temperature is used to predict this flow. The underestimation of leakage flow observed at 30rpm could be due to this effect but this does not explain why there is overestimation at higher speeds.

Another factor which is likely to have some effect on flow is the elasticity[70] of polymer melts. The much larger errors produced with the extrusion of highly elastic PVC melts compared with polystyrene melts using the same screws appear to indicate that the discrepancy between experimental and theoretical results could be due to the neglect of melt elasticity. If this is the case, then the absence of these overpredictions with screws B extruding polystyrene appears to indicate also that the elastic effect is more significant in some leakage flows more than others. Elastic effects could produce unstable flow conditions in small clearances and thus, could be responsible for a reduction in flow. Melt fracture[71] which has been associated with wall slip occurs at a critical shear stress usually of about $10^5 N/m^2$ for polystyrene incapillary flow and at about 1.4 times this value in slit flow.[72] From single-screw extrusion experiments of power measurements[30,73] and studies of the lubricating effect of melts[74] there is evidence which suggests that slip and melt fracture occur in the flight clearance with breaking down of the melt film and producing no flow over the flight. Viscosity measurements taken with polystyrene in capillary flow (see section 4.5) have shown, however that no slip/melt fracture took place for the wide range of shear rates used. This together with the fact that the flight clearances of the twin-screw extruder were about three times larger than what would normally be found in a single-screw machine[1,74] of the same diameter, suggests thst these effects would not be relevant for the screw geometries tested.

There are other flow situations in which the elastic properties of polymer melts become important. For instance, convergent pressure flow or channel flow with a constriction like flow in slit dies, and pressure

flow through capillary tubes. These cases have received considerable attention in the literature,[75-80] with both experimental and theoretical studies carried out to examine elastic effects on entry and exit losses of viscoelastic liquids in developing flows. Experimental results[78] indicate that entrance length for a viscoelastic fluid is longer than predicted for the corresponding viscoelastic liquid, in other words, all velocity profiles develop slower than the elastic predictions. Therefore, for polymer melts, the pressure losses in dies would be larger than for inelastic liquids indicating a reduction of flow for the same pressure drop with elastic melts. Elasticity level is usually assessed in terms of the Deborah number, D_e defined as the ratio of a relaxation time to a residence time of the flow.[75,76] For polymer melts the relaxation time can range from a few seconds to about 10 seconds.[75,76] For a $D_e = 1$, elastic effects are about the same order as viscous effects and for $D_e \ll 1$ the fluid is inelastic. For channel flow in single screw extruders, the residence time is usually large in comparison with the relaxation time and $D_e \ll 1$, thus elastic effects are usually neglected, although there is evidence which suggests that elasticity could be important in deep channel flow. For twin-screw extruders, however, $D_e \gg 1$ for both the chambers and in the leakage gaps and elasticity effects may be quite significant. Elasticity is essentially a memory effect which depends on the past history of the flowing melt.[83] This is seen in capillary flow as the phenomenon of die swell.[82] The melt is found to contract laterally in order to pass through the capillary before tending to recover elastically to its previous form. This and the increased resistance to flow is likely to have severe consequences for flows from the channel into and out of sudden contractions and expansions like in the case of the tetrahedron and side gaps but to a lesser extent in the calender passage because of the gradual convergence and divergence of the flow. In addition, the effect of elasticity on flows would increase

as residence time (and speed) increases, therefore, the effect would progressively become worse. This could be responsible for the observed increase in the overestimation of the leakageflow with increasing speed.

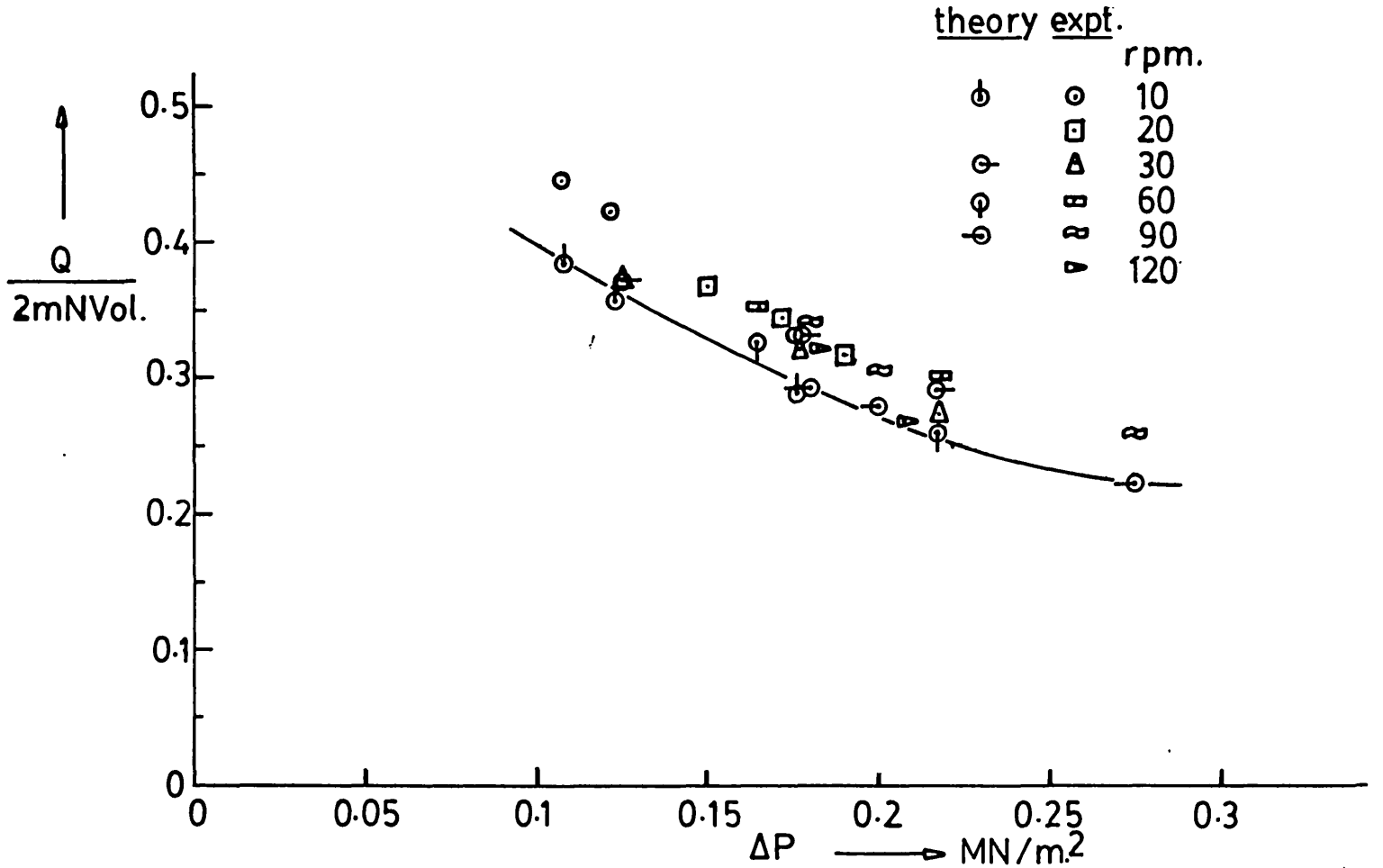

Figure 4.7.4 . Dimensionless throughput rate against axial pressure drop, screws A extruding polystyrene-CC37 at 200°C . The relationship can be represented by a single characteristic. —— theoretical curve.

CHAPTER 5

DISCUSSION AND CONCLUSIONS

The object of the study reported here has been to develop a theoretical method capable of realistically predicting flow behaviour in a counter-rotating twin screw extruder with a view to advancing extruder technology in both design and operating technique. One of the starting points in developing the theoretical model was the important pioneering work of Janssen who established the basic operating mechanisms of counter-rotating extruders, identified the various leakage flows and obtained accurate predictions of flow behaviour for Newtonian fluids. Although the value of Janssens contribution can in no sense be minimised it was believed that a considerable extension to his work was necessary to enable successful quantitative predictions to be made for polymer melts which are non-Newtonian. This, as was demonstrated in Chapter 4, proved to be the case; Newtonian and modified Newtonian analyses seriously overpredict output rates for polystyrene and the margin of error is too large to be acceptable for detailed design purposes.

Although the ultimate objective was to produce a model for non-Newtonian flow, an important stage in the development of the model was that it should accurately predict the much simpler condition of Newtonian flow. It was realised at an early stage that to base this analysis completely on Janssen's approach would not be satisfactory. This is because Janssen's method involved an experimentally determined relationship for flow in the important tetrahedron gap using an apparatus which consisted of a set of modified discs. This is a reasonable approach for Newtonian flow but for a non-Newtonian situation it was envisaged that separate tests would need to be carried out for all flow conditions and all polymers, hence being, arguably, only slightly easier than full scale testing on commercial

extruders. Therefore, the significant difference in the approach adopted here and Janssen's when describing Newtonian flow is that in this work a theoretical model of the tetrahedron gap is used whereas Janssen used an empirical relationship. The comparisons between the predictions obtained using this wholly theoretical model with both Janssen's predictions and experimental results presented in Chapter 3 (figures 3.11.4 (a) and (b)) show that agreement is good. This was particularly encouraging as in Janssen's tests the tetrahedron flow was the dominant leakage and in some cases predictions were superior to those of Janssen. The extension to non-Newtonian flow proved not to be merely a simple case of modifying the constitutive equations in the melt. This was because it was found that the model developed for the tetrahedron gap, although satisfactory for Newtonian predictions, was too crude for the non-Newtonian case. Therefore this model was modified, essentially by extending the regime considered and applying pressure boundary conditions at a greater distance from the intermeshing zone than in the prior case. Although this modelling is more complex it overcomes the problem, to some extent, of specifying boundary conditions along the perimeter of the intermeshing zone which must be uncertain. It also became clear that it was necessary to include curvature effects in analysing chamber flow to obtain reasonable accuracy. The resulting model is relatively sophisticated and the necessary computer programs to solve the governing equations needed to be developed without recourse to the programs of other workers although some of the principles adopted by others were followed.

The predictions of the final model compared to experiment as shown in figures 4.7.1 to 4.7.3 can be considered to be reasonably successful given the complexities of the process. Before commenting on these comparisons it is worth considering the predictions that are obtained from more simple approaches. The accuracy of these predictions will indicate whether the

additional complications involved in developing the analysis described here are justified. The simplest approach is to consider the polymer to be Newtonian and to apply Janssen's analysis or its equivalent. It has been shown that predictions based on this technique give large overpredictions of output rate when the viscosity of the melt is taken to be the viscosity in the channel (e.g. see figure 4.7.1 (a)). It is certain, however, that an improved prediction could be obtained by adopting a different viscosity, possibly the viscosity appropriate to the dominant leakage (if this can be determined at the outset) but the strategy involved in this approach still involves uncertainty and is likely to still present large inaccuracies. This conclusion can be argued if the modified Newtonian approach is considered. In this case the viscosity appropriate to each flow is based on the drag shear rate for that flow. At best this has shown to give only a modest improvement and at worst has shown a worsening of the prediction for that of Newtonian flow based on channel viscosity. This is because in some gaps the drag shear rate is very small hence implying high viscosities and underpredicting leakage. In these gaps pressure flow is the main factor in determining leakages and so if a mean shear rate based on combined drag and pressure flow is used then, once more, improvements can be expected in the predictive accuracy. However, this requires an iterative procedure and the simple approach will be found to become more and more complex to produce acceptable predictions. It is concluded, therefore, that the model which has been developed is necessary to describe the metering of polymer melts in counter-rotating twin screw extruders but, because of the discrepancies with experiment, it may not be sufficient.

Three factors have been considered to explain the differences between the predictions and the experimental results. These are inaccurate representation of the power law fluid model at low shear rates;

the effect of viscous heating on viscosity; and melt elasticity. The first of these factors is because at low shear rates a power law representation for which data is obtained at relatively high shear rates will overpredict viscosity and in the limit as shear rate tends to zero viscosity is predicted to be infinite. At low speeds the predictions for screws A, for which shear rates are lower in all passages than screws B, underestimate leakages. Using an estimated power-law relationship which gives lower viscosities at lower shear rates shows improved predictions as demonstrated in figures 4.7.1 and 4.7.2. At first sight it may appear surprising that a reduction in viscosities leads to a decrease in leakage flows. However, as explained in the previous chapter, this effect is attributed to the reduced pressure build-up in the chamber such that for a given pressure drop between corresponding points in adjacent chambers the pressure drop across the intermeshing zone is reduced, hence reducing leakages. It seems likely, therefore, that a more accurate flow curve representation in which data at low shear rates was experimentally obtained would increase the predictive accuracy of the theory.

The effects of shear heating are rather more difficult to assess. The uniformity of the pressure gradients over the length of the screws containing fully filled channels indicates that viscosity was constant and hence there was no bulk build-up of temperature which could cause viscosity changes. In the chambers of the extruder flow recirculates in both cross and down chamber directions thus enhancing heat transfer to the barrel, thus assisting the maintenance of constant temperature. If the effects of shear heating were very serious, however, some temperature rise and hence viscosity decrease as the die was approached would be expected. This evidence does not, however, prove that shear heating in the leakage gaps does not affect local viscosities which would cause increased leakage flows consistently along the screw. However consideration of relevant dimensionless

groups and estimates of the temperature rises in the leakage gaps assuming adiabatic conditions indicates that only in the flight gaps is there likely to be a serious influence of shear heating. This effect will be greater as screw speed is increased and may be a contributory factor in the general underprediction of output rate for screws B (with small gaps) but since the flight leakage is the least significant it is believed that the third factor, the neglect of melt elasticity, is a more likely cause of error.

The inclusion of melt elasticity in the analysis will have the effect of reducing flow in small clearances. However, incorporation of this property represents a further complexity in the analysis. As discussed in the previous chapter it is difficult to assess the influence of melt elasticity and precedent has been sought in work on single screw extrusion. Based on this it is believed that omission of melt elasticity effects is a contributing factor to the errors of the analysis. However it is unclear whether the additional complications and depth of analysis required to include elastic and viscous heating effects are justified by the potential improvement in accuracy which would follow given the complexities of the geometry and the problem generally.

The general conclusion is that the most serious errors, i.e. those found for screws A at low speeds, are more likely to be due to the limitations of the material data than the flow modelling. If this effect is allowed for, and also bearing in mind that in practice extruders will be run at the higher speeds, the theoretical predictions are satisfactory and give confidence in using the model for the assessment of other characteristics, for example power requirements and degrees of mixing. It is believed that the treatment presented here represents a significant improvement over simpler, pre-existing analyses for the prediction of the flow behaviour of polymers in counter-rotating twin screw extruders.

Appendix I.

The equation of Continuity in:

Cartesian coordinates (x,y,z),

$$\frac{\partial \rho}{\partial t} + \frac{\partial}{\partial x}(\rho v_x) + \frac{\partial}{\partial y}(\rho v_y) + \frac{\partial}{\partial z}(\rho v_z) = 0 \qquad (A)$$

Cylindrical polar coordinates (r,θ,z),

$$\frac{\partial \rho}{\partial t} + \frac{1}{r}\frac{\partial}{\partial r}(\rho r v_r) + \frac{1}{r}\frac{\partial}{\partial r}(\rho v_\theta) + \frac{\partial}{\partial z}(\rho v_z) = 0 \qquad (B)$$

Appendix II.

The Equations of motion in:

Cartesian coordinates (x,y,z),

$$\text{x-component, } \rho\left(\frac{\partial v_x}{\partial t} + v_x\frac{\partial v_x}{\partial x} + v_y\frac{\partial v_x}{\partial y} + v_z\frac{\partial v_x}{\partial z}\right) = -\frac{\partial p}{\partial x} - \left(\frac{\partial \tau_{xx}}{\partial x} + \frac{\partial \tau_{yx}}{\partial y} + \frac{\partial \tau_{zx}}{\partial z}\right) + \rho g_x \qquad (A)$$

$$\text{y-component, } \rho\left(\frac{\partial v_y}{\partial t} + v_x\frac{\partial v_y}{\partial x} + v_y\frac{\partial v_y}{\partial y} + v_z\frac{\partial v_y}{\partial z}\right) = -\frac{\partial p}{\partial y} - \left(\frac{\partial \tau_{xy}}{\partial x} + \frac{\partial \tau_{yy}}{\partial y} + \frac{\partial \tau_{zy}}{\partial z}\right) + \rho g_y \qquad (B)$$

$$\text{z-component, } \rho\left(\frac{\partial v_z}{\partial t} + v_x\frac{\partial v_z}{\partial x} + v_y\frac{\partial v_z}{\partial y} + v_z\frac{\partial v_z}{\partial z}\right) = -\frac{\partial p}{\partial z} - \left(\frac{\partial \tau_{xz}}{\partial x} + \frac{\partial \tau_{yz}}{\partial y} + \frac{\partial \tau_{zz}}{\partial z}\right) + \rho g_z \qquad (C)$$

Cylindrical polar coordinates (r,θ,z),

$$\text{r-component, } \rho\left(\frac{\partial v_r}{\partial t} + v_r\frac{\partial v_r}{\partial r} + \frac{v_\theta}{r}\frac{\partial v_r}{\partial \theta} - \frac{v_\theta^2}{r} + v_z\frac{\partial v_r}{\partial z}\right) = -\frac{\partial p}{\partial r} - \left(\frac{1}{r}\frac{\partial}{\partial r}(r\tau_{rr}) + \frac{1}{r}\frac{\partial \tau_{r\theta}}{\partial \theta} - \frac{\tau_{\theta\theta}}{r} + \frac{\partial \tau_{rz}}{\partial z}\right) + \rho g_r \qquad (D)$$

$$\theta\text{-component, } \rho\left(\frac{\partial v_\theta}{\partial t} + v_r\frac{\partial v_\theta}{\partial r} + \frac{v_\theta}{r}\frac{\partial v_\theta}{\partial \theta} + \frac{v_r v_\theta}{r} + v_z\frac{\partial v_\theta}{\partial z}\right) = -\frac{1}{r}\frac{\partial p}{\partial \theta} - \left(\frac{1}{r^2}\frac{\partial}{\partial r}(r^2\tau_{r\theta}) + \frac{1}{r}\frac{\partial \tau_{\theta\theta}}{\partial \theta} + \frac{\partial \tau_{\theta z}}{\partial z}\right) + \rho g_\theta \qquad (E)$$

$$\text{z-component, } \rho\left(\frac{\partial v_z}{\partial z} + v_r\frac{\partial v_z}{\partial r} + \frac{v_\theta}{r}\frac{\partial v_z}{\partial \theta} + v_z\frac{\partial v_z}{\partial z}\right) = -\frac{\partial p}{\partial z} - \left(\frac{1}{r}\frac{\partial}{\partial r}(r\tau_{rz}) + \frac{1}{r}\frac{\partial \tau_{\theta r}}{\partial z} + \frac{\partial \tau_{zz}}{\partial z}\right) + \rho g_z \qquad (F)$$

Appendix III.

The Equations of Energy in:

Cartesian coordinates (x,y,z),

$$\rho C_v \left(\frac{\partial T}{\partial t} + v_x \frac{\partial T}{\partial x} + v_y \frac{\partial T}{\partial y} + v_z \frac{\partial T}{\partial z} \right) = \left(\frac{\partial}{\partial x}\left(k \frac{\partial T}{\partial x}\right) + \frac{\partial}{\partial y}\left(k \frac{\partial T}{\partial y}\right) + \frac{\partial}{\partial z}\left(k \frac{\partial T}{\partial z}\right) \right)$$
$$- T\left(\frac{\partial p}{\partial T}\right)_\rho \left(\frac{\partial v_x}{\partial x} + \frac{\partial v_y}{\partial y} + \frac{\partial v_z}{\partial z} \right) - \left(\tau_{xx} \frac{\partial v_x}{\partial x} + \tau_{yy} \frac{\partial v_y}{\partial y} + \tau_{zz} \frac{\partial v_z}{\partial z} \right)$$
$$- \left(\tau_{xy} \left(\frac{\partial v_x}{\partial y} + \frac{\partial v_y}{\partial x} \right) + \tau_{xz} \left(\frac{\partial v_x}{\partial z} + \frac{\partial v_z}{\partial x} \right) + \tau_{yz} \left(\frac{\partial v_y}{\partial z} + \frac{\partial v_z}{\partial z} \right) \right) \qquad (A)$$

Cylindrical polar coordinates (r,θ, z),

$$\rho C_v \left(\frac{\partial T}{\partial t} + v_r \frac{\partial T}{\partial r} + \frac{v_\theta}{r} \frac{\partial T}{\partial \theta} + v_z \frac{\partial T}{\partial z} \right) = \left(\frac{1}{r} \frac{\partial}{\partial r}\left(rk \frac{\partial T}{\partial r}\right) + \frac{1}{r} \frac{\partial}{\partial \theta}\left(k \frac{\partial T}{\partial \theta}\right) + \frac{\partial}{\partial z}\left(k \frac{\partial T}{\partial z}\right) \right)$$
$$- T\left(\frac{\partial p}{\partial T}\right)_\rho \left(\frac{1}{r} \frac{\partial}{\partial r}(r v_r) + \frac{1}{r} \frac{\partial v_\theta}{\partial \theta} + \frac{\partial v_z}{\partial z} \right) - \left(\tau_{rr} \frac{\partial v_r}{\partial r} + \tau_{\theta\theta} \frac{1}{r} \left(\frac{\partial v_\theta}{\partial \theta} + v_r \right) + \tau_{zz} \frac{\partial v_z}{\partial z} \right)$$
$$- \left(\tau_{r\theta} \left(r \frac{\partial}{\partial r}\left(\frac{v_\theta}{r}\right) + \frac{1}{r} \frac{\partial v_r}{\partial \theta} \right) + \tau_{rz} \left(\frac{\partial v_z}{\partial r} + \frac{\partial v_r}{\partial r} \right) + \tau_{\theta r} \left(\frac{1}{r} \frac{\partial v_z}{\partial \theta} + \frac{\partial v_\theta}{\partial z} \right) \right) \qquad (B)$$

Appendix IV.

Components of Stress Tensor in:

Cartesian coordinates (x,y,z),

$$\tau_{xx} = -\mu\left(2\frac{\partial v_x}{\partial x} - 2/3\ (\nabla.v) \right) \qquad (A)$$

$$\tau_{yy} = -\mu\left(2\frac{\partial v_y}{\partial y} - 2/3\ (\nabla.v) \right) \qquad (B)$$

$$\tau_{zz} = -\mu\left(2\frac{\partial v_z}{\partial z} - 2/3\ (\nabla.v) \right) \qquad (C)$$

$$\tau_{xy} = \tau_{yx} = -\mu\left(\frac{\partial v_x}{\partial y} + \frac{\partial v_y}{\partial x} \right) \qquad (D)$$

$$\tau_{yz} = \tau_{zy} = -\mu\left(\frac{\partial v_y}{\partial z} + \frac{\partial v_z}{\partial y} \right) \qquad (E)$$

$$\tau_{zx} = \tau_{xz} = -\mu\left(\frac{\partial v_z}{\partial x} + \frac{\partial v_x}{\partial z} \right) \qquad (F)$$

$$(\nabla.v) = \frac{\partial v_x}{\partial x} + \frac{\partial v_y}{\partial y} + \frac{\partial v_z}{\partial z}$$

Cylindrical polar coordinates (r,θ,z),

$$\tau_{rr} = -\mu\left(2\frac{\partial v_r}{\partial r} - 2/3\ (\nabla.v) \right) \qquad (G)$$

$$\tau_{\theta\theta} = -\mu\left(2\left(\frac{1}{r}\frac{\partial v_\theta}{\partial \theta} + \frac{v_r}{r}\right) - 2/3\ (\nabla.v) \right) \qquad (H)$$

$$\tau_{zz} = -\mu\left(2\frac{\partial v_z}{\partial z} - 2/3\ (\nabla.v) \right) \qquad (I)$$

$$\tau_{r\theta} = \tau_{\theta r} = -\mu\left(r\frac{\partial}{\partial r}\left(\frac{v_\theta}{r}\right) + \frac{1}{r}\frac{\partial v_r}{\partial \theta} \right) \qquad (J)$$

$$\tau_{\theta z} = \tau_{z\theta} = -\mu\left(\frac{\partial v_\theta}{\partial z} + \frac{1}{r}\frac{\partial v_z}{\partial \theta} \right) \qquad (K)$$

$$\tau_{zr} = \tau_{rz} = -\mu\left(\frac{\partial v_z}{\partial r} + \frac{\partial v_r}{\partial z} \right) \qquad (L)$$

$$(\nabla.v) = \frac{1}{r}\frac{\partial}{\partial r}(rv_r) + \frac{1}{r}\frac{\partial v_\theta}{\partial \theta} + \frac{\partial v_z}{\partial z}$$

Appendix V.

One-dimensional power law flow between infinite parallel plates.

The power law equation for fluid flow is,

$$\tau_{yz} = -\mu_o \left| \frac{dv_z}{dy} \right|^n \qquad (A)$$

The momentum equation for force balance of an element of fluid in one-dimensional flow between infinite parallel plates reduces to,[1]

$$\frac{\partial p}{\partial z} = -\frac{\partial \tau_{yz}}{\partial y} = \mu_o \frac{\partial}{\partial y} \left(\left| \frac{dv_z}{dy} \right|^n \right) \qquad (B)$$

Dimensionless variables can be defined as,

$$\begin{aligned} &\text{clearance depth, } \xi = \frac{y}{h} \\ &\text{pressure gradient, } \pi_p = \frac{h^{s+1}}{V_z} \left(\frac{1}{\mu_o} \frac{dp}{dz} \right)^s \\ &\text{reciprocal of power law flow index, } s = \frac{1}{n} \\ &\text{velocity, } \vartheta = \frac{v_z}{pV_z} \end{aligned} \qquad (C)$$

Substituting these varaibles into equation (A) gives the differential equation,

$$\frac{d}{d\xi} \left(\left| \frac{d\vartheta}{d\xi} \right|^n \right) = 1 \qquad (D)$$

Positive pressure gradient.

For predominantly drag flow with dimensionless shear rate $\frac{d\vartheta}{d\xi} > 0$ everywhere in the velocity profile, equation (D) becomes,[1]

$$\frac{d}{d\xi} \left(\frac{d\vartheta}{d\xi} \right) = 1 \qquad (E)$$

Integrating this equation gives,

$$\frac{v_z}{V_z} = \frac{\pi_p}{s+1} (\xi + K_1)^{s+1} + \pi_p K_2 \qquad (F)$$

Using the boundary conditions $\frac{v_z}{V_z}(0)=0$ and $\frac{v_z}{V_z}(1)=1$,

$$K_2 = -\frac{K_1^{s+1}}{s+1}$$

and the dimensionless pressure gradient is,

$$\pi_p = \frac{s+1}{(K_1+1)^{s+1} - K_1^{s+1}} \tag{G}$$

Integrating the velocity equation over the clearance gives the dimensionless flow rate as follows,

$$\frac{Q}{V_z wh} = \frac{\pi_p}{s+1}\left[\frac{(1+K_1)^{s+2} - K_1^{s+2}}{s+2} - K_1^{s+1}\right] \tag{H}$$

and in terms of the dimensionless co-ordinate K_1 alone,

$$\frac{Q}{V_z wh} = \frac{\dfrac{(1+K_1)^{s+2} - K_1^{s+2}}{s+2} - K_1^{s+1}}{(K_1+1)^{s+1} - K_1^{s+1}} \tag{I}$$

The condition for predominantly drag flow is,

$$0.5 > \frac{Q}{V_z wh} \geqslant \frac{1}{s+2} \tag{Ia}$$

For predominantly pressure flow (Krosser and Middleman[37]), the differential equation, for the lower portion of the velocity profile where $\frac{d\vartheta_L}{d\xi} < 0$ and flow travels opposite to the principal direction, becomes,

$$-\frac{d}{d\xi}\left(\frac{d\vartheta_L}{d\xi}\right)^n = 1 \tag{J}$$

Integrating and using the boundary conditions $\frac{v_z}{V_z}(0)=0$ at the stationary surface and $\frac{d\vartheta_L}{d\xi} = 0$ at $\xi = \xi^*$,

$$\vartheta_L = \frac{1}{s+1}\left[(\xi^* - \xi)^{s+1} - (\xi^*)^{s+1}\right] \tag{K}$$

For the upper portion of the velocity profile where $\frac{d\vartheta_U}{d\xi} > 0$, the differential equation is the same as equation (E). Integrating and using the boundary conditions $\frac{v_z}{V_z}(1) = 1$ at the moving surface and $\frac{d\vartheta_U}{d\xi} = 0$ at $\xi = \xi^*$,

$$\vartheta_U = \frac{1}{s+1}\left[(\xi - \xi^*)^{s+1} - (1-\xi^*)^{s+1}\right] + \frac{1}{\pi_p} \tag{L}$$

Using the condition $\vartheta_L = \vartheta_U$ at $\xi = \xi^*$, the pressure gradient is obtained as follows,

$$\pi_p = \frac{s+1}{(1-\xi^*)^{s+1} - (\xi^*)^{s+1}} \tag{M}$$

By integrating the velocity equations over their respective regions of the clearance and summing the individual flows gives the dimensionless flow rate as,

$$\frac{Q}{V_z wh} = \frac{\pi_p}{s+1}\left[\frac{(\xi^*)^{s+2} + (1-\xi^*)^{s+2}}{s+2} - (\xi^*)^{s+1}\right] \qquad (N)$$

and in terms of the dimensionless co-ordinate ξ alone,

$$\frac{Q}{V_z wh} = \frac{\frac{(\xi^*)^{s+2} + (1+\xi^*)^{s+2}}{s+2} - (\xi^*)^{s+1}}{(1-\xi^*)^{s+1} - (\xi^*)^{s+1}} \qquad (O)$$

The condition for predominantly pressure flow is,

$$0 < \frac{Q}{V_z wh} \leqslant \frac{1}{s+2}$$

Negative pressure gradient.

As explained in section 2.5, Chapter 2, for predominantly drag flow, the dimensionless flow rate is given by,

$$\frac{Q}{V_z wh} = 1 - \frac{\pi_p}{s+1}\left[\frac{(1+K_1)^{s+2} - K_1^{s+2}}{s+2} - K_1^{s+1}\right] \qquad (P)$$

The dimensionless pressure gradient is given by equation (G).

In terms of the dimensionless co-ordinate K_1 alone,

$$\frac{Q}{V_z wh} = 1 - \left[\frac{\frac{(1+K_1)^{s+2} - K_1^{s+2}}{s+2} - K_1^{s+1}}{(K_1+1)^{s+1} - K_1^{s+1}}\right] \qquad (Q)$$

The condition for predominantly drag flow is,

$$0.5 < \frac{Q}{V_z wh} \leqslant \frac{s+1}{s+2} \qquad (Qa)$$

For predominantly pressure flow, the dimensionless flow rate is given by,

$$\frac{Q}{V_z wh} = 1 - \frac{\pi_p}{s+1}\left[\frac{(\xi^*)^{s+2} + (1-\xi^*)^{s+2}}{s+2} - (\xi^*)^{s+1}\right] \qquad (R)$$

The dimensionless pressure gradient is given by equation (M).

In terms of the dimensionless co-ordinate ξ alone,

$$\frac{Q}{V_z wh} = 1 - \frac{\frac{(\xi^*)^{s+2} + (1-\xi^*)^{s+2}}{s+2} - (\xi^*)^{s+1}}{(1-\xi^*)^{s+1} - (\xi^*)^{s+1}} \qquad (S)$$

The condition for predominantly pressure flow is,

$$\frac{s+1}{s+2} \leqslant \frac{Q}{V_z wh} < 1 \qquad (Sa)$$

Appendix VI

The method choosen for determining the equivalent viscosity which is used in the Finite Element analysis described in section 3.8, is as follows.[1,34] The dimensionless flow rate, $\pi_Q = Q/V_z WH$ for non-Newtonian flow is a function of $\pi_p^s = H/V_z((H/\mu_o)\partial p/\partial z)^s$ while for a Newtonian fluid it is a function of $H^2/\bar{\mu} V_z(\partial p/\partial z)$ where $\bar{\mu}$ is an average viscosity in the channel. There should exist a certain $\bar{\mu}$ value which will give the same flow rate with both equations. Defining a ratio k_R of these equations gives,

$$k_R = \frac{\pi_p^s}{H^2/\bar{\mu} V_z(\frac{\partial p}{\partial z})} = \bar{\mu}(\frac{H}{\mu_o}\frac{\partial p}{\partial z})^{s-1} \qquad (A)$$

Assuming the shear rate is positive everywhere (i.e. $\frac{1}{s+2} \leq \frac{Q}{V_z wh} \leq 0.5$), differentiating the velocity, equation(F), Appendix V, gives,

$$\frac{dv_z}{dy} = \frac{V_z}{H}\pi_p^s (\xi + K_1)^s \qquad (B)$$

where ξ is the dimensionless coordinate y/H and $K_1=\xi^*$, the position of the zero shear atress/ shear rate, and the shear rate at the barrel wall y=H,

$$\dot{\gamma}_w = (\frac{dV_z}{dy})_w = \frac{V_z}{H}\pi_p^s (1+K_1)^s = (\frac{H\partial p}{\mu_o \partial z})^s(1+K_1)^s \qquad (C)$$

Substituting equation (C) into (A) gives,

$$k_R = \bar{\mu}\frac{\dot{\gamma}_w}{(1+K_1)^s}\frac{\mu_o}{H(\frac{\partial p}{\partial z})} \qquad (D)$$

the shear stress at the wall is,

$$(-\tau_{yz})_w = \bar{\mu}\dot{\gamma}_w = k_R (1+K_1)^s \frac{H}{\mu_o}(\frac{\partial p}{\partial z}) \qquad (E)$$

Alternatively, the shear stress at the wall can be expressed as,

$$(-\tau_{yz})_w = \mu_o(\frac{dv_z}{dy})^n = \frac{H}{\mu_o}\frac{\partial p}{\partial z} (1+K_1) \qquad (F)$$

Eliminating the pressure gradient from the two equations gives,

$$\bar{\mu}\dot{\gamma}_w = k_R(1+K_1)^{s-1}(-\tau_{yz})_w \qquad (G)$$

Using the apparent viscosity at the wall, $(-\tau_{yz}/\dot{\gamma})_w = \mu_b$, this equation reduces to,

$$\bar{\mu} = \mu_b \, k_R (1+K_1)^{s-1} \qquad (H)$$

For a velocity profile with both positive and negative shear rates, i.e. $0 \leqslant \pi_Q \leqslant \frac{1}{s+2}$,

$$\bar{\mu} = \mu_b \, k_R (1-\xi^*)^{s-1} \qquad (I)$$

where ξ^* is the dimensionless coordinate of the stress neutral surface.

Appendix VII

Invariants of the rate of deformation tensor, expressed concisely in tensor notation,

$$I_1 = E_{ii} \qquad (A)$$

$$I_2 = \frac{1}{2} E_{ij}E_{ij} \qquad (B)$$

$$I_3 = \det(E_{ij}) \qquad (C)$$

where E_{ij} is the rate of deformation tensor and'det'means the determinant of the enclosed matrix (Refs. 1,30, Bird,R.B. et al, Dynamics of Polymeric Liquids: Vol.1, Fluid Mechanics, Wiley, 1977.).

References

1. Tadmor, Z., Klein, I., Engineering Principles of Plasticating Extrusion, Van Nostrand Reinhold, 1970.
2. Martelli, F., Twin Screw Extruders - A separate Breed, SPE Journal, vol 27, January 1971, p25.
3. Kaplan, A., Tadmor, Z., Theoretical Model for non-Intermeshing Twin Screw Extruders, Polymer Engineering and Science, Vol.14, No.1, Jan., 1974.
4. Shenkel, G., Plastic Extrusion Technology and Theory, Iliffe, 1966.
5. Janssen, L.P.B.M., Twin Screw Extruders, Elsevier, 1978.
6. Peek, W., Tackle rigid PVC with Twin screws, Plastics Engineering, July 1974, p23.
7. Thacker, G.A., Conical Twin Screw Extrusion of Rigid PVC, SPE ANTEC 1972, p628.
8. Pidgeon, B.J., A commercial look at twin screw preplasticizing, British Plastics, August 1963.
9. Suddenly there are a lot of twin-screw extruders. What's going on?, Modern Plastics, November 1969, p73.
10. Stinson, S.C., Twin-Screw Extrusion Swings into High Gear, Plastics Technology, v19, n2, Feb. 1973, p45.
11. Ferns, A.W.D., Twin screw Machines for Polymer Compounding Operations, New Tech. in Extrusion and Injection Moulding, Conf., Manchester, Engl, Apr. 11-12 1973, pap,7, 20p., Published by Plastics Institute, London, 1973.
12. Mack, W.A., Twin-Screw Extruders - where to use them and why, SPE 29th ANTEC, May 1971, p278.
13. Booy, M.L., Geometry of Fully Wiped Twin-screw Equipment, Polymer Engineering and Science, vol.18, no.12, Sept. 1978, p973.

14. Booy, M.L., Isothermal Flow of Viscous Liquids in Corotating Twin-Screw Devices, Polymer Engineering and Science, vol,20, no.18, Dec. 1980.

15. Denson, C.D., Hwang Jr., B.K., The influence of the Axial Pressure Gradient on Flow Rate for Newtonian Liquids in a Self-Wiping, Co-rotating Twin Screw Extruder, Polymer Engineering and Science, vol.20, no.14, Sept. 1980.

16. Todd, D.B., Residence Time Distribution in Twin-Screw Extruders, Polymer Engineering and Science, vol.15, no.6, June 1975.

17. Uhland, E., Dienst, M., Development Tendencies for Co-rotating Twin screw Extruders, SPE, 38th ANTEC, Plast. Prog. Through Process, New York, May 5-8, 1980, p36.

18. Rauwendaal, C.J., Analysis and experimental Evaluation of Twin-Screw Extruders, Polymer Engineering and Science, vol.21, no.16, Nov. 1981, p1092.

19. Denson, C.D., Hwang Jr., B.K., The Effect of Leakage and Cross Channel Flows on the Performance of Co-rotating Twin-Screw Extruders, SPE, 38th ANTEC, Plast. Prog. Through Process, New York, May 5-8, 1980, p107.

20. Wyman, C.E., Theoretical Model for Intermeshing Twin-screw Extruders: Axial velocity Profile for shallow channels, Polymer Engineering and Science, vol.15, no.8, August 1975.

21. Maheshri, J.C., Wyman, C.E., Mixing in an Intermeshing Twin screw Extruder Chamber: Combined Cross and Down Channel Flow, Polymer Engineering and Science, vol.20, no.9, June 1980.

22. Janssen, L.P.B.M, A Phenomenological study on twin screw extruders, Thesis (1976), Delft University.

23. McKelvey, J.M., Polymer Processing, John Wiley and Sons, Inc, New York, 1962.

24. Martin, B., Numerical Studies of Steady State Extrusion Processes, PhD. Thesis, Cambridge University, England, 1969.

25. Gaskell, R.E., The Calendering of Plastic Materials, Journal of Applied Mechanics, Sept. 1950, p334.

26. Janssen, L.P.B.M., Smith, J.M., Comparison of different classes of extruders, Plastics and Rubber: Processing, Sept./Dec. 1980, p115.

27. Pinkus, O., Sternlicht, B., Theory of Hydrodynamic Lubrication, McGraw-Hill, New York, 1961.

28. Cameron, A., Basic Lubrication Theory, London, Longmans, 1970.

29. Wilkinson, W.L., Non-Newtonian Fluids, Pergamon Press, London, 1960.

30. Fenner, R.T., Extruder Screw Design, Iliffe, 1970.

31. Fenner, R.T., Principles of Polymer Processing, MacMillan, 1979.

32. Bagley, E.B., End Corrections in Capillary Flow of Polyethylene, J. of Applied Physics, v28,no5, 1957, p624.

33. Rabinowitsch, B., Z. Phys. Chem. v145A, no1, 1929.

34. Weeks, D.J., Allen, W.J., screw Extrusion of Plastics, Journal of Mechanical Engineering Science, vol.4, no.4, 1962.

35. Jacobi, H.R., Screw Extrusion of Plastics, London, Iliffe Books Ltd., 1963.

36. Glyde, B.S., Holmes-Walker, W.A., Screw Extrusion of Thermoplastics, International Plastics Engineering, vol.2, pt.8, Aug. 1962.

37. Krosser, F.W., Middleman, S., The Calculation of Screw Characteristics for the Extrusion of non-Newtonian Melts, Polymer Engineering and Science, vol.5, Oct. 1965.

38. Kennaway, A., Weeks, D.J., Extrusion Problems and Screw Design, Polythene Ed. Renfrew and Morgan, Iliffe, London, 1960.

39. Griffith, R.M., Fully developed Flow in Screw Extruders, Ind. Eng. Chem. Fundermentals, vol1, no.3, Aug. 1962.

40. Klein, I., Tadmor, Z., Computer Design of Plasticating Extruder Screws, Modern Plastics, Sept. 1969.

41. Tadmor, Z., Non-Newtonian Tangential Flow in Cylindrical Annuli, Polymer Engineering and Science, July 1966, p203.

42. Pearson, J.R.A., Non-Newtonian flow and die design, Trans. Plastics Institution, vol.30, 1962, p230.

43. Fenner, R.T., Designing extruder screws and dies with the aid of computers, Plastics and Polymers, June 1974.

44. Fenner, R.T., Nadiri, F., Finite Element Analysis of Polymer Melt Flow in Cable-covering Crossheads, Polymer Engineering and science, vol.19, no.3, Feb. 1979.

45. Booy, M.L., Influence of Channel Curvature on Flow, Pressure Distribution, and Power requirements of Screw pumps and Melt Extruders, SPE Trans., July 1963, p176.

46. Middleman, S., The Flow of Power-law fluids in Rectangular Ducts, Trans. Soc. Rheol., 9, no1, 1965, p83.

47. Palit, K., Fenner, R.T., Finite Element Analysis of Slow non-Newtonian Channel Flow, AIChE Journal, vol18, no.3, May 1972, p628.

48. Dyer, D.F., A Numerical Solution for the Single-Screw Extrusion of Polymer Melt, AIChE Journal, v15,n6, 1969.

49. Hami, M.L., Pittman, J.F.T., Finite Element Solutions for Flow in a single-screw Extruder, including curvature effects, Polymer Engineering and Science, vol.20, no5, March 1980, p339.

50. Choo, K.P., Hami, M.L., Pittman, J.F.T., Deep Channel Operating Characteristic of a single Screw Extruder: Finite element Predictions and Experimental Results for isothermal non-Newtonian Flow, Polymer Engineering and Science, vol.21, no2, Feb. 1981, p100.

51. Carley, J.F., Fundermentals of Melt Rheology, Heat Generation, and Heat Transfer as Applied to Polymer Processing, Polymer Engineering and Science, April 1966, p158.

52. Wilkinson, W.L., An introduction to heat transfer concepts involved in plastics processing, Plastics and Polymers, England, October 1974, p221.

53. Pearson, J.R.A., Heat-transfer Effects in Flowing Polymers, Progress in Heat and Mass Transfer, vol.V by Schowalter, Minkowyez, Afgan and Luikov, Pergamon Press, New York, 1972, p73.

54. Pearson, J.R.A., The lubrication approximation applied to non-Newtonian Flow Problems: A Perturbation approach, Proc. of the symposium on solution of non-Linear Partial Differential Equations, p73, (ed. W.F. Ames), Academic Press, New York, 1967.

55. Benis, A.M., Laminar flow of power-law fluids through narrow three-dimensional channels of varying gap, Chemical Engineering Science, vol.22, 1967, Pergamon Press Ltd., Oxford, England.

56. Fenner, R.T., Finite element Methods for Engineers, MacMillan, London, 1975.

57. Schechter, R.S., The Variational Method in Engineering, McGraw-Hill, New York, 1967.

58. Gosman, A.D., Pun, W.M., Rundal, A.K., Spalding, D.B., Wolfshtein, M., Heat and Mass Transfer in Recirculating Flows, Academic Press, 1969.

59. Palit, K., Fenner, R.T., Finite Element Analysis of Slow non-Newtonian Channel Flow, AIChE Journal, vol.18, no.3, May 1972, p628.

60. Zienkiewicz, O.C., The Finite Element Method in Engineering Science, McGraw-Hill, London, 1971.

61. Martin, H.C., Finite Element Analysis of Fluid Flows, Proc. Second Conf. on Matrix Methods in Structural Mech. Alright-Patterson Air Force Base, Ohio, 1968.

62. Lai-Fook, R.A., Worth, R.A., Rheodynamic Lubrication of Screw Flights to reduce wear in Single-screw Extruders, SPE, 36th ANTEC TECH PAPERS vol.XXIV, April 1978, p450.

63. Scheid, F., Theory and problems of Numerical Analysis, Schaum's Outline Series, McGraw-Hill, 1968, p315.

64. Janssen, L.P.B.M., Private communication.

65. Tadmor, Z., Broyer, E., and Gutfinger, C., Flow Analysis Network- A method for solving flow problems in Polymer Processing, Polymer Eng. Sci., v14, 1974, p660.

66. Broyer, E., Gutfinger, C., and Tadmor, Z., Evaluating Flows of non-Newtonian Fluids by the Method of Equivalent Newtonian Viscosity, AIChE Journal, v21, n1, Jan. 1975.

67. Pearson, J.R.A., Mechanical Principles of Polymer Melt Processing, Pergamon Press, 1966.

68. Martin, B., Some Analytical Solutions for Viscometric Flows of Power-law fluids with Heat generation and temperature dependent viscosity, J. Non- Linear Mechanics, Vol 2, 1967.

69. Winter, H.H.V., Rheologica Acta 11, 216-223, 1972.

70. Lodge, A.S., Elastic Liquids, Academic Press, London, 1964.

71. Benbow, J.J., Charley, R.V., Unstable Flow of Molten Polymers, Nature, v 192, no 4799, Oct. 1961.

72. Tadmor, Z., Gogos, C.G., Principles of Polymer Processing, John Wiley and Sons, 1979.

73. Worth, R.A., Helmy, H.A.A., and Parnaby, J., Wall slip and its implications in the design of Single-screw Plastics Melt-Fed Extruders, Polymer Engineering and Science, Vol 17, No.14, April 1977.

74. Carlile, D.R., and Fenner, R.T., On the Lubricating Action of Molten Polymers in Single-screw Extruders, J. Mech. Eng. Sci., 20, 1978.

75. Mitsoulis, E.,Vlachopoulos, J., Mirza, F.A., Finite Element Analysis of Two-dimensional Polymer Melt Flows, Polymer Processing Engineering, 1 (3), 1983-84.

76. Walters, K., Rheometry, Chapman and Hall, London, 1975.

77. Black, J.R., Denn, M.M., Converging Flow of a Viscoelastic Liquid, J. of non-Newtonian Fluid Mechanics, 1, 1976.

78. Tan, K.L., Tiu, C., Entry Flow behaviour of Viscoelastic Fluids in an Annulus, J. of non-Newtonian Fluid Mechanics, 3, 1977/1978.

79. Brocklebank, M.P., Smith, J.M., Developing laminar flows with viscoelastic and non-Newtonian liquids, Rheologica Acta, 9, v3, 1970.

80. Crochet, M.J., Pilate, G., Plane Flow of a Fluid of Second Grade through a Contraction, J. of Non-Newtonian Fluid Mechanics, 1, 1976.

81. Choo, K.P., Hami, M.L., Pittman, J.F.T., Deep Channel Operating Characteristic of a Single-Screw Extruder: Finite Element Predictions and Experimental Results for isothermal Non-Newtonian Flow, Polymer Engineering and Science, vol. 21, No.2, Mid-Feb. 1981.

82. Tanner, R.I., A Theory of Die-Swell, Journal of Polymer Science: Part A-2, Vol.8, 1970.

83. Petrie, C.J.S., Elongational Flows, Pitman, London, 1979.